POLITECNICO DI MILANO

Facoltà di Ingegneria Industriale

Dipartimento di Energia

Corso di Dottorato in Scienze e Tecnologie Energetiche e Nucleari

Thermodynamic and economic analysis of advanced systems for CO_2 capture

Supervisor: Prof. Ennio Macchi

Co-supervisors: Ing. Giampaolo Manzolini

Tutor: Prof. Stefano Campanari

Coordinator: Prof. Carlo Enrico Bottani

PhD candidate

Matteo GAZZANI

XXV cycle

RINGRAZIAMENTI

Fermandomi a riflettere sui tre anni passati al Dipartimento di Energia non posso che trovare soddisfazione per aver intrapreso il miglior percorso possibile. Certamente sono state le persone che mi hanno accompagnato ad aver reso indimenticabile quest'esperienza.

Per questo, il mio primo ringraziamento va al gruppo di ricerca GECoS nel suo complesso, indubbiamente il miglior ambiente di lavoro che si possa desiderare.

Un grazie speciale al Prof. Macchi per avermi permesso d'intraprendere il percorso di dottorato, per i preziosi insegnamenti, i consigli, la passione e l'entusiasmo con i quali ha sempre seguito il mio lavoro.

Grazie a Giampaolo Manzolini per la continua disponibilità e l'impegno con cui mi ha seguito e indirizzato durante l'attività di ricerca, nonché durante le numerose e divertenti trasferte estere.

Grazie a Paolo Chiesa e Matteo Romano per le molteplici discussioni tecniche che mi hanno insegnato più di qualsiasi libro di testo, sempre accompagnate da simpatia e ilarità.

Grazie a Stefano Campanari e al Prof. Lozza per i preziosi consigli e insegnamenti.

Desidero ringraziare calorosamente tutte le persone dell'ufficio dottorandi, amici più che colleghi, con cui ho condiviso buona parte degli ultimi anni; soprattutto Bino, Vince, Gio e Asto, ma anche tutti coloro che hanno fatto o fanno parte dell'ufficio.

Un ringraziamento sentito al Prof. Ghoniem per la calorosa ospitalità con cui mi ha accolto nel suo gruppo di ricerca durante il periodo al MIT. Grazie anche ad Antonio, Christian, Chris, Alberto e Francesco, che hanno reso il soggiorno a Boston spensierato e divertente.

Grazie ai miei genitori che mi hanno sempre sostenuto e incoraggiato a perseguire i miei obiettivi.

Grazie a mio fratello, unico nella tenacia e nella capacità di non arrendersi davanti ai problemi.

Infine grazie a Lisa per la felicità che mi dona da sempre.

Table of Contents

SUMMARY

INTRODUCTION AND METHODOLOGY

Rising world energy demand has mostly been met by expanding the use of fossil fuels, resulting in higher concentrations of carbon dioxide in the atmosphere. The possible consequences of these trends, in particular global warming, have driven the search for alternative electricity generation technologies capable of limiting CO_2 emissions. It is very likely that carbon dioxide reduction will have to be achieved while fossil fuels continue to be the major source of primary energy for several decades to come. Carbon dioxide capture and storage, is recognized as one of the most promising options because it addresses the impact of the largest primary energy sources and the largest source of CO_2.

The final goal of the PhD research activity was the techno-economic assessment of fossil fuelled power plants with carbon capture by two different innovative technologies: one based on advanced sorbents (Sorption Enhanced Water Gas Shift) and one based on membranes (hydrogen selective membranes). SEWGS application to NGCC, IGCC and steelworks plant is investigated while membranes are integrated only in IGCC plant. Both the technologies were developed in two FP7 projects: CAESAR and CACHET-II. The PhD work was exclusively theoretical but with input from experiments carried out by the projects partners (ECN, SINTEF). The best plant configurations have been established limiting the thermodynamic and economic penalization of CCS application.

In order to study advanced technologies together with innovative power production configurations, different investigation levels have been considered:

1. **Detailed reactor model**: it aims at reproducing the behavior of the most critical reactors involving detailed chemical kinetic mechanisms. Due to the high level of details and the required implementation time, two different reactors have been investigated using this model approach: i) the coal gasifier and ii) the hot gas clean-up system. The first one is the most important reactor in a coal gasification plant whilst the second one is critical for limiting the penalization of desulfurization process. Both the components work in two/three phase conditions and the kinetic approach is mandatory to correctly predict the performances or the design. It must be remarked that the detailed modeling of the SEWGS and the H_2 membranes was performed by other partners inside the project consortium (SEWGS: Air Product; Membranes: SINTEF). Chapter 4 and 5 are dedicated to the Shell kinetic model and hot gas desulfurization, respectively.
2. **Specific process model**: it is focused on the most important processes adopted in a defined configuration; this simulation involves only the required physical phenomena. Single system model has been adopted to reproduce the behavior of hydrogen fuelled gas turbine and the Shell coal gasification process. The latter is briefly reported together with the Shell kinetic model. Chapter 6 is dedicated to hydrogen gas turbine simulations.
3. **Overall techno-economic plant simulation**: the thermodynamic evaluation is based on mass and energy balances and it allows integrating all the component required for power production with CCS. All the data obtained in the single reactor and process modeling are

implemented in this step. Chapter 7 and 8 report the thermodynamic analysis of SEWGS and hydrogen membranes respectively. Economics of the two technologies are reported in chapter 9.

The results obtained in the single reactor and system modeling are implemented in the overall plant simulations; in particular: i) the coal gasification kinetic model as well as the IGCC process simulations have supplied data for all the IGCC-based plants, ii) the hot gas desulfurization kinetic model is applied to the CACHET-II membrane investigation, iii) the hydrogen fuelled GT model have given input for all the overall plant cases.

All the analyses have been carried out using several software: the overall integration and the single process simulations were developed with the proprietary code GS or the commercial tool Aspen Plus whilst the single model simulations are based on brand new code written in Aspen Custom Modeler (gasification reactor) or in Matlab (Hot gas clean up). Finally, overall economic evaluation is based on excel VBA with calculation of the Levelized Cost of Electricity according to the IEA method.

RESULTS

A Reduced Order Model (ROM) was developed in order to predict the performance of the Shell-Prenflo gasifier. As result of the Shell ROM modeling, several parameters were calculated for a gasifier of about 3000 tons per day, for example: i) syngas, particles and gasifier wall temperature, ii) syngas and particle composition and iii) overall gasification temperature and pressure. The ROM predicts quite accurately the syngas conditions at the scrubber outlet; the simulation of the quench mixing resulted to be the main source of difference with the actual process. The equilibrium simulation results are accurate when given gasifier compositions are available for tuning. The CGE predicted by both the ROM and the equilibrium modes are close to the Shell value; additionally, the ROM can be applied to a variety of coal or with different operating conditions. Sensitivity analyses were used to further investigate effects of main variables: i) oxygen to coal ratio, ii) coal feed amount and iii) CO_2 feed as carrier gas.

A kinetic model of hot gas desulfurization based on zinc sorbents was developed to design the reactor at different operating conditions and estimating its cost. The process is based on fluidized beds: the desulfurizer is a fast fluidized bed while the regenerator is a bubbling fluidized bed. The model has in input the system conditions which are defined by the gasification technology adopted and the desulfurization level to be achieved. The model was then adapted to the Cu-based sorbent developed by Sintef and applied to membrane integration in IGCC.

Hydrogen fuelled gas turbine was investigated, comparing premixed vs. diffusive flame combustor. With respect to natural gas, hydrogen combustion causes a variation of the flame properties, mainly temperature, speed and geometry and a higher water concentration in the product gases. All these variations, along with the change of the fuel flow rate due to a change in the LVH, bring about a modification of the machine design specifications. One of the main concerns is limiting the NO_X emissions provided that: i) lean premixed combustors used with natural gas, at present are not commercially available for hydrogen because of technical hurdles posed by the very high reactivity of hydrogen; ii) the flame temperature of hydrogen is significantly higher than natural gas. The analysis showed that:

- In order to achieve STFT=2200K, the diluent to hydrogen ratio must be equal to 7.6 and 16 for steam and nitrogen dilution respectively.
- Dilution always negatively affects the combined cycle efficiency: the higher the diluent to hydrogen ratio the lower the CC efficiency. Comparing the two diffusive flame cases, nitrogen always achieves higher efficiency than steam at equal stoichiometric flame temperature.
- The CC efficiency penalty due to inert dilution is limited as far as the TIT and the blade metal temperature are kept at the nominal values. A decrease of the allowed blade metal temperature reflects into a twice reduction of the TIT with a noticeable efficiency decay.
- The efficiency of the simple cycle GT engine is remarkably affected by an increase of the pressure drop in the combustor. However, because of the simultaneous TOT increase, the efficiency decay of the CC is much less sensible. On other hand, at fixed expander geometry and compressor pressure ratio, the combustor pressure drop causes a significant mass flow rate decrease which results in a proportional reduction of the power output.

The previous analyses (gasifier, desulfurization and hydrogen gas turbine) have been then adopted to simulate SEWGS and membranes cases.

Several sensitivity analyses were carried out in order to assess the best techno-economic plant configurations. CO_2 purity, reactor CCR, purge pressure, size and quantity of vessels and cycle time were investigated in the SEWGS integrations. On the other hand, hydrogen recovery factor, feed pressure, use of the separated hydrogen and gasifier lock hopper system were considered for the membrane based plants.

Table 1and Table 2 show an overview the thermodynamic and economic results for all the best cases in term of CO_2 capture cost.

SEWGS technology has shown good thermodynamic in all the investigated configurations. In NGCC the SEWGS allows limiting the efficiency penalty compared to the reference technologies, the minimum SPECCA is about 2.5 MJ/kg_{CO2}. In IGCC application SEWGS stands out thanks to: i) the simultaneous H_2S-CO_2 capture, ii) the low steam demand for sorbent regeneration and iii) the decrease of the equipment number. The achieved net electric efficiency is between 38% and 39% with CO_2 avoidance between 96% and 86% respectively. The resulting SPECCA is about 2.5 MJ/kg_{CO2}, which is considerable lower than reference IGCC with capture via Selexol (3.7 MJ/kg_{CO2}) and ASC with amine scrubbing (4.2 MJ/kg_{CO2}). SPECCA can be reduced down to 2.0 MJ/kg_{CO2} with the new improved sorbent. Considering the blast furnace application it was found that SEWGS reaches good performances with around 85% CO_2 avoidance.

From thermodynamic point of view, hydrogen membranes are a promising solution for CO_2 capture plant in IGCC plants. The computed efficiency and SPECCA are very high in each developed configuration. Carbon capture avoided ranges between 85-95% depending on the feeding technology and the efficiency of the purification process. Provided the good thermodynamic performances, the membrane area become the most effective evaluating parameters. It was found that membrane area features huge variations depending on the type of membrane and the operating conditions adopted. Pd-alloy membrane does not harness its sulfur

tolerance in conventional Selexol process. Both in nitrogen- or CO_2-based gasifier, the pure Pd membrane requires low HRF and high feed pressure in order to limit as much as possible the surface. The new configuration developed with post-firing results to be the most promising because of the higher efficiency and lower membrane area. Pd-alloy and HGD is a promising solution for long-term application but more R&D is required. Finally, CO_2-based gasifier can be an innovative solution, most of all if combined with HRSG post-firing as for the nitrogen case.

From an economic point of view, the application of SEWGS to NGCC does not show evident advantages compared to commercial ready technology. On the other hand, SEWGS application to IGCC leads to a substantial decrease in the cost of CO_2 avoided, in the order of 35%. The cost of CO_2 avoided approaches 20 €/ton_{CO2} values when advanced sorbent is considered.

Concerning hydrogen membrane application to IGCC, the cost of CO_2 avoided is not competitive as far as all the hydrogen is produced and sent to the gas turbine. Nevertheless, the cost of CO_2 avoided decreases below the reference technology at about 30 €/ton_{CO2} when advanced layout is considered.

Table 1: main thermodynamic end economic values for all the natural gas-based plant investigated.

	Reference NGCC			SEWGS	
	No cap	MEA Cap	MDEA Cap	α	β
Net Electric Efficiency $_{LHV}$, %	58.34	49.9	50.3	51.1	51.9
SPECCA, MJLHV/kg_{CO2}	N/A	3.36	3.07	2.88	2.51
Specific costs, €/kW	630.4	969.9	1280.6	1168.1	1072
COE, €/MWh	54.1	69.1	74.6	72.8	69.9
Cost of CO_2 avoided €/t_{CO2}	N/A	47.5	63.8	58.4	49

Table 2: main thermodynamic end economic values for all the coal-based plant investigated.

	Reference		SEWGS		Pd-membrane			
COAL	No Cap	Cap	α	β	base N_2	N_2 PF	HGD	Base CO_2
Net Electric Efficiency$_{LHV}$, %	47.12	36.0	39.3	39.8	39.0	39.1	40.2	39.2
SPECCA, MJ_{LHV}/kg_{CO2}	N/A	3.71	2.39	2.07	2.52	2.49	2.18	2.19
Specific costs, €/kW	2093	2881	2743	2599	3309	2918	3079	3434
COE, €/MWh	66.32	89.6	85.8	82.3	96.6	87.7	90.7	99.2
Cost of CO_2 avoided, €/t_{CO2}	N/A	36.7	30.6	23.5	48.3	33.9	40.1	46.2

1 MOTIVATIONS OF THE STUDY

1.1 INTRODUCTION TO CLIMATE CHANGE

The increasing energy demand in recent years has been satisfied by fossil fuels leading to a rising concentration of carbon dioxide in the atmosphere. Monitoring has shown that the amount of CO_2 is approaching 400 ppm comparing to pre-industrial levels of 280 ppm [1].

According to the IPCC [1] (Intergovernmental Panel on Climate Change) there is strong evidence that most of the global warming observed over the past 50 years is attributable to GreenHouse Gas (GHG) emissions, whose largest contribution is by far carbon dioxide. The IPCC estimated that by 2100, the increase in global average temperature could range between 1.1-6.4 °C depending on the level of greenhouse gas emission during this century. Recent studies confirm that an increase of 6°C will be very likely achieved [2]. Energy-related CO_2 emissions account for about 60% of the total global anthropogenic GHG emissions [3]. Domestic transport contributes to almost the remaining part.

Figure 1-1 shows the world CO_2 emissions from 1971 to 2010 by fuel type; there is a clear constant increase due to the growth of the world primary energy consumption. The largest global source of fossil fuel emissions comes from coal-fired power plant. Simultaneously, the adoption of coal as fuel for electricity production becomes more and more strategic because of its lower price and well-established and spread reservoirs compared to oil and natural gas.

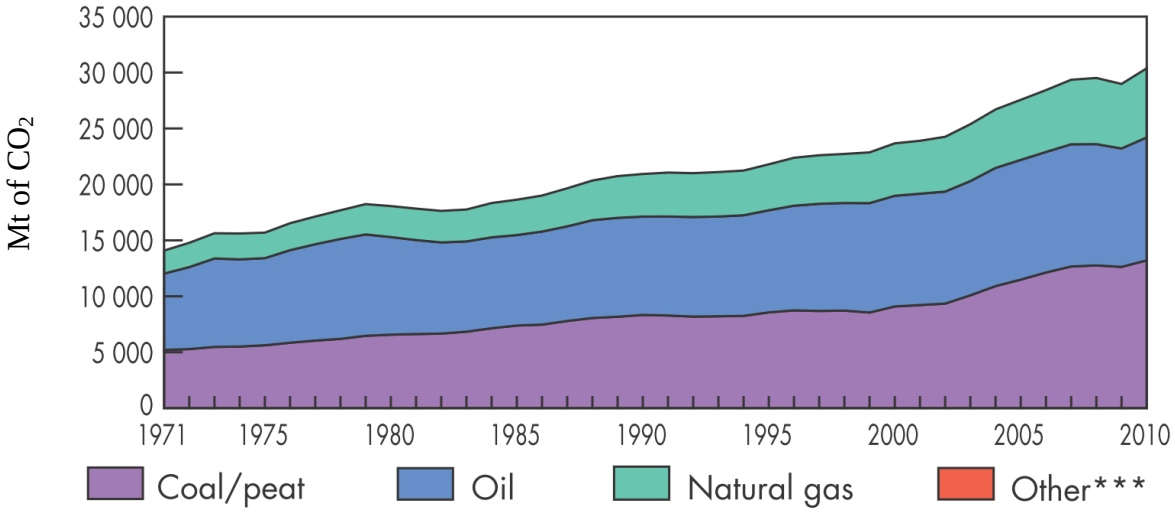

Figure 1-1: world CO_2 emissions from 1971 to 2010 by fuel [4].

1.2 OPTIONS FOR MITIGATING CLIMATE CHANGE

The future economic development policies may impact greenhouse gas emissions as strongly as policies and technologies especially developed to address climate change. The major factors influencing the CO_2 emissions from the supply and use of energy are summarized in the identity:

$$CO_2 emissions = Population \times \left(\frac{GDP}{Population}\right) \times \left(\frac{Energy}{GDP}\right) \times \left(\frac{Emissions}{Energy}\right)$$

This shows that the level of CO_2 emissions depend directly on the size of the human population, on the level of global wealth, on the energy intensity of the global economy, and on the emissions arising from the production and use of energy. At present, the population continues to rise and average energy use is also rising, whilst the amount of energy required per unit of GDP is falling in many countries, but slowly [1]. So achieving deep reductions in emissions will, all other aspects remaining constant, require major changes in the third and fourth factors in this equation.

There is a wide variety of technological options to reduce net CO_2 emissions:

- Reducing energy consumption improving the efficiency of energy conversion, transport and end-use, enhancing less energy intensive economic activities;
- Switching to less carbon-intensive fossil fuels, for example NG instead of coal;
- Increasing use of low- and near-zero-carbon energy sources as renewable energies (wind, solar, biomass, hydro, geothermal, tidal power) or nuclear energy;
- Sequestering CO_2 by enhancing biological absorption capacity in forest and soils;
- Capturing and storing CO_2 chemically or physically.

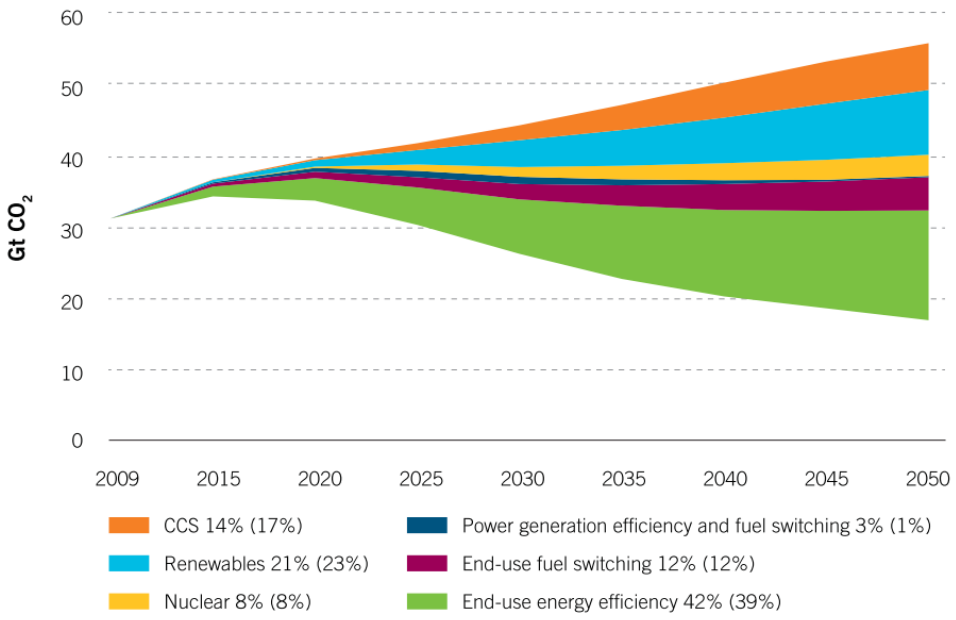

Figure 1-2: Energy-related CO_2 emission reductions by technology. Percentages represent share of cumulative emissions reduction to 2050. Percentages in brackets represent share of emissions reductions in the year 2050. Source: [3] [5].

As shown in Figure 1-2, capturing CO_2 accounts for a large GHG reduction; indeed it is one of the most recognized technologies to limit the impact of fossil fuel on the environment [6] [7].

CO_2 capture can be hardly applied to small distributed sources while suits well in large industrial applications or power generation units. Consistently, CCS is investigated only in the latter cases. Figure 1-3 reports the current CCS project deployment: 16 out of 75 projects are currently operating or in construction with a combined capture capacity of around 36 million tonnes per annum [3]. During the past years there has been a slow but steadily increase of projects.

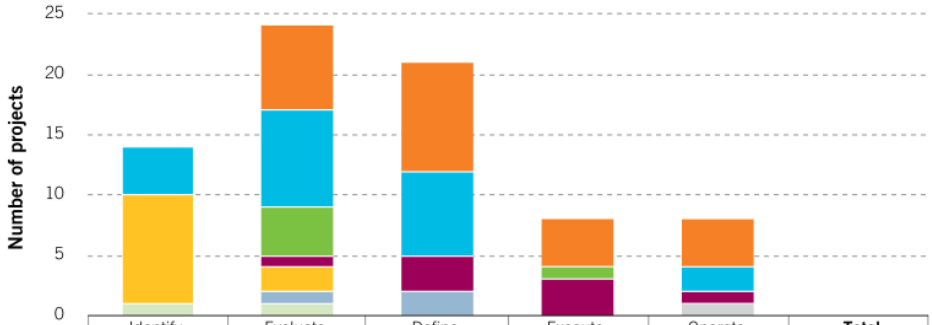

	Identify	Evaluate	Define	Execute	Operate	Total
United States	0	7	9	4	4	**24**
Europe	4	8	7	0	2	**21**
Australia and New Zealand	0	4	0	1	0	**5**
Canada	0	1	3	3	1	**8**
China	9	2	0	0	0	**11**
Middle East	0	1	2	0	0	**3**
Other Asia	1	1	0	0	0	**2**
Africa	0	0	0	0	1	**1**
Total	**14**	**24**	**21**	**8**	**8**	**75**

Figure 1-3: overview of large-scale integrated CCS projects. Source: [3].

There are three main routes for CO_2 capture in large fossil fuel plants: i) post-combustion CO_2 capture, ii) oxy-combustion and iii) pre-combustion decarbonisation. The first category is based on capturing CO_2 in the exhaust gases via chemical or physical absorption of CO_2: amine scrubbing [8] [9] is the state-of-the-art, while chilled-ammonia [10] or even fuel cells like molten carbonate [11] [12] can be considered as advanced solutions.

Oxy-combustion separation consists of a close-to-stoichiometric oxygen combustion: the main products are a mixture of CO_2 and steam which can be easily separated for gravity, even if CO_2 purity constraints requires additional processing to get rid of the excess O_2. The last category is pre-combustion decarbonisation which implies the energy transfer from methane or syngas to hydrogen; hydrogen can then be used as a fuel in a combined cycle, without any CO_2 emission.

This work aims at assess the potentialities of two advanced pre-combustion capture technologies.

REFERENCES

[1] **IPCC.** *Carbon Dioxide Capture and Storage.* s.l. : Cambridge Unversity Press, 2005.

[2] **IEA.** World Energy Outlook . 2011.

[3] **Global CCS Institute.** The Global Status of CCS 2012.

[4] **IEA.** 2012 Key World Energy Statistics. 2012.

[5] —. Summing up the parts: Combining policy instruments for least-cost climate mitigation strategies. *Information Paper.* 2011.

[6] **DOE.** *Carbon Sequestration Technology Roadmap and Program Plan.* s.l. : US department of Energy, 2007.

[7] **International Energy Agency.** *CO2 capture and storage - A Key Carbon Abatement Option.* 2008. ISBN 978-92-64-041400.

[8] **Wang M, Lawal A, Stephenson P, Sidders J, Ramshaw C.** Post-combustion CO2 capture with chemical absorption: A state-of-the-art review. *2011.* s.l. : Chemical Engineering Research and Design . Vol. 89. 1609-1624.

[9] **Rao AB, Rubin ES.** A technical economic and environmental assessment of amine-based CO2 capture technology for power plant greenhouse gas control. s.l. : Enviornmental technology, 2002. Vol. 36. 4467-4475.

[10] **Valenti G, Bonalumi D, Macchi E.** A parametric investigation of the Chilled Ammonia Process from energy and economic perspectives. s.l. : Fuels, In press 2011. dx.doi.org/10.1016/j.fuel.2011.06.035.

[11] **Chiesa P, Campanari S, Manzolini G.** CO2 cryogenic separation from combined cycle integrated with molten carbonate fuel cells. s.l. : Internatonal Journal of Hydrogen Energy . Vols. 2011, In press. DOI: 10.1016/j.ijhydene.2010.09.068.

[12] **Campanari S, Chiesa P, Manzolini G.** CO2 capture from combined cycles integrated with Molten carbonate Fuel Cells. s.l. : International Journal of Greenhouse Gas Control, 2010. Vol. 4, 3. 441-451.

2. METHODOLOGY AND SIMULATION TOOLS

Nomenclature and Acronyms

ACM: Aspen Custom Modeler
CACHET: CArbon Capture and Hydrogen production with membranes
CAESAR:CArbon-free Electricity by SEWGS: Advanced Materials, Reactor and process design
CCS: Carbon Capture and Storage
GT: Gas Turbine
HGCU: Hot Gas Clean Up
SEWGS: Sorption Enhanced Water Gas Shift
WP: Work Package

The final goal of the PhD research activity was the techno-economic assessment of fossil fuelled power plants with carbon capture by two different innovative technologies: one based on advanced sorbents (Sorption Enhanced Water Gas Shift) and one based on membranes (hydrogen selective membranes). Both the technologies were developed in two FP7 projects: CAESAR and CACHET-II. Therefore, the agenda and the tasks required for the investigation were defined according to the projects development. The PhD work was exclusively theoretical but with input from experiments carried out by the projects partners (ECN, SINTEF, Air Product).

Briefly, the features of both the considered technologies are:

- **Sorption Enhanced Water Gas Shift**: SEWGS comprises of multiple fixed beds operating in parallel that adsorb CO_2 at high temperature and pressure, and release it at low pressure. The combination of CO_2 conversion and removal enhances H_2 production and the purity of the stream feeding the Gas Turbine combustor, whilst a separate CO_2 by-product can be recovered from the adsorbent by regenerating the bed. The SEWGS technology has been recently developed and neither process integration nor economic assessments are available in literature. In this work, SEWGS application to natural gas, coal and steelworks plant are presented.
- **Hydrogen membranes**: hydrogen permeable membranes are an attractive technology for pre-combustion carbon capture in both coal and gas fired power stations because they combine the simultaneous production and separation of hydrogen while capturing the remaining carbon dioxide. The carbon dioxide is produced at high pressure, reducing the compression energy for transport and storage. Despite this technology is extensively studied, there are no detailed works in literature which links together experimental results, membrane module design, plant integration and economic evaluation. In this work hydrogen membrane application to coal plant is presented

The PhD work aimed at investigating both the technologies, supplying the evaluations not yet available in literature and previously mentioned. The analyses were carried out developing the best plant configurations both from thermodynamic and economic point of view.

When CO_2 pre-combustion capture is applied to power production plant, the resulting system becomes a hybrid between chemical and power station. In fact, as in chemical workshop, the

layout complexity features a large number of reactor and streams linked together. In addition, the plant will have to work with all the constraints set by a common power plant and following the electrical system load. From a simulation point of view, such a type of plant requires a comprehensive approach which moves from detailed physical phenomena inside a specific reactor up to an overall view of the plant.

In order to fulfill this requirement, in the present work different levels of analysis were considered.

1. **Detailed reactor model**: it aims at reproducing the behavior of the most critical reactors involving detailed chemical kinetic mechanisms. Due to the high level of details and the required implementation time, only two different reactors have been investigated using this model approach: i) the coal gasifier and ii) the hot gas clean-up system. The first one is the most important reactor in coal gasification plant whilst the second one is critical for limiting the penalization of desulfurization process. Both the components work in two/three phase conditions and the kinetic approach is mandatory to correctly predict the performances or the design. It must be remarked that the detailed modeling of the SEWGS and the H_2 membranes was performed by other partners inside the project consortium (SEWGS: Air Product; Membranes: SINTEF). Chapter 4 and 5 are dedicated to the Shell kinetic model and hot gas desulfurization, respectively.
2. **Specific process model**: it is focused on the most important processes adopted in a defined configuration; this simulation involves only the required physical phenomena. Single system model has been adopted to reproduce the behavior of hydrogen fuelled gas turbine and the Shell coal gasification process. The latter is briefly reported together with the Shell kinetic model. Chapter 6 is dedicated to hydrogen GT simulations.
3. **Overall techno-economic plant simulation**: the thermodynamic evaluation is based on mass and energy balances and it allows integrating all the component required for power production with CCS. All the data obtained in the single reactor and process modeling are implemented in this step. Chapter 7 and 8 report the thermodynamic analysis of SEWGS and hydrogen membranes respectively. Economics of the two technologies are reported in chapter 9.

The results obtained in the single reactor and system modeling are implemented in the overall plant simulations as shown in Figure 2-1. In particular: i) the coal gasification kinetic model as well as the IGCC process simulations have supplied data for all the IGCC-based plants, ii) the hot gas desulfurization kinetic model is applied to the CACHET-II membrane investigation, iii) the hydrogen fuelled GT model have given input for all the overall plant cases.

The present manuscript is organized following the different simulation levels. Firstly both the detailed reactor models are introduced; then the investigation on hydrogen fuelled gas turbine is presented. Eventually, the overall techno-economic assessments are presented.

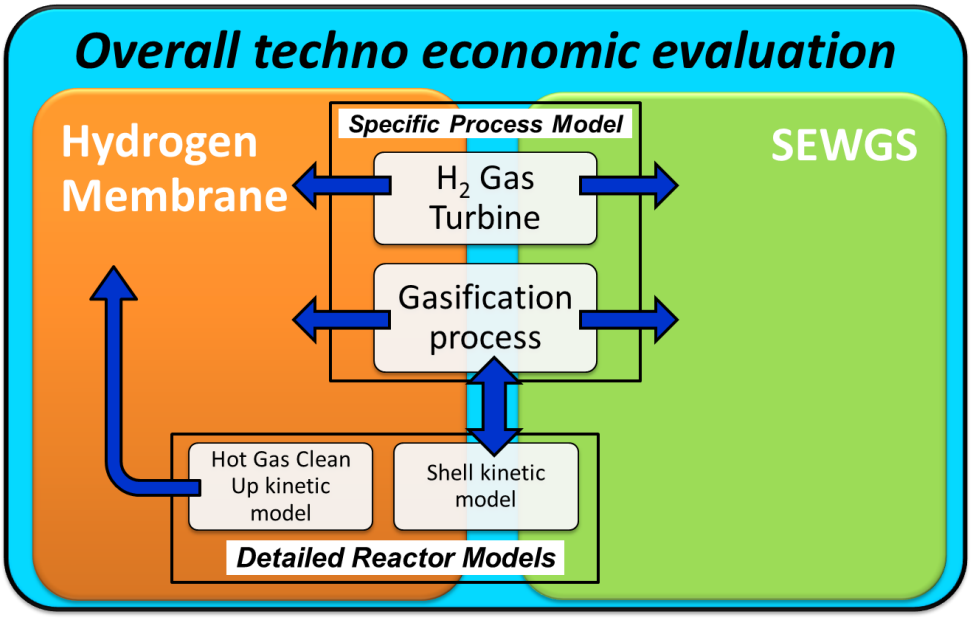

Figure 2-1: representation of the different simulation levels considered in the PhD work, with emphasis on data exchange between the several sections. The specific process models provide information to both the overall techno-economic evaluation as well the shell kinetic model; the HGCU model is applied only in membrane assessment.

2.1 Addressing the Critical Technologies

In pre-combustion capture plant different technologies can be identified as the most critical, mainly depending on the fossil fuel input.

Certainly, the CO_2 separation technology is the first process which must be adequately investigated: both the SEWGS and hydrogen membranes are advanced concepts which require a dedicated simulation. Experimental and theoretical investigations have been largely addressed during the collaborative European projects by other team partners. Therefore, in this work no dedicated tools have been implemented for the SEWGS or hydrogen membranes but results from other Work Packages have been used to assess the performance and reproduce the mass&energy balances.

Considering a coal fed power plant, the gasifier reactor is the component which mainly affects the plant performance and availability. Another critical technology is by far the sulfur removal process, most of all when the CO_2 capture system is not sulfur tolerant.

Moving to the natural gas fed plant, the fuel conversion system is once again a critical process which affects the overall performances.

Finally, both in coal and natural gas fuelled plants, running the gas turbine with hydrogen rich stream represent a critical issue which must be carefully investigated.

Table 2-1: critical technologies for pre-combustion CO_2 capture by SEWGS and membranes in coal and natural gas fed plants. In green the technologies developed using the detail reactor model, in light violet using the single process model and in orange adopting the overall system model.

	Pre-combustion CCS	
	H_2 Membrane	**SEWGS**
Coal fuelled power plant	Gasifier reactor	
	Gas desulfurization	--
	Hydrogen fuelled gas turbine	
	Membrane CO_2 separation	SEWGS CO_2 separation
Natural Gas fuelled power plant	Autothermal reforming	
	Hydrogen fuelled gas turbine	
	Membrane CO_2 separation	SEWGS CO_2 separation

It can be noted from Table 2-1 that the PhD work covers well the critical issues which should be addressed when applying hydrogen membrane and SEWGS process.

Finally, the modeling approach implemented in this work is shown in Figure 2-2: the different analysis levels are strictly linked together and information are continuously gathered among the three. For example, the Shell gasification process supply the mass balance to the kinetic model which, on the other hand, predicts the data required to calibrate the overall analysis. When modifications to the reference technology are implemented (see CO_2 feed in chapter 8) the data flows the other way round, starting from kinetic to process to overall assessment. Thanks to this information cycle, the PhD investigation became very flexible.

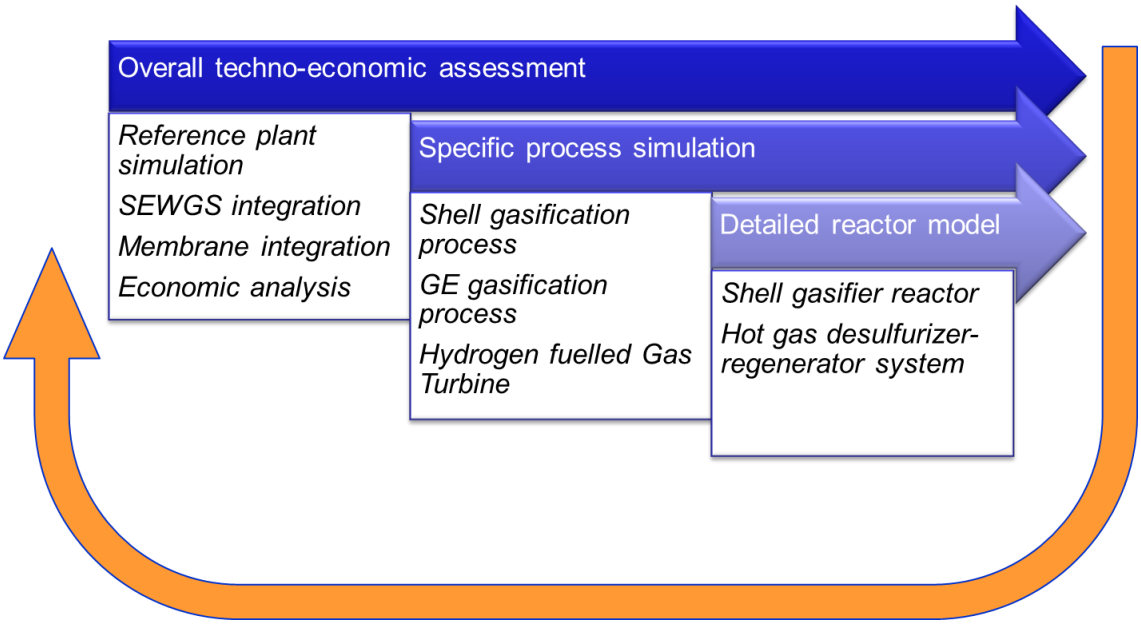

Figure 2-2: data flow among overall techno-economic assessment, specific process simulation and detailed reactor model.

2.2 SIMULATION TOOLS

2.2.1 GS

Mass and energy balances have been estimated by a proprietary computer code (GS) developed by the GECoS group at the Department of Energy of the Politecnico di Milano to assess the performance of gas/steam cycles [1], CO_2 capture systems, as well as a variety of other plant options, including IGCC, membranes, etc. [2] [3] [4]. The plant scheme is reproduced by assembling in a coherent network the different components selected in a library containing over 20 basic modules, whose models have been previously implemented. Built-in rules for efficiency prediction of turbomachines (gas and steam turbine, compressors), as a function of their operating conditions, as well as built-in correlations for predicting gas turbine cooling flows allow the code to generate very accurate estimations of combined cycles performance, even for off-design conditions [5]. The gas turbine model in GS is calibrated to correctly predict the performance of advanced gas turbines, accounting for all the relevant phenomena occurring fluid-dynamic losses, cooling circuit performance, changes in gas turbine fuel and working fluid composition.

Input parameters and equations governing mass and energy balances vary with the type of component. The heat exchanger and the mixer allow for the variation of the chemical composition of input flows until chemical equilibrium is reached according to Gibbs free energy minimisation. The combustor always assumes complete oxidation of the fuel. The cooled expansion that takes place in modern gas turbines is based on simplified machine design as extensively explained in chapter 6. The heat recovery steam cycle includes the heat recovery steam generator (which can have up to three pressures levels and reheat), the steam turbine, the condenser, the feedwater heaters, the feedwater pump, etc.

Once the system to be calculated is been defined and the coherence of the component characteristics and their interconnections are verified, the code sequentially calculates mass, energy and atomic species balances of all plant components until convergence is reached. Convergence is reached when both the following conditions are verified: i) mass flow rate, temperature and pressure difference of each stream between two successive iterations differs less than 0.01% and ii) mass and energy balance of each component is respected with a maximum error of 0.005%.

Ideal behavior is assumed for all mixtures; thermodynamic properties are calculated by means of NASA polynomials.

2.2.2 ASPEN PLUS®

Aspen Plus® was extensively adopted to simulate the chemical process where ideal gas law cannot be assumed. The considered process are: MEA CO_2 separation, MDEA CO_2 separation, CO_2 compression, cryogenic purification and Rectisol AGR.

2.2.3 ASPEN CUSTOM MODELER®

Aspen Custom Modeler can be adopted to '*quickly create rigorous models of processing equipment and to apply these equipment models to simulate and optimize continuous, batch, and semi-batch processes. It is used across many industries, including chemicals, power, nuclear, food and beverage, metals and minerals, pharmaceuticals, and consumer goods. Aspen Customer Modeler is a core element of AspenTech's aspenONE® Engineering applications*' [6]. Aspen Custom Modeler is the core software for the kinetic simulation of the Shell gasifier reported in chapter 4.

2.2.4 MATLAB®

The Hot Gas Desulfurization algorithm have been implemented in Matlab®.

2.3 IMPORTANT NOTE TO THIS MANUSCRIPT

The present manuscript should not be regarded as a paper collection of the PhD period. Nevertheless, this work is strongly based on different papers either already published or soon available in international journals and conference proceedings. The link between chapter and papers is the following:

Chapter 3:

- Manzolini G, Macchi E, Binotti M, Gazzani M: *Integration of SEWGS for carbon capture in Natural Gas Combined Cycle. Part B: Reference case comparison*. International Journal of Greenhouse Gas Control 2011;5:214-25. DOI: 10.1016/j.ijggc.2010.08.007
- Gazzani M, Macchi E, Manzolini G: *CAESAR: SEWGS Integration in an IGCC plant.* 10th International Conference on Greenhouse Gas Control Technologies, Amsterdam, September 19-23 2010

Chapter 4:

- Gazzani M, Manzolini G, Macchi E, Ghoniem A.F: *Reduced order modeling of the Shell-Prenflo entrained flow gasifier*. Fuel 2012. DOI: 10.1016/j.fuel.2012.06.117

Chapter 6

- Gazzani M, Chiesa P, Martelli E, Sigali S, Brunetti I*: Using Hydrogen as Gas Turbine Fuel: Premixed versus Diffusive Combustors* ASME Turboexpo 2013, San Antonio 3-7 June.

Chapter 7

- Gazzani M, Macchi E, Manzolini G: *CO_2 capture in natural gas combined cycle with SEWGS. Part A: Thermodynamic performances*. International Journal of Greenhouse Gas Control 2012. DOI: 10.1016/j.ijggc.2012.06.010
- Gazzani M, Macchi E, Manzolini G: *CO_2 capture in Integrated Gasification Combined Cycle with SEWGS - Part A: Thermodynamic performances*. Fuel 2012. DOI: 10.1016/j.fuel.2012.07.048
- Gazzani M, Romano M, Manzolini G: *Application of Sorption Enhanced Water Gas Shift for Carbon Capture in Integrated Steelworks* 11th International Conference on Greenhouse Gas Control Technologies, Kyoto, November 19-23 2012

- Gazzani M, Romano M, Manzolini G, Arcara G: *Application of SEWGS process for CO_2 capture and power generation from blast furnace gas* Tenth Annual Conference on Carbon Capture and Sequestration, Pittsburgh May 2-5 2011

Chapter 8

- Manzolini G, Gazzani M, Turi DM, Macchi E: *Application of hydrogen selective membranes to IGCC*. 11th International Conference on Greenhouse Gas Control Technologies, Kyoto, November 19-23 2012

Chapter 9

- Manzolini G, Macchi E, Gazzani M: *CO_2 capture in natural gas combined cycle with SEWGS. Part B: Economic assessment*. International Journal of Greenhouse Gas Control 2012. DOI**:** 10.1016/j.ijggc.2012.06.021
- Manzolini G, Macchi E, Gazzani M: *CO_2 capture in Integrated Gasification Combined Cycle with SEWGS - Part B: Economic assessment*. Fuel 2012. DOI**:** 10.1016/j.fuel.2012.07.043
- Manzolini G, Gazzani M, Turi DM, Macchi E: *Application of hydrogen selective membranes to IGCC*. 11th International Conference on Greenhouse Gas Control Technologies, Kyoto, November 19-23 2012

REFERENCES

[1] **Politecnico di Milano.** Software presentation: GS (Gas-Steam Cycles). *http://www.gecos.polimi.it/software/gs.html.* [Online] 2009.

[2] **Consonni S, Lozza G, Macchi E, Chiesa P, Bombarda P.** Gas turbine-based cycles for power generation. Part A: calculation model. 1991.

[3] **Lozza, G.** Bottoming steam cycles for combined gas-steam power plants: a theoretical estimation of steam turbine performance and cycle analysis. New Orleans, USA : ASME Cogen-Turbo, 1990.

[4] **Manzolini G, Dijkstra JW, Macchi E, Jansen D.** Technical Economic Evaluation of a system for electricity production with CO2 capture using membrane reformer with permeate side combustion. 2006.

[5] **Chiesa P, Macchi E.** A thermodynamic analysis of different options to break 60% electric efficiency in combined cycle power plants. 2004, Vol. 126, 770-785.

[6] **Tech, Aspen.** http://www.aspentech.com/products/aspen-custom-modeler.aspx. [Online]

3 GENERAL ASSUMPTIONS AND REFERENCE POWER PLANTS

Nomenclature and Acronyms

ASC: Advanced Supercritical Plant
ASU: Air Separation Unit
ATR: Autothermal Reformer
EBTF: European Benchmark Task Force
GHR: Gas Heated Reformer
HHV: High Heating Value
HR: Heat Rate
HRSC: Heat Recovery Steam Cycle
HRSG: Heat Recovery Steam Generator
HTS: High Temperature Shift
IGCC: Integrated Gas Combined Cycle
LHV: Low Heating Value
LTS: Low Temperature Shift
MDEA: N-Methyldiethanolamine
MEA: Monoethanolamine
NG: Natural Gas
NGCC: Natural Gas Combined Cycle
SPECCA: Specific Primary Energy Consumption for CO_2 Avoided
TIT: Turbine Inlet Temperature
TOP: Turbine Outlet Pressure
TOT: Turbine Outlet Temperature
WGS: Water Gas Shift

3.1 EBTF ACTION

This chapter presents three study cases of reference power plants without and with CO_2 capture. The final goal is to develop comprehensive cases which are adopted to evaluate the innovative capture technologies presented in the following chapters. The three reference cases are: i) an Advanced Supercritical Pulverized Coal plant, ii) an Integrated Gasification Combined Cycle and iii) a Natural Gas Combined Cycle. For each case, a general description of the case is presented, followed by the specifications of the process streams, operational characteristics and operational performance. As aforesaid, all the new plants are then compared to the performance of these three cases.

All performance data presented refer to plants operating at nominal base-load, *"new and clean"* conditions. For all considered cases, the energy cost related to CO_2 capture is given by the Specific Primary Energy Consumption for CO_2 Avoided (SPECCA), which is defined as:

$$SPECCA = \frac{HR - HR_{REF}}{E_{REF} - E} = \frac{3600 \cdot \left(\frac{1}{\eta} - \frac{1}{\eta_{REF}} \right)}{E_{REF} - E}$$

Where:

- HR is the heat rate of the plants, expressed in kJ_{LHV}/kWh_{el}
- E is the CO_2 emission rate, expressed in kg_{CO2}/kWh_{el}
- η is the net electrical efficiency of the plants
- $_{REF}$ refers to the value found for the same plant without CCS.

The contents of this chapter partially follow the work carried out for the European Benchmark Task Force (EBTF) [1]: a team of members of three FP7 european projects (CAESAR, CESAR and DECARBIT) jointly established the performances and the assumptions

of the abovementioned reference case. All cases were thoroughly discussed within the EBTF so that every effort was made to ensure that the results reflect, as much as possible, the views of the European community of carbon capture researchers.

For two out of the three study cases without CO_2 capture, i.e. the Advanced Super-Critical 800 MW steam power plant and the Natural Gas Combined Cycle 834 MWe power plant, their calculations reproduce the actual performance of a large number of existing state-of-the-art power plants. Hence the calculated net electric efficiency and specific power are fully consistent with values reached by the major plant manufacturers. A completely different situation occurs for the Integrated Gasification Combined Cycle study case: the EBTF calculations depict a power generation technology based on the theoretical performance of a large number of state-of-the-art components. This technology is not yet applied in several large-scale plants which could validate the presented results. A similar situation occurs for the three capture study cases: presently, only small-scale pilot plants have been built.

3.2 GENERAL ASSUMPTIONS

3.2.1 AMBIENT CONDITIONS AND FUEL COMPOSITIONS

Air, ambient conditions, natural gas features and coal analysis are reported in Table 3-1, Table 3-2 and

Table 3-3.

The characteristics of the fuel are fundamental in energy and mass balance calculations and in the definition of processes such as gasification, gas reforming, gas cleaning and combustion. Even though the fuel composition and conditions strongly affect efficiency and economic results, this work is based on one gaseous (NG) and one solid (coal) fuel type. In fact, this allows consistently comparing several different plants, showing positive and negative features. Nevertheless, when evaluating two different technologies, for example one sulfur not tolerant and one not sulfur tolerant, the different fuel can lead to completely different scenario.

Table 3-1: air and ambient conditions

Air conditions	
Ambient conditions:	
T_{ISO}, °C	15.0
P_{ISO}, bar	1.013
Relative Humidity, %	60.0
Air composition, dry molar fraction, %	N_2 78.08%, CO_2 0.04%, Ar 0.93%, O_2 20.95%

Table 3-2: natural gas properties

Natural Gas features and composition	
T, °C	10.0
P, bar	70.0
HHV, MJ/kg	46.502
LHV, MJ/kg	51.473
NG, dry molar fraction, %	CH_4 89.00, C_2H_6 7.00, C_3H_8 1.00, C4-i 0.05, C4-n 0.05, C5-i 0.005, C5-n 0.004, CO_2 2.00, $N_2$0.89, S< 5 ppm

Table 3-3: properties of a typical Douglas Premium coal; proximate, ultimate and ash analyses

Proximate Analysis [%]		Ash Analysis [%]	
Moisture	8.00	SiO_2	45
Ash	14.15	Al_2O_3	30
Volatiles	22.90	Fe_2O_3	3
Fixed Carbon	54.90	CaO	7.5
Total Sulphur	0.52	MgO	1.2
		TiO_2	2
Ultimate Analysis [%]		K_2O	0.4
Carbon	66.52	Na_2O	0.2
Hydrogen	3.78	SO_3	3.5
Nitrogen	1.56	P_2O_5	2
Total Sulphur	0.52		
Ash	14.15	Ash fushion temperature	°C
Chlorine	0.009	Initial deformation	1340
Moisture	8.00	Softening	1380
Oxygen (by difference)	5.46	Hemispherical	1400
		Flow	1430
HHV, MJ/kg	26.230		
LHV, MJ/kg	25.170		

3.2.2 GAS TURBINE

Certainly, the Gas Turbine simulation is the most critical in the power island section. The motivation is double folded: from one side the thermo-fluid-dynamic simulation is critical because of the complexity of the machine; on the other side, this technology is strictly guarded from the few existing manufacturers. Nonetheless, the in-house code GS introduced in chapter 2 allows rebuild the machine geometry starting from few calibration data: i) the machine net power, ii) the compressor ratio, iii) the turbine outlet temperature and, iv) the gas turbine gross efficiency. The gas turbine model in GS is then calibrated to correctly predict the performance of a given gas turbines, accounting for all the relevant phenomena: fluid-dynamic losses, cooling circuit performance, changes in gas turbine fuel and working fluid composition.

In this work, the gas turbine simulated is a generic 50 Hz "F Class" with a single combustor stage. Table 3-4 shows the assumptions and the results obtained.

Table 3-4: assumptions and results for the calibration of a generic F class gas turbine.

Gas Turbine assumptions		
	Iso Condition	
Pressure loss at inlet, kPa	1	
Pressure loss at outlet, kPa	1	
Pressure ratio	18.1	
Air flow rate, kg/s	650.0	
TIT, °C	1360	
Results	*Combined cycle*	*Simple cycle*
Specific work, kJ/kg	419.5	424.5
Net electric efficiency, %	38.33	38.51
Fuel flow rate, kg/s	15.30	
COT, °C	1443.3	
TOT, °C	608.0	603.5
TOP, bar	1.043	1.023
η_{Poly} (cooled stages)	92.15	
η_{Poly} (uncooled stages)	93.15	
Amount of cooling flow, kg/s	121.9	
% of cooling flow on air at comp inlet, %	17.7	
coolant 1st stage, kg/s	76.1	
coolant 2nd stage, kg/s	33.6	
coolant 3rd stage, kg/s	12.2	

As far as pre-combustion capture is concerned, another relevant issue arises considering the GT: the use of hydrogen mixtures instead of natural gas. In fact, butning hydrogen introduces different technology limitations and modifies the general fluid-dynamic behaviour of the machine. This issue is very important and chapter 6 is completely dedicated to better investigate the gas turbine behaviour when using hydrogen fuelled diffusive or premixed flame combustor.

Briefly, two different philosophies can be followed:

- The gas turbine design is fixed: the variations of cycle efficiency are compute when using hydrogen through an off-design investigation (not reengineered case).
- Reengineered gas turbine is assumed: the gas turbine performance is computed considering a design from scratch of the new machine.

All the calculations carried out in this work consider a re-engineered gas turbine.

3.2.3 STEAM CYCLE (STEAM TURBINE AND HRSG)

The steam cycle, contributing to more than one third of the total power, is a very important section of the plant. This is stressed in pre-combustion capture plant as there is the need of a tight integration between the fuel conversion island and the power block. Table 3-5 reports the assumptions adopted for all the steam cycle calculation in this work. The most important differences between the coal and natural gas cases are the HP and IP pressure levels which, as far as IGCC is concerned, must meet the gasifier pressure. Other options could be selected, e.g. standalone gasifier steam cycle, but the commercial applications are almost all based on linked

syngas cooler-HRSG. In all layouts the HRSG features a triple pressure, single reheat configuration; before being sent to the reheat section, the superheated IP steam and the cold steam from HP steam turbine are mixed. Natural circulation is considered inside the HRSG.

Table 3-5: operating conditions of the Heat Recovery Steam Cycle for NGCC and IGCC application

Steam Turbine	
Turbine isentropic efficiency, %	
HP	92
IP	94
LP	88
Pressure losses for steam extraction, %	
HP extraction pipe + preheater	3
LP extraction pipe + preheater	5
Heat Recovery Steam Cycle	
Steam evaporation pressures NGCC case, bar	130, 28, 4
Steam evaporation pressures IGCC case, bar	144, 54, 4
SH and RH temperature, °C	565
Pinch point ΔT, °C	10
Sub cooling ΔT, °C	5
Minimum ΔT in SH and RH, °C	25
Thermal losses, %LHV	0.7
Pressure losses, gas side, kPa	3
Pressure losses for each HRSG heat exchanger water side, %	3
Pressure losses reheat, total, %	10
Pressure losses steam-pipe valve, HP, IP, LP, %	7,9,12
Temperature losses from super/re-heater to turbine, kJ/kg	1
Condenser	
Natural draft tower – water cooled steam condenser	
Condensation pressure, bar	0.048 (32°C)
Pumps	
Efficiency, %	70

3.2.4 AIR SEPARATION UNIT

Air supplied to the Air Separation Unit may come from the compressor of the gas turbine, from an entirely independent compressor or part from the gas turbine and part from an independent compressor. So, 100% integration of the air separation process with the power plant means that all air supplied to the process comes from the compressor of the gas turbine. An integration of 0% means that all air comes from an entirely independent compressor. The present experience with power plants based on coal gasification recommends a maximum of 50% integration, on grounds of reliability and availability. So, for purposes of definition of base cycles, this is the value adopted [1].

Table 3-6: Air separation unit features and operating conditions

ASU	
Oxygen Purity	95%
Nitrogen Purity	99%
Oxygen temperature entering the gasifier	180 °C
Oxygen pressure entering the gasifier	48 bar
Oxygen and Nitrogen temperature leaving ASU	22 °C

3.2.5 WGS

Depending on the type of fuel considered, the shift process can be sulfur or not sulfur tolerant. All the cases based on natural gas adopt sulfur free catalyst which can be at high temperature (High Temperature Shift) or at low temperature (Low Temperature Shift). As far as coal is concerned, in all the SEWGS cases the WGS is sour whilst in all membrane cases the WGS is not sulfur tolerant.

Table 3-7: WGS operating conditions

WGS	
Steam / CO	1.9
Pressure loss, bar	0.5

3.2.6 GHR-ATR

The natural gas reforming process, as already introduced in Chapter 2, can be regarded as a critical technology for natural gas pre-combustion plants. This is because of the large exergy penalties arising when irreversible chemical reactions take place. Nontheless, this technology has already been installed in several plants and can be considered commercially available and proved. Therefore, in this work it is considered only from thermodynamic equilibrium point of view with the assessment of all the mass and energy streams involved.

The hydrocarbons steam reforming is a catalytic reaction described by the following equation:

$$C_nH_m + nH_2O \leftrightarrow nCO + (n + \frac{m}{2})H_2 \qquad (3\text{-}1)$$

This reaction is highly endothermic and is promoted at high temperatures (750°C-850°C) and low pressures. Nevertheless the process usually operates in intermediate pressure in order to reduce the reactor volumes and the temperature is further increased as much as possible. The reached conversion depends on the amount of steam available (Steam/C ratio) and on the catalyst activity.

The methane steam reforming, coherently with (3-1), is:

$$CH_4 + H_2O \leftrightarrow CO + 3H_2 \qquad (\Delta H°_{298K} = 206 \text{ kJ/mol}) \qquad (3\text{-}2)$$

At the same time other secondary reactions can lead to coke formation:

methane pyrolysis $CH_4 \leftrightarrow C + 2H_2$ (3-3)

carbon monoxide reduction $CO + H_2 \leftrightarrow C + 3H_2O$ (3-4)

Boudouard reaction $2CO_2 \leftrightarrow C + CO_2$ (3-5)

The pyrolysis reaction is not very significant in the steam reforming and it can be neglected. In order to avoid the catalyst poisoning it is important to work with operating conditions in which the carbon destruction speed is higher than the carbon formation speed. Increasing the S/C ratio the equilibrium of (3-4) moves left; the adoption of special catalyst promote the CO formation reducing the coke production.

The steam reforming reaction in the studied plants layout takes places into two different reactors: the Gas Heated Prereformer (GHR) and subsequently the Auto Thermal Reforming (ATR). Before entering the GHR-ATR, the desuphured NG is mixed with the steam required for the reactions.

The initial steam reforming stage is carried out passing the steam-hydrocarbon mixture through the GHR. The heat required for the reactions is provided by the gas exiting the ATR. Second law losses are reduced since energy is transferred at high temperature into the same stream flow.

The temperature of the flow entering the primary reformer is typically in the range 300-500°C, in the studied case this temperature has been set equal to 380°C. The primary reforming catalyst may be nickel supported on a refractory support such as rings or pellets of calcium aluminate cement, alumina, titania, zirconia. Alternatively a combination of a nickel and precious metal catalyst may be used. The temperature of the resulting partially reformed gas is preferably in the range 650-850° C; the syngas will contain greater than 10% hydrogen by volume.

The outflow of the GHR enters the ATR adiabatic reactor in which both combustion and reforming reactions occur (secondary reforming).

Differently from the GHR, the heat for the reaction in the ATR is provided by the combustion. The ATR reactor is fed with air. This choice has been taken for different reasons: i) the syngas dilution allows to lower the NO_x production ii) no syngas purity is required and iii) no ASU unit is needed. The feedstock mixture of the ATR is partially converted through a pressurized combustion with fuel excess and the conversion of the hydro carbonates in the row syngas is finished in a fixed catalytic bed. Autothermal or secondary reforming serves three purposes: i) the increased temperature resulting from partial combustion and subsequent adiabatic steam reforming results in a higher reactions rates ii) the increased temperature favors the reverse shift reaction so that the carbon monoxide to carbon dioxide ratio is increased and iii) the partial combustion effectively consumes some of the hydrogen present in the steam-reformed gas. Preferably the cooled reformed gas mixture leaves the heat exchange reformer at a temperature in the range 500-650° C.

The ATR reactor can be divided into three different areas: the combustion zone, the thermal zone and the catalytic zone. The combustion zone is where the oxygen and the molecules of hydro carbons mix together in a turbulent diffusion flame that can be described with the following reaction:

$$CH_4 + \frac{3}{2}O_2 \leftrightarrow CO + 2H_2O \qquad \Delta H°_{298K} = -519 \text{ kJ/mol} \qquad (3\text{-}6)$$

The O_2/CH_4 ratio in the flame is around 1.5.

In the thermal zone above the catalytic bed there is a further conversion with gaseous phase reactions slower than in the flame zone. The main reactions are the methane reforming and the shift reaction:

$$CO + H_2O \leftrightarrow CO_2 + H_2 \qquad \Delta H°_{298K} = -41 \text{kJ/mol} \qquad (3\text{-}7)$$

In this zone, reactions between nitrogen and hydrocarbon radicals can lead to HCN and NH_3 formation.

The catalytic zone allows completing the hydro carbons conversion through a series of catalytic heterogeneous reactions. The gas flow temperature at the catalytic bed inlet is around 1200-1300°C and the outlet temperature is around 1000°C; the bed can be considered adiabatic. Because of the high temperatures the catalyst must be highly stable with the temperature and has to limit pressure drops. The most used catalyst are nickel based on a suitable support such as alumina ($\alpha - Al_2O_3$) or magnesium and aluminum spinels ($MgAl_2O_4$). The most used shape in order to assure high activity and low pressure dorps is the pellet.

A GS model of the GHR-ATR reactor has been developed in order to simulate the reforming process as much realistic as possible; therefore the model is calibrated on US patent [2] and [3]. In the process, feedstock is typically compressed to a pressure in the range 10-100 bar preferably 20-60 bar. In the studied case, the natural gas pressure is around 30 bar at the GHR-ATR inlet. It is preferred that the steam to carbon ratio is below 1.5, more preferably 0.5-1.0. The chosen S/C ratio, according with the data suggested by the CAESAR project partners, has been set equal to 1.1. According to this simulation, in all the different cases, the ATR outlet temperature has been set equal to 950°C.

An example of the model is shown in Figure 3-1.

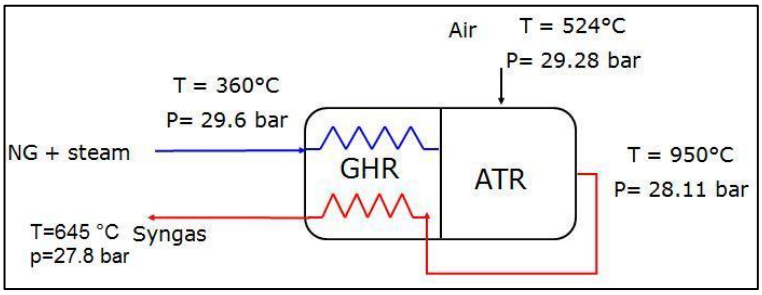

Figure 3-1: GHR-ATR GS modelisation with temperature and pressure of the incoming-out coming flows.

Table 3-8: GHR-ATR main assumptions

GHR-ATR properties	
Equilibrium temperature, °C	950
S/C ratio	1.1
Pressure	set in order to have a fuel pressure at combustor of 23.1 bar
Pressure drop, %	6.0

3.2.7 HEAT EXCHANGER

General assumptions for heat exchanger simulation are reported in Table 3-9.

Table 3-9: main characteristics of a general heat exchanger considered in the simulations

Heat Exchanger pinch points and pressure losses	
Gas / Gas, °C	25
Gas / boiling or liquid phase, °C	10
Liquid / liquid, °C	10
Condensing / liquid, °C	3
Gas phase pressure loss for cold and hot side, %	2.0
Liquid phase pressure loss for cold and hot side, MPa	0.04
Heat loss, %	0.7

3.2.8 ELECTRICAL & AUXILIARIES

General assumptions for electrical equipment and auxiliaries are reported in Table 3-10.

Table 3-10: efficiency assumptions for electrical devices

Electrical auxiliaries efficiency	
Driver efficiency, %	95
Generator efficiency, %	98.5
Mechanical efficiency, %	99.6

3.2.9 MEA

The CO_2 capture section based on MEA is simulated with ASPEN® adopting the RK-SOAVE calculation method. A schematic layout of the carbon capture section simulated in Aspen is reported in Figure 3-2 while the main process parameters are reported in Table 3-11. In the power plant, there are two absorbers and two strippers lines, one for each HRSG, in order to limit column size and diameter. Nevertheless, it is assumed to adopt only one CO_2 compressor. Exhaust gases are cooled after the HRSG in order to achieve a temperature of 40°C required by the absorber. The absorption and stripper column are simulated, respectively, with 4 and 9 vapour-liquid equilibrium stages. Results are consistent with EBTF and, in particular, with TNO simulations for the Cesar project [4]. In Figure 3-2 the MEA loop is shown as open with a splitter and make-up introduced on the stream from the stripper to the absorber. In real applications MEA circulates in a closed loop and make-up is necessary only for degradation processes which are not simulated.

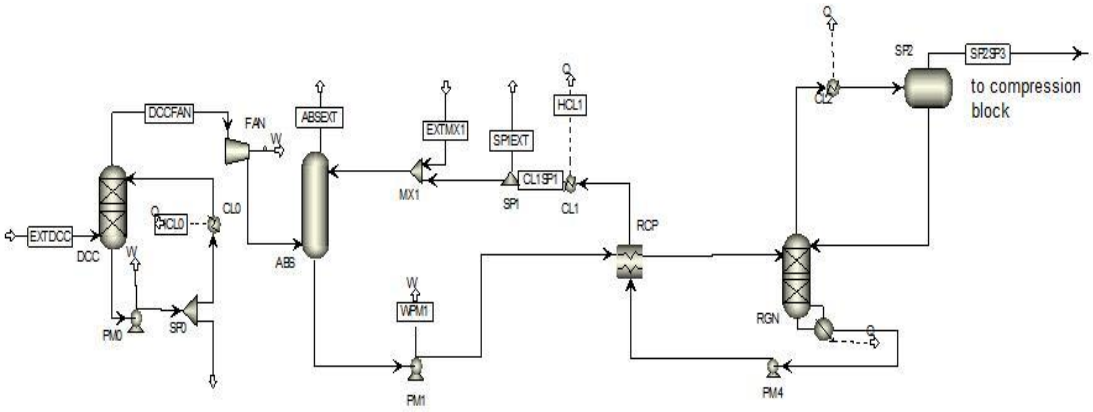

Main Blocks:
DCC – exhaust gas cooler
ABS – absorber
PM1,2,3,4 - pumps
RGN - stripper
CL0,1,2 – heat rejection
FAN – forced fan
SP2 – flash tank
RCP – regenerative heat exchanger

Main Flows:
EXTDCC – flow exiting the HRSG
ABSEXT – decarbonised flue gas
SP2SP3 – CO_2 rich mixture

Figure 3-2: schematic of the CO_2 capture section by MEA

Table 3-11: main assumptions for post-combustion CO_2absorption process by MEA.

Mass Flows for each absorber	
Exhaust gases mass flow, kg/s	665.3
CO_2 Captured, kg/s	36.93
Booster Fan	
Pressure ratio	1.1
Isentropic efficiency, %	85
Driver efficiency, %	95
Regenerative Heat exchanger	
ΔT_{min}, °C	5
Absorption Column	
Column pressure, bar	1.1
Number of stages	4
Stripper Column	
Column pressure, bar	1.8
Number of stages	9
Heat for solvent regeneration, $MJ_{th}/kgCO_2$	3.95
Steam pressure for solvent regeneration, bar	4.0
Absorber and Stripper Pumps	
Head, bar	10
Hydraulic efficiency, %	75
Driver efficiency, %	95
Solution parameter	
Solvent concentration, wt%	30
CO_2 loading rich amine, mol/mol	0.466
CO_2 loading lean amine, mol/mol	0.257
Rich stream regeneration, %	50

3.2.10 MDEA

The MDEA process is based on Di-Ethanol Amine partial thermal regeneration in a stripper with low pressure steam and partial physical regeneration in a low pressure flash, like in the BASF MDEA process [5] [6]. It is simulated with Aspen Plus® MDEA package, with Electrolyte NRTL model and Redlich-Kwong equation of state and chemical equilibrium calculations according to [7]. A schematic of MDEA layout is shown in Figure 3-3 while main operating conditions are reported in Table 3-12.

Rich solution exiting the absorber is first sent to a high pressure flash where most of the hydrogen, carbon monoxide and nitrogen are desorbed and recycled back to the absorber. Afterwards, it enters a low pressure flash where it is partially regenerated. The semi-lean solution exiting the LP flash is partly sent to a stripper where carbon dioxide is stripped with the steam generated in a reboiler. A low pressure steam flow extracted from the steam turbine is condensed in the reboiler to supply the required heat. Vapor flow exiting the stripper, mainly composed of carbon dioxide and steam, is sent to the LP flash where water condenses providing heat to the rich solution and enhancing semi-lean solvent regeneration. Considering the two regeneration levels attained in the process, the CO_2 absorber is fed with a lean solution at the top of the column and with a semi-lean solution at an intermediate stage (whose position was optimized in the simulations).

Energy consumptions for CO_2 capture in MDEA process are: (i) steam usage for reboiler, (ii) compression work for syngas recycle and solvent circulation and (iii) heat rejection. Main assumptions for MDEA process simulation are summarized in Table 3-12.

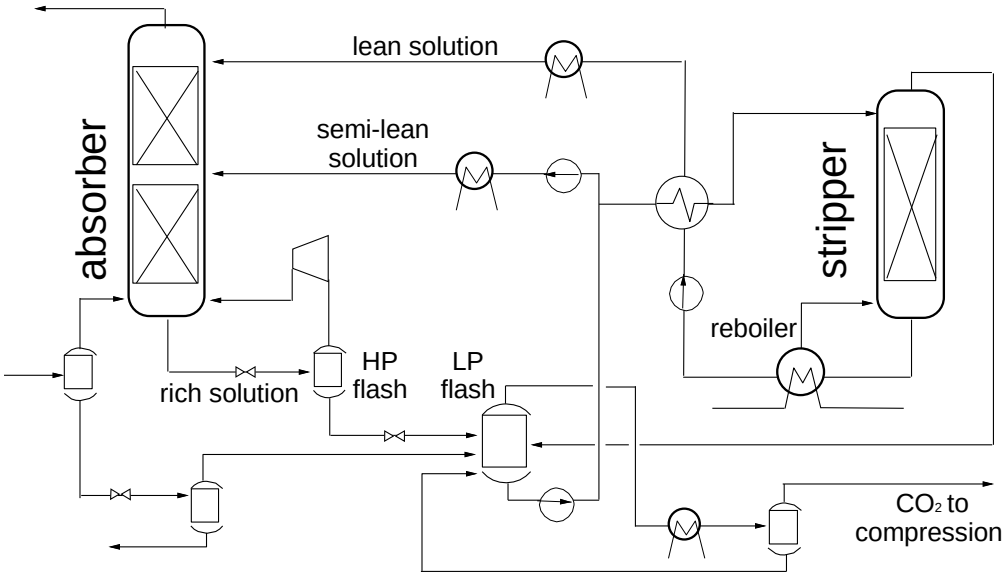

Figure 3-3: schematic of the MDEA process for CO_2 absorption

Table 3-12: main assumptions used for MDEA process.

MDEA process	
Absorber tray efficiency, %	35
MDEA concentration in the solution, %wt.	40
Lean solution CO_2 loading, mol-CO2/mol-MDEA	0.005
HP / LP flash pressure, bar	5 / 1.1
Stripper ideal stages	5
Reboiler pressure, bar	1.3
Reboiler heat duty, MJth/kg_{CO2}	1.34
Minimum ΔT in reboiler / regenerative HE, °C	5 / 10
Pumps hydraulic / mech.-electric efficiency, %	75 / 95
Recycle compressor isentropic / mech.-electric efficiency, %	80 / 95

3.2.11 CO_2 COMPRESSION TRAIN

An Aspen Plus sheet (see Figure 3-4) was implemented in order to match the chemical behaviour of the mixture, with particular attention to the real gas effects; the thermodynamic properties were calculated using the PC-Saft equations of state [8], which according to [9] of AspenTech is the best correlation for H_2O-CO_2 mixtures. The model aimed to minimize the process energy demand.

The compression train is composed by: i) a five stages-four intercoolers compressor with one aftercooler and, ii) a pump with a final aftercooler. The compressor provides an outlet pressure of 80 bar while the pump provides a fixed delivery pressure of 110 bar. All the water inside the CO_2 stream is removed before the fourth intercooler.

The stages included between two intercoolers have an overall pressure set as: $\beta_{group} = \sqrt[n]{\beta_{tot}}$; with n equal to the number of stages groups (i.e. 5 groups see Figure 3-5). The compressor isentropic efficiency and the pump hydraulic efficiency are fixed and set equal to 0.85 and 0.75 respectively. Main assumptions for each section are shown in Table 3-13.

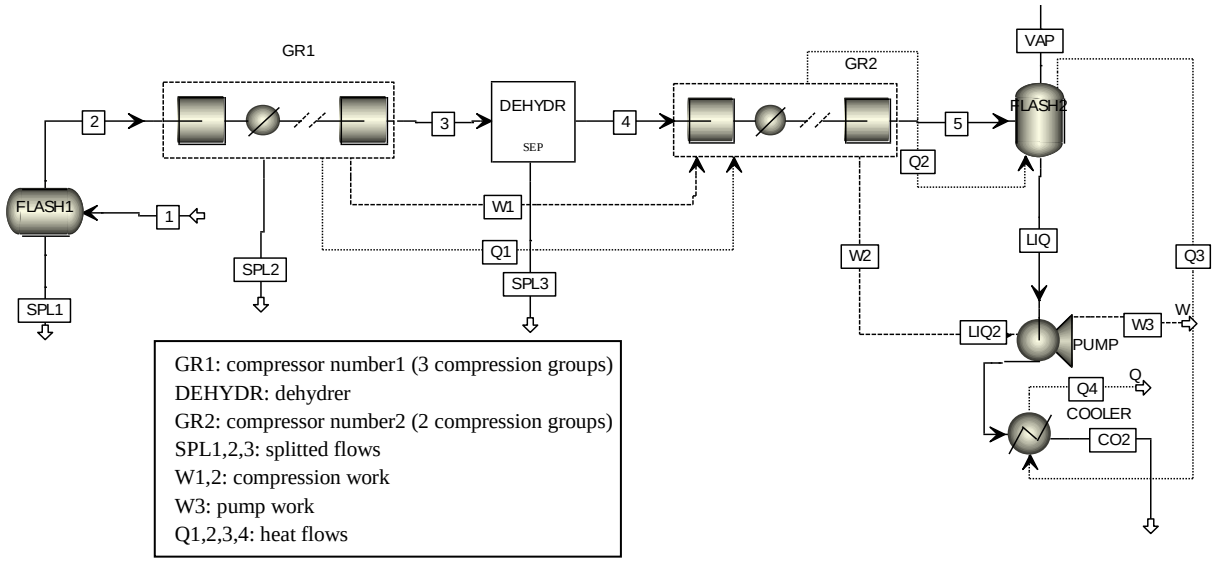

Figure 3-4: schematic of Aspen scheme adopted for CO2 compression work calculation

Table 3-13: carbon dioxide compression specifications

CO_2 delivery pressure, bar	110
CO_2 delivery temperature, °C	25
CO_2 condensation pressure, bar	80
CO_2 *compressor*	
Number of stages groups	5
Number of intercooled stages groups,	4
Intercooler pressure drops, %	1
CO_2 temperature after intercooler,	35
Isentropic efficiency for each stage, %	85
Driver efficiency, %	95
After cooler	
Pressure drop, %	1
CO_2 temperature,	25
Pumps	
Hydraulic efficiency, %	75
Driver efficiency, %	95

Figure 3-5 and Table 3-14 show the T-s diagram and the results for the CO_2 compression. It must be noted that in the T-s diagram the isobars don't match between inlet and outlet conditions for the intercooler 1, 2 and aftercooler 1; this is due to the water condensation and the following composition variation that moves the isobar left.

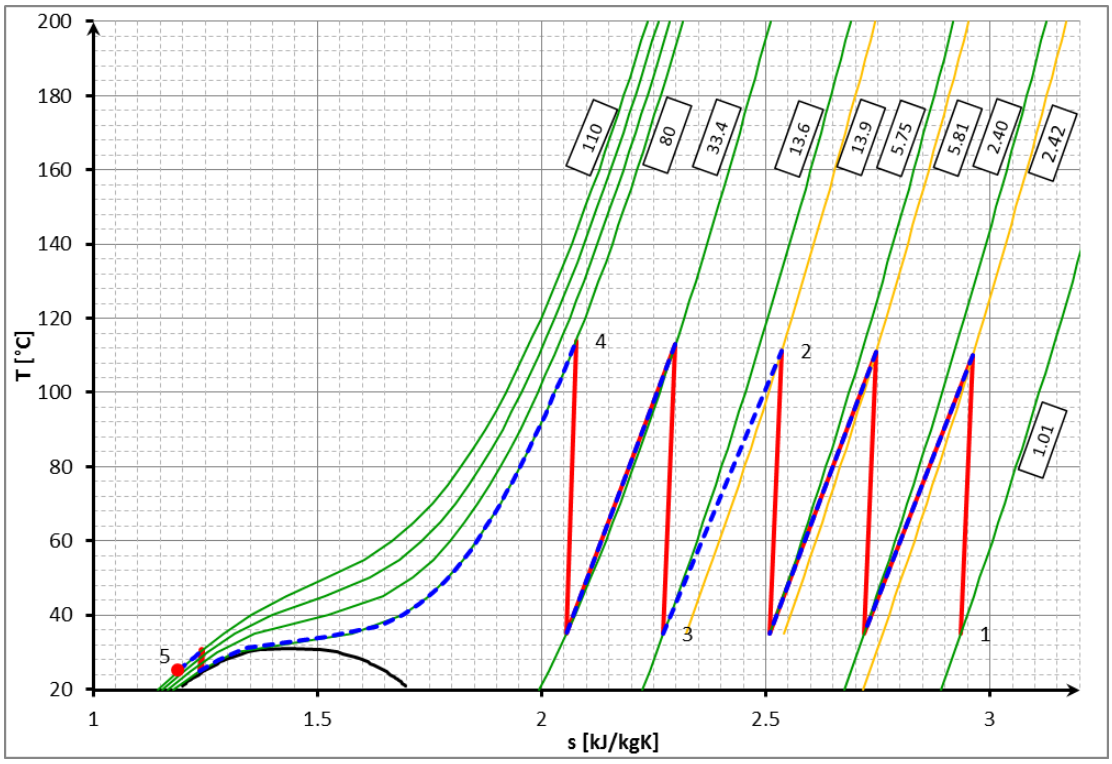

Figure 3-5: T-s diagram for the CO_2 compression; for the first compressor the yellow isobars refer to the composition entering the intercoolers while the green isobars refer to the composition exiting the intercoolers.

Table 3-14: thermodynamic conditions along CO_2 compression, point refers to Figure 3-5.

	T [°C]	s [kJ/kg K]	P [bar]	V [m^3/s]
1	35.0	2.94	1.01	25.4
2	111.3	2.54	13.92	2.17
3	35.0	2.27	13.64	1.68
4	114.0	2.08	80	0.324
5	25.0	1.19	110	0.051

Some cases concerning the SEWGS applications feature a lower inlet pressure, requiring little modifications to the compression train. Accordingly, the pressure ratio is calculated as previously discussed, but limiting the maximum temperature after the stage to 125°C. The number of stages increases up to 7.

It must be stressed that thermodynamic conditions close to critical point as assumed for CO_2 liquefaction models have several uncertainties leading to scattered results: for example, H_2 dissolution in liquid CO_2 ranges from 20 to 100%. In this work, all the hydrogen is assumed to dissolute with CO_2 considering the very low concentration. Assuming that all hydrogen is recovered, the overall efficiency would increase by about 0.25%point.

3.3 NATURAL GAS COMBINED CYCLE

3.3.1 EBTF REFERENCE CASE WITHOUT CARBON CAPTURE

The selected reference NGCC for electricity production without carbon capture is based on two large-scale identical gas turbines (GT), "F class", each equipped with a heat recovery steam generator (HRSG), and a single steam turbine; the plant layout is shown in Figure 3-6 [10]. This 2+1 arrangement is quite popular among utilities, since it adds operational flexibility as required by a competitive electricity market.

The HRSG is a three pressure level + reheat type. Before feeding the gas turbine combustor, natural gas is preheated up to 160°C by means of feed water extracted from the intermediate pressure (IP) drum, increasing the overall plant efficiency. The fuel flow rate to the gas turbine combustor is set to obtain an assumed Turbine Inlet Temperature (TIT) of 1360°C.

Characteristics of the main streams as compositions and thermodynamic conditions are reported in Table 3-15.

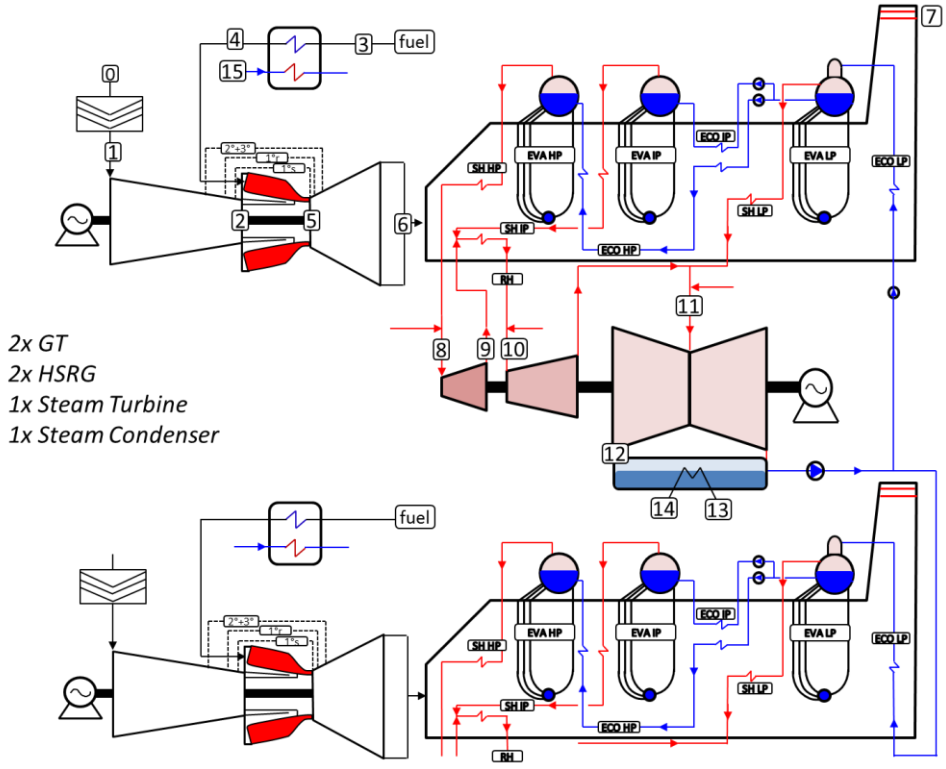

Figure 3-6: Layout of the NGCC plant without carbon capture.

Table 3-15: mass flow rate, pressure, temperature and composition of the main fluxes of NGCC reference plant (Numbers refer to Figure 3-6); for point 5 (maximum cycle temperature) the table indicates the three most commonly used definitions in the international literature. (*) 2GT

Point	G	T	P	X	Composition, %mol.					
	[kg/s]	[°C]	[Bar]		Ar	N_2	O_2	CO_2	H_2O	NO_x
0	650.0	15.0	1.01	--						
1	650.0	15.0	1.00	--			Air, see Table 3-1			
2	523.4	417.5	18.16	--						
3	15.3	10.0	70.0	--						
4	15.3	160.0	70.0	--			NG composition, see Table 3-2			
	538.7	COT 1443.3	17.6	--	0.88	73.71	10.47	4.87	10.07	$1.4\cdot10^{-3}$
5		TIT 1360.0	-	-	-	-	-	-	-	-
		TIT_{iso} 1265.7	-	-	0.89	74.38	12.39	3.96	8.38	$1.4\cdot10^{-3}$
6	665.3	608.0	1.04	--	0.89	74.38	12.39	3.96	8.38	$1.4\cdot10^{-3}$
7	665.3	86.8	1.01	--	0.89	74.38	12.39	3.96	8.38	$1.4\cdot10^{-3}$
8*	153.7	559.5	120.9	1	-	-	-	-	100.	-
9*	153.7	337.7	28.0	1	-	-	-	-	100.	-
10*	185.0	561.0	22.96	1	-	-	-	-	100.	-
11*	20.9	299.0	3.52	1	-	-	-	-	100.	-
12*	205.9	32.2	.048	0.93	-	-	-	-	100.	-
13*	11172	19.2	1.01	0	-	-	-	-	100.	-
14*	11172	29.2	1.01	0	-	-	-	-	100.	-
15	6.84	230.0	28.00	0	-	-	-	-	100.	-
Net Power Output				**829.9**	**MW**	**Net Electric Efficiency**			**58.3**	**%**

3.3.2 EBTF REFERENCE CASE WITH POST-COMBUSTION CO2 CAPTURE WITH MEA

Post-combustion CO_2 capture consists of CO_2 chemical absorption with 30wt% MEA. The pressure in the absorption column is set at 1.06 bara with a booster fan upstream, in order to account for pressure drops and keep the GT exhaust pressure equal to a conventional NGCC without carbon capture. The absorption temperature is set to about 50°C, so a cooler is required after the HRSG. The CO_2 captured by MEA in the absorption column is released in the stripper, where heat is required at the reboiler. This heat is supplied by steam extracted from the steam turbine and attempered with water. Stripper pressure at the bottom of the column is set at 1.8 bara and the reboiler process side temperature is 119 °C. The CO_2 released in the stripper column is compressed in an inter-cooled compressor and, after reaching liquid phase liquefaction in the 80 bar after-cooler, pumped to the delivery pressure fixed at 110 bar.

The nominal net output decreases because of the steam required for amine regeneration and the additional auxiliary power consumption (amine circulation pumps, fans for overcoming the gas pressure losses, additional cooling water pumps, CO_2 compressor). The amount of energy for regeneration is assumed equal to 3.95 GJ/tonne$_{CO2}$ with steam at a pressure of 4.0 bar [11], which corresponds to about 1.85 kg of steam for every kg of CO_2 captured. This value is consistent adopting a superheating and a subcooling of the steam of 10°C at the assumed pressure. A summary of the main streams are reported in Table 3-16.

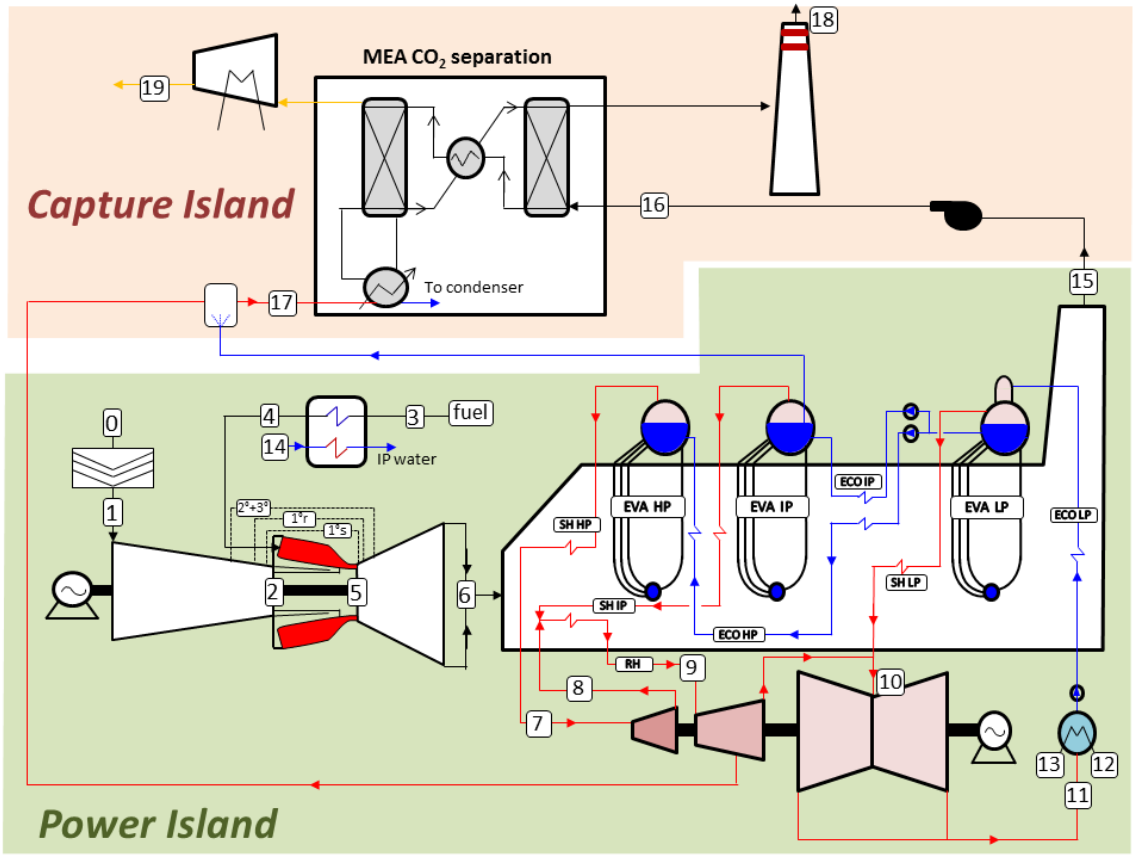

Figure 3-7: Schematic of the reference NGCC with CO_2 capture power plant; for simplicity only one GT and HRSG are represented

Because of the fan upstream of the amine absorption column, the GT working conditions do not change compared to NGCC without CO_2 capture. LP steam production slightly decreases (20.7 kg/s vs. 20.9 kg/s) because of water extraction from the LP drum for steam de-superheating. The higher temperature of HRSG outlet gases is because of the water return from the stripper reboiler at about 120°C with consequent less heat demand for water pre-heating.

Table 3-16: mass flow rate, pressure, temperature and composition of the main fluxes of NGCC reference plant with carbon capture by MEA (Numbers refer to Figure 3-7). (*) 2GT

Point	G	T	P	X	Composition, %mol.					
	kg/s	°C	Bar		Ar	N_2	O_2	CO_2	H_2O	NO_x
0	650.0	15.0	1.01	--						
1	650.0	15.0	1.00	--			Air, see Table 3-1			
2	523.4	417.5	18.2	--						
3	15.30	10.0	70.0	--						
4	15.30	160.0	70.0	--			NG composition, see Table 3-2			
5	538.7	COT 1443.3 TIT 1360.1 TIT_{iso} 1265.7	17.6	--	0.88	73.71	10.47	4.87	10.08	$1.4 \cdot 10^{-3}$
6	665.3	608.0	1.04	--	0.89	74.38	12.39	3.96	8.38	$1.4 \cdot 10^{-3}$
7*	153.7	559.9	120.9	1	-	-	-	-	100.	-
8*	153.7	337.7	28.0	1	-	-	-	-	100.	-
9*	185.0	561.0	23.0	1	-	-	-	-	100.	-
10*	20.7	299.0	3.5	1	-	-	-	-	100.	-
11*	90.4	32.2	0.048	0.92	-	-	-	-	100.	-
12*	4921	19.2	1.01	0	-	-	-	-	100.	-
13*	4921	29.2	1.01	0	-	-	-	-	100.	-
14	6.84	230.0	28.0	0	-	-	-	-	100.	-
15	665.0	101.5	1.01	--	0.89	74.38	12.39	3.96	8.38	$1.4 \cdot 10^{-3}$
16	659.7	48.7	1.06	--	0.90	75.39	12.56	4.02	7.14	-
17	66.3	154.0	4.0	--	-	-	-	-	100.	-
18	642.4	51.8	1.01		0.89	74.57	12.43	0.38	11.74	
19	36.95	25.0	110.0	0.05	-	0.01	<0.01	99.93	-	-
	Net Power Output		**709.9**	**MW**	**Net Electric Efficiency**				**49.9**	**%**

3.3.3 NATURAL GAS FIRED WITH PRE-COMBUSTION CARBON CAPTURE BY MDEA

Compared to post-combustion technology, pre-combustion significantly modifies the power cycle because of the decarbonization process required upstream of combustion. In particular, main components of the power plant with pre-combustion MDEA-based technology are:

- A GHR-ATR that converts a steam-methane mixture into hydrogen using two sequential steps: a pre-reforming gas heated reformer (GHR) and a more conventional air blown autothermal reformer (ATR) [2] [3]. In order to avoid catalyst poisoning from sulphur components present in the NG, a desulphurization section is required in front of the reformer;
- Two water-gas shift reactors (WGS) that convert CO in the syngas produced by the ATR into CO_2 and H_2. The first WGS reactor works at high temperature allowing a fast conversion (smaller catalyst surfaces). The water-gas shift reaction is exothermic with

the exit temperature rising over 400 °C and the heat released is recovered by producing HP steam in a wasted heat boiler. The second WGS reactor operates at lower equilibrium temperatures (around 230°C), where the reaction is promoted and enhances further CO conversion;

- A CO_2 separation unit (carried out with MDEA technology) to capture CO_2 from the syngas exiting the WGS in order to produce a decarbonised fuel (H_2 and N_2 with some traces of CH_4, CO and H_2O remaining from the previous reactions) which is then fed into the gas turbine combustor;
- Two direct contact saturators: the first saturator humidifies and heats the NG before the pre-reformer reactor using HP and IP water from the HRSG; this reduces the amount of steam bled from the turbine in order to reach the desired Steam-to-Carbon ratio (S/C ratio). The second saturator humidifies the syngas before the combustor inlet lowering the flame temperature with benefits on NO_x formation;
- A combined cycle with the same parameters as the reference case.

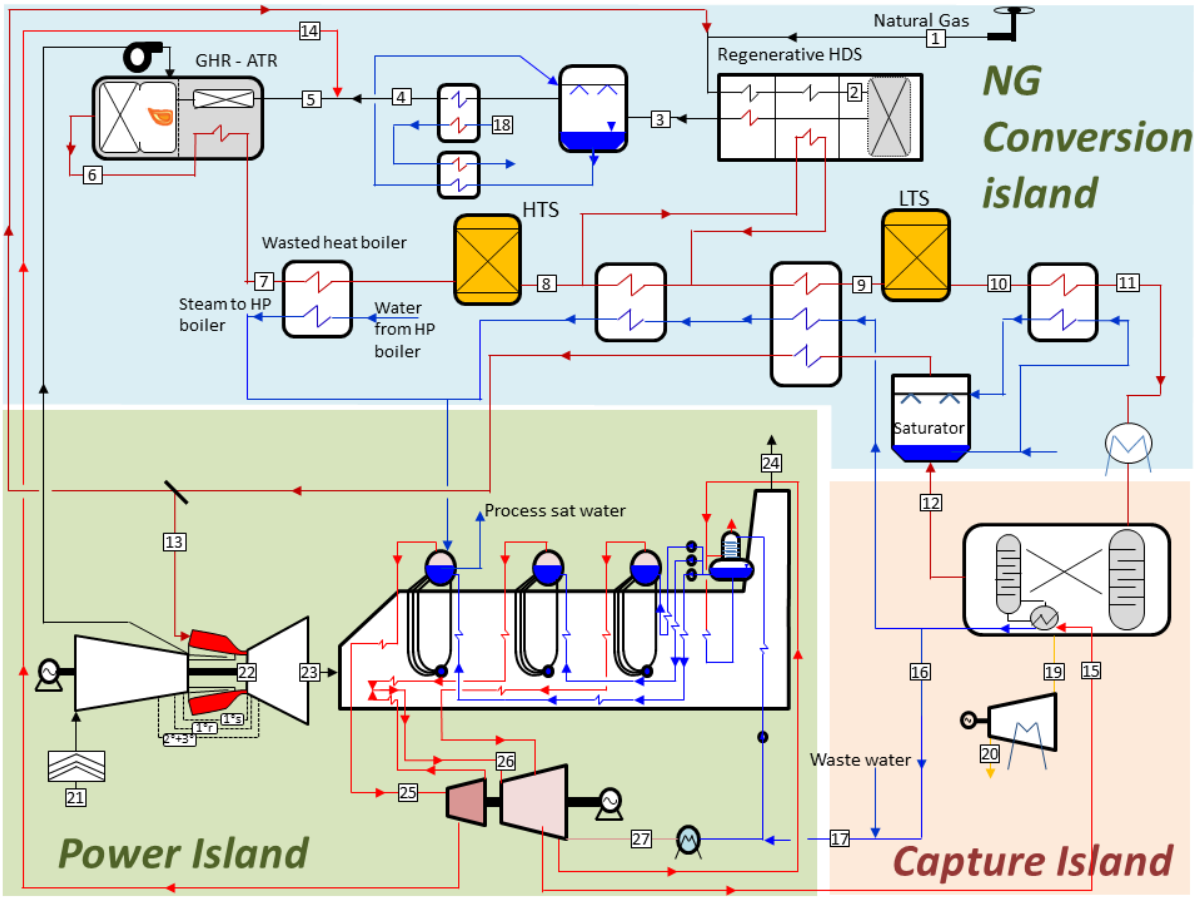

Figure 3-8: Layout of the NGCC power plant with CO_2 capture by MDEA

In the choice between a hydrogen island decoupled from the power section and a tight integration, the latter is chosen for analysis as this limits exergy losses and achieves the highest electric efficiency. In this work, the layout is taken from a previous paper [7], but the results are

slightly different because assumptions have been modified according to [11]. Figure 3-8 shows the proposed layout.

Following Figure 3-8, the NG is fed at 70 bar and 10 °C, and preheated to 380 °C as required by the Hydro DeSulphurization reactor (HDS) through a recuperative heat exchanger and a syngas heat exchanger. Before HDS, a hydrogen-rich gas must be mixed to the NG to achieve 2% hydrogen content in the stream as required by the desulphurization process. Then the NG is saturated in a direct contact saturator and further pre-heated before the GHR-ATR: saturation reduces the amount of steam bled from the turbine for the reforming; the heat required is supplied by cooling HP and IP water taken from the HRSG. The syngas leaving the ATR at 950 °C is cooled in the GHR to 645 °C whilst heating the natural gas-steam mixture up to 625 °C and providing heat for the reforming reaction in the GHR. After the GHR the syngas is cooled to 350 °C by producing HP steam and then enters the first adiabatic water gas shift reactor. The syngas leaves the High Temperature Shift (HTS) at an equilibrium temperature of about 450 °C where it is cooled by parallel heat exchangers: in the first the syngas is cooled to 340 °C by evaporating HP water and supplies the heat required by the desulphurization process; in the second, the syngas is cooled to 190 °C by heating GT fuel and preheating HP water. Then, an adiabatic Low Temperature Shift (LTS) is adopted.

A second saturator is used on the hydrogen rich mixture stream and allows heating to reduce the NO_x production in the GT combustor using feed water heated by the syngas at the MDEA inlet. The heat necessary for the CO_2 stripping from the MDEA solution is obtained by bleeding LP steam from the turbine.

Table 3-17: mass flow rate, pressure, temperature and composition of the main fluxes of NGCC with carbon capture by MDEA. (*) 2GT (Numbers refer to Figure 3-8)

Point	G	T	P	x	Composition, %mol.								
	kg/s	°C	Bar		Ar	CH_4	CO	CO_2	C_xH_y	H_2	H_2O	N_2	O_2
1	18.8	10.0	70.00	--	NG composition, see Table 3-2								
2	18.8	380.0	65.80	--									
3	18.3	118.4	29.73	--	.02	85.52	.02	1.94	7.78	2.00	.56	2.16	-
4	22.3	320.8	29.14	--	.01	70.48	.02	1.60	6.39	1.65	17.97	1.85	-
5	47.1	317.4	29.14	--	.01	33.45	.01	.76	3.04	.78	61.10	.84	-
6	122.2	949.9	27.41	--	.35	.35	10.90	4.63	-	32.93	20.66	30.18	-
7	122.2	645.8	26.87	--	.35	.35	10.90	4.63	-	32.93	20.66	30.18	-
8	121.8	400.0	26.06	--	.35	.35	3.18	12.35	-	40.65	12.94	30.18	-
9	121.8	190.0	25.54	--	.35	.35	3.18	12.35	-	40.65	12.94	30.18	-
10	121.8	224.2	25.28	--	.35	.35	.44	15.09	-	43.38	10.21	30.18	-
11	121.8	90.0	24.28	--	.35	.35	.44	15.09	-	43.38	10.21	30.18	-
12	66.6	78.4	24.13	--	.47	.46	.59	.51	-	57.49	.47	40.00	-
13	81.1	300.0	23.17	--	.41	.40	.51	.44	-	49.37	14.54	34.34	-
14	24.9	342.8	29.14	1.	-	-	-	-	-	-	100.	-	-
15	19.8	217.4	1.77	1.	-	-	-	-	-	-	100.	-	-
16	19.8	115.0	1.73	0.	-	-	-	-	-	-	100.	-	-
17	45.0	109.1	1.73	0.	-	-	-	-	-	-	100.	-	-
18	11.7	164.0	128.7	0.	-	-	-	-	-	-	100.	-	-
19	44.3	32.4	1.10	--	-	-	-	99.96	-	0.03	-	0.01	-
20	44.3	25.0	110.	--	-	-	-	99.96	-	0.03	-	0.01	-
21	650.0	15.0	1.01		Air composition, see Table 3-1								
	520.0	COT 1434.8	17.61	--	.84	-	-	.43	-	-	20.17	70.20	8.37
22		TIT 1359.9											
		TIT_{ISO} 1253.0			.85	-	-	.35	-	-	16.57	71.53	10.70
23	656.9	591.2	1.04	--	.85	-	-	.35	-	-	16.46	71.57	10.77
24	656.9	76.2	1.01	--	.85	-	-	.35	-	-	16.46	71.57	10.77
25*	231.1	559.5	120.9	1.	-	-	-	-	-	-	100.	-	-
26*	193.3	560.9	22.96	1.	-	-	-	-	-	-	100.	-	-
27*	161.0	32.2	.048	.93	-	-	-	-	-	-	100.	-	-
Net Power Output					**830.0**	**MW**		**Net Electric Efficiency**				**50.3**	**%**

3.4 COAL PLANT REFERENCE CASES WITH AND WITHOUT CO_2 CAPTURE

3.4.1 ASC

The plant is based on an Advanced Super Critical (ASC) Boiler and Turbine producing about 820 MWe (gross) without any carbon capture. The auxiliary power consumptions require 65 MW leading to a final net power plant output is 754.3 MWe, yielding a net cycle efficiency of 45.5% [12]. The general arrangement layout for the reference power plant is based on an inland site with natural draft cooling towers and delivery of the coal by rail. For the control of combustion product emissions, the power plant is equipped with selective catalytic reduction (SCR) DeNOx plant located between the boiler exit and air heater inlet, electrostatic precipitators and wet limestone based desulphurization plant before exhausting to atmosphere via a flue stack. NO_x ad SO_x emission limits are assumed to 120 mg/m^3 and 85 mg/m^3, respectively. For ash handling, a dry ash conveying system is employed for fly ash and a continuous ash removal system with submerged chain conveyer for furnace bottom ash.

3.4.2 IGCC

The reference IGCC technology is based on an entrained flow, oxygen blown, dry feed slagging Shell gasifier. The adoption of a Shell gasifier among other technologies (i.e. GE) is justified by the highest efficiency as well as availability of gasification heat and mass balances provided by Shell within EBTF [13]. The assumed lay-out, shown in Figure 3-9, reflects Shell experience.

The gasification pressure is 44 bar, high enough to feed the gas turbine without syngas compression. The choice of a dry feed gasifier with high carbon conversion (99%) gives a higher cold gas efficiency and consequently higher plant efficiency, compared to slurry fed gasifier. Due to the high gasification temperature, the gasifier wall must be water cooled; water pressure has to be higher than syngas. During the operation the main thermal barrier is provided by the ash layer, composed by a solidified part attached to the wall and a melted part which flows towards the bottom of the reactor; the slag layer also prevents corrosion of the wall. Before feeding, coal is pulverised and dried with an auxiliary fuel.

One gasification train is assumed, generating syngas for one gas turbine. Oxygen is produced in an air separation unit (ASU) whose distillation column is assumed to work at 5.76 bar; N_2 and O_2 (95 mol% pure) are available at atmospheric pressure. An expander between the gas turbine compressor and the ASU is adopted to recover part of the compression work. The advantages obtained integrating the gas turbine compressor with the ASU main compressor are driven by the higher GT flexibility. The low LHV of the syngas feeding the gas turbine leads to lower air demand at compressor inlet with possible stall issues; GT integration with ASU partially balances this issue leading to a reduction of the air volumetric flow at the compressor inlet of about 8% compared to the reference case; this condition is in the range of Variable Guide Vanes (VGV) application. Concerning the compressor duty, no significant advantages exist when power and gasification island are integrated: the GT compressor features higher isentropic efficiency whilst the ASU main compressor is intercooled; this results in an overall equivalent compression work at different integration levels. N_2 produced in the ASU is compressed and

used in (i) lock hoppers for coal feeding, (ii) periodic cleaning of candle filters and (iii) moderation of the gas turbine combustor stoichiometric temperature (in order to limit the NO_x formation). Only part of the N_2 used for lock hopper operation (about 50%), reaches the gasifier, while the remaining is vented during feeding process[1]. Hot syngas exiting the gasifier at about 1550°C, is quenched to 900°C with cold recycled syngas. Molten slag entrained by the gas stream solidifies and the syngas is cooled to 300°C in the syngas coolers, producing HP and IP steam. Some is then recycled back for syngas quench by means of a recycle fan. The remaining syngas is then sent to a scrubber where solids and soluble contaminants are removed. Liquid water from the scrubber is clarified in a sour water stripper by means of LP steam and subsequently recycled back to the scrubber. Syngas exits the scrubber at about 170°C and, after regenerative heat exchangers, is sent to a catalytic bed for COS hydrolysis. Low temperature heat is recovered producing hot water for the saturator. Syngas is then further cooled with cooling water and sent to acid gas removal (AGR) unit after condensate separation.

H_2S is removed in the AGR section by means of a Selexol cycle and sent to the sulphur recovery unit. Zero net steam is assumed from the sulphur recovery unit, i.e. the steam raised by H_2S combustion in the Claus plant is balanced by the heat required to keep S molten and to regenerate the SCOT solvent. After the AGR unit, syngas is mixed with nitrogen from the ASU and then saturated in order to preheat GT fuel and limit NO_x formation.

Before being burnt, syngas is further preheated up to 200°C with saturated water taken from the HRSG IP drum. Assuming the gas turbine has the same air compressor, the same pressure ratio and TIT of the natural gas fired case are kept by regulating air mass flow rate by means of the VGVs. This ensures a high gas turbine performance and maintains a sufficient stall margin. It must be outlined that the TIT is assumed to be constant recalculating the blade cooling flows which guarantee the same maximum metal temperature.

Three pressure level heat recovery steam cycle (at 144, 54 bar and 4) is used to recover heat from gas turbine flue gas and syngas cooling. IP pressure is higher compared to natural gas application, which is in the range of 30 and 40 bar [12] [14], because it is adopted in the gasification island as reaction medium as well as coolant. In order to avoid sulphuric acid condensation, a higher stack temperature (115°C) is assumed compared to natural gas fired combined cycle. Because of the high stack temperature and large steam production outside HRSG, exhaust gas heat is not sufficient for a complete feed-water heating, thus low pressure regenerative pre-heaters must be adopted as also in [11].

[1] The amount of nitrogen required for coal feeding was determined according to [20], while all other assumptions as oxygen consumption or syngas composition at gasifier outlet are taken from EBTF document [12]

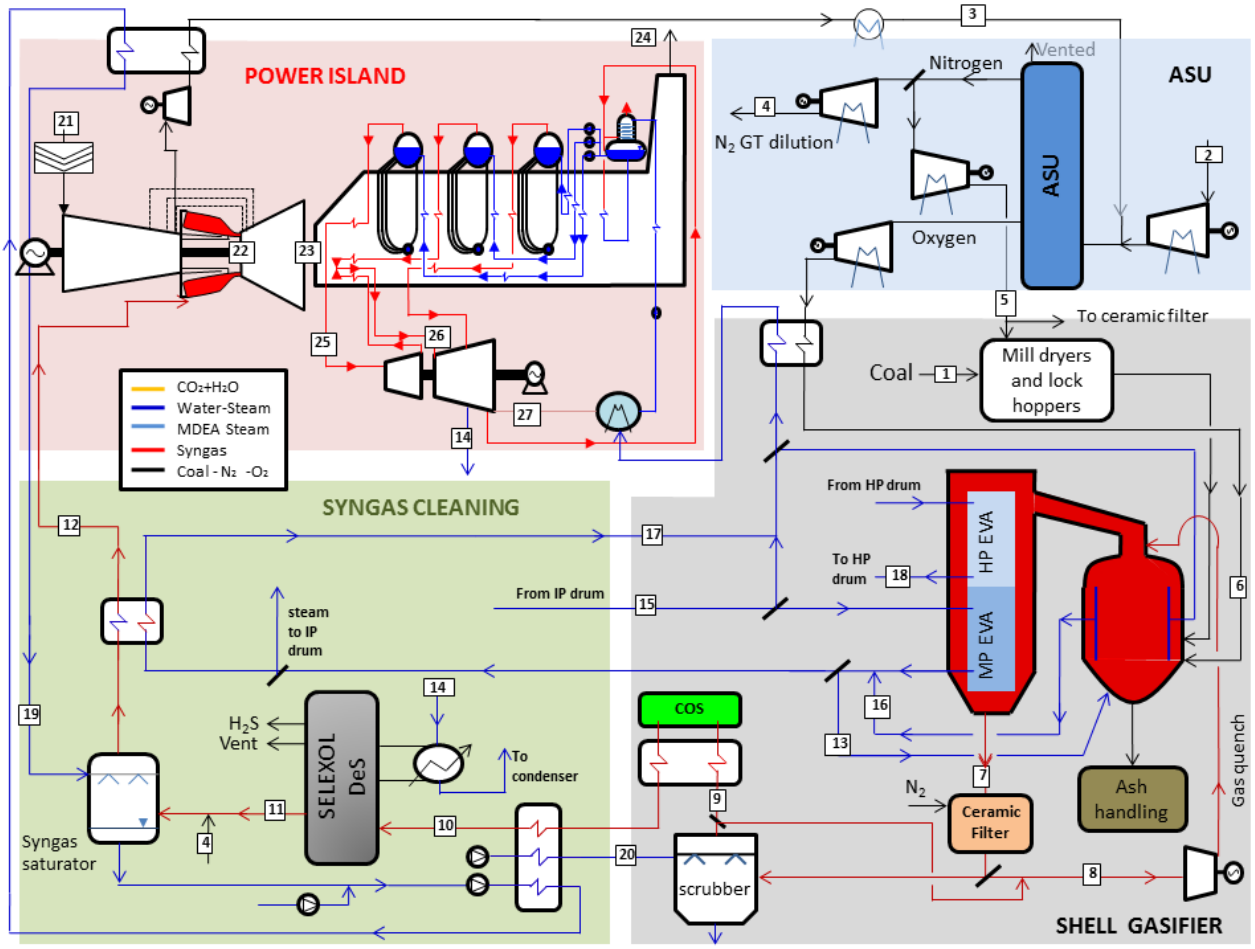

Figure 3-9: layout for the reference IGCC SHELL dry gasifier case

The main flows and compositions from the IGCC simulation are shown in Table 3-18. Higher net plant LHV efficiencies are obtained compared to those previously reported in the literature for Shell gasifier-based IGCCs [15] [16] [17] [18], but these results were approved by Shell and consistent with EBTF test cases.

Table 3-18: mass flow rate, pressure, temperature and composition of the main fluxes of IGCC reference plant.

Point	G	T	p	Composition, %mol.								
	kg/s	°C	bar	CH_4	CO	CO_2	H_2	H_2O	Ar	N_2	O_2	H_2S
1	32.9	15.0	44.0	Dry Coal 2%, see Table 3-3								
2	60.3	15.0	1.01	Air, see Table 3-1								
3	60.3	30.0	5.8									
4	65.2	260.6	27.2	-	-	-	-	-	-	100.0	-	-
5	9.2	80.0	88.0	-	-	-	-	-	-	100.0	-	-
6	28.9	180.0	48.0	-	-	-	-	-	3.1	1.9	95.0	-
7	113.7	300.0	41.1	.01	56.9	2.8	26.3	4.8	.9	8.0	-	.18
8	48.2	200.0	41.1	.01	52.4	2.6	24.3	11.4	.8	8.3	-	.16
9	76.3	170.0	40.3	.01	50.7	2.5	23.5	14.3	.8	8.0	-	.16
10	76.3	35.0	36.7	.01	50.7	2.5	23.5	14.3	.8	8.0	-	.16
11	66.58	80.0	26.9	.01	59.3	2.8	27.5	.1	.9	9.7	-	0.001
12	143.8	200.0	25.1	.01	30.2	1.4	14.0	11.0	.5	42.9	-	0.001
13	2.9	300.0	54.0	-	-	-	-	100.0	-	-	-	-
14	1.67	273.6	6.0	-	-	-	-	100.0	-	-	-	-
15	17.7	268.8	54.0	-	-	-	-	100.0	-	-	-	-
16	10.2	300.0	54.0	-	-	-	-	100.0	-	-	-	-
17	6.0	195.0	53.5	-	-	-	-	100.0	-	-	-	-
18	86.7	339.0	144.0	-	-	-	-	100.0	-	-	-	-
19	79.2	155.0	70.0	-	-	-	-	100.0	-	-	-	-
20	9.7	158.0	41.1	-	-	-	-	100.0	-	-	-	-
21	581.5	15.0	1.01	Air, see Table 3-1								
22	537.0	COT 1439.4 TIT 1360.1 TIT_{ISO} 1259.4	17.6	-	-	10.5	-	9.09	.8	71.5	8.0	-
23	665.0	614.7	1.04	-	-	8.5	-	7.5	.8	72.6	10.5	-
24	665.0	115.0	1.01	-	-	8.5	-	7.5	.8	72.6	10.5	-
25	124.1	559.2	133.9	-	-	-	-	100.0	-	-	-	-
26	134.8	559.1	44.2	-	-	-	-	100.0	-	-	-	-
27	121.0	32.2	0.048	-	-	-	-	100.0	-	-	-	-
Net Power Output				**422.4**	**MW**		**Net Electric Efficiency**				**47.1**	**%**

3.4.3 ASC WITH CO_2 CAPTURE

CO_2 capture in the considered pulverized coal plant is based on post-combustion technology with conventional amine scrubbing process. The capture plant is designed to operate for the whole life of the plant capturing 90% of the CO_2 contained in the flue gas. Operation of the plant at full load conditions is considered. The flue gas is initially cooled to 50ºC and fed to the absorber, where it is contacted with the 30% wt MEA solvent which is considered the benchmark technology thanks to the several industrial applications. Regeneration is carried out with steam from the IP/LP crossover, at about 5.2 bar, in order to take into account pressure drop from the power block to the stripper. Stripper working conditions are: temperature of 134°C, pressure 3.05 bar and specific heat duty for regeneration of 3.75 GJ/t_{CO2} [12] [19].The condensate is returned to the boiler feed water train. Detailed description of the CO_2 capture island is reported in [12] [19].

3.4.4 IGCC WITH CO_2 CAPTURE

The plant configuration for an IGCC plant with pre-combustion carbon capture is shown in Figure 3-10. Differences from the reference case without carbon capture start after scrubbing: before entering the shift section, syngas is mixed with steam bled from turbine in order to have the desired steam to carbon ratio for the shift reaction. Sour water gas shift reaction is performed in two reactors to convert as much CO as possible into CO_2 and hydrogen. In the first reactor, the majority of CO is converted and the heat of reaction is recovered by producing high pressure saturated steam in a waste heat boiler; in the second one, the shift reaction is almost completed thanks to the lower equilibrium temperature which enhances products formation. A Steam-to-CO ratio of 1.9 is set at WGS inlet to control temperature along the reactor [12]. Compared to reference case without CO_2 capture, COS hydrolysis is directly carried out in the WGS avoiding a dedicated reactor and thermal swing. Because of the higher water concentration in syngas at the shift section outlet, condensation occurs at higher temperature compared to the no-capture case; hence, condensation heat can be recovered for saturator and HP water pre-heating.

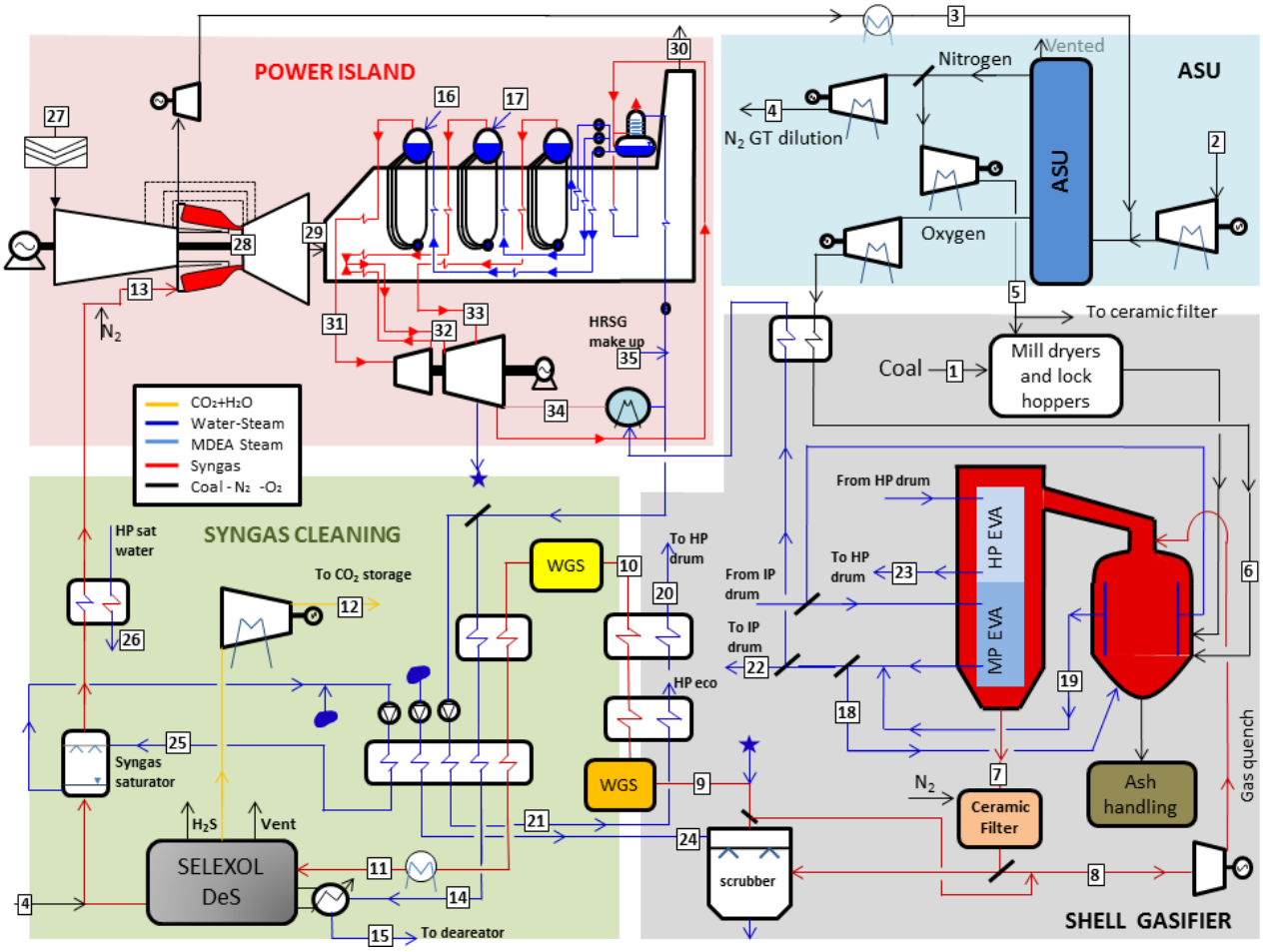

Figure 3-10: Layout of the IGCC power plant with CO_2 capture by Selexol

Carbon dioxide is removed from the syngas by a Selexol process at ambient temperature. A two-stage Selexol process is adopted where H_2S is removed in the first stage and CO_2 in the second stage of absorption. The process results in three product streams: (i) the rich fuel gas, (ii) a CO_2 rich stream and (iii) an acid gas fed to the Claus plant. The CO_2 stream is purified before the final compression and H_2-CO are recycled back to the process. Despite the fact that H_2S and CO_2 co-capture is a process currently carried out for natural gas sweetening, increased risks and costs are associated with transport of CO_2 contaminated with H_2S. Separate CO_2 and H_2S capture was therefore assumed in this study. The Selexol process is designed to capture about 90% of the CO_2 in the syngas. Carbon dioxide emissions will therefore originated from: (i) CO_2 not captured in the Selexol process, (ii) unconverted CO and CH_4 burned in the gas turbine combustor and (iii) CO_2 captured along with H_2S and vented in the Claus plant.

After the dilution with nitrogen from ASU for NO_x control, the hydrogen-rich fuel gas is saturated by using low temperature heat available from syngas cooling and then preheated to 200°C with IP water. Finally, the hydrogen rich fuel gas is sent to the power island and burned in the gas turbine combustor. Differences in volumetric air flow ratio at compressor inlet compared to the NG case are in the range of 1-2%, thus negligible. The calculated energy penalty efficiency related to capture is of approximately 11% points.

Table 3-19: mass flow rate, pressure, temperature and composition of the main fluxes of IGCC with carbon capture by Selexol. (Numbers refer to Figure 3-10)

Point	G	T	p	Composition, %mol.								
	kg/s	°C	bar	CH_4	CO	CO_2	H_2	H_2O	Ar	N_2	O_2	H_2S
1	39.0	15.0		Dry Coal 2%, see Table 3-3								
2	71.3	15.0	1.0	Air, see Table 3-1								
3	71.3	30.0	5.8									
4	49.9	257.6	23.9	-	-	-	-	-	-	100.00	-	-
5	10.8	80.0	88.0	-	-	-	-	-	-	100.00	-	-
6	34.2	180.0	48.0	-	-	-	-	-	3.1	1.9	95.0	-
7	136.9	298.0	41.1	0.0	56.3	2.9	26.0	4.8	0.9	9.0	-	0.2
8	57.8	200.0	41.1	0.0	56.3	2.9	26.0	4.8	0.9	9.0	-	0.2
9	153.1	263.1	40.2	0.0	27.9	1.4	12.9	52.8	0.4	4.4	-	0.1
10	15.1	250.0	39.4	0.0	4.4	24.9	36.4	29.3	0.4	4.4	-	0.1
11	153.1	35.0	36.7	0.0	0.9	28.4	39.9	25.8	0.4	4.4	-	0.1
12	91.0	25.0	110.0	-	0.0	99.0	0.4	-	-	0.6	-	-
13	9.0	200.0	23.2	0.0	1.1	2.3	48.0	15.3	0.5	32.8	-	-
14	15.5	146.0	4.0	-	-	-	-	100.0	-	-	-	-
15	10.3	140.0	4.0	-	-	-	-	100.0	-	-	-	-
16	138.2	337.2	144.0	-	-	-	-	100.0	-	-	-	-
17	15.8	300.0	144.0	-	-	-	-	100.0	-	-	-	-
18	3.5	300.0	54.0	-	-	-	-	100.0	-	-	-	-
19	11.9	300.0	54.0	-	-	-	-	100.0	-	-	-	-
20	20.7	343.0	144.0	-	-	-	-	100.0	-	-	-	-
21	13.3	148.5	144.0	-	-	-	-	100.0	-	-	-	-
22	15.7	300.0	54.0	-	-	-	-	100.0	-	-	-	-
23	102.5	339.0	144.0	-	-	-	-	100.0	-	-	-	-
24	10.9	130.0	41.1	-	-	-	-	100.0	-	-	-	-
25	165.8	158.0	28.4	-	-	-	-	100.0	-	-	-	-
26	13.32	148.5	144.0	-	-	-	-	100.0	-	-	-	-
27	643.3	15.0	1.0	Air, see Table 3-1								
28	526.7	COT 1439.9	17.6					-				
		TIT 1360.0		-	-	1.1		21.3	0.9	69.1	7.7	-
		TIT_{ISO}1258.1		-	-	-	-	-	-	-	-	-
29	665.0	600.6	1.0	-	-	-	-	-	-	-	-	-
30	665.0	115.0	1.0	-	-	0.9	-	17.4	0.9	70.6	10.2	-
31	156.7	559.2	133.9	-	-	0.9	-	17.4	0.9	70.6	10.2	-
32	110.7	559.0	44.2	-	-	-	-	100.0	-	-	-	-
33	6.08	253.7	3.5	-	-	-	-	100.0	-	-	-	-
34	102.6	32.2	0.0	-	-	-	-	100.0	-	-	-	-
35	15.0	66.9	1.01	-	-	-	-	100.0	-	-	-	-
Net Power Output			**379.6**	**MW**		**Net Electric Efficiency**				**36.0**		%

Synthesis of thermodynamic results for four reference cases (two without capture and two with CO_2 capture) are shown in Table 3-20. Specific Primary Energy consumption for CO_2 avoided (SPECCA) is lower when ASC is assumed as reference case because it has a lower efficiency than IGCC.

Table 3-20: summary of reference cases power balances and emissions

	ASC	ASC with CO_2	IGCC	SELEXOL
Net Power Output, [MW]	758.6	562.4	422.4	379.6
Thermal Power Input$_{LHV}$, [MW]	1676.5	1676.5	896.5	1053.5
Net Electric Efficiency$_{LHV}$, [%]	45.25	33.55	47.12	36.03
Net Electric Efficiency$_{HHV}$, [%]	43.42	32.19	45.21	34.58
Emissions, [g_{CO2}/kWh_{el}]	772	104	732	99
CO_2 avoided, [%]	--	86.51	--	86.54
SPECCA (IGCC) (MJ_{LHV}/kg_{CO2})	--	4.92	--	3.71
SPECCA (ASC) (MJ_{LHV}/kg_{CO2})	--	4.16	--	3.02

REFERENCES

[1] **European Benchmark Task Force.** European best practice guide for assessment of CO2 capture technologies. 2011. Vol. http://www.energia.polimi.it/news/D%204_9%20best%20practice%20guide.pdf.

[2] **Abbott et al.** *Process for the production of Hydrocarbons. US 7,087,652 B2* United States, August 8, 2006.

[3] —. *Production of hydrocarbons by steam reforming and fisher-tropsch reaction. US 7,323,497 B2* USA, January 29, 2008.

[4] **Eva Sanchez, TNO researcher, personal communication December 2009.**

[5] **Kohl A, Nielsen R.** *Gas purification.* s.l. : Gulf Publishing Company, 5th edition, 1997.

[6] **Meissner III RE, Wagner U.** Low-energy process recovers CO2 . *Oil-Gas Journal.* Vols. 81, 55-58.

[7] **Romano M, Chiesa P, Lozza G.** Pre-combustion CO2 capture from natural gas power plants with ATR and MDEA processes. October 2008.

[8] **Gross, J and Sadowski, G.** *Perturbed-Chain SAFT: An Equation of State Based on a Perturbation Theory for Chain Molecules.* s.l. : Res. Ind. Eng. Chem. American Chemical Society, 01 18, 2001. Vol. 40, 4, pp. 1244-1260. 10.1021/ie0003887.

[9] **Chen, Chau-Chyun.** Personal Communication.

[10] Gas Turbine World . *Handbook.* 2009.

[11] **Franco F, Bolland O, Manzolini E, Macchi E, Booth N, Rezvani S, Pfeffer A.** *Common Framework Definition document.* 2009.

[12] **Franco F, Anantharaman R, Bolland O, Booth N, et al.** Common framework and test cases for transparent and comparable techno-economic evaluations of CO2 capture technologies - the work of the European Benchmark task Force. *Proceedings of GHGT-10 international conference, Amsterdam 2010.*

[13] **Shell Global Solutions.** *Shell Coal Gasification Process for Generic IGCC with Carbon Capture Evaluations.* April 2009.

[14] **Manzolini G, Macchi E, Binotti M, Gazzani M.** Integration of SEWGS for carbon capture in Natural Gas Combined Cycle. Part B: Reference case comparison. *International Journal of Greenhouse Gas Control.* 2011. Vol. 5, 2, Pag 214-225.

[15] **NETL.** Shell Gasifier IGCC Base Cases. *www.netl.doe.gov/technologies/coalpower/gasification/pubs/pdf/system/shell3x.pdf.* [Online] April 2008.

[16] **Foster Wheeler.** *Potential for Improvement in Gasification Combined Cycle Power Generation with CO2 Capture.* s.l. : IEA , 2003. PH4/19.

[17] **NETL.** *Cost Performance Baseline for Fossil Energy Plants.* s.l. : www.netl.doe.gov/energy-analyses/pubs/BituminousBaselineFinalReport.pdf, April 2008.

[18] **Stork Engineering Consultancy B.V.** *Leading Options for the Capture of CO2 Emissions at Power Station.* s.l. : IEA, February 2000. PH3/14.

[19] **Valenti G, Bonalumi D, Macchi E.** A parametric investigation of the Chilled Ammonia Process from energy and economic perspectives. s.l. : Fuel 2011. dx.doi.org/10.1016/j.fuel.2011.06.035.

[20] **Prins, Mark and Shell.** Personal communication.

4 SHELL GASIFIER MODEL

Nomenclature and Acronyms

ACM: Aspen Custom Modeler
ASU: Air Separation Unit
CFD: Computational Fluid Dynamic
CGE: Cold Gas Efficiency
COS: Carbonyl Sulfide
DSZ: Downstream Zone
ERZ: External Recirculation Zone
GT: Gas Turbine
HHV: Higher Heating Value
HP: High Pressure
HPHT: High Pressure High Temperature
IGCC: Integrated Gasification Combined Cycle
IP: Intermediate Pressure
IRZ: Internal Recirculation Zone
JEZ: Jet Expansion Zone
LH: Lock Hopper
LHV: Lower Heating Value
LP: Low Pressure
PFR: Plug Flow Reactor
ROM: Reduced Order Model
RNM: Reactor Network Model
WGS: Water Gas Shift
WSR: Well Stirred Reactor

4.1 GASIFICATION TECHNOLOGY

Gasification is the process which allows producing energetically valuable gaseous product starting from carbonaceous feedstock. Devolatilization, combustion and gasification reactions occur in the gasifier, producing syngas, which consists mainly of CO and H_2. The range of potential fuels covers coal, biomass, oils and wastes.

There are three general families of commercial gasifier designs: fixed bed, fluidized bed and entrained flow. The syngas composition of each family and design of gasifier is different because of the operating conditions associated with each as reported in Table 4-1.

Table 4-1: main characteristics of different gasifier families.

Category	Fixed bed	Fluidized bed	Entrained flow
Ash conditions	Dry or slagging	Dry or agglomerating	Slagging
Feed characteristics			
- Size, mm	6-50	6-10	<100 μm
- Preferred coal rank	Any if dry process, high if slagging	Low or any	Any
Operating features			
- Outlet gas temperature, °C	425-650	900-1050	1250-1600
- Pressure range, bar	1-27	1-68	1-82
- Oxidant type	Air or oxygen	Air or oxygen	Air or oxygen
- Oxidant demand	Low	Moderate	High
- Steam demand	High for dry, low for slagging	Moderate	Low
Application	Synfuels or chemicals	IGCC or chemicals	IGCC or chemicals

Nowadays, the entrained flow gasifier is the only one which has been commercialized in several units, most of all for electric energy production or chemical synthesis (ammonia and methanol). This is mainly due to the ability to handle practically any coal as feedstock and to

produce a clean, tar-free gas [1]. Moreover, the ash is produced in the form of an inert slag. Entrained flow gasifier are definitely become the preferred gasifier type for hard coals and majority of commercial-sized IGCC.

Entrained flow gasifiers can be subdivided into a large variety of alternatives based on the design approach as reported in Table 4-2. Over 90% of syngas production capacity is accounted for by four designs: i) Shell Coal Gasification Process (SCGP), ii) GE, iii) ConocoPhillips (CoP) E-Gas and iv) MHI [2]. A brief description of the GE, E-Gas and MHI peculiarities are reported here and shown in Figure 4-1, whilst the SCGP, being the core of this work, is widely described in the rest of the chapter.

Table 4-2: Features of the important entrained-flow process, readapted from [1].

Process	Stages	Feed	Flow	Reactor wall	Syngas Cooling	Oxidant
Shell SCGP	1	Dry	Up	Membrane	Gas/water quench or syngas cooler	Oxygen
GE energy	1	Slurry	Down	Refractory	Water quench and/or syngas cooler	Oxygen
E-Gas	2	Slurry	Up	Refractory	Two-stage gasification	Oxygen
Siemens	1	Dry	Down	Membrane	Water quench and/or syngas cooler	Oxygen
MHI	2	Dry	Up	Membrane	Two-stage gasification	Air
Eagle	2	Dry	Up	Membrane	Two-stage gasification	Oxygen

- GE gasifier: the GE process for coal gasification uses a slurry feed downflow entrained-flow gasifier. The reactor is not cooled and a refractory lining is employed to make the gasification almost adiabatic. Syngas cooling is flexible and can adopt direct quench or radiant cooler with final quench. The slurry is charged into the reactor with a pump at the ractor typical pressure (50/60 bar). The feed burner is located on the top of the gasifier. The hot syngas leaves the gasifier from the bottom whilst the slag is sent to a quench bath where it solidifies.
- E-Gas gasifier: The E-Gas gasifier is a two-stage coal-water slurry feed entrained flow slagging gasifier. In the process scheme, the sub-bituminous coal-water slurry is injected into the hot gases leaving the first slagging stage, resulting in a much cooler exit gas. This mixture at about 1040 °C passes through a fire-tube syngas cooler, after which the char is separated from the gas in a particulate-removal unit featuring metallic candle filter. The char is then injected together with oxygen and/or steam into the first slagging stage at about 1400°C.
- MHI gasifier: the MHI gasifier combines the advantages of a dry feed entrained-flow reactor with two-stage feeding. The first zone, acting as a combustor, releases gas at very high temperature while liquid slag is easily separated. The oxidant is slightly enriched air. In the second stage more coal is introduced; heat for the endothermic gasification reactions is supplied by the very same gas of the first stage. Most of the char is gasified, the unconverted amount is separated in cyclones and candle filter and then recycle back to the first stage. Carbon conversion approaches 99.8%.

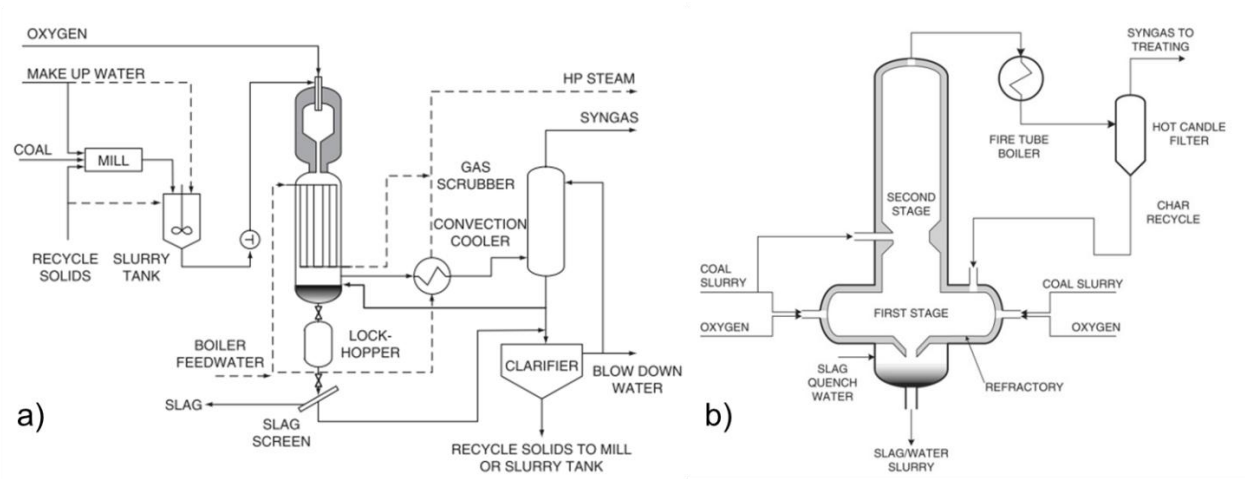

Figure 4-1: layout representation of: a) GE gasification process and b) E-Gas gasification process; readapted from [1].

4.2 GASIFIER KINETICS

The kinetic of coal gasification has been and still is a subject of intensive investigation. Despite of this, general commercial gasifier design is based on thermodynamic approach because homogeneous reactions can be described by simple equations. This cannot be applied for the heterogeneous equations, which imply complex mass transport phenomena in three phase system (a mechanism overview is shown in Figure 4-2). A simplified sequence of the heterogeneous reaction is: i) devolatilization (350-800°C) ii) volatiles combustion and iii) char gasification.

The overall gasification process is controlled by different mechanisms as mainly function of the temperature: in the hot zone the diffusion of gaseous reactants through the bulk results to be the controlling step whilst in the colder zone the chemical reaction rate is controlling. Finally, in the medium temperature zone, both the diffusion and chemical characteristic times play an important role.

The system aforesaid described is very complex and, so far, was likely to be accessible only via separated software; CFD for the fluid-dynamic and dedicated chemical tools for the kinetics. Nonetheless, as illustrated in paragraph 4.4, a new approach towards reactor modeling allows simulating the overall gasification process without simplifying the kinetic system. The core of this chapter illustrates a kinetic simulation of the overall Shell gasifier process; it is based on the work presented in [3].

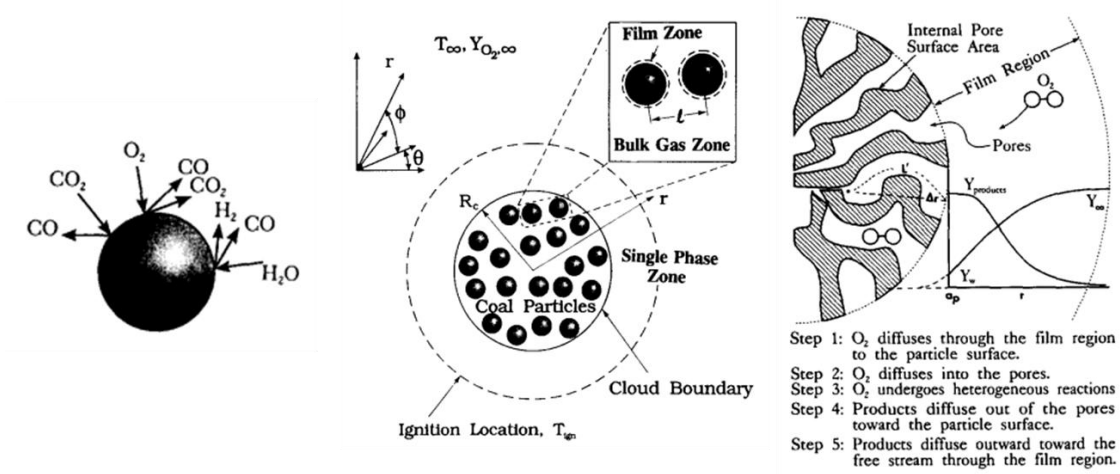

Figure 4-2: representation of the coal gasification process: on the left the heterogeneous reaction with a single particle, at the center a group of coal particles within a gas cloud and on the right the pore diffusion mechanism. Readapted from [4].

4.3 SHELL GASIFICATION PROCESS

The Shell gasifier is an upflow entrained flow reactor fed with pulverized coal through a number of diametrically opposed burners (4-6) placed in the bottom part of the reactor. The Shell process provides almost separate outlets for the syngas and the ash, with the gas leaving from the top and the larger amount of ash flowing out at the bottom side in the form slag. More than 70% of the ash content in the feed leaves as slag while the remaining stays with the syngas as flyash. The adoption of a dry feed gasifier with high carbon conversion (>99%) leads to higher gasifier efficiency (measured in terms of Cold Gas Efficiency) and higher plant efficiency, when compared to slurry fed gasifiers. Another advantage of the Shell process is the wide variety of coal that can be gasified in this dry-fed system. By using dry gases to pressurize the pulverized coal, there is no limitation on coal composition and the operating conditions. Moreover, the amount of oxygen required for gasification is lower than in slurry fed gasifiers. On the other hand, the gain in cold gas efficiency comes at the cost of higher plant complexity and cost; the higher operating temperature inside the gasifier results in more waste heat and a larger syngas cooler, and requires a water cooled reactor jacket. Even though the reliability of the dry coal feeding system has been one of the main issues during the initial stages of development, the issue has addressed and it no longer contributes significantly to the total downtime [5].

According to Shell, the gasification pressure is set up to 44 bar; there is a trade-off between the efficiency, which is higher at lower pressures, and the vessel size. Oxygen is produced in an ASU which is partially integrated with the gas turbine (GT) compressor: 50% of the air at the ASU distillation column comes from the GT compressor. Oxygen is fed to the gasifier at 180 °C [6]. Coal is dried before feeding it to the gasifier, limiting its moisture content to 2% by mass, to improve the flow through the lock hoppers and lower the amount of oxidant. The coal carrier is typically nitrogen, produced in the ASU, although it may be replaced by CO_2 for carbon-capture plants. Of the N_2 used for coal feeding, only part flows into the gasifier (around 40-50%), while the remaining is vented during the cyclic operation of the feeding process [7]. Finally a small

amount of N_2 is used to regenerate the candle filters for the syngas purification after the convective coolers. The hot syngas exiting the gasifier is quenched to 900°C with cold recycled syngas (at around 200°C). Molten slag entrained by the gas stream solidifies during the quench process while the syngas is cooled to 300°C in the syngas coolers, producing saturated HP and IP steam. The last syngas purification step inside the gasifier train is the wet scrubbing, where the remaining solids and soluble contaminants are removed. Syngas exits the scrubber at about 170°C and, after the regenerative heat exchangers, is sent to a catalytic bed for COS hydrolysis. The latter step is not required in case of pre-combustion CO_2 capture as COS is converted inside the WGS reactor.

Figure 4-3 shows a detailed representation of the Shell gasification process as described above. Data reported in Table 4-3 were obtained at the Politecnico di Milano by calibrating the property 0-D code (GS) in order to reproduce the Shell experimental data at the scrubber exit; this simulation is based on chemical equilibrium, adopting the approach-to-equilibrium method. The overall gasification process for a specific coal was reproduced and validated, and it was used to support the kinetic simulation developed in this work, and in assigning the values of oxidant, coal and moderator at the reactor inlet. Different Shell plant configurations based on chemical equilibrium are reported in [8].

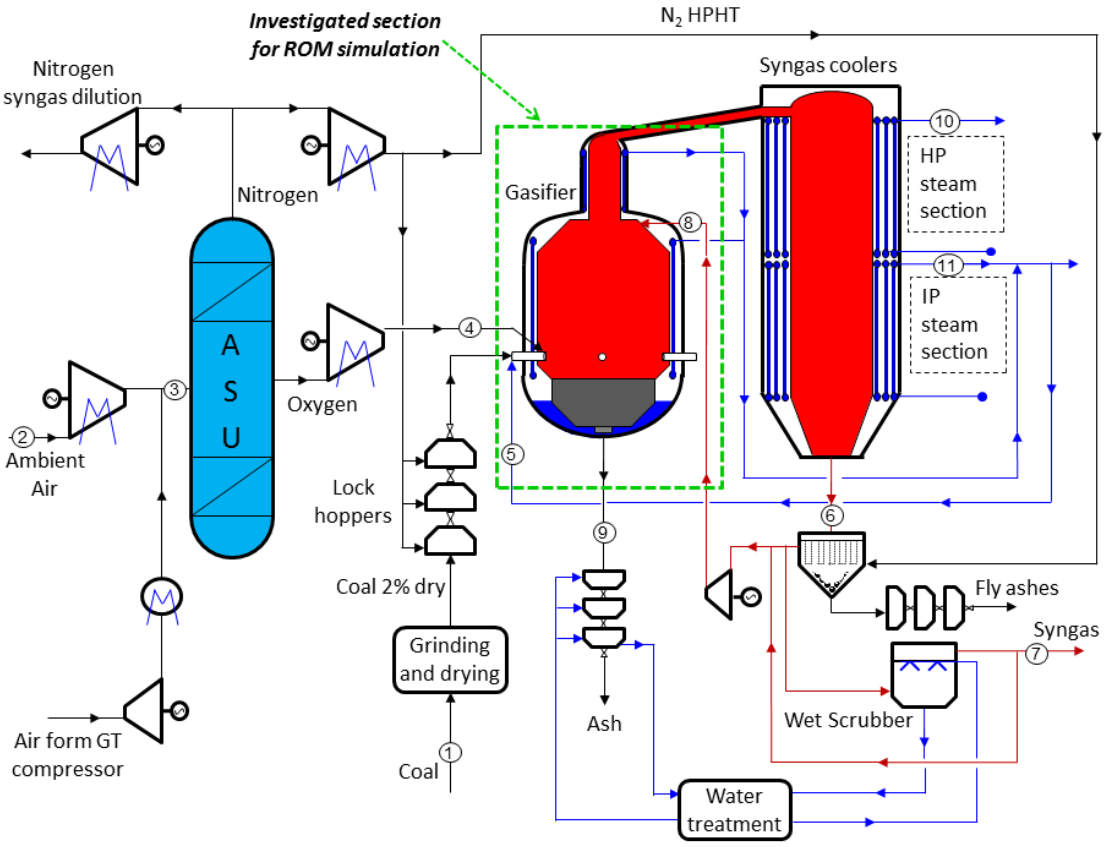

Figure 4-3: Overview of the Shell gasification process; gases and coal flows are shown in black lines, water in blue and syngas in red; the green dashed line emphasizes the gasifier section investigated in this study and reported with more details in Figure 4-4.

Table 4-3: Mass flow, pressure, temperature and composition of the reference Shell gasifier data [9]; data are obtained by calibrating a 0D simulation on the experimental measurements provided by Shell.

Point	G	T	p	Composition, %mol.								
	kg/s	°C	bar	CH_4	CO	CO_2	H_2	H_2O	Ar	N_2	O_2	H_2S
1	35.0	15.0	1.01	Premium Douglas coal as received, see Table 4-7								
2	60.7	96.0	5.76	-	-	0.03	-	1.03	0.92	77.28	20.74	-
3	121.4	60.7	5.76	-	-	0.03	-	1.03	0.92	77.28	20.74	-
4	29.1	180.0	48.0	-	-	-	-	-	3.09	1.91	95.0	-
5	2.97	300.0	54.0	-	-	-	-	100.0	-	-	-	-
6	115.1	300.0	41.1	0.009	56.66	2.92	26.22	5.09	0.86	8.07	-	.0176
7	76.7	158.5	41.06	0.008	50.55	2.61	23.39	14.47	0.78	8.04	-	0.157
8	49.3	213.8	44.44	0.008	52.22	2.69	24.16	11.66	0.79	8.31	-	0.162
9	5.0	> $T_{melting}$	48.0	Ashes [9]								
10	87.2	339.0	144.00	-	-	-	-	100.00	-	-	-	-
11	7.9	300.0	54.00	-	-	-	-	100.00	-	-	-	-

4.4 REDUCED ORDER MODEL

The structure, development and implementation of the Reduced Order Model (ROM) are reported in [10] [2] [11] and [12]. Only the basic concepts of the ROM are briefly described here. In the ROM the gasifier is represented by a Reactor Network Model (RNM). The RNM is based on using idealized chemical reactors (0-D WSR or 1-D PFR) to model different parts of the gasifier. For this reason, the ROM simulation may require some input from CFD. For modeling the current gasifier, the RNM model developed in [2] is chosen, which is based on work in [13] and [14]. The original model was set up for the GE or MHI gasifiers, which are different in several aspects from the Shell process [1]: i) the wall design (a refractory lining in GE, a membrane wall in Shell and MHI), ii) the flow direction (downward in GE, upward in Shell and MHI), iii) the number of burners (1 in GE, 4/6 in Shell, >4 in MHI), iii) the coal feeding system (wet in GE, dry in Shell and MHI) and iv) the number of stages (one in GE and Shell, two in MHI). The Shell gasifier and the correspondent RNM are shown in Figure 4-4 while Table 4-4 reports the geometry data. The Shell gasifier is subdivided into 4 zones:

- IRZ: Internal Recirculation Zone
- JEZ: Jet Expansion Zone
- ERZ: External Recirculation Zone
- DSZ: Downstream Section Zone

The formation of an ERZ downstream of the burner zone is caused by the low value of H/D. The radial dimension of the gasifier allows the stream to expand as it flows downstream with recirculation forming due to the wall impingement. The IRZ zone forms thanks to the high swirl number induced by the injection of coal at a finite angle with the radial direction. One of the main variables affecting the calculation is the diameter and the number of the burners. The cross-sectional area of the JEZ must be equal to the sum of the burners cross-sectional area; this is necessary to avoid unrealistic expansion or compression moving from the IRZ towards the JEZ. Therefore, the Shell ROM is implemented so that, given the geometry and the number of the burners, the JEZ inlet area will automatically have the correct value.

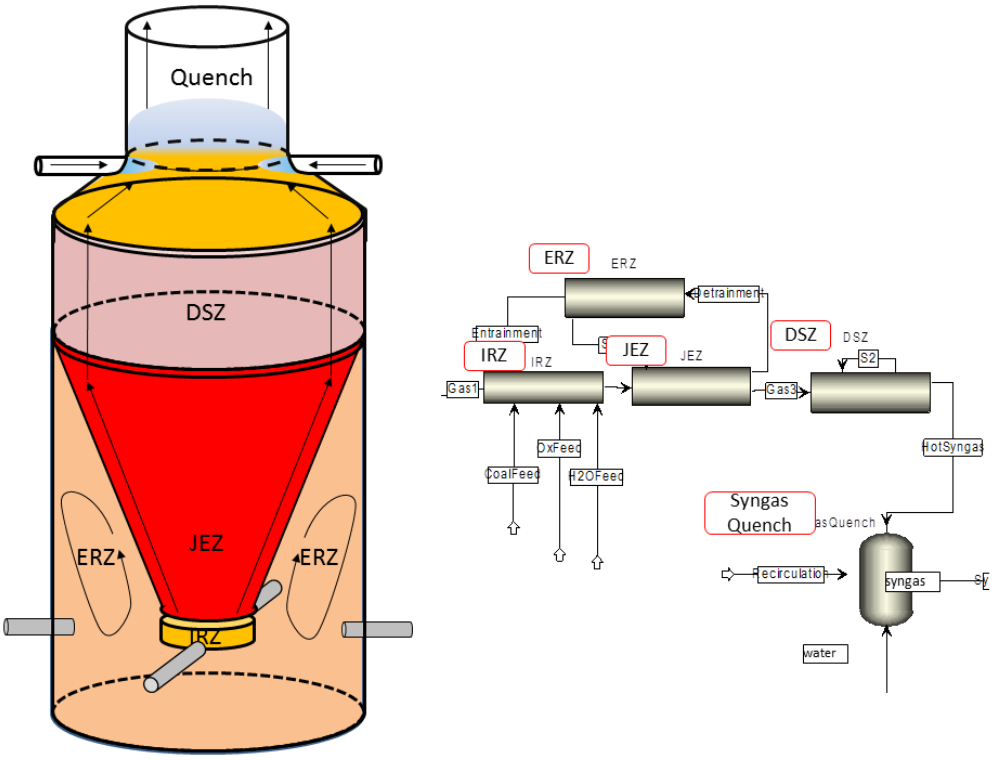

Figure 4-4: Shell gasifier RNM representation. On the left-hand side the physical macro areas subdivision inside the gasifier; on the right-hand side the equivalent reactor network model in Aspen Custom Modeler.

Table 4-4: The diameter and length of the gasifier reactor zones.

Zone	D inlet [m]	D outlet [m]	Length [m]
IRZ	0.25	0.25	0.20
JEZ	0.50	3.00	7.31
ERZ	n.a	n.a	7.56
DSZ	3.00	3.00	1.44

Figure 4-5 shows the organization of the ROM model: once the gasifier design is defined (geometry, recirculation ratio after JEZ and expansion angle) the reactors are sized and linked. Each reactor has its own set of conservation equations, 0-D or 1-D if WSR or PFR respectively, which require several submodels to close the system. In the absence of CFD simulations, the parameters for these reactors are chosen based on experience and some modeling. The modular structure of the ROM makes the model flexible and applicable to several types of entrained gasifiers. Once the geometry and the preliminary design are defined, the user can easily switch to different configurations modifying the conservation equations and adjusting the pre-defined parameters [10]. Anyway, a flow field CFD simulation is recommended in order to validate the zone division.

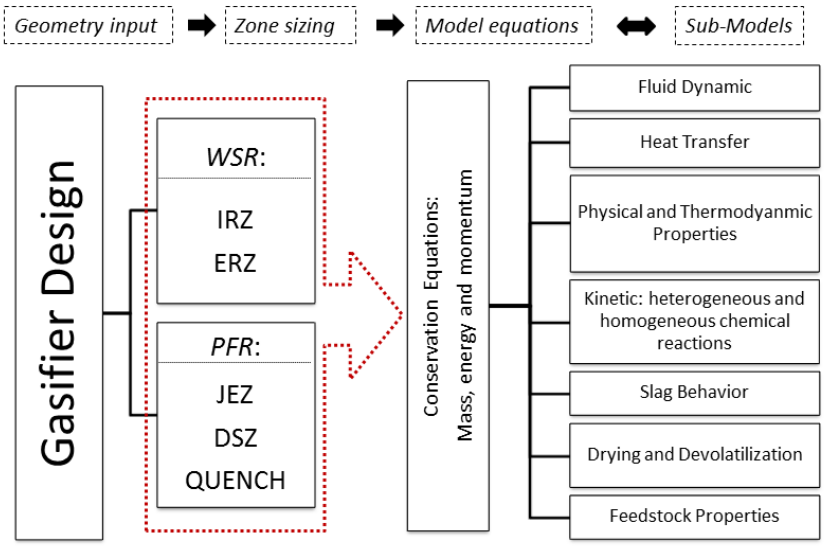

Figure 4-5: Shell gasifier ROM layout; the gasifier design supplies input to the zone sizing for each idealized reactor. Conservation equations for mass, energy and momentum (both gas and solid) are solved supplemented with several sub-models.

As mentioned above, the recirculation of gases between the JEZ to the ERZ is one of the most important parameter to be assigned. Ideally, it should be provided by CFD simulations [15] [16], which are currently not available for this family of gasifiers. Thus, this value was determined as in [2], using the method of Thring and Newby [17]. The effect of this value on the exit temperature and exit gas molar composition was investigated using sensitivity analysis and reported in Table 4-5. Results indicate that this sensitivity is very low.

Table 4-5: The parameters varied in the sensitivity study (temperature and composition at the gasifier reactor outlet) for different values of recirculation ratio. Sensitivity x→y is defined as x/y*(Δy/Δx).

Recirculation ratio	Temperature [°C]		CO dry [%mol]		H_2 dry [%mol]		CO_2 dry [%mol]	
Set value (2.3)	1588.62		63.41		26.40		1.07	
Variation [%]	ΔT [°C]	Sensitivity	CO [%]	Sensitivity	H_2 [%]	Sensitivity	CO_2 [%]	Sensitivity
1.8 (-22.0 %)	-1.4	0.006	+0.015	0.001	+0.022	0.003	-0.023	0.08
2.17 (-6.5 %)	-0.6		+0.004		+0.006		-0.006	
2.47 (+6.5 %)	+0.6		-0.004		-0.005		+0.006	
2.7 (+17.0 %)	+1.3		-0.006		-0.011		+0.011	

4.5 GEOMETRY AND COMPONENTS

The information reported in the next paragraphs were obtained through a comprehensive review of the literature and discussions with Shell for the EBTF project [9]. The gasifier is fed with around 3000 tons/day of coal, a common value for large Shell IGCC plant. The gasifier dimensions for this size have been inferred and approximated as follows: L = 9m, D = 3m. These values are consistent with recent literature [18] although they have been obtained separately and in different time.

4.5.1 BURNERS

The most common burner type is co-annular with coal, a carrier (N_2) and a moderator injected at the center, and oxygen injected from an annular passage [1]. Special attention is given to prevent burner front damage by employing internal cooling, and ensuring the contact of the fresh coal-oxygen stream with the hot syngas inside the reactor to initiate ignition [19]. Two techniques adopted to improve mixing include the use of different injection angles for the oxygen inside the burner before entering the gasifier, and arranging the burner at an angle with respect to the radial direction to create a swirling flow inside the gasifier [20]. Furthermore, the oxygen injector inside the burner can incorporate a swirler to improve mixing between oxygen and coal [1].

Some basic information is required here in order to determine the volume of the IRZ and the boundary conditions with the JEZ. Figure 4-6 reports the geometry considered, dimensions has been inferred from the Shell patent literature and then adapted to the reactant mass flow considered in this study.

4.5.2 MEMBRANE WALL

The Shell gasifier is equipped with a water-cooled membrane wall where IP steam is produced inside high-pressure steel tubes all around the reactor jacket. During operation, the primary thermal barrier is provided by the ash layer, composed by a solidified layer attached to the wall and a melted layer which flows towards the bottom of the reactor. A thin layer of castable refractory (generally silicon carbide) is anchored to the tube surface between the steel and the solidified ashes to prevent local damage and corrosion of the membrane wall [21]. As the membrane wall cannot stand large pressure difference, vessel pressurization is maintained by an outer steel vessel which incorporates an air layer between the gasifier outer wall and the membrane wall [1]. On the other hand, the amount of thermal energy removed from the reactor is higher than in the case of a refractory lined gasifier (such as the GE or the MHI). As such, the heat loss calculation is much more complex and critical for the accurate gasifier simulation (see paragraph 4.6). Heat losses through the reactor walls are in the range of 2-4% of the coal heating value [1].

4.5.3 TEMPERATURE CONTROL

The very short residence time in entrained flow gasifiers (in the range of 1-3 seconds [1]) complicates the control of the reactor operation. The Shell gasifier temperature can be controlled through two different parameters:

- The oxygen/coal ratio, which can provide large variation in the gasification temperature whose average is 1540 °C.
- The gasifier steam production, which can be used to lower the average gasification temperature, but with lower range than the oxygen/coal ratio variation.

In this work the oxygen to coal ratio is considered fixed. The simulation aims to model the process while fixing the incoming gasifier streams as shown in paragraph 4.3. The results, in

terms of the temperature and composition at the outlet, will then be compared with the available data.

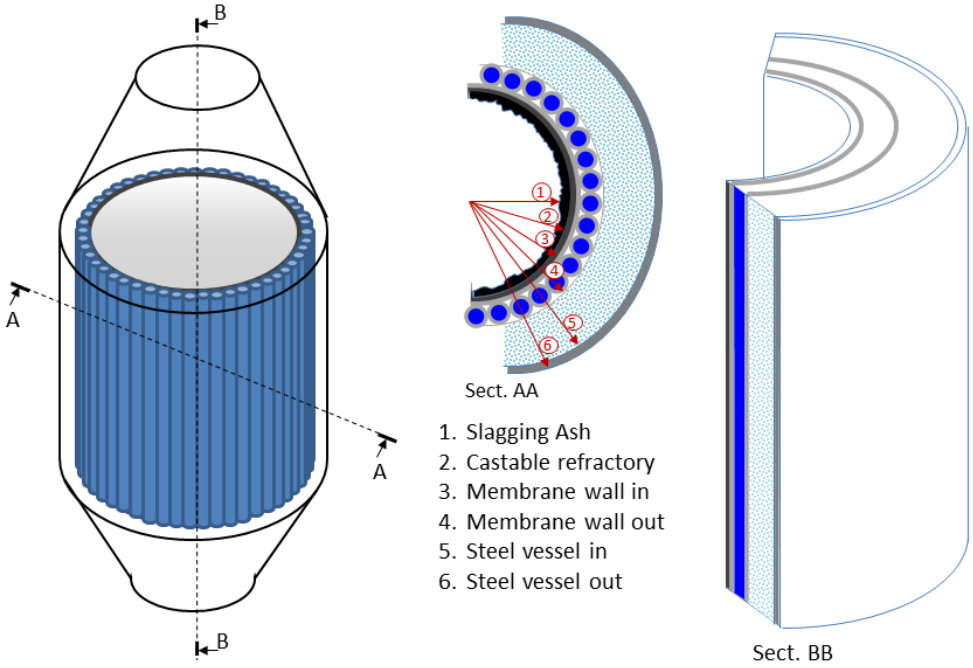

Figure 4-6: Representation of the Shell gasifier membrane wall; an overall view of the gasifier is shown on the left, horizontal and vertical sections are shown on the right.

4.5.4 SYNGAS QUENCH

The gas quench is carried out at the reactor outlet where the exiting stream temperature is around 1500 – 1600 °C. Most of the syngas cooling is then carried out in the syngas cooler through its membrane wall.

4.6 MEMBRANE WALL THERMAL MODEL

The membrane composite wall requires heat transfer analysis in the radial and axial directions. Energy balance is written for each wall layer in order to obtain the heat flux and the temperature profile. As shown in Figure 4-7, the composite wall can be divided into 6 layers:

1. Slag and solid ash layer: the model is based on a single ash layer of variable thickness along the vertical wall, modeling the slag layer built up as molten ash flows from the reactor interior toward the wall. Subdividing the layer into liquid and solid parts [22] would have required many more nodes and would have dramatically increased the cost of the calculations [2]. To analyze the mass and energy balances across a control volume of the slag layer, the following fluxes are considered: (i) the convective flux from gas to wall, (ii) the radiative flux from char particles to the wall, (iii) the mass flow of ash/slag approaching the wall (iv) the mass flow entering and exiting the control volume along the vertical and (v) the conduction flow to the thin castable wall.
2. Silicon carbide (refractory) layer: characterized by high conductivity, this layer receives heat from the attached slag layer releasing it to the membrane wall through conduction.

3. Tube jacket: this is the core of the composite gasifier wall and it is made of a number of vertical water tubes used to cool the wall. The water tubes are in contact with the refractory layer, and the buffer air layer. A steam-water mixture flows inside the tubes. The model must account for the complex heat transfer along the tube. Detailed description of the model is reported in paragraph 4.6.1.
4. Steam-water mixture: Heat is conducted across the tube walls into the water flowing through the tube, which experiences phase change while flowing upwards. Determining the heat transfer coefficient requires complex calculation, which takes into account the steam-liquid conditions at each location. Detailed description of the calculation is reported in 4.6.2. Considering a control volume of steam-water, the energy terms are: (i) the convective heat flow from the tube and (ii) the enthalpy of the incoming/exiting water mixture.
5. Air layer: the tube wall at high temperature transfers heat to the pressurized steel vessel through radiative exchange and to the air layer through natural convection.
6. Steel vessel and ambient air layer: in this final layer, heat is rejected to the ambient air through radiative and convective exchange.

No external insulation has been considered because no reference to external insulation was found. However, it may be required for the safe operation of the plant if the external wall temperature is higher than the safe minimum temperature. This would not make a significant contribution to the gasifier energy balance but it would slightly increase the steam production rate as it lowers the heat released to the ambient.

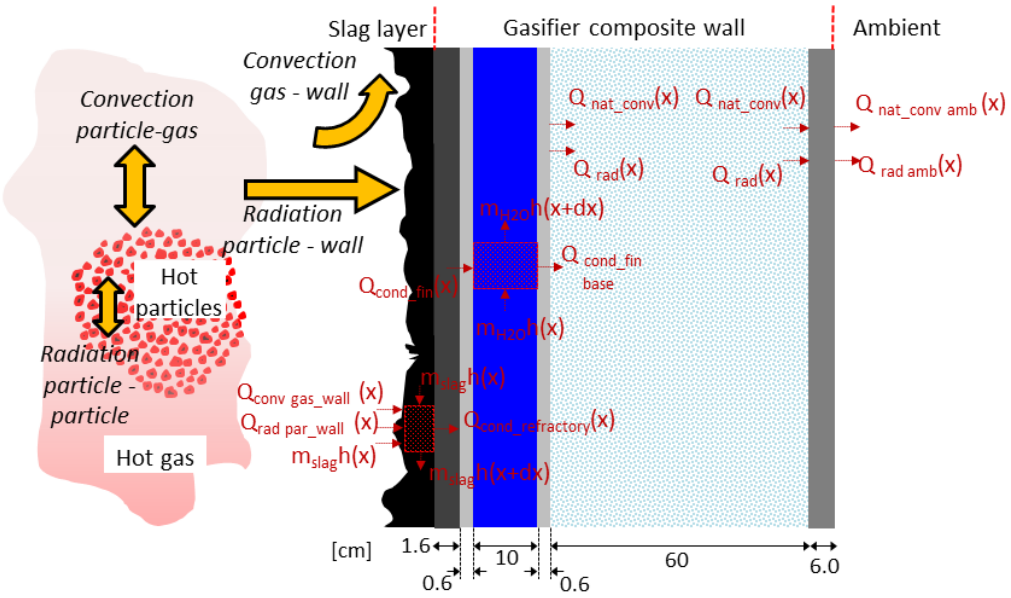

Figure 4-7: detailed schematics of the gasifier wall with a representation (red) of the heat fluxes considered in the energy conservation equations. Moving from inside to outside, the gasifier wall is composed of: (i) slag layer, (ii) castable refractory, (iii) membrane wall tubes (steel and water), (iv) air layer and (v) steel vessel.

4.6.1 EQUIVALENT MODEL FOR THE MEMBRANE WALL

Heat is transferred axially because of the peak temperature near the burners, and radially towards the walls. Nevertheless, because of the temperature distribution and the material heat conductivity, the heat transfer pathways can be simplified: in the radial direction heat flows from the refractory layer to the steel tubes. Indeed, thanks to the high convective heat transfer coefficient inside the tube, almost all the heat is transferred to the water, leaving a small amount to flow to the environment through the outer walls. Thus the tube wall temperature is approximately constant, slightly above the water saturation temperature. This can mathematically be represented using an equivalent fin model as shown in Figure 4-8. As shown in Figure 4-8a, half of the tube circumference acts as an extended surface which transfers heat to the water and to the air layer. Considering a pair of half tubes, the extended surface can be modeled as a fin whose thickness is twice the single duct thickness with a prescribed temperature at the fin (Figure 4-8b). This temperature has to be adjusted in order to satisfy the energy balance across the fin: the conductive heat transfer from the refractory layer must be equal to the convective heat transfer to the water plus the heat transferred to the air layer (both radiative and convective). Conservation of energy allows neglecting the heat transfer to the air layer, except at the end of the fin. Nevertheless, since the heat transferred to the air is a very small fraction of the total heat transferred to the gasifier wall, the temperature difference along the tube is small making this approximation acceptable.

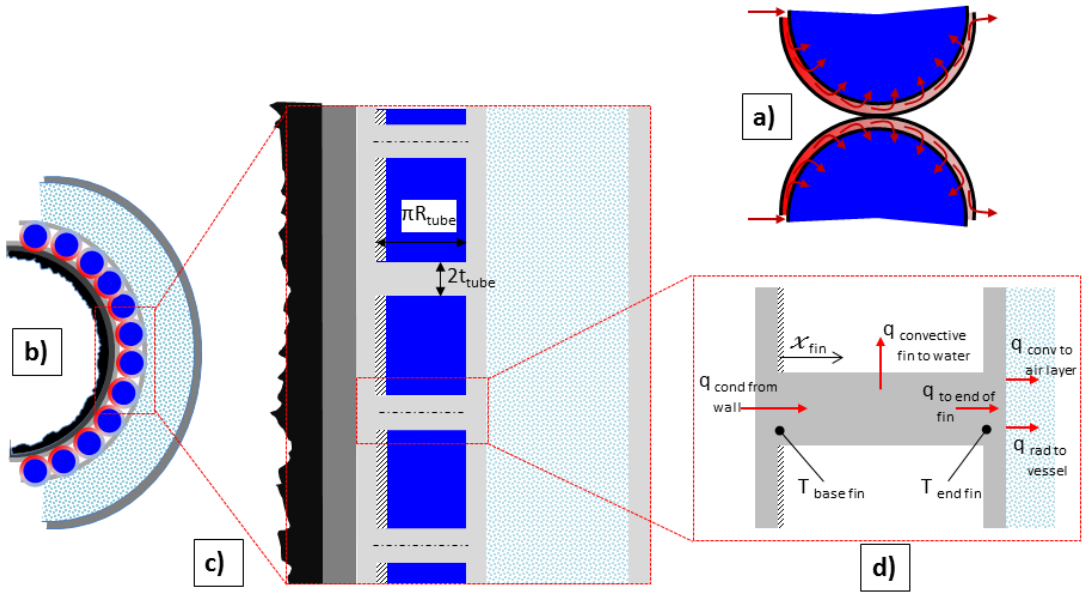

Figure 4-8: Schematic representation of the equivalent fin model. (a) ideal pathways for the heat along the tube section;(b) horizontal section of the gasifier with emphasis on tube layer; (c) horizontal sketch of the equivalent fin model; (d) detailed representation of one fin with the heat fluxes and main temperatures.

The equivalent fin model is described below. Equation (5-1) and (5-2) show the temperature and heat flux for a uniform cross section fin with prescribed tip temperature; applying the boundary conditions both at the fin base and at the fin end (the temperatures are given once the profile is obtained), the heat flux is obtained and shown in (5-3) and (5-4). The energy

conservation equations for the fin base, the coolant flow and the fin tip are written in (5-5), (5-6) and (5-7) respectively.

$$\vartheta(x) = \frac{\vartheta_0 \, sinh\big(m(L-x)\big) + \vartheta_L \, sinh(mx)}{sinh(mL)} \tag{4-1}$$

$$q_{fin}(x) = -kA_c \left[\frac{\vartheta_L m}{sinh(mL)} cosh(mx) - \frac{\vartheta_0 m}{sinh(mL)} cosh\big(m(L-x)\big)\right] \tag{4-2}$$

$$q_{fin}(0) = kA_c \left[\frac{\vartheta_0 m}{tanh(mL)} - \frac{\vartheta_L m}{sinh(mL)}\right] \tag{4-3}$$

$$q_{fin}(L) = kA_c \left[\frac{\vartheta_0 m}{sinh(mL)} - \frac{\vartheta_L m}{tanh(mL)}\right] \tag{4-4}$$

$$\frac{T_{refractory} - T_{basefin}}{R'_{equivalent}} = q'_{fin}(0) = 2kt \left[\frac{\vartheta_0 m}{tanh(mL)} - \frac{\vartheta_L m}{sinh(mL)}\right] \tag{4-5}$$

$$\begin{aligned} \frac{1}{L}\frac{d\dot{H}}{dx} &= q'_{fin}(0) - q'_{fin}(L) \\ &= 2kt \left[\frac{\vartheta_0 m}{tanh(mL)} - \frac{\vartheta_L m}{sinh(mL)}\right] - 2kt \left[\frac{\vartheta_0 m}{sinh(mL)} - \frac{\vartheta_L m}{tanh(mL)}\right] \end{aligned} \tag{4-6}$$

$$q'_{fin}(L) = q'_{rad-air} + q'_{conv-air} \tag{4-7}$$

The equivalent fin model allows the accurate calculation of the heat transferred to the water using vertical tube boiling correlations for power plant boilers. The flow parameters are calculated for a single tube, results are then extended to all the ducts (i.e. the correspondent equivalent fins).

4.6.2 TWO PHASE FLOW HEAT TRANSFER

Two-phase flow and heat transfer are complex processes. Internal convective boiling heat transfer is associated with bubble formation along the inner surface of the heated tubes where the liquid is flowing. Several correlations for two-phase heat transfer are available in literature [23] [24]. For this study, a recent correlation proposed by Steiner and Taborek, which accounts for the evaporation inside vertical tubes, is adopted. The local flow boiling heat transfer coefficient is obtained considering convective and nucleate heat transfer obtained from:

$$h_{tp} = \left[\left(h_{nb,0} F_{nb}\right)^3 + \left(h_{Lt} F_{tp}\right)^3\right]^{1/3} \tag{4-8}$$

The method for calculating the parameters in Equation (4-8) is not discussed here as it is extensively reported in literature [25]. The two-phase flow multiplier F_{tp} is a function of the steam quality, which can be calculated once the heat transfer coefficient has been found; therefore the wall heat problem solution is iterative. The procedure adopted for the temperature profile calculation is shown in Figure 4-9 and can be summarized as: the first step lies in the resolution of the energy conservation equations as set by the equivalent fin model; once local water enthalpy has been obtained, all the water properties can be inferred as function of pressure and enthalpy, included the steam quality. Next, h_{tp} is calculated and the temperature profile is obtained.

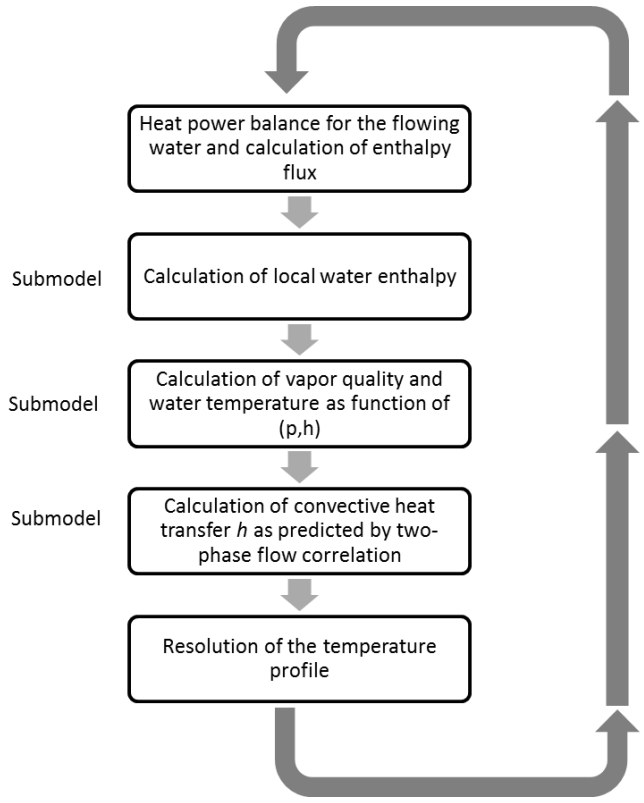

Figure 4-9: Process schematics for the heat transfer calculation steps for the two-phase flow prediction inside the tube.

Particular attention is paid to the conditions reached inside the tube in order to guarantee the system integrity. In particular, steam bubbles must not be allowed to stick to the tube wall as this could lead to local damages. Hence, the steam quality and the inlet velocity must be checked in order to satisfy two conditions: (i) bubble or slug flow inside the tube and (ii) good turbulent wet wall flow; that is, respectively, maximum steam quality of 0.4 and minimum inlet velocity of 0.15 [m/s] [26]. System control is carried out inside the ROM while modifying the global amount of water circulating in the membrane wall.

4.6.3 NATURAL CONVECTION AND RADIATION INSIDE AIR LAYER

Heat inside the air layer is transferred through radiation and natural convection, with the latter less important but still not negligible. The radiative component is calculated assuming radiative heat transfer for long concentric cylinders; emissivity is function of temperature. Due to the high

gasifier diameter, plane wall correlation is used to find an approximation of the natural convection term.

4.7 SYNGAS QUENCH AND COOLING

The Shell gasification process features several composition and temperature changes not only inside the gasifier but also in the syngas cooler, scrubbing and the COS hydrolysis. As mentioned before, the syngas quench is carried out by mixing hot syngas with cold recirculating syngas. Being at high temperature (syngas leaves the gasifier reactor at 1500-1600°C), cooling and quench are necessary for further reactions. Homogeneous chemical reactions during quench can contribute to hydrogen formation if the water-gas shift rate is sufficient. The WGS reaction inside the quench depends on the mixing rate: if the mixing rate is fast, the temperature gradient is high with a steep temperature drop at the inlet of the quench zone. In this case, since the uncatalyzed water-gas shift rate is sufficient at least above 1000-1100 °C, hydrogen production is negligible. On the other hand, if mixing is slow along the quench section, the temperature change of the incoming hot gases is slower allowing the WGS to remain reactive. In entrained flow gasifiers, a critical issue which must be addressed is ash sticking on the syngas cooler wall. Fly ash together with other solid particles leaving the gasifier must be cooled rapidly to values below the ash melting temperature, reaching the solid state before approaching the non-slagging wall. That is, mixing has to be vigorous enough to guarantee a high temperature gradient. Although hydrogen production is probably negligible inside the quench zone, kinetic simulation during gas mixing has been implemented in order to make the Shell ROM as flexible as possible.

Under quench operating conditions, the syngas quench zone is modeled as a plug flow reactor with two different choices for the mixing of the fresh and recirculating syngas: (i) perfect mixing at the recirculation inlet, or (ii) progressive mixing along the duct using two discretization zones, ten nodes with user defined mixing ratios. Both cases are not adiabatic but feature the interaction with the wall, which is considered to be a membrane jacket as in the reactor zone.

As carbon conversion is possible only inside the gasifier reactor, it is assumed that the solid particles are chemically frozen in the quench zone, i.e. no heterogeneous reactions are allowed during quench. The particles are mainly composed by ash and unconverted carbon, which accounts for the carbon left in the particle at the end of gasification. In this zone, particles interact with their environment only via heat and momentum exchange. Being below the melting temperature and having assigned composition, the particle structure is considered fixed along the quench duct.

The primary role of the quench kinetics model is to assess whether the gas mixing is at equilibrium but not to evaluate change in particle composition. The considered conservation equations for this section of the model are reported in Table 4-6

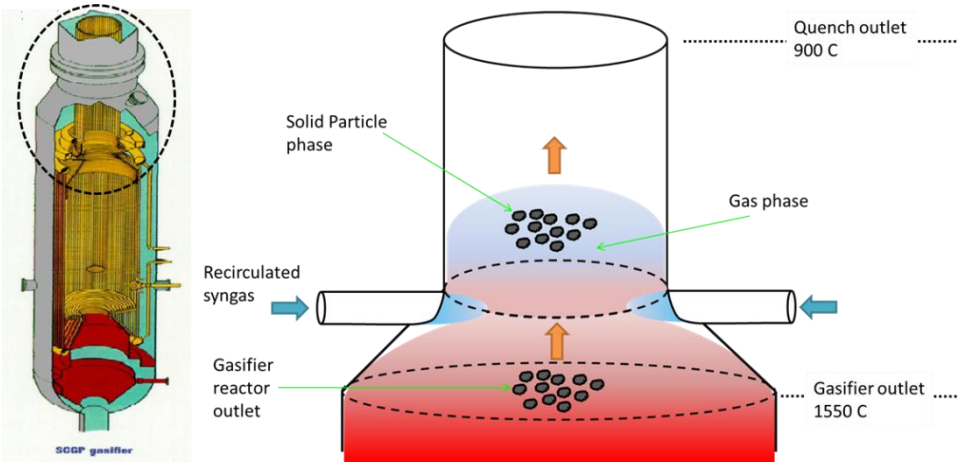

Figure 4-10: A schematic drawing of the gas quench process; on the left-hand side the quench area of the gasifier, on the right-hand side, a representation of quench process.

Table 4-6: Conservation equations considered in the syngas quench model.

	Gas phase	Solid phase
Mass Balance	• Axial Diffusion • Axial Convection • Homogeneous reactions	• Constant
Energy Balance	• Axial conduction • Axial convection • Convection gas-particle • Convection gas-wall	• Axial Convection • Convection gas-particle • Radiation particle-wall • Radial radiation particle
Momentum Balance	• Axial momentum flux • Axial pressure gradient • Axial gravitational force • Viscous interaction gas-wall • Viscout interaction gas-particle	• Axial momentum flux • Axial gravitational force • Viscous interaction gas-particle

4.8 ASSUMPTIONS AND METHODOLOGY

The modeling study was carried out using Aspen Custom Modeler®. Aspen Plus® and GS© were adopted in order to model water scrubbing and the overall gasification process, respectively. Coupling these tools, which provide different levels of detail, allows a more comprehensive gasification process simulation. The RNM was developed and solved in Aspen Custom Modeler (ACM), an AspenTech product. ACM is used to create rigorous models of process equipment and to apply these equipment models to simulate and optimize continuous, batch, and semi-batch processes [27].

Other simulation assumptions are reported in Table 4-7. The membrane wall design has been inferred from available information; Von Mises and Mariotte criteria have been used to check the thickness of the pressurization vessel and the membrane wall tubes respectively. Both thicknesses were sufficient to support the stresses induced by gasification pressure (44 bara) and intermediate steam pressure (54 bara); moreover recent literature [28] reports almost same design values.

Table 4-7: Simulation assumptions.

Ambient conditions	15 °C / 1.013 bar / 60% RH			
Air composition, dry molar fraction (%)	N_2 78.08%, CO_2 0.04%, Ar 0.93%, O_2 20.95%			
Douglas Premium coal characteristics [9]				
Ultimate analysis [%]	C	66.52	O	5.46
	N	1.56	Clorine	0.009
	H	3.78	Moisture	8.0
	S	0.52	Ash	14.15
Proximate analysis [%]	Fixed Carbon 54.9, Volatiles 22.9, Moisture 8.0, Ash 14.15, Total Sulphur 0.52			
Coal LHV, HHV	25.17 MJ/kg, 26.23 MJ/kg			
Oxygen composition	95% O_2, 3.1% Ar, 1.9% N_2			
Oxygen conditions	180 °C, 48 bar			
Moderator steam	300 °C, 54 bar			
Nitrogen for coal feeding (lock hoppers)	80 °C, 88 bar			
Gasifier Geometry				
Height	10 m			
Inner diameter	3 m			
Inner quench diameter	1 m			
Steel vessel thickness	0.06 m			
Gasifier pressure	44 bar			
Membrane Wall				
Tube diameter	0.1 m			
Tube Thickness	0.006 m			
Steel emissivity at 250 °C	0.24			
Steel emissivity at 50 °C	0.22			
Membrane wall internal pressure	54 bar			

4.9 RESULTS AND DISCUSSIONS

The reference simulation was performed using the mass balance reported in Table 4-3, for a 3000 ton per day of coal. Sensitivity analyses were used to investigate the effects of primary variables.

4.9.1 SYNGAS, PARTICLES AND GASIFIER WALL TEMPERATURE

Temperature profiles inside the gasifier are shown in Figure 4-11. The gas and particle temperatures are shown along the centerline whilst the slag temperature is shown at the wall. The gas and particles are in thermal equilibrium for almost all of the gasifier length except in the combustion zone where the volatiles are burnt to supply energy for char gasification. A temperature peak is observed in the combustion zone at the JEZ inlet. The temperature decreases sharply in the zone where gasification takes place. Following carbon conversion, the temperature changes due to the heat loss to the membrane wall. The temperature decreases a bit steeper in the DSZ than in the last part of the JEZ. Along the JEZ, convective heat transfer to the wall is computed using the gas temperature of the recirculation zone (ERZ) which, because it is modeled as a WSR, is spatially uniform. However this does not affect the radiation term and results in a negligible, although visible, variation.

The computed temperature at the exit is 1588 °C, which is higher than the value assumed for the 0-D simulation reported in paragraph 4.3 (1550 °C) but still consistent with the temperature range generally provided by Shell (1550-1600 °C) [29] [30] and [31]. The slag temperature refers to the inner value of the slag layer; the corresponding variation along the gasifier is small thanks to the contact with the membrane wall which prevents high temperature peak.

The steam quality and the two-phase heat transfer along the gasifier are shown in Figure 4-12. The heat transfer coefficient is strongly dependent on the heat flux at the wall; hence the highest value occurs in the combustion zone, decreasing smoothly in the rest of the gasifier. Consequently, steam quality features a steeper increase in the combustion zone where the heat transfer coefficient is higher while it increases in the rest of the gasifier. The outlet steam quality fraction is around 0.25 which is typical of the evaporative section inside large steam generator. This would also fit well with standalone gasifier steam plant.

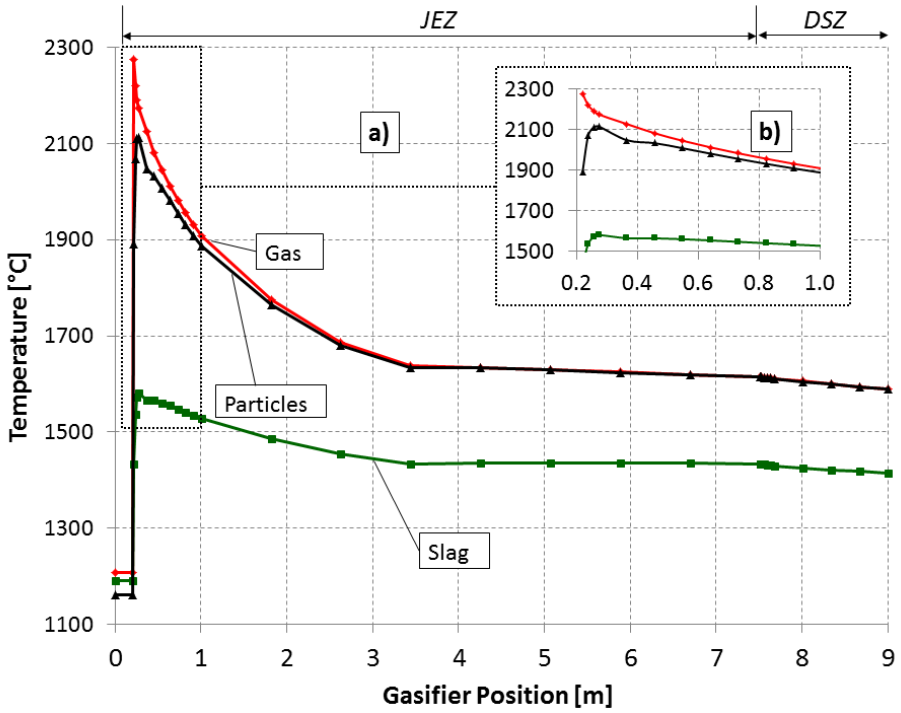

Figure 4-11: Gas, particle and slag temperature profile inside the gasifier; (a) overall gasifier reactor and (b) details from inlet to 1m height.

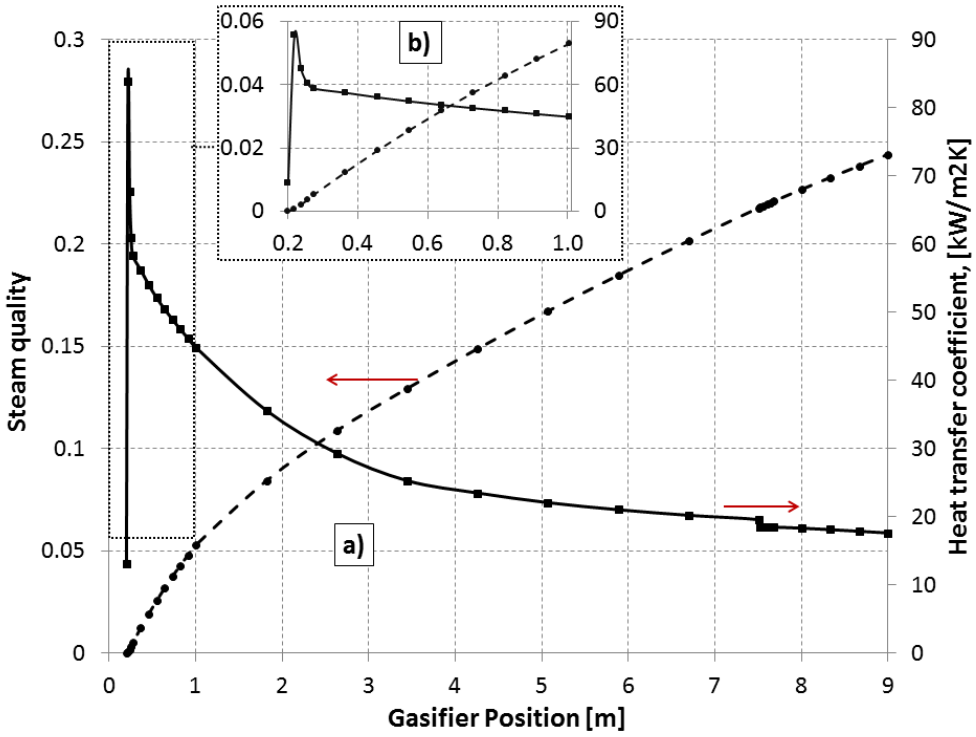

Figure 4-12: (a) The steam quality and the two phase heat transfer coefficient variation along the gasifier. Steeper steam quality variation is seen in the combustion zone, where the heat transfer coefficient experiences a peak; (b) detail of steam quality and two-phase heat transfer along the first part of the gasifier.

Figure 4-13 shows the temperature profile along the gasifier wall. The largest temperature gradient is located across the slag layer allowing the membrane walls to stay relatively cool. This is consistent with values obtained in CFD simulations [32] [33]. Moreover, [1] reports that the tubes are almost at the water-steam temperature, within a range of 250-300 °C depending on the evaporation pressure. Nevertheless it must be noted that the ROM underestimates the slag layer thickness (there is no calculation for a liquid-solid interface). The refractory temperature is close to the tube temperature because of the high thermal conductivity of steel compared to the solidified slag. The external vessel temperature is around 50 °C. This is because the air layer thickness guarantees good insulation despite the radiative term.

Figure 4-14 shows a comprehensive representation of the tube temperature along the entire gasifier length (x-axis), moving from the inside to the outside (y-axis). The temperature variation is reduced by the high two-phase heat transfer value; therefore the tube temperature is within the range of 280-260 °C. Accordingly, the peak temperature is located in the combustion zone.

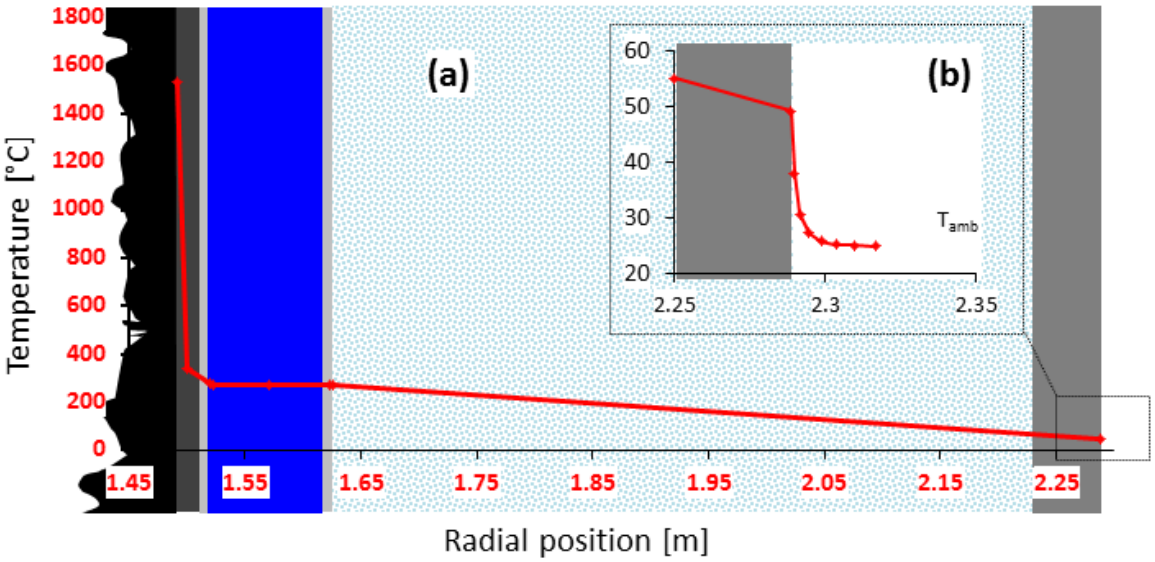

Figure 4-13: (a) The temperature profile along the gasifier composite wall; slag, refractory, tube, evaporating water, air layer and steel vessel. Values refer to the middle position of the overall height; (b) detail of the temperature profile at the steel vessel - ambient interface.

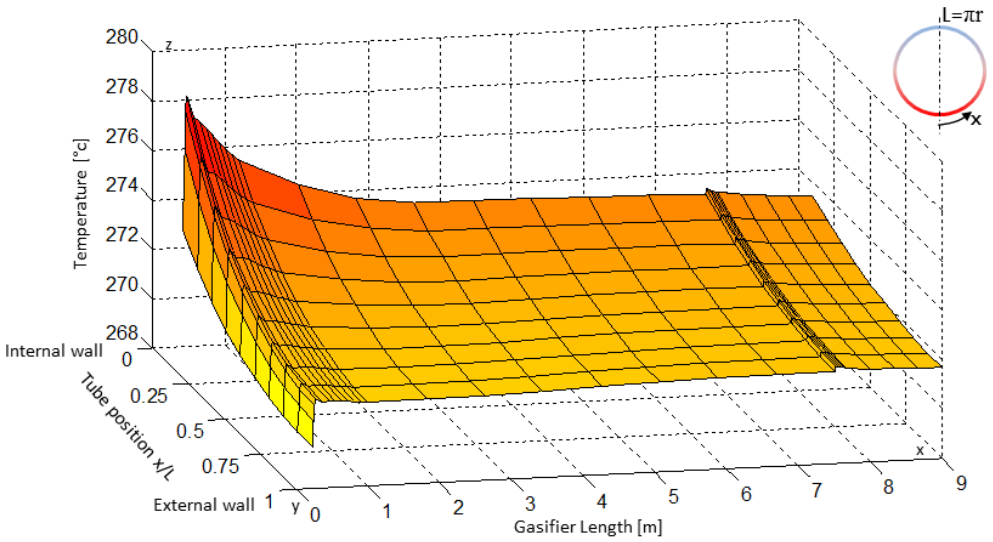

Figure 4-14: The temperature variation along the membrane jacket. On the x axis, the radial position of the tube measured with respect to the overall semi circumference (i.e. 0 corresponds to the inner face while 1 to the external face), on the y axis the gasifier length and on the z axis the temperature distribution. The small step visible around y=8 is due to the sudden change from the JEZ to the DSZ as assumed by the ROM.

4.9.2 SYNGAS COMPOSITION

The gas composition inside the gasifier is shown in Figure 4-15. At the combustor inlet, inside the IRZ, devolatilization and coal drying take place; all moisture leaves the particles upon heating whilst part of the non-carbon and the carbon species remain in the char after the devolatilization (Merrick model has been adopted here [10]). The products of devolatilization are: char, CH_4, C_2H_6, CO, CO_2, tar, H_2, H_2O, NH_3 and H_2S. As the mixture enters the JRZ, O_2 is almost instantaneously consumed; H_2O and CO_2 are formed as a result of the combustion of H_2 and char with O_2. As the particle-gas mixture leaves the combustion zone, char gasification takes place; H_2O and CO_2 decrease due to hydro-gasification, the water-gas shift and Boudouard reaction. Hydrogen increases thanks to the WGS. As shown in Figure 4-16a, the most important heterogeneous reaction is the hydro-gasification which has the highest rate, the Boudouard gasification reaction, and partial combustion are noticeable although the reaction rates are respectively one or two order of magnitude lower than the water gasification. According to the simulation results shown in Figure 4-16b, almost complete carbon conversion is already reached few meters after the inlet; this seems to be a common feature of most commercial entrained flow gasifier, especially GE and Shell, and it is consistent with several CFD simulations [34]. This result can be explained considering that the initial gasifier designs have probably been conservative; it would also be consistent with the recent operator tendency to increase the coal feedrate to the same gasifier (till 4500 tons/day for a Shell gasifier). Finally, it must be underlined that the power-law kinetic tends to predict higher conversion rate.

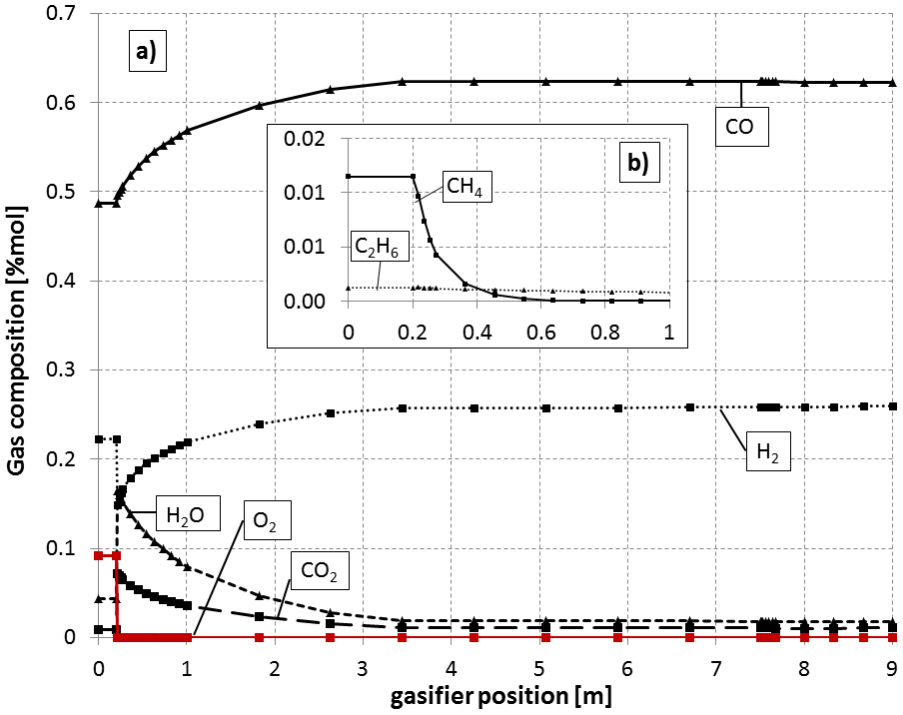

Figure 4-15: Gas species molar composition along the gasifier; (a) CO, H_2, O_2, H_2O, CO_2, (b) Zooming at gasifier inlet for CH_4 and C_2H_6.

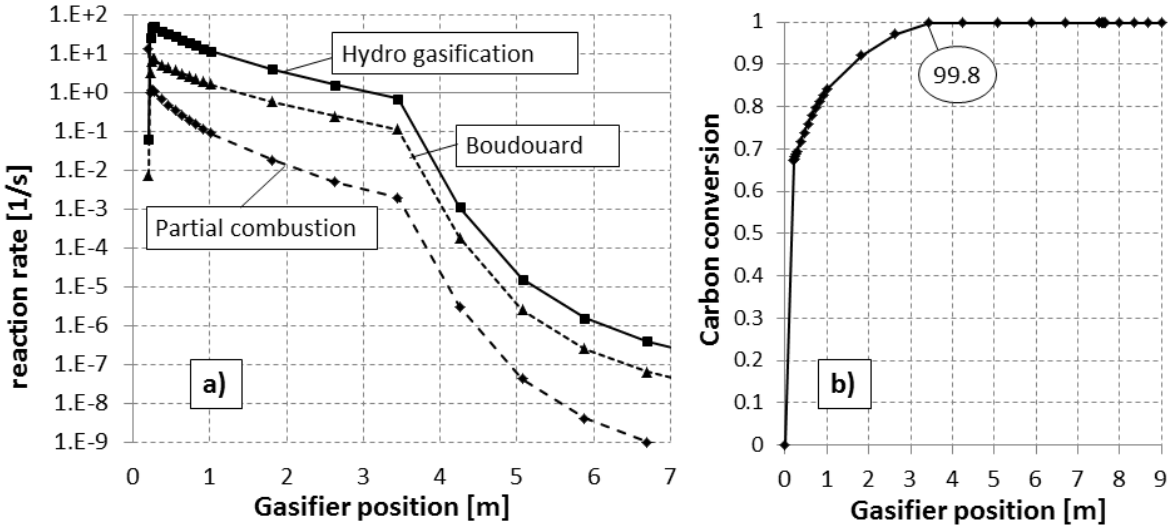

Figure 4-16: (a) The reaction rate profile along the gasifier length for the heterogeneous reactions (steam gasification, Boudouard and partial oxidation); (b) carbon conversion along the gasifier length. The steep drop in the reaction rate in (a) at around 4 m corresponds to approaching the maximum carbon conversion in (b).

The axial velocity and pressure are shown in Figure 4-17. Once injected in the IRZ, the flow expands in the JEZ reaching the maximum velocity as soon as the expansion starts. Particles peak velocity is lower and is delayed compared to the gas velocity due to the higher solids inertia. Around three meters after the reactor inlet, the solids and the gas velocity profiles match. The pressure field reflects the velocity profile: after a minimum at the expansion inlet (the region with higher speed) the pressure increases as the gas slows down. To the first approximation, the

residence time is function of the gasifier axial velocity profile; minimum values calculated for the higher local velocity are: i) IRZ: 0.003 [s], ii) JEZ: 0.616 [s] and iii) DSZ: 0.952 [s]. Because the gasifier is operating at steady state, the recirculation zone does not affect the total residence time. Hence, considering the IRZ, the JRZ and the ERZ the total residence time is about 1.6 [s], a value consistent with the residence time for entrained flow gasifiers reported in [1] (1-5 [s]).

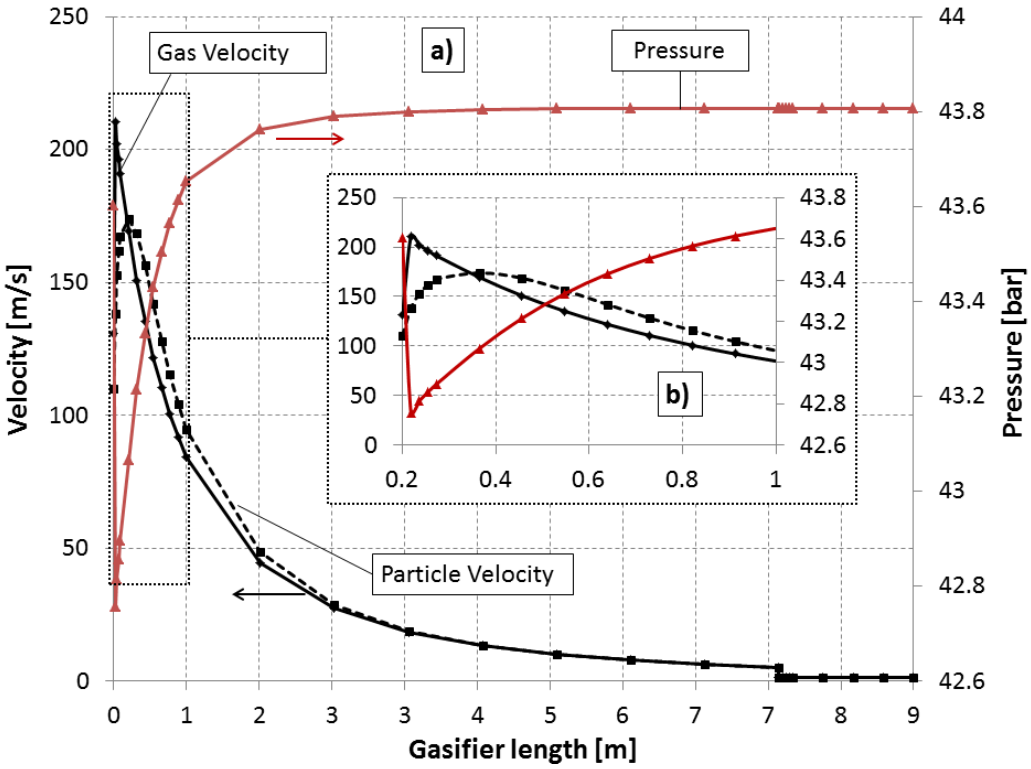

Figure 4-17: The gas velocity, particle velocity and pressure along the gasifier. The pressure and velocity are linked in the momentum equation. The steep decrease of velocity along the boundary from JEZ to DSZ is are caused by the drop in the mass flow arte due to recirculation.

4.9.3 OVERALL GASIFICATION TEMPERATURE AND COMPOSITION

The overall gasification process can be represented by three different zones, placed at the outlet of: i) the gasifier reactor, ii) the quench exit and iii) the scrubber exit. The ROM provides detailed information for both the gasifier reactor and the quench, whilst scrubber process has been simulated in Aspen Plus. Table 4-8 shows the temperature, pressure, mass flow and molar composition for the gas phase at the outlet of abovementioned sections. The change in molar composition along the quench is mainly due to the mixing with the recirculated syngas partially after the convective coolers and partially after the scrubber. The scrubber process can be represented as saturation and gas purification which does not affect the chemical composition but only the water content. One of the main objectives of this study was to develop a kinetic simulation which could reproduce the gasification process without requiring calibration against supplied composition data (for example adjusting the degree of reaction or the approach to the equilibrium). Table 4-8 reports a comparison between the ROM results, the equilibrium results for the same flow and the Shell data (available only at the scrubber exit). The equilibrium case

does not consider methane formation throughout the gasifier and reflects only gas phase equilibrium, i.e. an equivalent gas composition for incoming coal is adopted which satisfy atomic balance and LHV-HHV values.

Equilibrium simulation produces results close to the ROM as far as the gasifier reactor outlet is concerned; this, as shown in Figure 4-15 and Figure 4-16, is due to the fast complete char conversion in the gasifier. It must be emphasized that the equilibrium model is limited to the gas phase and does not describe the solid particle behavior. Larger differences arise when quench is considered; equilibrium calculations are affected by the higher conversion of CO due to water-gas shift. Outlet quench temperature is higher thanks to the heat released by the exothermic reaction. The scrubber process is not affected by the chemical reactions; hence the differences are only due to the incoming composition (the temperature and pressure are the same after the syngas coolers). According to the results shown in Figure 4-18, where it is also compared with the data provided by Shell, the final dried gas composition calculated using equilibrium is influenced by the overprediction of carbon dioxide and hydrogen. On the other hand the ROM model predicts lower H_2 and CO_2 content, i.e. lower WGS reaction rate. The cold gas efficiency is few percent points above 80%, which is in good agreement with typical Shell values, here available only after the scrubber. The ROM predicts 82.5%, very close to reference 82.8%. Equilibrium case CGE is lower, 82.0%, due to higher CO conversion. From an overall process point of view, the gasification itself accounts for most of the efficiency loss while only 0.7 percent points are lost in the quench and the scrubbing process (0.9 for the equilibrium case). The cold gas efficiency at the quench exit is not meaningful due to the gas recirculation. The results predicted by the equilibrium model are meaningful as long as CH_4 is excluded from reactions, most of all during the quench, otherwise around 1% of methane would be present at the scrubber outlet.

Table 4-8: Temperature, pressure, mass flow, composition and cold gas efficiency for the gas phase at the most relevant points of the gasification process. Values are reported using the ROM developed in this work and for an equilibrium model with the same boundary conditions. CGE for Shell data are calculated using the syngas composition reported in this table [35].

	T [°C]	p [bar]	G [kg/s]	Chemical species molar concentration [%mol]								CGE [%]
				CO	H_2	CO_2	H_2O	CH_4	H_2S	N_2	Ar	
Kinetic ROM model												
Gasifier exit	1588.0	43.8	65.9	62.28	25.93	1.05	1.78	--	0.17	7.87	0.91	83.2
Quench exit	932.0	43.8	115.1	58.20	24.32	0.99	7.50	--	0.15	7.97	0.87	--
Scrubber exit	160.6	41.1	76.7	51.90	21.72	0.84	16.70	--	0.13	7.94	0.77	82.5
Equilibrium model												
Gasifier exit	1536.6	43.8	65.9	62.09	25.91	1.16	1.87	--	0.19	7.88	0.91	82.9
Quench exit	1001.2	43.8	115.1	55.32	27.66	4.32	3.59	--	0.18	8.07	0.86	--
Scrubber exit	154.0	41.1	76.7	48.98	24.53	3.65	13.96	--	0.15	7.98	0.76	82.0
Shell data												
Scrubber exit	165.0	41.0	--	48.74	22.37	2.34	17.97	0.02	0.13	7.37	0.95	82.8

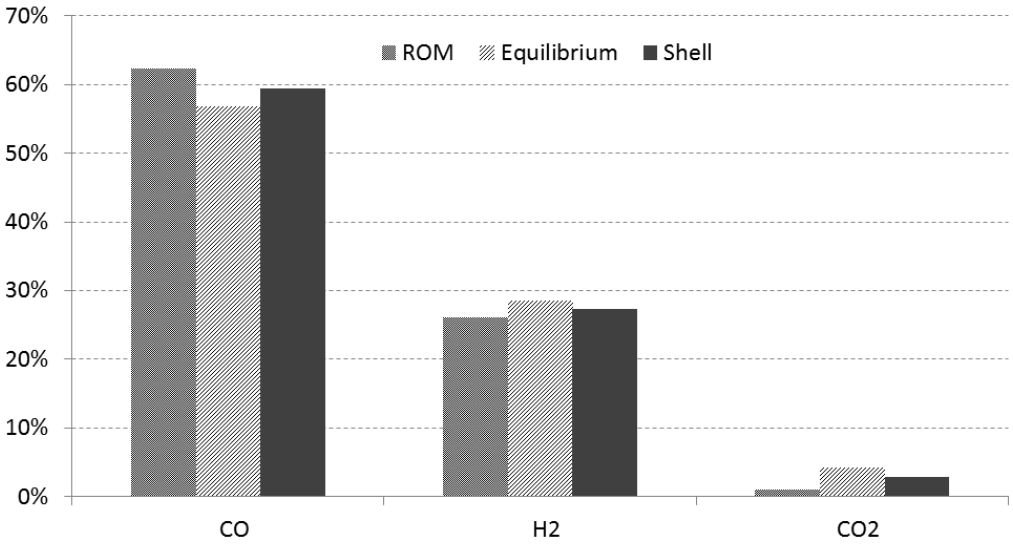

Figure 4-18: The dry molar gas concentration obtained using the kinetic ROM model, the equilibrium model and Shell data at the scrubber exit.

Results reported in Figure 4-18 are limited to the gas phase because of equilibrium. Shell data fall in the range between ROM and equilibrium and this is probably related to the WGS activity during the quench. This is directly related to the mixing process in the first part of the quench and it would require a more detailed fluid dynamic simulation (CFD). Indeed, the actual mixing process features several non-ideal effects which affect the temperature gradient inside the flow and, therefore, the WGS activity in this section: a vigorous mixing implies a large temperature change and a lower CO conversion along the quench. This is consistent with the results shown in Figure 4-18: the perfect mixing model adopted in this ROM simulation lowers the WGS activity as compared to the actual non-perfect mixing case. Regarding the equilibrium results, they are close to Shell data. However the simulation process does not provide as much information as the ROM and requires specific calibration using given operator data.

Figure 4-19 reports the gas and solid particles temperature profiles for: gasifier reactor, quench, convective coolers and scrubbing. The slag temperature is reported only for the gasifier reactor. If perfect mixing is assumed at the quench inlet, the temperature falls immediately down to around 1000 °C; in the following quench section, cooling is due to the membrane wall heat loss. Syngas is cooled in the convective heat exchangers from 930 °C to 300 °C. Finally, the gas supplies heat for water evaporation in the scrubbing process leaving it at around 160 °C.

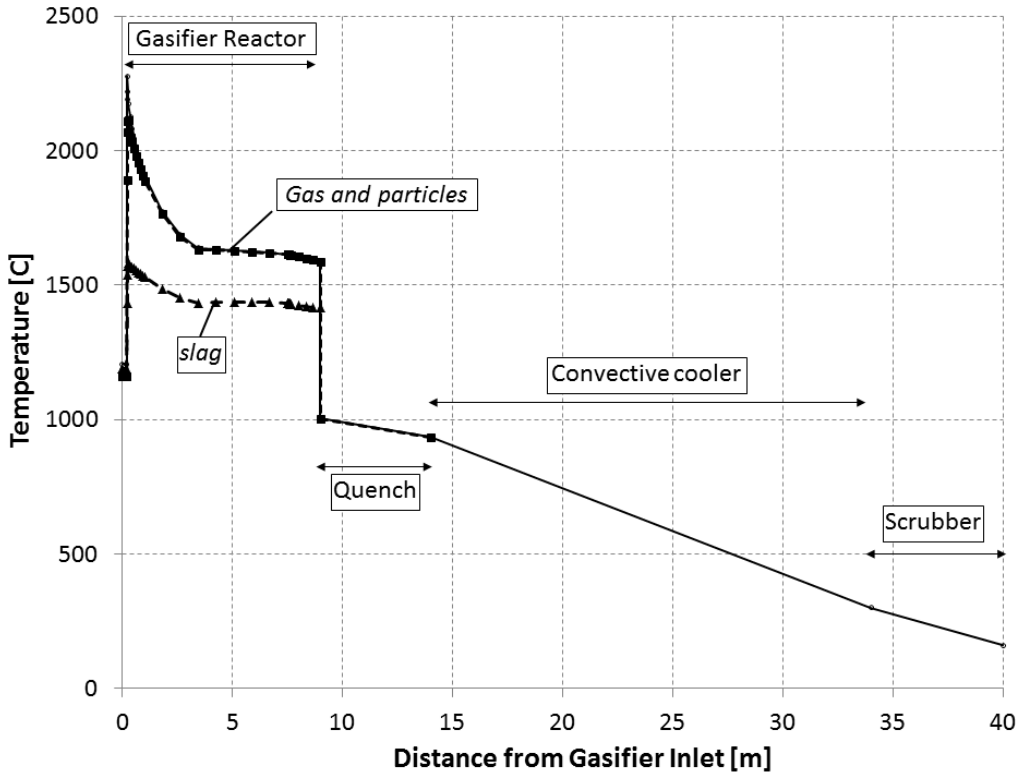

Figure 4-19: The overall temperature profile for the gasification process; the temperature is reported as function of the distance from the gasifier inlet, syngas cooler and scrubber length are set as 20 and 5 [m] respectively.

4.10 SENSITIVITY ANALYSIS

4.10.1 OXYGEN-TO-COAL RATIO

The oxygen needed for the gasification process is one of the most important parameters: it strongly affects the conditions inside the gasifier and contributes to the efficiency penalty. The ROM kinetic model allows predicting accurately the chemical response of the process when boundary conditions change. When the oxygen-to-coal ratio is lowered, the 99.8 carbon conversion is achieved few meters downstream of the location predicted for the base case. In the meantime, the temperature is lower all along the reactor: while oxygen is still abundant at the combustor inlet, the peak temperature is lower but without changing dramatically. On the other hand, within the gasification zone, the lack of thermal energy due to oxygen depletion is balanced by the reactants sensible energy; this results in a lower outlet temperature. As shown in Table 4-9, gas composition at the gasifier exit reflects the described mechanism: CO molar composition slightly increases as less carbon is burned. Moreover, more carbon is gasified by steam and the water percent sharply decreases. CO_2 content is lower because less is produced in the combustion zone; the Boudouard reaction also consumes more CO_2 along the reactor. This behavior is confirmed by the extrinsic reaction rate in the combustion zone: switching from O/Coal = 0.83 to O/Coal = 0.78, the carbon combustion reaction rate decreases from 13 to 5.8 [s^{-1}] respectively. On the other hand the steam gasification and Boudouard reaction rates are significant for a longer part of the reactor: for O/Coal = 0.78 reactions rates approach zero at

around 7.5 meters from the inlet instead of 3.5 (base case). Results obtained in this analysis and reported in Figure 4-20, show high sensitivity towards oxygen availability: by lowering the oxygen flow by about 6% the reactor length required to reach near complete carbon conversion almost doubles while the exit temperature decreases by about 9%. This is quite different from the results reported in [18] where oxygen sensitivity seems too low.

Table 4-9: molar concentrations at gasifier reactor outlet for CO, H_2, CO_2 and H_2O; CO

O_2/coal	CO	H_2	CO_2	H_2O
		Molar composition [%]		
0.83	62.28	25.93	1.05	1.78
0.80	62.91	26.91	0.44	0.68
0.78	63.31	27.50	0.02	0.03

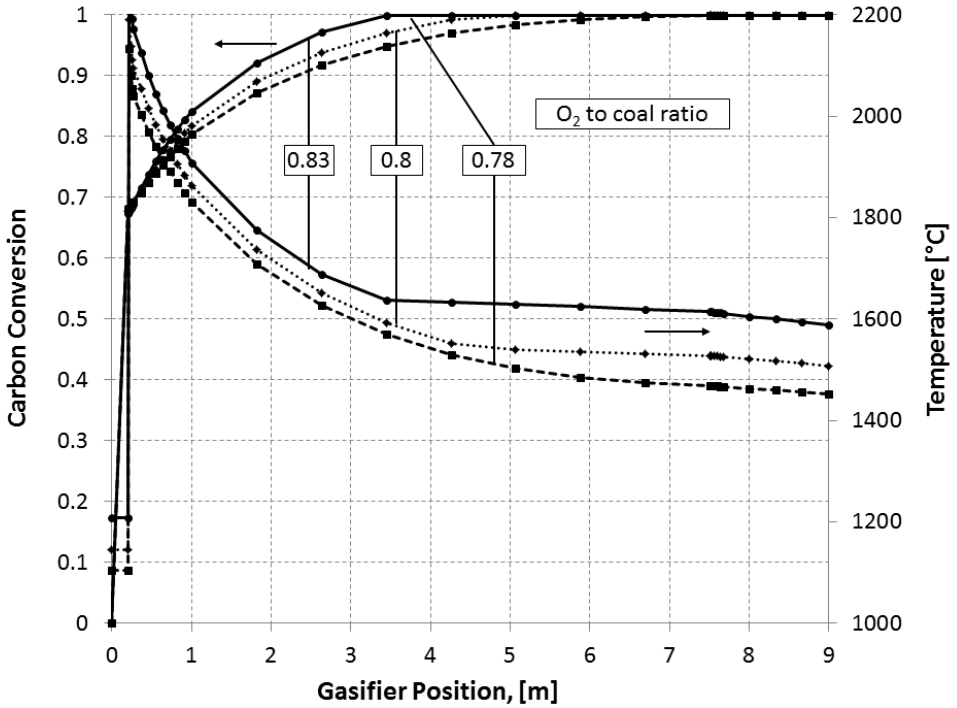

Figure 4-20: carbon conversion and temperature profile for different oxygen to coal ratios (0.83 = base case, 0.8 and 0.78); influence of oxygen feed on the temperature profile is high: if less O2 is supplied, carbon conversion slows down and the energy required for gasification lowers the temperature.

4.10.2 COAL FEED RATE

Increasing the coal feed, while fixing the O/Coal, N/Coal ratio, moderator and gasifier geometry, is a reasonable approach to increasing the syngas output at almost constant investment cost. A sensitivity analysis is performed to examine the impact of the coal feed rate. Results are shown in Table 4-10 and Figure 4-21. An increase in the coal feed reduces the residence time, the fluid dynamic and transport process, e.g., the gas diffusion towards char particle, but it does not affect the equilibrium chemistry (as O/C and Steam/C are kept fixed). Within the range of values used here, the ROM predicts negligible change in the overall carbon conversion, although as shown in the figure, carbon conversion does slow down. This, while surprising, is not an uncommon observation in operating entrained flow gasifiers, that is, changing the feedrate of

coal within a relatively narrow range does not have a significant negative impact on carbon conversion. One reason is that while increasing the feedrate of coal while holding the coal/oxygen ratio constant, the pressure inside the gasifier also increases, speeding up the kinetic rate and overall conversion rate. Changing the flow rate also changes the flow pattern inside the gasifier.

Table 4-10: residence times for several coal feed rate. For the same gasifier geometry, increasing coal flow rate lowers the residence time in each zone

Coal Input		3500	4000	4500
IRZ	[s]	0.002	0.002	0.001
JEZ	[s]	0.50	0.43	0.38
DSZ	[s]	0.76	0.66	0.58
Tot	[s]	1.26	1.09	0.96

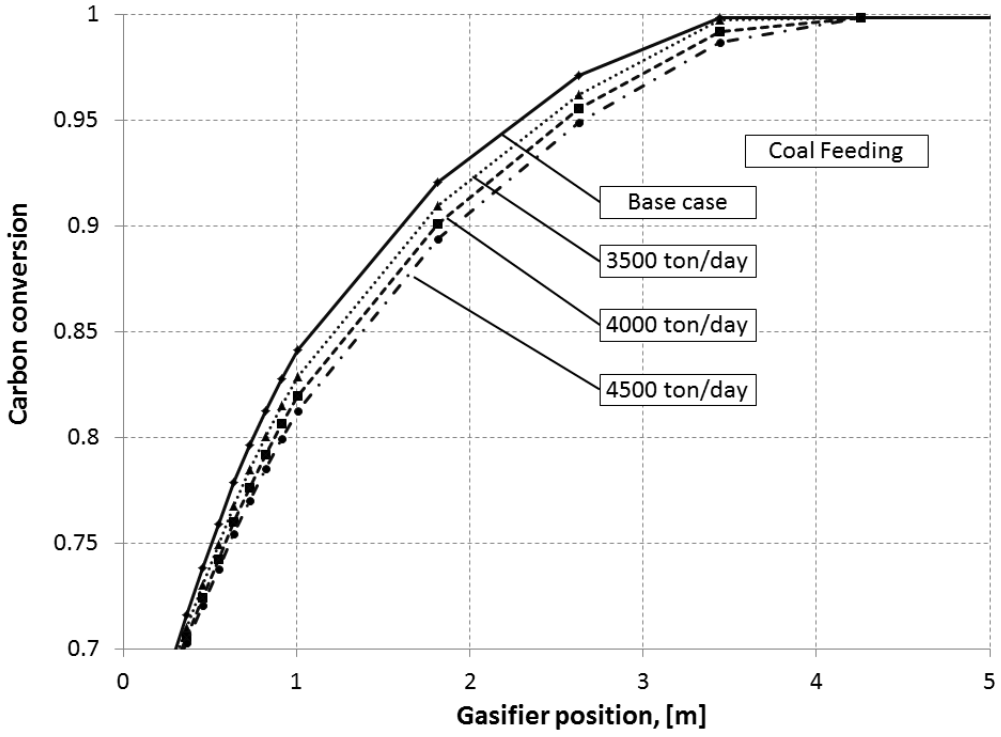

Figure 4-21: carbon conversion profiles for several coal feed rates. Carbon conversion curves are smoother for higher feedrates, reaching 99.8% at longer distance from the reactor inlet.

4.10.3 CO_2 FEED

Dry feed endows the Shell gasifier with flexibility regarding the coal type. Nitrogen is usually used to charge the lockhoppers. In some applications such as CCS or Fischer-Tropsch applications (Coal to Liquid), it is important to minimize the diluent content of the syngas in order to increase the CO_2 purity after the separation (i.e. for hydrogen membranes) or to increase the partial pressure of the reactants (for FT liquid). Analysis is performed using CO_2 instead of N_2 to charge the lockhoppers while keeping the steam and oxygen flowrates as constant, as suggested by Shell [6]. CO_2 mass flow is recalculated keeping the volumetric flow for the lockhoppers pressurization the same which causes the mass flow rate to double. Switching feed

gas changes the reactor chemistry due to the increase of CO_2 and hence shifting the Boudouard equilibrium. Results are shown in Figure 4-22 and Table 4-11. The temperature is lower because of the extra inert in the flow. Moreover the larger contribution of the Boudouard reaction increases the temperature difference as the gasification reactions take place along the reactor. This is confirmed by the increase of CO content at the gasifier exit. Finally, the CO_2 concentration outside the gasifier train rises from 2.3% to 5.75% (the increase between quench exit and scrubber exit is due to the candle filter purge flow). The CGE is higher thanks to the lower combustion reaction rate and the lower mean temperature inside the gasifier, i.e. energy released to the water decreases.

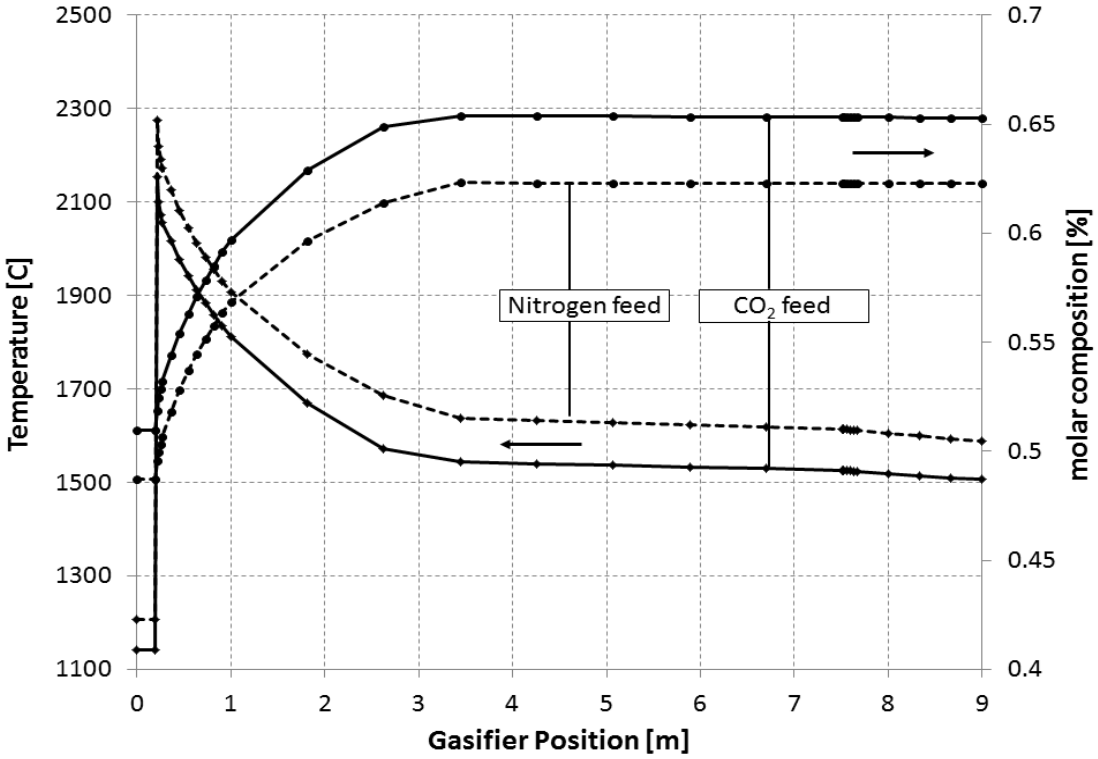

Figure 4-22: Temperature and CO molar content for gasification with CO2 and N2. Higher CO2 feed raises the mass flow in order to keep the volumetric flow constant at the lock hoppers. The temperature decreases because of the higher feed gas and because of the Boudouard reaction. Likewise, the CO content increases thanks to Boudouard gasification.

Table 4-11: Temperature, pressure, mass flow, molar content and CGE for gasification with CO_2 feed gas.

	T [°C]	p [bar]	G [kg/s]	Chemical species molar concentration [%mol]								CGE [%]
				CO	H_2	CO_2	H_2O	CH_4	H_2S	N_2	Ar	
Gasifier exit	1505.5	43.8	71.6	65.29	21.21	5.01	5.92	--	0.16	1.33	1.02	83.7
Quench exit	984.0	43.8	111.1	62.21	20.42	5.50	9.43	--	0.16	1.29	0.98	n.a.
Scrubber exit	164.9	41.1	71.6	55.57	18.27	5.75	18.24	--	0.13	1.15	0.88	83.5

4.11 CONCLUSIONS

A reduced order model of the Shell-Prenflo entrained flow gasifier was developed; two well-stirred and three plug flow reactors were used to reproduce each gasifier macro zone. The development of new simulation tools accounting for the wall heat transfer and the quench process allowed reproducing all the features of this gasifier family. The sensitivity analyses with respect to the recirculation level inside the reactor showed that the ROM provides interesting results even without the adoption of a CFD simulation.

The fin-based heat transfer model yields to a peak in the two-phase flow heat transfer coefficient next to the combustion zone where the heat flow is the highest; the calculated steam quality shows the same trend as the heat transfer coefficient. Gas and solid particle outlet temperature is 1588 °C while ashes are around 1400 °C. Temperature variation is strongly non-linear in the first part of the gasifier while it becomes linear when the gasification is almost completed. The tube temperature gradient is limited both along its circumference and axial direction. The ROM predicts quite accurately the syngas conditions at the scrubber outlet; the simulation of the quench mixing resulted to be the main source of difference with the actual process. The equilibrium simulation results are accurate when given gasifier compositions are available for tuning. The CGE predicted by both the ROM and the equilibrium modes are close to the Shell value; additionally, the ROM can be applied to a variety of coal or with different operating conditions. Sensitivity analyses showed that the ROM is able to accurately predict the chemical behavior such as a change in oxygen feed rate while limits arises when only the fluid dynamic is concerned. Finally, substitution of N_2 with CO_2 as transport gas was investigated highlighting the different gasification regimes for the two cases.

4.12 ACKNOWLEDGEMENTS

This study has been carried out thanks to MIT-Politecnico di Milano collaboration funded by Rocca Project framework.

REFERENCES

[1] **Higman, C. and van der Burgt, M.** *Gasification.* Second Edition. s.l. : Gulf Professional Publishing - Elsevier, 2008. ISBN: 978-0-7506-8528-3.

[2] **Monaghan, R.F.D.** Dynamic Reduced Order Modeling of Entrained Flow Gasifier. *PhD thesis.* s.l. : Massachusetts Institute of Technology, February 2010.

[3] **Gazzani, M, et al.** Reduced order modeling of the Shell-Prenflo entrained flow gasifier. *Fuel.* s.l. : Elsevier, 2012. Vol. 104, pp. 822-837. DOI:10.1016/j.fuel.2012.06.117.

[4] **Annamalai, K, Ryan, W and Dhanapalan, S.** Interactive Processes in Gasification and Combustion - Part III: Coal/Char particle arrays, streams and clouds. *Progress in Energy Combustion Science.* s.l. : Pergamon, 1994. Vol. 4, pp. 487-618. 0360-1285(94)00020-4.

[5] **Jancker, Steffen.** Delivering performance in Chinese operations. [on-line presentation]. Dresden : s.n., May 5, 2010. http://www.gasification-freiberg.org/desktopdefault.aspx/tabid-16.

[6] **Prins, M.** Personal communication. s.l. : Shell.

[7] **IEA.** *Potential for Improvement in Gasification Combined Power Generation with CO2 capture.* May 2003. Report Number PH4/19.

[8] **Martelli, E, et al.** Shell coal IGCCS with carbon capture: Conventional gas quench vs. innovative configurations. *Applied Energy.* s.l. : Elsevier, 2011. Vol. 88, pp. 3978-3989. doi:10.1016/j.apenergy.2011.04.046.

[9] **Franco F., Bolland O., Manzolini G., Macchi E., Booth N., Rezvani S., Pfeffer A.** Common Framework Definition document. [Online] 2009. http://caesar.ecn.nl/downloadslinks/.

[10] **Monaghan, R.F.D. and Ghoniem, A.F.** A dynamic reduced order model for simulating entrained flow gasfiers. Part I: Model development and description. *Fuel.* s.l. : Elsevier, August 2011. doi: 10.1016/j.fuel.2011.07.015.

[11] —. A dynamic reduced order model for simulating entrained flow gasifiers. Part II: Model validation and sensitivity analysis. *Fuel.* s.l. : Elsevier, August 2011. doi:10.1016/j.fuel.2011.08.046.

[12] **Monaghan, R.F.D., Kumar, M., Singer, Simcha L, Zhang, C., Ghoniem, A.F.** Reduced Order Modeling of Entrained Flow Solid Fuel Gasification. Lake Buena Vista : s.n. IMECE2009-12985.

[13] **Pedersen, L.S., Breithaupt, P., Dam-Johansen, K., Weber, R.** Residence Time Distributions in confined Swirling Flames. s.l. : Taylor & Francis, 1997. Vol. 127. dx.doi.org/10.1080/00102209708935696.

[14] **Pedersen, L.S., Glarborg, P., Dam-Johansen, K., Hepburn, P.W., Hesselmann, G.** A Chemical Engineering Model for Predicting NO Emissions and Burnout from Pulverised Coal Flames. s.l. : Taylor & Francis, 1998. Vol. 132. dx.doi.org/10.1080/00102209808952017.

[15] **Kumar, M. and Ghoniem, A.F.** Multphysics simulations of entrained flow gasification. Part I: validating the non-reacting flow solver and the particle turbulent dispersion model. *Energy and Fuels.* s.l. : ACS Publications, 2012. Vol. 26, 1, pp. 451-463. DOI: 10.1021/ef200884j.

[16] —. Multiphysics simulations of entrained flow gasification. Part II: constructing and validating the overall model. *Energy and Fuels.* s.l. : ACS publications, 2012. Vol. 26, 1, pp. 464-479. DOI: 10.1021/ef2008858.

[17] **Beer J M and Chigier N A.** *Combustion Aerodynamics.* London : Applied Science Publishers, Ltd, 1972. ISBN: 978-0898745450.

[18] **Lee, H, Choi, S and Paek, M.** A simple process modelling for a dry-feeding entrained bed coal gasifier. s.l. : Proceedings of the Institution of Mechanichal Engineers, Part A: Journal of Power and Energy, February 2011. Vol. 225, 1, pp. 74-84. DOI: 10.117/2041296710394249.

[19] **Klaus Kohnen and Hans Niermann.** *Arrangement for gasifying finely divided particularly solid fuel under high pressure. 4,818,252* [ed.] Krupp Koppers GmbH. United States, March 23, 1987.

[20] **Ian Poll.** *Method and Apparatus for the Combustion of Solid Fuel. 4,350,103* [ed.] Shell Oil Company. United States, Spetember 26, 1980.

[21] **de Graaf, J.D.** Shell Coal Gasification Technology. *Lecture.* s.l. : Technische Universiteit Eindhoven, 2011.

[22] **Yong, S.Z., Gazzino, M. and Ghoniem, A.F.** Modeling the slag layer in solid fuel gasification and combustion - formulation and sensitivity analysis. *Fuel.* s.l. : Elsevier, February 2012. Vol. 92, 1, pp. 162-170. dx.doi.org/10.1016/j.fuel.2011.06.062.

[23] **Incropera, et al.** *Fundamentals of Heat and Mass Transfer.* sixth edition. s.l. : Wiley. ISBN: 0-471-45728-0.

[24] **Bejan, Adrian and Kraus, Allan D.** *Heat Transfer Handbook.* s.l. : Wiley, 2003. ISBN: 0-471-39015-1.

[25] **Thome, John R.** *Engineering Data Book III.* s.l. : Wolverine Tube Inc.

[26] **Rayaprolu, Kumar.** *Boilers for Power and Process.* s.l. : CRC Press, Taylor & Francis Group, 2009. ISBN: 978-1-4200-7536-6.

[27] **Aspen Custom Modeler.** [Online] AspenTech. http://www.aspentech.com/products/aspen-custom-modeler.aspx.

[28] **Yang, Zhiwei, et al.** Dynamic Model for an Oxygen-Staged Slagging Entrained Flow Gasifier. s.l. : ACS Publications, 2011. 25, pp. 3646-3656. dx.doi.org/10.1021/ef200742s.

[29] **Uhde GmbH - ThyssenKrup.** *Press Information No.02.* Dortmund : s.n., 2008.

[30] **Volk, Jim.** Shell Coal Gasification: Delivering performance in Chinese operations today, developing technology and deployment solutions for tomorrow. *GTC November 2010.*

[31] **Chhoa, Thomas.** Shell Gasification business in action. *GTC October 2005.*

[32] **Seggiani, M.** Modelling and simulation of time varying slag flow in a Prenflo entrained-flow gasifier. s.l. : ELSEVIER, November 1998. Vol. 77, 14. dx.doi.org/10.1016/S0016-2361(98)00075-1.

[33] **Bockelie, Michale J., et al.** CFD Modeling for Entrained Flow Gasifiers. *Gasification Technologies Conference.* 2002. http://www.reaction-eng.com/downloads/publications.html.

[34] **Kumar, M.** Personal Communication. *MIT - Reacting Gas Dynamic Laboratory.*

[35] **Shell.** *Information package for DECARBIT: Shell Coal Gasification Process for generic IGCC with carbon capture evaluations.* March 3, 2010.

[36] Gecos group. *Energy Department, Politecnico di Milano.* [Online] www.gecos.polimi.it.

5 HOT GAS DESULFURIZATION

Nomenclature and Acronyms

FGD: Flue Gas Desulfurizer
HHV: High Heating Value
HGCU: Hot Gas Clean Up
HGD: Hot Gas Desulfurization
IGCC: Integrated Gas Combined Cycle
LHV: Low Heating Value
MCFC: Molten Carbonate Fuel Cell
PAFC: Phosphoric Acid Fuel Cell
Ppm: part per million
SOFC: Solid Oxide Fuel Cell
TG: Thermo Gravimetric
TGA: Thermo Gravimetric Analysis
ZF: Zinc Ferrite
ZT: Zinc Titania

5.1 BACKGROUND

In IGCC power plants, coal is converted into a fuel gas, which must be cleaned before its use in the combustion turbine in order to: i) protect the gas turbine from corrosion, erosion, fouling and ii) minimize the pollutant emissions to the environment. Gas clean-up can be carried out by conventional absorption processes, operating at near–ambient temperature, or by advanced methods, based on hot gas filtering and desulfurization. The primary incentive for developing a process that can remove hydrogen sulfide from gas streams at high temperature is the potential of improving the thermal efficiency of IGCC power plants [1].

Purification of the fuel gas close to the generation temperature avoids the energy losses associated with cooling it to a conventional purification process temperature and reheating it to the required gas turbine feed temperature. Although the development of a high-temperature desulfurization process can be justified on the basis of its effect on IGCC system efficiency, it also offers potential benefits for other applications such as the purification of feed gases for high-temperature fuel cells and catalytic synthesis operations. The tolerable level of sulfur for different important applications is shown in Table 5-1.

Table 5-1: Allowable sulfur level for different processes. Readapted from [2]

Application	Allowable sulfur levels [ppmv]
Ammonia production	< 0.1
Methanol synthesis	< 0.5
Fuel Cell	
- SOFC	< 0.2
- PAFC	< 50
- MCFC	< 0.5
Fischer-Tropsh process	< 1
Gas Turbine	< 20
H_2 Membrane	
- Pure Palladium	< 1
- Pd-Au or Pd-Cu	< 10

Two basic approaches have been considered for high temperature sulfur removal from gases: contact with reactive molten salts and contacts with reactive solids. The molten salt approach has encountered several problems, including containment materials corrosion, salt vaporization, and

salt solidification on cooling [1]. Consistently, only the use of reactive solids has been considered and will be discussed in the present work.

The hydrogen sulfide is removed from the gas by reacting with a metal oxide to form a stable, non-volatile metal sulfide. The minimum H_2S concentration in the treated syngas is determined by the equilibrium concentration based on the syngas composition and metal oxide. Reaction kinetics determine how rapidly the H_2S reacts to reach the equilibrium concentration and therefore the H_2S slip for a given velocity and reactor geometry. The metal sulfide is then subjected to a regeneration step in which it reacts with oxygen and/or water vapor to remove the sulfur usually as sulfur dioxide and produce reusable metal oxide. Both the sorption and regeneration steps are carried out at elevated temperature, but not necessary the same.

The main problems encountered for industrial application are: sorbent evaporation, formation of metal sulfates, chemical changes and mechanical attrition. From a system point of view other issues are represented by the reactor adopted: fixed-bed requires high temperature, high-pressure valves and produce a regeneration gas stream that varies in composition and quantity during cycle. Fluidized and moving bed systems are very susceptible to particle attrition problems and require a complex solids transport control system when operating at high pressure.

A number of metals known to have a strong affinity for sulfur have been considered in several pilot/experimental activities. The materials are classified into two groups: alkaline earth metal compounds and transition metal compounds. The key reactions of several metal oxides with hydrogen sulfide and the logarithms of the equilibrium constants for the reaction are given in Table 5-2 (re-adapted from [1]).

Table 5-2: reaction of metal oxides with H_2S at 1000K and their logK values. Readapted from [1]

Reaction	log**K**
$CaO + H_2S \leftrightarrow CaS + H_2O$	3.36
$MgO + H_2S \leftrightarrow MgS + H_2O$	-1.79
$FeO + H_2S \leftrightarrow FeS + H_2O$	2.29
$FeO + 2H_2S \leftrightarrow 2FeS + H_2O + H_2$	0.58
$1/2Fe_2O_3 + 3/2H_2S \leftrightarrow FeS + 3/2H_2O + 1/4S_2$	2.40
$1/2Fe_2O_3 + 2H_2S \leftrightarrow FeS_2 + 3/2H_2O + 1/2H_2$	1.77
$1/3Fe_3O_4 + 4/3H_2S \leftrightarrow FeS + 4/3H_2O + 1/6S_2$	1.99
$1/3Fe_3O_4 + 2H_2S \leftrightarrow FeS_2 + 4/3H_2O + 2/3H_2$	0.99
$MnO + H_2S \leftrightarrow MnS + H_2O$	2.80
$ZnO + H_2S \leftrightarrow ZnS + H_2O$	3.88
$MoO_2 + 2H_2S \leftrightarrow MoS_2 + 2H_2O$	5.2
$MoO_3 + 3H_2S \leftrightarrow MoS_2 + 3H_2O + 1/2S_2$	8.7
$CoO + H_2S \leftrightarrow 1/9Co_9S_8 + H_2O + 1/18S_2$	3.10
$NiO + H_2S \leftrightarrow NiS + H_2O$	4.1
$NiO + H_2S \leftrightarrow 1/3Ni_3S_2 + H_2O + 1/6S_2$	2.76

Among the transition metal oxides, the zinc-based sorbents seem to be the most promising. Zinc oxide is known to be among the best metal oxide sorbents as it shows the most favorable sulphidation thermodynamics. Extensive research work has been carried out focusing on two types of zinc oxide based materials: zinc ferrite (ZF) and zinc titanate (ZT). ZF sorbent showed several practical problems during the regeneration [2], while ZT compounds have emerged as sorbents with most of the advantages and few of the limitations of ZF. Especially Zn-Ti-O

compounds have shown interesting properties: ZnO possesses one of the highest thermodynamic efficiencies for H_2S removal and the most favorable reaction kinetics of all the active oxide materials within the 149 to 371 °C temperature range. Furthermore, Zn-Ti-O sorbents allows increasing the operating temperature for gas desulphurization as a result of the lower ZnO reduction rate. At temperature in the range of 400 to 700°C similar activation energies were found for both Zn-Ti-O and ZnO sorbents [2].

5.2 ZINC BASED HOT GAS SULFUR REMOVAL SYSTEM

As aforementioned, zinc ferrite and zinc titanate sorbents appear to be the leading sorbent for high-temperature, high-pressure sulfur removal in fluidized bed. They have been extensively evaluated for fixed-bed reactors; however, according to [3] this configuration has limited practical potential because of: i) the need for high-temperature, high-pressure valves, ii) the difficulty of handling the heat released during regeneration and iii) the non-uniform composition of the regeneration offgas during the cycle period. On the other hand, fluidized bed systems showed high potentialities for this application leading to the realization of several lab or demo scale project [4] [5] [6]. In this case, the difficulty of operating interconnected fluidized bed at high pressure is an issue, but some examples of successful operations in lab-scale facilities [7], the delivery of demo scale systems [8] as well as the application of pressurized dual fluidized bed systems in other fields (e.g. the commercial process for cracked-gasoline and diesel sulfur removal developed by Conocophillips [9]) make this option a real candidate for future applications.

With such a configuration, the sorbent can be transported through the two reactors, undergoing several cycles of absorption and regeneration. Both the reactors operate at a pressure very close to the gasification one.

When HGD is based on zinc titanate, the reactions to be taken into account are:

- *Sulfur removal:*

$$\frac{1}{x}Zn_xTi_yO_{x+2y}(s) + H_2S(g) \leftrightarrow ZnS(s) + \frac{y}{x}TiO_2(s) + H_2O(g) \quad (5\text{-}1)$$

- *Regeneration:*

$$ZnS(s) + 1.5O_2(g) + \frac{1}{x}Ti_yO_{2y}(s) \leftrightarrow ZnO(s) + SO_2(g) + \frac{1}{x}Ti_yO_{2y}(s) \quad (5\text{-}2)$$

The SO_2 produced upon regeneration can be treated further to yield Calcium sulfate in a conventional FGD system or H_2SO_4 in a sulfuric acid plant. At regeneration conditions, beside reaction (5-2) undesired zinc sulfate can form with the following reactions [10] [11]:

$$ZnO(s) + SO_2(g) + 0.5O_2(g) \leftrightarrow ZnSO_4(s) \quad (5\text{-}3)$$

$$ZnS(s) + 2O_2(g) \leftrightarrow ZnSO_4(s) \quad (5\text{-}4)$$

If these reactions occur, part of the sulfur is not desorbed leading to a sorbent capacity decrease; moreover the solid material behaves as oxygen carrier from the regenerator to the desulfurizer, eventually oxidizing part of the syngas through the $ZnSO_4$ decomposition to ZnS.

As reported in [6] and shown in the Zn-S-O phase diagram in Figure 5-1, from a thermodynamic point of view the regeneration should be carried out at high temperature and low SO_2 and O_2 partial pressure to prevent $ZnSO_4$ formation. However, the kinetic behavior affects reactions (5-3) and (5-4) more than the reaction thermodynamic. Bagajewicz [10] showed that zinc sulfate formation through reaction (5-4) is insignificant while low amount of freshly formed ZnO can lead to $ZnSO_4$. Woods et al [12] showed that the reaction rates of these secondary reactions are very low: when the O_2 concentration is varied from 1 to 8% the reaction rate of regeneration increased with no sign of $ZnSO_4$ formation at ambient pressure. At 20 bar the regeneration rate decreased but there was no evidence in $ZnSO_4$ formation. Finally also Siriwardane and Woodruff showed that at 550-650 °C the reaction rate of (5-3) is much lower than reaction (5-2).

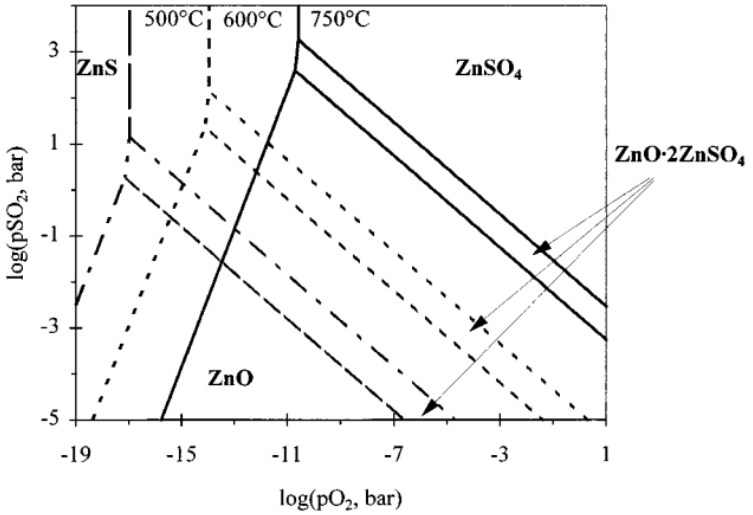

Figure 5-1: Zn-O-S phase stability diagram [13]

In this study, the hot raw syngas is supposed to fluidize the desulfurizer. The entrained solid particles are separated by a cyclone and partly ducted to the regeneration reactor, while the syngas exiting from the top of the cyclone is cleaned from fines in a hot gas filter. The sulfur-laden solids pass through the regenerator and interact with a mixture of air and nitrogen delivered by a compressor, so reaction (5-2), which is highly exothermic, occurs. As described above, reactions (5-3) and (5-4), i.e. the possible $ZnSO_4$ formation during regeneration, are kinetically neglected in this model. In fact, zinc sulfate, whose formation can occur at the bottom of the regenerator where oxidizing conditions subsist, is expected to be very limited considering the reducing conditions in the rest of the fluidized bed and the lack of oxygen in the gaseous stream at regenerator outlet. This pressurized stream, after solid separation and filtration, is expanded in a turbine, driving the regeneration stream compressor. The expanded gas contains the removed sulfur as SO_2, whose concentration can vary significantly according to the O_2 content in the sorbent regeneration stream. Therefore, regeneration off-gas must be

treated before being vented to the atmosphere either in a standard wet FGD unit or in a sulfuric acid production process.

5.3 MODELING THE HGD PROCESS

In order to develop and scale-up a reactor system, it is essential to obtain a reliable model for the performances prediction and bed design. The best approach to model the chemical behavior of fluidized bed reactors is to describe the nonideal flow of gas and solids by considering separate phases, how gas and solid contact and react and which are the vertical and radial distributions of solids [14] [15]. This leads to a three-phase model with a lumped bed conversion parameter and an appropriate average concentration between the gas inlet and exit. Another method for modeling non-ideal flow of gas, as shown in [16] and introduced by [17], is to adopt a certain number of linked completely-stirred reactors. The tanks-in-series model is quite simple and at the same time can be adapted to complicated kinetics and can be extended without too many difficulties to any arrangement of compartments.

In both the reactors, the model must satisfy the following mass balance:

- Desulfurizer:

$$\dot{N}_{sulfur} \cdot \eta_{S-conversion} = \dot{N}_{Zn} \cdot \frac{dX_{Zn}}{dt} \tag{5-5}$$

- Regenerator:

$$\dot{N}_{O_2} \cdot \eta_{O_2-conversion} = 1.5\dot{N}_{ZnS} \cdot \frac{dX_{ZnS}}{dt} \tag{5-6}$$

When the accuracy of the simulation increases using a higher number of slices, the plug flow model can be directly adopted. The equations which describe the first-order reversible reaction in the plug-flow reactor are:

- Desulfurizer:

$$\frac{n_{sorb} rate_{sorb}}{n_{gas,in}} = \frac{M + X_{H2S,equil}}{M + 1} ln\left(\frac{X_{H2S,equil}}{X_{H2S,equil} + X_{H2S,out}}\right) \tag{5-7}$$

$$y_{H2S,out} = y_{H2S,in}\left[1 - X_{H2S,equil}\left(1 - e^{\frac{-n_{sorb} rate_{sorb}}{n_{gas,in}\beta}}\right)\right] \tag{5-8}$$

Where:

$$M = \frac{y_{H2O,in}}{y_{H2S,in}} \quad X_{H2S,equil} = 1 - \frac{M}{k_{equil}} \tag{5-9}$$

$$\beta = \frac{M + X_{H2S,equil}}{k_{equil} M + 1} \approx 1 \quad rate_{sorb} = \frac{C_{H2S,in}}{dF/dX_{ZnS-des}} \tag{5-10}$$

$$X_{ZnS-des} = \frac{\dot{N}_{ZnO\_converted}}{\dot{N}_{ZnO\_in}} = \frac{X_{H2S}\dot{N}_{H2S_{in}}}{\dot{N}_{ZnO_{in}}} \quad (5\text{-}11)$$

- Regenerator:

$$X_{ZnS-reg} = \frac{\dot{N}_{O_2} * (1 - e^{-\frac{1.5\dot{N}_{ZnS_{in}} k_{regeneration} \tau_{bed} (1-X_{ZnS})^2}{\dot{V}_{gas}}})}{1.5\dot{N}_{ZnS_{in}}} \quad (5\text{-}12)$$

$$y_{SO2,out} = \frac{y_{O2,in}}{1.5}(1 - e^{-\frac{1.5\dot{N}_{ZnS_{in}} k_{regeneration} (1-X_{ZnS})}{\dot{V}_{gas}}}) \quad (5\text{-}13)$$

$$X_{ZnS-reg} = \frac{\dot{N}_{ZnS\_regenerated}}{\dot{N}_{ZnS\_in}} = \frac{X_{O2}\dot{N}_{O2_{in}}}{1.5\dot{N}_{ZnS_{in}}} \quad (5\text{-}14)$$

In both the desulfurizer and regenerator, the solid phase is assumed to be perfectly mixed, which means that the concentration of the reactive solid is not dependent on the bed position. On the contrary, the gas phase is modeled assuming a plug flow distribution.

5.3.1 DESULFURIZER KINETIC EQUATIONS

In order to reproduce the kinetic of the desulfurization process, the unreacted shrinking core modeling approach can be adopted. This model assumes the unreacted shrinking core of the particle as the reaction surface, equal to the particle external surface at the initial time. Compared to the overlapping grain model [18], where the real behavior of the sorbent is pursued describing the radius-time variation, the USC is easier and suits well the fluidized bed simulation.

Nonetheless, a more general version of the USC has been obtained in order to describe the changes of the internal structure of the porous solid as consequence of the reactions. This means that the assumption of constant effective diffusivity D_{eff} in modeling is no longer valid. Zevenhoven et al [19], have introduced a more general definition for effective diffusivity, where this parameter is a function of the overall particle conversion. The effective diffusivity is defined as:

$$\frac{V_{pore} + V_{pl}}{D_{eff}} = \frac{V_{pl}}{D_{pl}} + \frac{V_{pore}}{D_{pore}} \quad (5\text{-}15)$$

There are two mechanism included in this parameter: i) diffusion in the pores of the particle (gas phase diffusion and Knudsen diffusion) and ii) diffusion through a solid nonporous product layer. These two mechanisms occur in series: the gas diffuses through the pores and then through the product layer. It comes out that the D_{eff} is linked to the relative volume fractions which all change during the conversion.

The USC time-conversion equations give the combination of reaction kinetics and intraparticle diffusion as in the following expressions:

$$t = \tau_{kin} * f_{kin}(X) + \tau_{diff} * \frac{1+BX}{1+AX} f_{diff}(X) \quad (5\text{-}16)$$

$$f_{kin}(X) = (1-(1-X)^{\frac{1}{3}}) \qquad f_{diff}(X) = \left(\frac{Z-(1+ZX-X)^{2/3}}{Z-1} - (1-X)^{\frac{2}{3}}\right) \quad (5\text{-}17)$$

$$\frac{dX}{dt} = \frac{C_{H2S}}{dF/_{dX}} \quad (5\text{-}18)$$

Where:

$$\tau_{kin} = \frac{R_{pore}\rho_{mol,sorbent}}{kC_{H2S}} \quad \tau_{diff} = \frac{{R_{pore}}^2\rho_{mol,sorbent}}{6D_{eff,0}C_{H2S}} \quad (5\text{-}19)$$

$$A = \frac{1-\varepsilon_0}{\varepsilon_0} \quad B = \frac{A * D_{eff,0}Z}{D_{product-layer}} \quad (5\text{-}20)$$

$$F = \frac{R_{pore}\rho_{mol,sorbent}}{k} f_{kin}(X) + \frac{{R_{pore}}^2\rho_{mol,sorbent}}{6D_{eff,0}} \frac{1+BX}{1+AX} f_{diff}(X) \quad (5\text{-}21)$$

$$X = X_{ZnS-des} \quad (5\text{-}22)$$

Where:

- ε_0: porosity
- $D_{eff,0}$: initial effective diffusivity
- D_{pl}: product layer diffusivity
- k: reaction rate constant

5.3.2 Regenerator Kinetic Equations

The rate of regeneration is assumed to follow the expression of the progressive conversion model [20]: reactant gas enters and reacts throughout the particle all times, most likely at different rates at different locations within the particle. Solid reactant is converted continuously and progressively. Therefore, in the regenerator, the gaseous reactant O_2 is assumed to be present evenly throughout the ZnS-containing solid particle and reacts with a solid everywhere.

$$\frac{dX}{dt} = k_{reaction}(1-X){C_{O2}}^N \quad (5\text{-}23)$$

$$X = X_{ZnS-reg} \quad (5\text{-}24)$$

Where:

- X is the fractional conversion of ZnS to ZnO,
- C_{O2} is the concentration of oxygen
- N is the order of reaction
- $k_{reaction}$ is the reaction rate constant

As reported in [6] the order of O_2 in the regeneration can be assumed to be 1. According to the experimental results and the following kinetic parameters, the rate of SO_2 release is strongly

dependent on process temperature and the rate of $ZnSO_4$ formation at high temperature and pressure is negligible.

5.3.3 MODEL VALIDATION

As previously introduced, the model developed in this work to reproduce the hot gas clean-up process is based on the work of Konttinen et al. [5] [16] [21] [6]. Not only does this reference reports experimental data of a demo plant but also the kinetic parameters and equations which could be used to reproduce the desulfurization and regeneration processes. In order to continue with the design and extend the model (see paragraph 5.3.4), a comprehensive validation with the cited references has been carried out. Results of the validation are shown in Figure 5-2 and Figure 5-3.

The critical issue of this process is to extrapolate all the information required to simulate the references operating conditions. Moreover, the detail level of the equation resolution or the gas properties calculation can be very different compared to what carried out in the reference (a clear example is the H_2S diffusivity calculation in the syngas). Nevertheless, the results show good agreement with the reference data. In literature, the desulfurizer and the regenerator are considered as standalone components, therefore there are no validations on the connected system but just on the single component.

As far as the desulfurizer is concerned, the H_2S slip vs. the sorbent conversion is plotted in Figure 5-2; the predicted H_2S level is very close to the reference in all the reported range. The absolute difference between the two models is in the range of few ppm whilst the curve shape is very much the same.

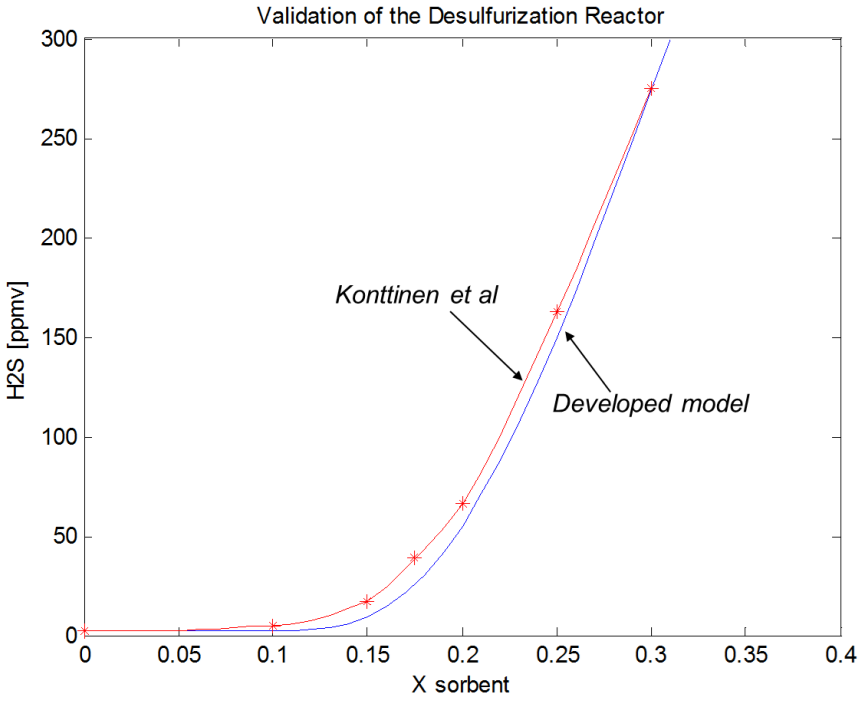

Figure 5-2: H2S level in the syngas exiting the reactor as function of the ZnO conversion. Model results are in blue, literature results in red.

Table 5-3: Desulfurizer data for the validation.

Input data for the validation	Desulfurizer						
Inventory, g	500						
Reactor temperature, °C	550.0						
Pressure, bar	20.0						
Superficial gas velocity, m/s	0.21						
Sorbent							
- Bulk density, kg/m^3	1500						
- Porosity	0.412						
- Median pore diameter, A	4500						
- Zn/Ti, molar ratio	1.46						
- Average particle size, μm	308						
- Shape	sphere						
Syngas Composition, %mol	CO	H_2	H_2O	H_2S	N_2	Ar	CO_2
	.18	.13	.11	.0015	.4984	.0001	.08

The regeneration reactor validation, shown in Figure 5-3, reports the level of the regeneration (as unreacted sulfur to regenerated sorbent ratio) and the oxygen conversion as function of the reactor temperature. The model predictions and the literature data are very close each other, most of all concerning the oxygen conversion. The sorbent conversion is slightly shifted towards lower value in all the range. This can be due to difficulty in extrapolating the parameters used in the reference.

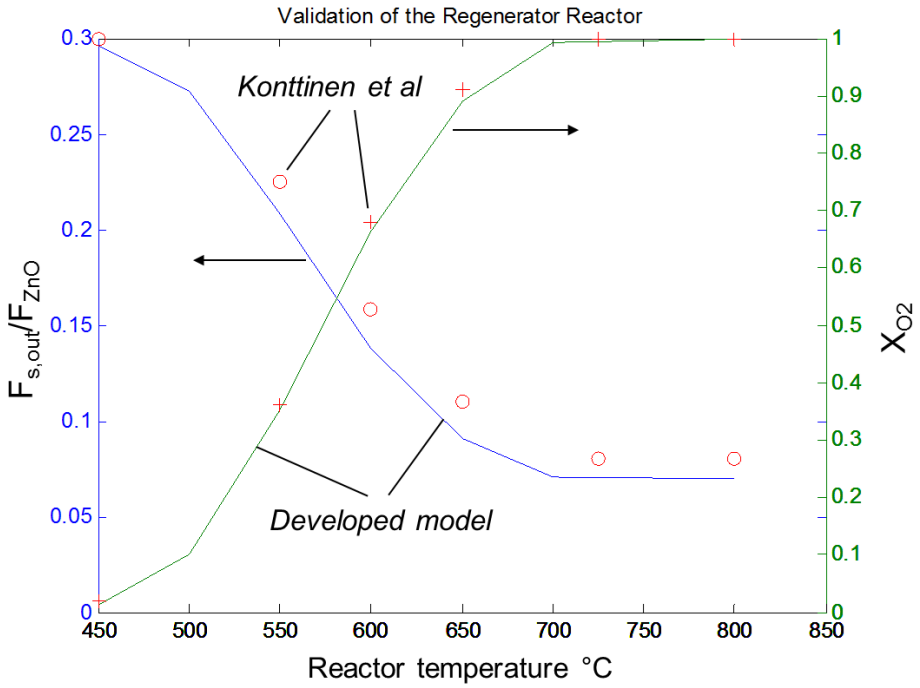

Figure 5-3: results of the model validation for the regeneration reactor; on the left axis the unreacted sulfur to exiting ZnO ratio as function of the regenerator bed temperature. On the right axis the conversion of the entering oxygen as function of the regenerator temperature.

Table 5-4: Regenerator data for the validation

Input data for the validation	Regenerator
Incoming sorbent, mol/s	1
Temperature, °C	600.0
Pressure, bar	20.0
Solid residence time, s	3600
Regeneration air	
- Volume flow, m^3/s	0.08-0.12
- O_2 composition, %mol	0.04

5.3.4 Model Extension And Design Approach

After the validation, the model has been further developed and extended in order to: i) simulate connected fluidized bed systems, ii) predict the raw design and cost of the reactors and, iii) obtain the energy balance of the reactors and the circulating solids. The global model layout is shown in Figure 5-4: the input conditions are defined by the IGCC scheme, i.e. the gasification technology, and the solid composition inside the reactors. Once these preliminary conditions are set, the desulfurizer and the regenerator blocks solve the kinetic equations using several submodels. Finally, the reactor design, the energy balance and the reactor cost are computed. The gas properties are based on Refprop correlations (integrated with matlab) whilst solid properties are given from reference [5].

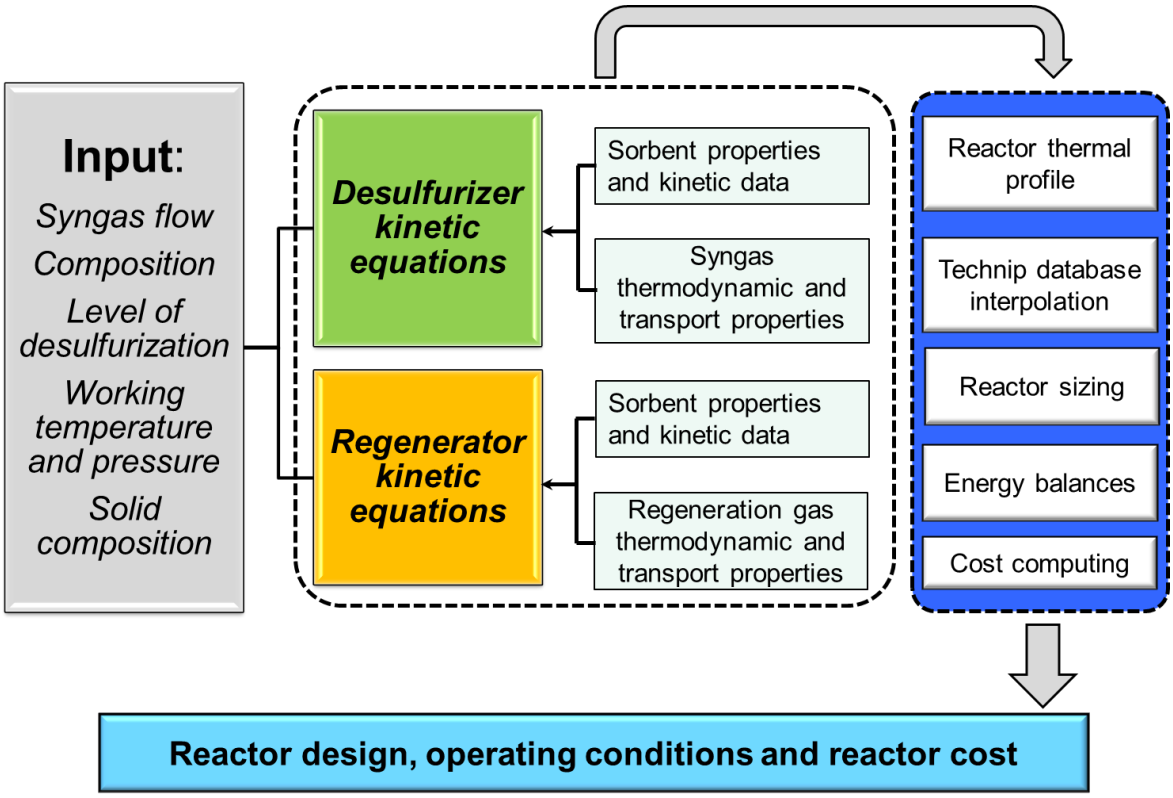

Figure 5-4: Hot gas desulfurization model layout: given the conditions at the reactor inlet, the desulfurizer and regenerator models solve the kinetic and rate equations thanks to many other submodels. The reactor design, the main thermodynamic parameters and the reactor cost are obtained.

The design of the each reactor is carried out assigning the operating conditions (T, p, syngas composition), the relative sorbent conversion, the oxygen concentration in the regeneration air and a tentative gas superficial velocity.

In order to clearly link the desulfurizer and regenerator models, the definition if the solid conversion through the reactors is rearranged, making explicit the sulfidation level of the desulfurizer and regenerator inventory, $X_{S\text{-}DES}$ and $X_{S\text{-}REG}$ respectively. The sorbent conversion indicated in (5-11) and (5-14), which are still the input to the kinetic equations aforesaid, are no more defined independently but are obtained with the following procedure: i) the required syngas desulfurization and therefore the amount of removed H_2S are defined, ii) the level of sulfidation inside the beds is set, iii) the circulating zinc is calculated, iv) the amount of ZnO and ZnS inside each reactor (and therefore exiting each reactor because of the completely stirred reactor approach) are calculated and, v) the reactor conversions as in (5-11) and (5-14) are obtained. The corresponding equations are here reported:

$$X_{S-DES} = \left|\frac{N_{ZnS}}{N_{ZnS} + N_{ZnO}}\right|_{inside\ Desulfurizer} \tag{5-25}$$

$$X_{S-REG} = \left|\frac{N_{ZnS}}{N_{ZnS} + N_{ZnO}}\right|_{inside\ Regenerator} \tag{5-26}$$

$$\dot{N}_{H2S\ removed} = \dot{N}_{H2S\ syngas\ in} \cdot \varepsilon_{H2S-removal} \tag{5-27}$$

$$\dot{N}_{Zinc-circulating} = \frac{\dot{N}_{H2S\ removed}}{X_{S-DES} - X_{S-REG}} \tag{5-28}$$

$$\dot{N}_{ZnS,in-DES} = \dot{N}_{Zinc-circulating} \cdot X_{S-REG} \tag{5-29}$$

$$\dot{N}_{ZnS,in-REG} = \dot{N}_{Zinc-circulating} \cdot X_{S-DES} \tag{5-30}$$

$$\dot{N}_{ZnO,in-DES} = \dot{N}_{Zinc-circulating} - \dot{N}_{ZnS,in-DES} \tag{5-31}$$

$$\dot{N}_{ZnO,in-REG} = \dot{N}_{Zinc-circulating} - \dot{N}_{ZnS,in-REG} \tag{5-32}$$

Generally: $$\dot{N}_{Zinc-circulating} = Sorbent\ converted + Sorbent\ not\ converted]_{Des\ or\ Reg} \tag{5-33}$$

Out Desulfurizer: $$\dot{N}_{Zinc-circulating} = \dot{N}_{ZnS,in-REG} + \dot{N}_{ZnO,in-DES}(1 - X_{ZnS-Des}) \tag{5-34}$$

Out Regenerator: $$\dot{N}_{Zinc-circulating} = \dot{N}_{ZnO,in-DES} + \dot{N}_{ZnS,in-REG}(1 - X_{ZnS-Reg}) \tag{5-35}$$

Finally, the conversion inside a reactor is obtained rearranging equations (5-34) and (5-35):

$$X_{ZnS-Des} = 1 - \frac{\dot{N}_{Zinc-circulating} - \dot{N}_{ZnS,in-REG}}{\dot{N}_{ZnO,in-DES}} \tag{5-36}$$

$$X_{ZnS-Reg} = 1 - \frac{\dot{N}_{Zinc-circulating} - \dot{N}_{ZnO,in-DES}}{\dot{N}_{ZnS,in-REG}} \quad (5\text{-}37)$$

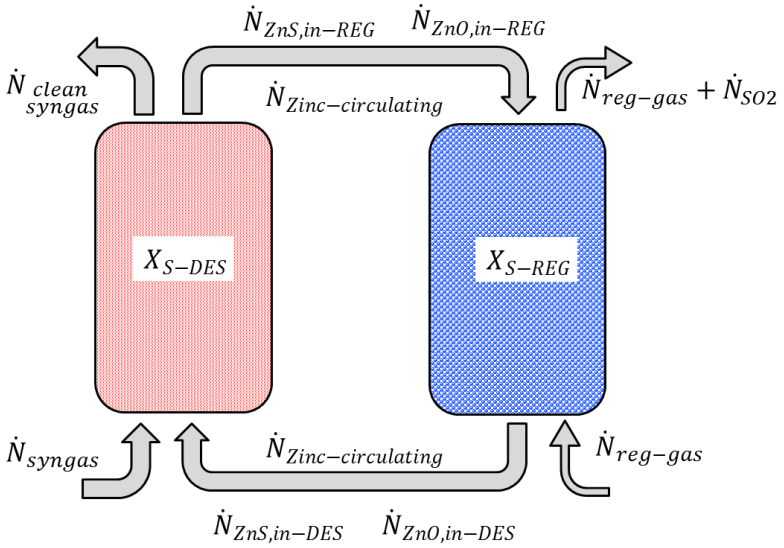

Figure 5-5: simplified representation of the fluidized bed system; on the left in red the desulfurizer, on the right in blue the regenerator.

The computational steps of the overall model are shown in Figure 5-6. The reactor design is carried out singularly for the desulfurizer and the regenerator, taking into account that the fluid-dynamic conditions inside the reactors are different. The circulating sorbents are computed at the beginning after imposing the sulfidation level. The heat balances are calculated after the reactor geometry is defined. Concerning the desulfurizer, a tentative value for the superficial gas velocity is assigned and the design is computed. If the H/D ratio is out of the defined range (3-15), the model modifies the assumed velocity.

As far as the regenerator is concerned, the superficial velocity is assigned as function of an over-velocity compared the minimum fluidization velocity; the typical value of $v_{gas}/v_{min\text{-}fluid}$ for a bubbling fluidized bed reactor is 3 [14]. At this point the model checks that the obtained value is lower than the terminal velocity, if not the over-velocity is reduced. The reactor volume is computed by means of the diameter, the average fill degree and the required inventory. Finally, the reactor design is iteratively computed as consequence of the wall geometry explained in the following.

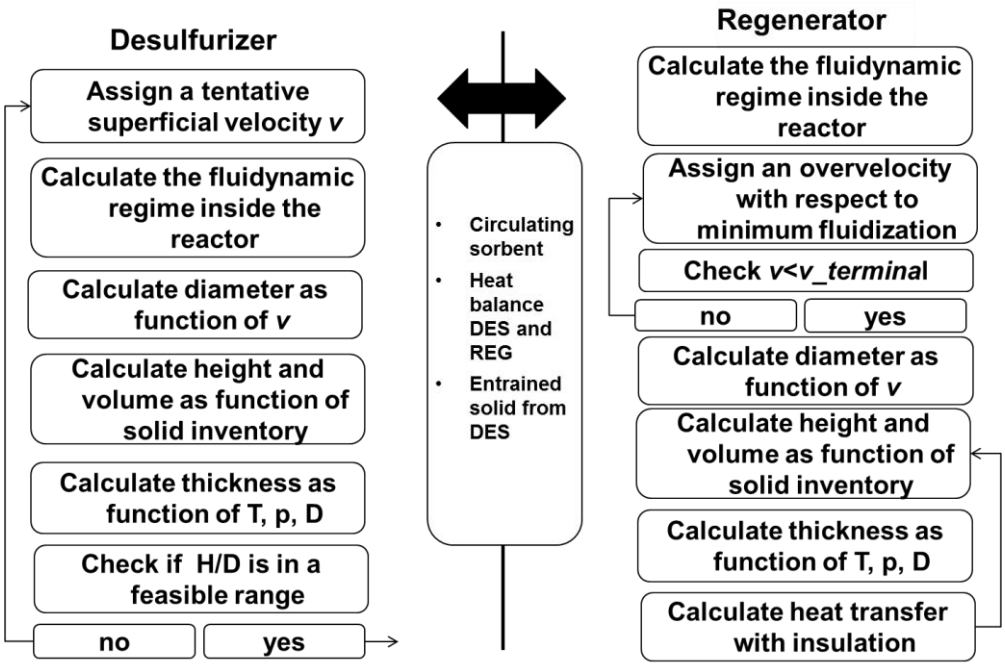

Figure 5-6: model computational steps; on the left side the desulfurizer resolution scheme, on the right side the regenerator resolution scheme.

As well as the fluid-dynamic conditions inside each reactor, also the wall thermal profile affects the reactor design. As explained in section 5.3.7, the reactor geometry and its cost are function of the working temperature. In order to optimize the system, the choice of the reactor configuration, e.g. cooled or adiabatic, is carried out limiting the material quality and the thickness of the vessel wall.

Concerning the desulfurizer, the adoption of a membrane wall jacket sharply decreases the steel vessel temperature: thanks to the high heat exchange coefficient of a two-phase flow, the steel temperature is very close to the evaporating water (e.g. at 85 bar, 300 °C). This configuration allows working inside the reactor at around 450-550°C with wall at around 300°C. The exothermic heat of adsorption reaction is completely released to the evaporating water; the amount of flowing water permits to control the heat released from the reactor and it makes this process almost isothermal.

As far as the regeneration reactor is concerned, the configuration must take into account the higher working temperature required to promote the desorption but should limit the increase of the reactor cost. One possibility to keep the process almost adiabatic at moderately high temperature but with controlled vessel temperature is to adopt a refractory lining. This configuration is successfully applied to the GE gasifier. In this case, it is essential to adopt a material which can cope with the high level of erosion due to metal-based sorbent. Moreover, in order to avoid an increase of the vessel temperature, an evaporative water membrane jacket is preferred to an external insulation. In such a way, the vessel is almost at the steam temperature but the heat losses are limited thanks to the internal insulation. The radial thermal profile is assigned solving equation (5-38) (iterative on s_{steel} and with $s_{refractory}$ unknown).

$$\frac{T_{bulk\,in} - T_{refractory}}{{}^{1}/_{h_{wall-to-bed}2\pi r_{in}} + {}^{ln\left(\frac{r_{ref}}{r_{in}}\right)}/_{k_{ref}2\pi}} = \frac{T_{refractory} - T_{bulk\,steam}}{{}^{ln\left(\frac{r_{steel}}{r_{ref}}\right)}/_{k_{steel}2\pi} + {}^{1}/_{h_{steam}2\pi r_{steel}}} \quad (5\text{-}38)$$

The wall-to-bed heat transfer coefficient inside the desulfurizer is assumed constant (150 W/m^{2}K and chosen from graph in [22] while for the regenerator it is calculated adopting the correlation 6.49 for heat exchange in bubbling fluidized bed given in [22].

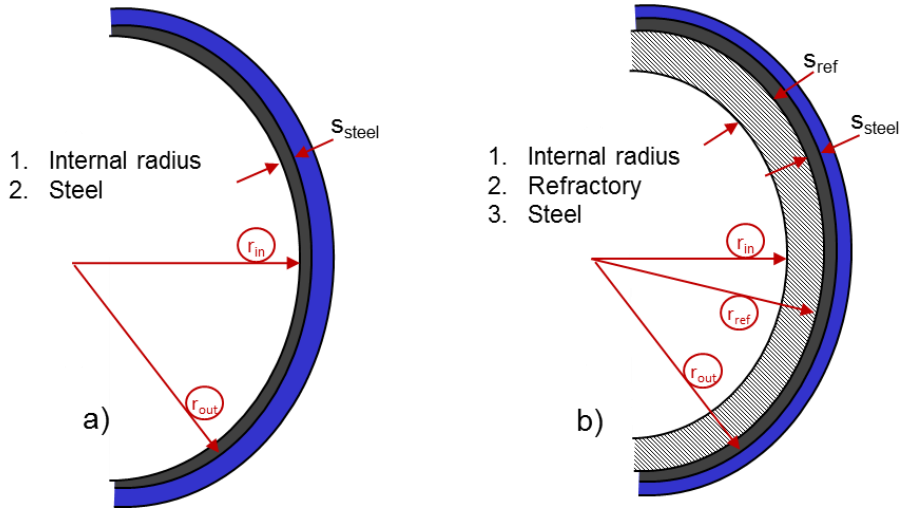

Figure 5-7: vessel radial geometry configuration: a) the desulfurizer reactor configuration and, b) the regenerator vessel configuration.

5.3.5 FLUIDIZATION CONDITIONS

In order to obtain an insight of the reactor properties and the fluidization regime, the most important fluidization parameters are computed (as in [17]): i) the minimum fluidization velocity (5-39), ii) the minimum bubbling to minimum fluidization ratio (5-40), iii) the Archimedes number (5-41) and, iv) the terminal velocity. The fluidization regime for each reactor is identified by means of the Grace diagram [23]. The amount of suspended particles carried by the gas is calculated using the entrainment G_s [kg/m$_2$s] correlation (5-42). The amount of entrained solid allows verifying the condition of completely stirred reactor for the solid phase: in a fast fluidized bed the higher the amount of recirculation the more the solids are mixed. Finally, the bed height is adjusted considering the extra space for the transport disengaging height (for the regenerator) (5-44).

$$u_{mf} = \frac{{d_p}^2(\rho_{solid} - \rho_{gas})g}{150\,\mu} \frac{{\varepsilon_{mf}}^3 {\emptyset_s}^2}{1 - \epsilon_{mf}} \quad (5\text{-}39)$$

$$\frac{u_{mb}}{u_{mf}} = \frac{4.125 \cdot 10^4 \mu^{0.9} {\rho_g}^{0.1}}{(\rho_{solid} - \rho_{gas}) d_p g} \quad (5\text{-}40)$$

$$Ar = \frac{{d_p}^3(\rho_{solid} - \rho_{gas})g}{\mu^2} \quad (5\text{-}41)$$

$$G_s = 0.01\rho_{solid}(v_{desulfurizer} - v_{terminal}) \quad (5\text{-}42)$$

$$m_{entrained\ solid} = G_s \cdot Surface\ area \quad (5\text{-}43)$$

$$TDH = \frac{{v_{rig}}^2}{g \cdot 10^{-3}} \quad (5\text{-}44)$$

5.3.6 ENERGY BALANCES

The energy balances are computed in both the reactors in order to calculate the heat which must be provided or extracted to sustain the process. In steady state conditions the balance accounts for: i) heat of the reactions (5-1) and (5-2), ii) sensible heat of the circulating solids which works at two different temperature levels (T_{REG} and T_{DES}), iii) sensible heat of the gas phases and, iv) heat released from the reactor to the ambient or to the heat recovery system (membrane wall or water jacket). In equations (5-45) and (5-46) the balance of the desulfurizer and regenerator are respectively reported, explicitly showing on the left side the net term to be added or removed. Both the reactions are exothermic. In the desulfurizer the sensible heat of the solids is released to the bed inventory while the syngas sensible heat is negligible (when HGD is applied after the WGS); therefore the heat released to the wall must balance the sum of the other terms avoiding a temperature increase. On the contrary, in the regenerator the solids coming from the desulfurizer must be heated up to the vessel working temperature as well as the air for the regeneration process. If the oxidation does not supply all the heat required, the reactor will cool down loosing eventually all the regeneration capacity. In this case an external heat source must be provided.

$$Q_{balance\ Des} = Q_{reaction} + Q_{sensible\_solids} - Q_{sensible\_gas} - Q_{wall} \quad (5\text{-}45)$$

$$Q_{balance\ Des} = Q_{reaction} - Q_{sensible_{solids}} - Q_{sensible\_air} - Q_{wall} \quad (5\text{-}46)$$

5.3.7 REACTOR THICKNESS DESIGN

The vessel thickness is calculated using the input data provided by Technip in the FP7 project CACHET-II. Once the design temperature and pressure are defined, the material required to withstand the working conditions is set. Therefore, the thickness is calculated as function of the diameter, temperature and pressure. The code interpolates inside the range of data supplied by Technip. An example of the data interpolation is reported in Figure 5-8 for an internal pressure of 60 bar. The overall range of validity is: 100 < T < 650 °C and 40 < p < 60 bar. The vessel material is a chromium-molybdenum alloy steel (A387gr11/22) when the temperature is below 400°C and incoloy when it is higher. The combination of high temperature and large diameter makes the steel thickness to increase sharply; therefore, when the reactor working temperature is higher than 500°C, it is worth to adopt an internal refractor.

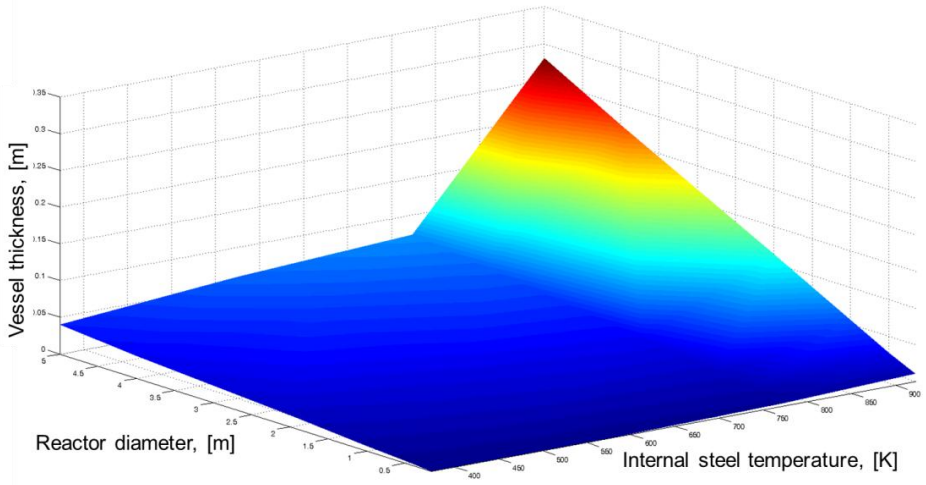

Figure 5-8: vessel thickness as function of the internal reactor diameter and the steel temperature; data reported for a given pressure equal to 60 bar. For a higher temperature and a larger reactor diameter the vessel stresses increase, requiring a larger thickness.

5.4 RESULTS

After being validated, the model has been adopted to simulate the desulfurization of a syngas obtained with a commercial size Shell gasifier. Before being sent to the desulfurization process, the syngas is partially converted in a high temperature/sulfur tolerant shift. This layout allows desulfurizing at high temperature keeping unchanged the gasification section, i.e. gasifier, syngas coolers and scrubber. This solution is more reliable than desulfurizing inside the gasification island; nevertheless some drawbacks arise: i) the syngas mass flow rate is higher because of the steam dilution for the shift reaction and, ii) the water partial pressure is higher with negative effects on the desulfurization equilibrium.

Table 5-5 reports the overall assumptions for the overall system. All the data reported in the next section refer to a given H_2S removal efficiency; the H_2S concentration in the incoming and treated syngas is kept fixed. The chosen sorbent is the same reported in Table 5-3.

Table 5-5: assumptions and inputs for the simulation of a commercial size desulfurizer unit.

Input data for the syngas desulfurization							
Syngas treated, kg/s	100						
Pressure, bar	40						
H_2S concentration in the treated syngas, ppmv	20						
Average void fraction desulfurizer	0.15						
Average void fraction regenerator	0.35						
Syngas Composition, %mol	CO	H_2	H_2O	H_2S	N_2	Ar	CO_2
	.18	.13	.11	.0015	.4984	.0001	.08

Figure 5-9 shows the flow regime diagrams for both the desulfurizer and the regenerator as consequence of the design approach defined in paragraph 5.3.4. The desulfurizer is designed to work in the fast fluidization region: this is reasonable as the treated syngas features a high mass flow rate. On the other side, the amount of converted sulfur is relatively limited, which keeps the regeneration air mass flow low. Consistently, the regenerator works in the region of bubbling flow fluidization. The reported considerations are not permanent rules since several parameters

can be modified in order to change the fluid-dynamic conditions of the two reactors (starting from the particle diameter). Nevertheless, this flow regime diagram is an useful tool when developing from scratch the reactors design.

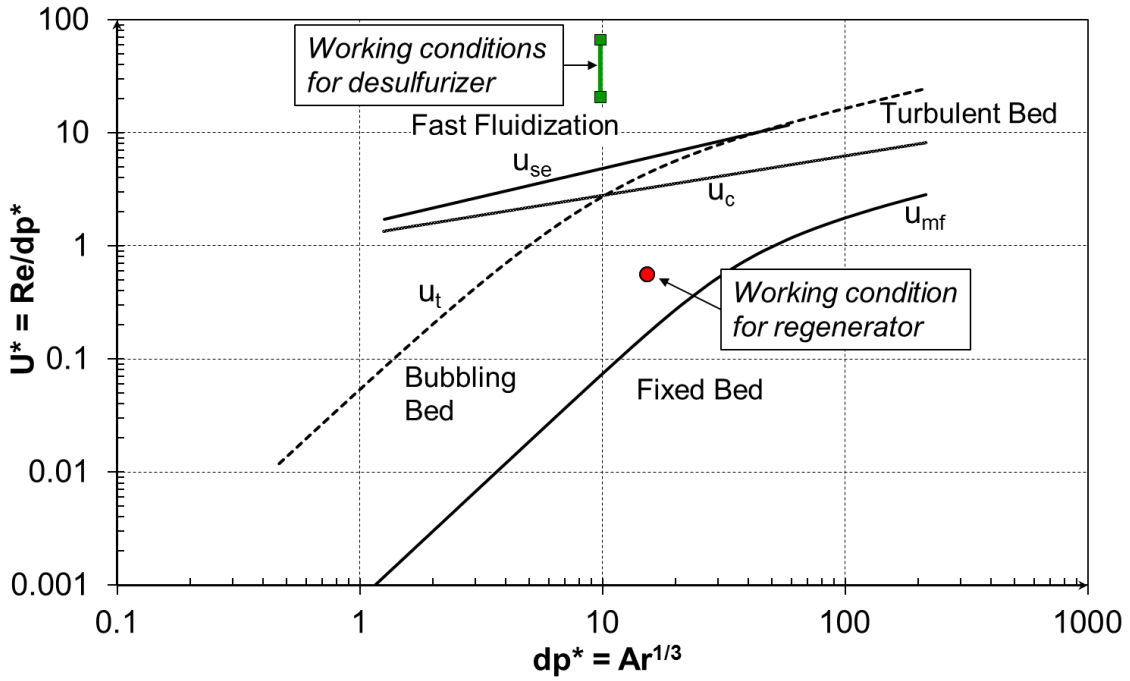

Figure 5-9: flow regime diagram for the whole range of gas-solid contacting. In green and red the working points of the desulfurizer and regenerator, respectively (obtained with fixed conditions reported in Table 5-5, but varying the sulfidation level inside each reactor); adapted from Grace [23].

Starting from the aforesaid considerations, a qualitative reactor layout has been realized and is reported in Figure 5-10. The desulfurizer (on the left hand side) is a turbulent/fast fluidization reactor with a heavy load cyclone for gas filtration and recirculation of the entrained solids. A loop seal must be adopted to avoid gas exchange between the two reactors. As the amount of entrained particles is higher than the regenerator demand, the larger part of solids is sent back to the desulfurizer through a loop-seal internal return leg. This behavior, confirmed by results presented in Figure 5-15, makes consistent the hypothesis of well stirred reactor for the solid phase. The regenerator reactor (on the right hand side) is a bubbling fluidized bed, with a cyclone for preliminary de-dusting and sorbent recovery. Once the solid is regenerated, it is sent back to the desulfurizer from the bottom part of the reactor as there are no entrained solids in a bubbling fluidized bed. Again, a loop seal is required to keep compartmentalized the gas phases and the solid phases.

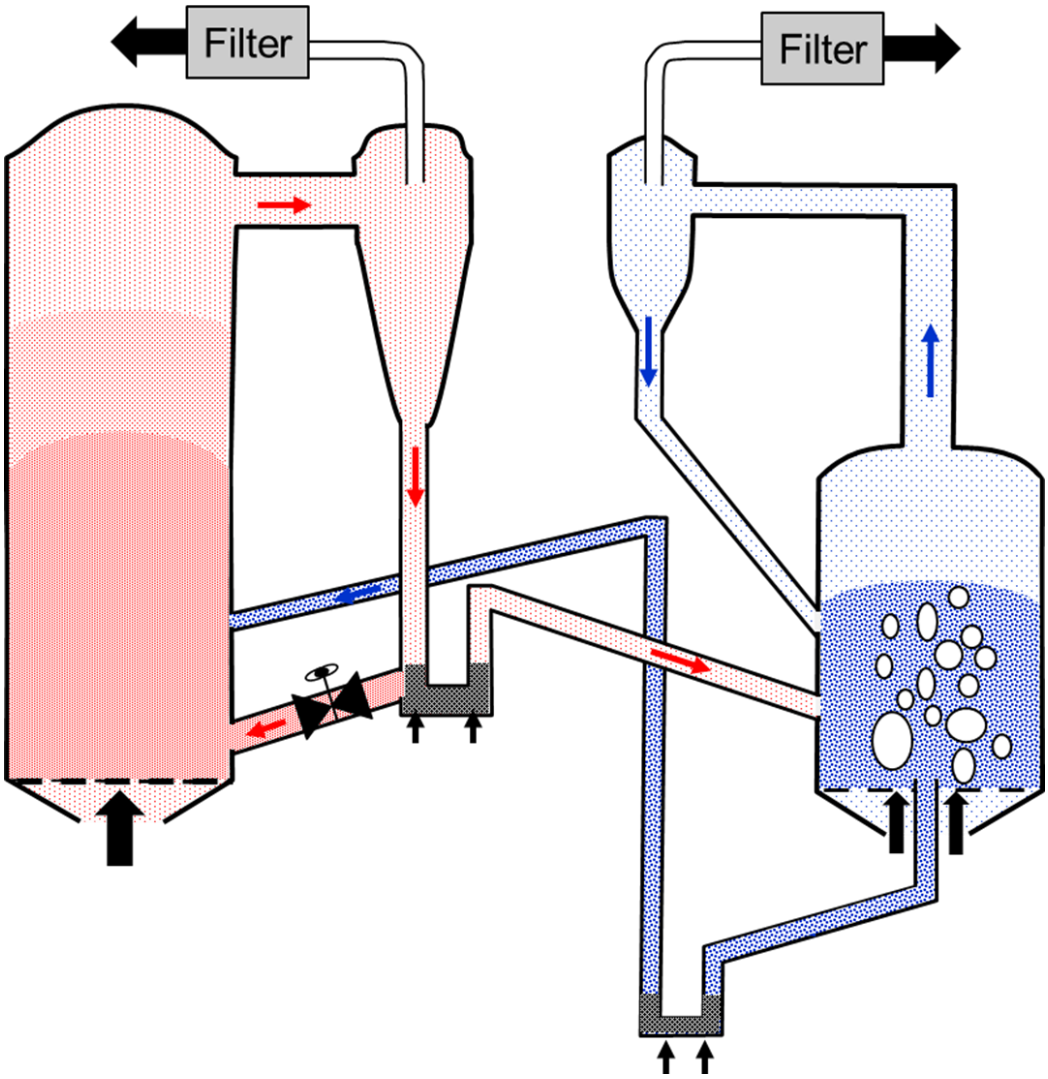

Figure 5-10: representation of the circulating fluidized bed system. On the left side, in red, the desulfurization reactor; on the right side, in blue, the regeneration reactor. As first design tentative, the desulfurizer is represented as a fast circulating fluidized bed while the regenerator as a bubbling fluidized bed.

The model of a circulating fluidized bed system features several variables which are deeply linked each other; therefore, the optimum reactor design can be obtained only analyzing the different working maps. In the following paragraph, several sensitivity analyses are presented trying to identify the most convenient operating parameters.

5.4.1 DESULFURIZER WORKING CONDITIONS

At constant H_2S removal level and entering syngas conditions, the desulfurizer is mainly affected by the working temperature and the inventory sulfidation level. The sorbent inventory required for different desulfurization temperatures and solid compositions is reported in Figure 5-11. It can be noted that:

- For $T_{desulfurizer}$ and $X_{desulfurizer}$ ranging between 500-600 °C and 0.4-0.6, respectively, the desulfurizer inventory varies between 65-1200 kmol of sorbent.

- The solid inventory is strongly dependent on the sulfidation level: the more sulfur present, the less active the material, due to the higher chemical and diffusive resistances. Coherently with the kinetic model, the solid inventory is more sensitive toward the sulfidation level at lower working temperature (the product layer diffusivity is exponentially function of the temperature).
- Similarly to the sulfidation level, also the working temperature strongly influences the sorbent inventory; at low sulfidation level the material is already active at lower temperature (500°C) while at high sulfidation level the inventory steeply decreases moving from 500 to 600°C. It must be stressed that the inventory-temperature curve features a minimum at about 590-595 °C; this is because of the temperature influence on the equilibrium concentrations. At temperature above 600°C the desulfurization is limited by the equilibrium (being the reaction exothermic, equilibrium is not favored at high T).

As briefly shown in the previous discussion, the desulfurizer working conditions should ideally imply: i) as lower as possible sulfidation level of the sorbent and, ii) moderately high temperature. Nevertheless, as shown in the next paragraphs, in a sustainable process the sulfidation level in the desulfurizer is limited by that one in the regenerator.

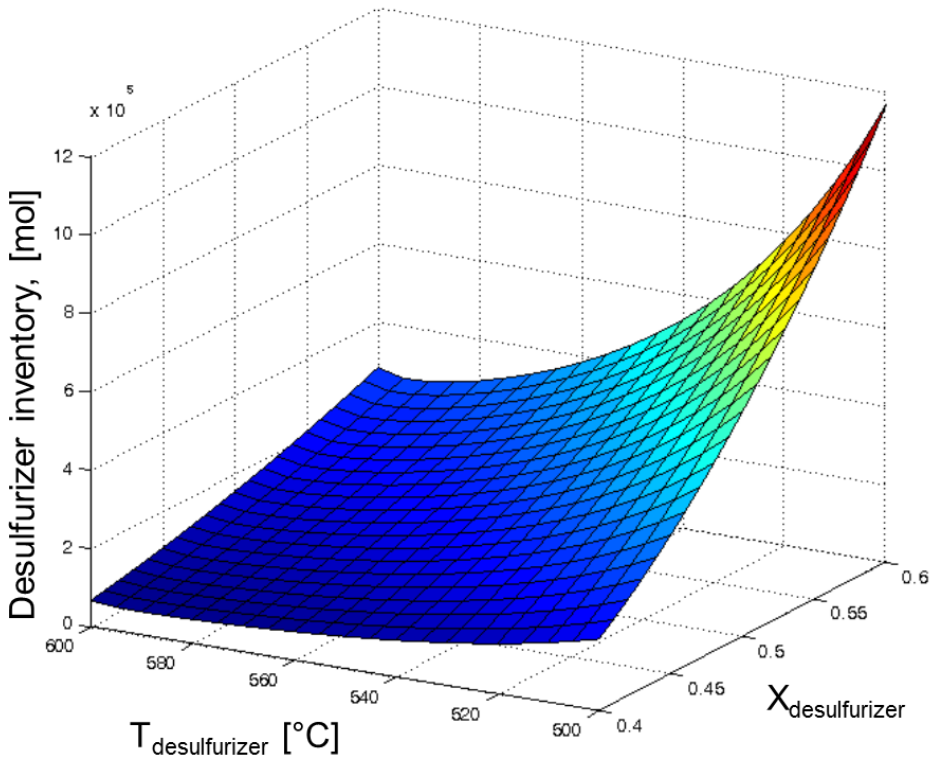

Figure 5-11: desulfurizer inventory required as function of the desulfurizer temperature and inventory composition.

5.4.2 REGENERATOR WORKING CONDITIONS

As aforesaid for the desulfurizer, also the regenerator strongly depends on the working temperature and sulfidation level. Provided the regenerator kinetic model (section 5.3.2), the process efficiency results to be particularly sensitive towards the reactor temperature as shown in Figure 5-12. It can be noted that the inventory-temperature correlation is very sharp: lowering the temperature from 700°C to 500°C brings about an inventory increase from 20 to 1500 kmol. This clearly remarks that the regeneration temperature must be as high as possible once the material and the structural limits are set. Similarly, the regenerator inventory is affected by the solid composition inside the reactor: when the sulfur level is higher (higher $X_{regenerator}$) the sorbent is more active towards reaction (5-2) and the inventory required for a given sulfur removal is lower.

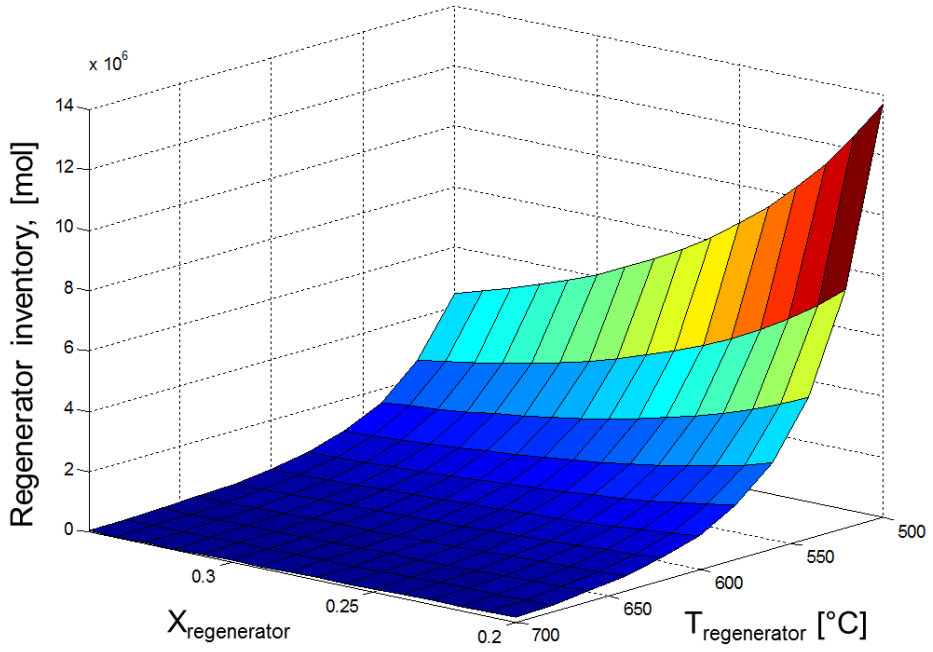

Figure 5-12: regenerator inventory as function of the sulfidation level of the solids in the regenerator and the working temperature.

In addition to the sulfidation level and regenerator temperature, the regeneration process is affected by the oxygen partial pressure in the regeneration gas and the amount of oxygen supplied compared to the stoichiometric one, which is fixed by the reaction (5-2) and the regeneration conversion. The definition of the oxygen overflow is defined in equation (5-47). Consistently, Figure 5-13 reports the sensitivity analysis towards oxygen partial pressure (upper side of the graph) and oxygen-overflow (lower side of the graph). At the same sulfidation level and temperature, e.g. 0.3 and 630 °C, the regenerator sorbent inventory lowers from 600 to 200 and to 100 kmol switching the O_2 molar fraction from 0.02 to 0.06 and to 0.1, respectively. This behavior is observed also increasing the amount of oxygen supplied at constant molar fraction due to the higher oxygen average availability along the reactor. It is straightforward that the higher the oxygen provided, either in term of molar fraction or molar flow, the lower the amount of sorbent required. Nevertheless, this must cope with the possibility of $ZnSO_4$ formation, which

would be detrimental for the good operation of the reactor. Therefore, values higer than x_{O2} = 0.1 or oxygen-overflow = 1.1 have not been considered.

$$oxygen\ overflow = \frac{\dot{N}_{O_2 entering\ the\ reactor}}{\dot{N}_{O_2 stochiometric}} \tag{5-47}$$

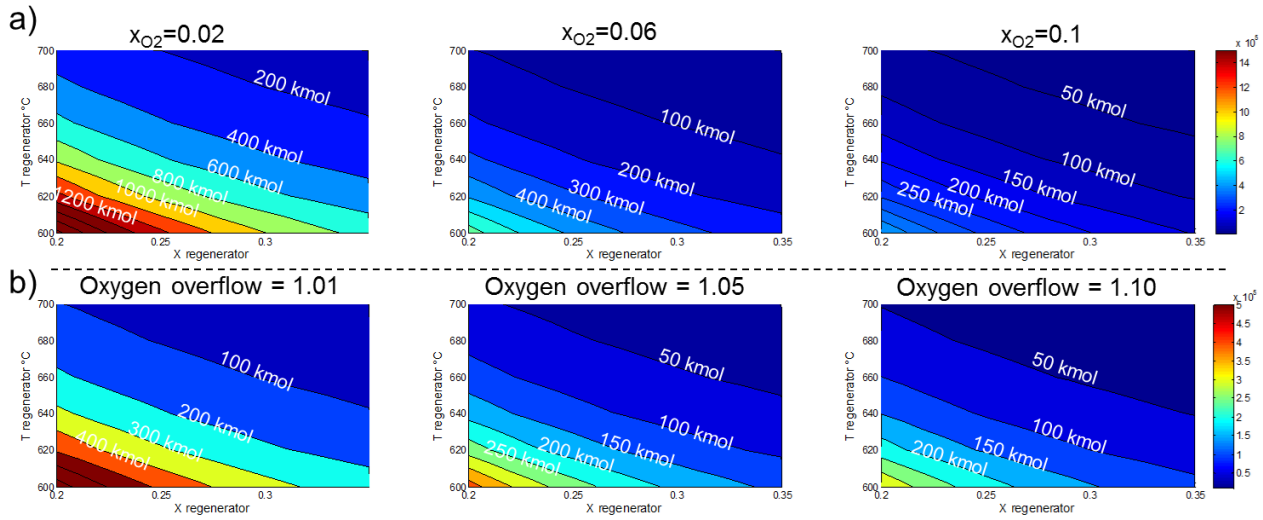

Figure 5-13: sensitivity analysis on the regenerator inventory at different X_{REG} and T_{REG} as function of: a) the oxygen concentration in the regeneration air (x values from 0.02 to 0.1; oxygen overflow=1.01); b) the extra amount of oxygen supplied compared to the stechiometric value (oxygen overflow values from 1.01 to 1.10, x_{O2}=0.06). Fixed parameters: T_{DES}=580 °C, X_{DES}=0.04.

5.4.3 *Overall system: Inventory, Circulating Zinc and Power Balances*

Concerning the overall system and besides the single vessel operating conditions, it is fundamental to establish the best combination of the sulfidation level in each reactor ($X_{S\text{-}DES}$ $X_{S\text{-}REG}$). These values are linked together as shown in paragraph 5.3.4 and establish both the circulating sorbent and the single reactor sorbent conversion ($X_{ZnS\text{-}Des}$, $X_{ZnS\text{-}Reg}$). As reported in Figure 5-14, both the reactor inventories are minimized when the difference $X_{S\text{-}DES}$-$X_{S\text{-}REG}$ is limited. In fact, provided that this value must be positive to keep the process self-sustainable (considering negligible the effect of make-up of fresh sorbent), the desulfurizer requires as low as possible $X_{S\text{-}DES}$ whilst the regenerator requires as high as possible $X_{S\text{-}REG}$. On the other hand, the more similar the sulfidation levels, the higher the required amount of circulating sorbent (see Figure 5-15). Nevertheless, it must be emphasized that the circulating sorbent flow is fairly low in IGCC applications; this is because of the moderate amount of sulfur to be removed, generally always below 10000ppm, and consistently the required Zn.

The power balances, shown in Figure 5-16, are affected by the sulfidation level similarly to the circulating sorbent: as far as the circulating solids are contained, the reaction heat is the main component in both equations (5-45) and (5-46). This results in a net power which must be released from the reactors. In such cases the desulfurizer and the regenerator must be equipped with a heat exchange surface, e.g. a membrane wall or flooded tubes system. Nevertheless, the required surface is limited because of the low amount of energy produced by the reactions. When the circulating sorbents increase, the sensible heat required for the thermal swing between

the desulfurizer and the regenerator temperature becomes predominant. For example when T_{DES}=550°C and T_{REG}=700°C, the desulfurizer has to release up to 1.6 MW, whilst the regenerator requires an external heat input up to 0.3 MW. This can be critical because: i) the heat surface inside the desulfurizer can be not sufficiently large and, ii) the heat to be supplied to the regenerator is at high temperature. One possible solution would require the use of extended fins inside the desulfurizer (or external heat exchanger) and a partial combustion of the regeneration air. In the latter case, in view of the small amount of fuel required, there would be a positive effect thanks to the lower quantity of diluent (which must be compressed up to the working pressure).

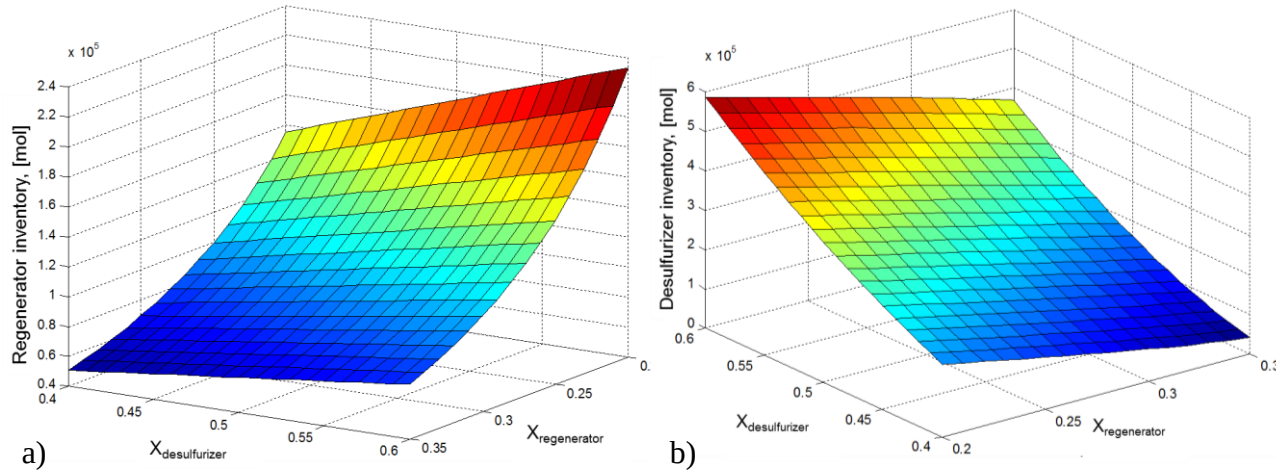

Figure 5-14: sorbent inventory as function of the sulfidation level in the desulfurizer X_{DES} and in the regenerator X_{REG}. a) regenerator inventory; b) desulfurizer inventory. Results obtained with: T_{DES}=550 °C, T_{REG}=700 °C, x_{O2}=0.04, oxygenoverflow = 1.01.

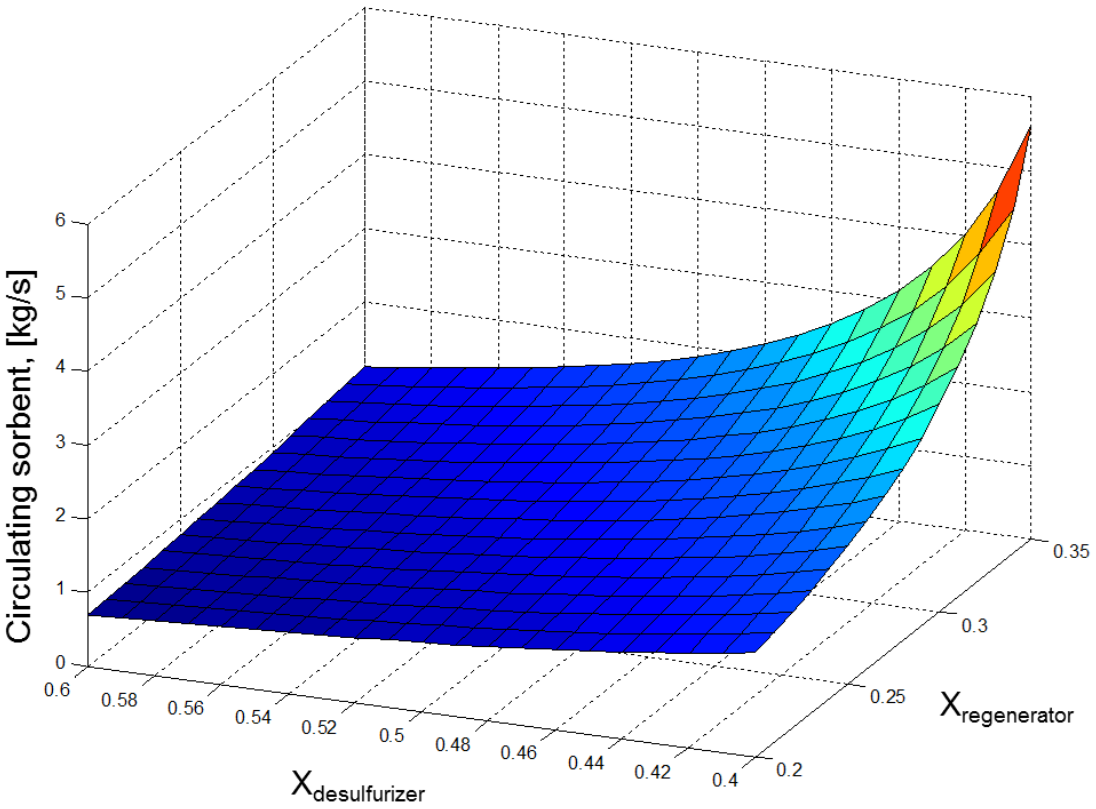

Figure 5-15: circulating sorbent as function of the desulfurizer and regenerator sulfidation level. Results obtained with: T_{DES}=550 °C, T_{REG}=700 °C, x_{O2}=0.04, oxygen-overflow = 1.01.

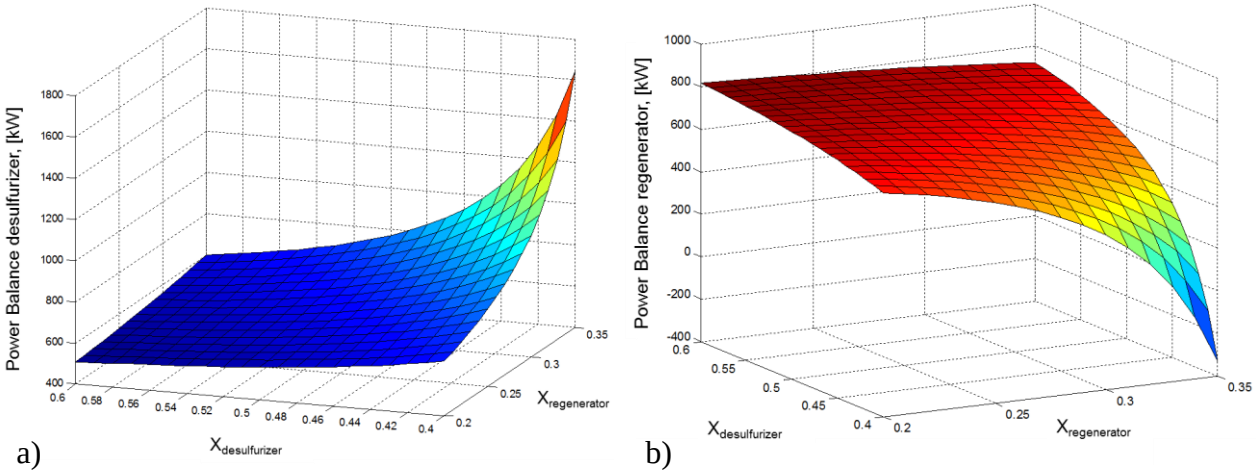

Figure 5-16: net power to be released (when > 0) or supplied (when < 0) from the desulfurizer and regenerator reactors; obtained with: T_{DES}=550 °C, T_{REG}=700 °C, x_{O2}=0.04, oxygen-overflow = 1.01

Finally, the main design parameters at different desulfurizer/regenerator sulfidation level are reported in Table 5-6.

Table 5-6: main design parameters for different value of sulfidation level inside the desulfurizer (0.4, 0.45 and 0.5) and the regenerator (0.25, 0.3, 0.35).

		DESULFURIZER						REGENERATOR				
$X_{S\text{-}DES}$	$X_{S\text{-}REG}$	v_{DES}, m/s	H_{DES}, m	D_{DES}, m	H/D	GS_{DES}, kg/sm^2	$solid_{DES}$ kg/s	v_{REG}, m/s	H_{REG}, m	D_{REG}, m	H/D	Thick. m
0.40	0.25	13.91	5.50	1.81	3.03	193.6	500.9	0.08	3.69	1.68	2.19	0.05
	0.30	18.38	4.77	1.58	3.02	261.1	511.2	0.08	2.79	1.68	1.66	0.05
	0.35	27.09	3.91	1.30	3.01	392.7	521.5	0.08	2.25	1.68	1.34	0.05
0.45	0.25	10.63	6.29	2.08	3.03	144.1	487.8	0.08	4.05	1.68	2.41	0.05
	0.30	13.10	5.69	1.87	3.04	181.4	498.2	0.08	3.05	1.68	1.81	0.05
	0.35	17.31	4.91	1.63	3.02	245.0	509.2	0.08	2.44	1.68	1.45	0.05
0.50	0.25	8.46	7.01	2.33	3.01	111.3	473.5	0.08	4.42	1.68	2.62	0.05
	0.30	9.92	6.50	2.15	3.02	133.3	483.8	0.08	3.30	1.68	1.96	0.05
	0.35	12.22	5.88	1.94	3.04	168.1	495.0	0.08	2.63	1.68	1.56	0.05

5.4.4 COST ESTIMATION

In this early stage of the system design, the reactors cost has been computed considering the amount and the quality of steel required for a given design, as already described in section 5.3.7.

Figure 5-17 reports three sensitivity analysis on the overall system cost as function of the sulfidation level inside each reactor:

1. Sensitivity analysis on the desulfurizer temperature, Figure 5-17a.
2. Sensitivity analysis on the regenerator temperature, Figure 5-17b.
3. Sensitivity analysis on the oxygen molar fraction in the regenerator, Figure 5-17c.

Considering that the system cost is proportional to the vessel dimensions which, in turn, are functions of the solid inventory, the overall cost is always minimized for values of $X_{S\text{-}DES}$ $X_{S\text{-}REG}$ as close as possible. Increasing the desulfurizer temperature makes the cost diagram smoother, lowering the maximum value but keeping similar the minimum cost (which in this case would be mainly affected by the regenerator). On the other hand, when the regenerator temperature is increased all the cost area lower: moving from 600°C to 700°C both the maximum and the minimum decrease to about one third of the first value. From Figure 5-17 a) and b) it is therefore clear that the temperature must be high enough to promote the reactions, limit the cost and, most of all, broaden the working condition intervals where the cost is minimized (for example, increasing the ΔX with no influence on the total costs). Finally, the sensitivity analysis on the oxygen molar fraction shows that the cost are similar between two different oxygen partial pressure; however the low-cost area is wider for x_{O2}=0.08.

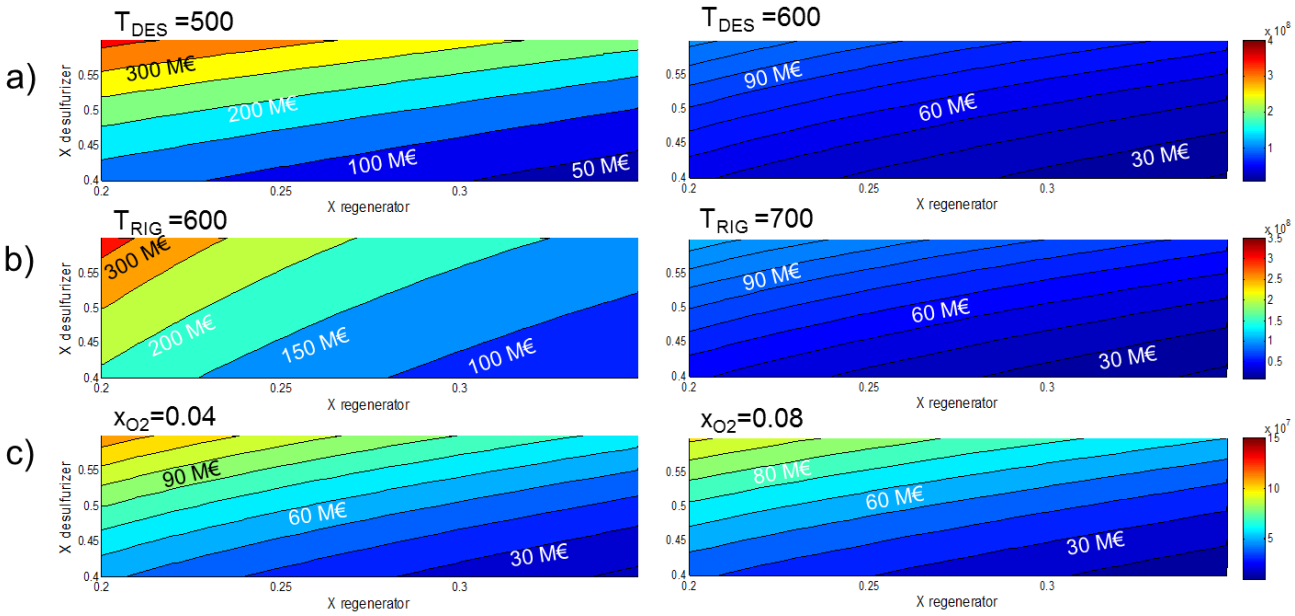

Figure 5-17: sensitivity analysis on the total reactor cost for different X_{REG} and X_{DES} as function of: a) desulfurizer working temperature (with T_{REG}=700 °C, x_{O2}=0.06, oxygen-overflow = 1.1); b) regenerator working temperature (with T_{DES}=580 °C, x_{O2}=0.06, oxygen-overflow = 1.1) and c) oxygen molar fraction (with T_{DES}=580 °C T_{REG}=700 °C, oxygen-overflow = 1.1).

5.5 Model Application to CACHET II Cu-Based Sorbents

The work package 3 in the EU research project CACHET II (Carbon Capture and Hydrogen Production with Membranes) focuses on high temperature (200-500°C) selective sulphur removal from hydrogen rich gas produced from sulphur containing fuel. Sulphur containing gas is a challenge to the Pd membranes that separates hydrogen from CO_2 and H_2O, and to ensure sufficient lifetime of the Pd-membrane the targeted sorbent cleaning efficiency (slippage) is 5-20 ppm H_2S upstream of the membrane.

The theoretical model above-described has been adapted to the Cu-based sorbent developed by Sintef. Unfortunately, the characteristics of the sorbent didn't completely match with the tool: being based on Cu, it requires two regeneration reactors for the conversion of CuO and $CuSO_4$ (see reactions (5-49) and (5-50)); on the contrary the ZnO based model considers only one regeneration reactor. However, the most important step of oxidative desulphurization could be well predicted by the model. A hypothetic reactor configuration is reported in Figure 5-18.

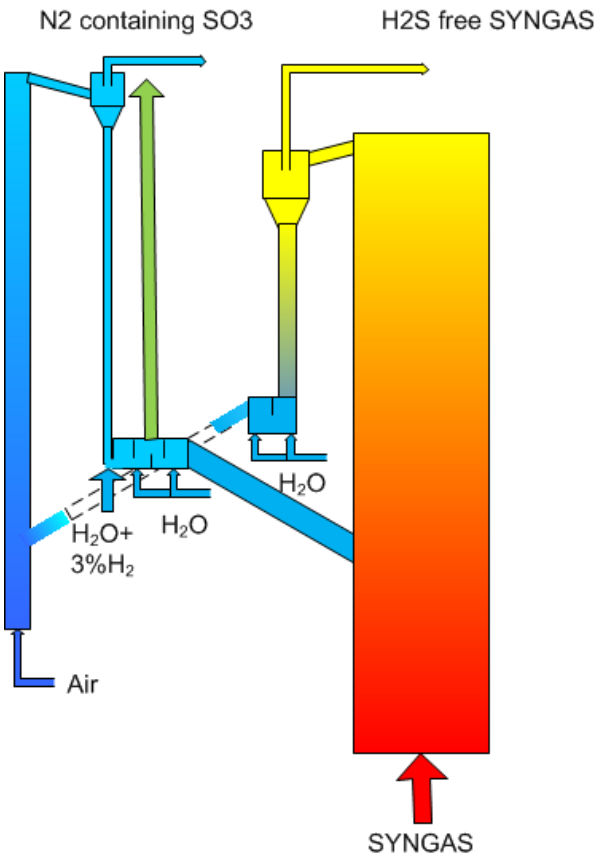

Figure 5-18: representation of one possible circulating fluidized bed system based on Cu sorbents, on the left in blue the regeneration reactors; on the right side in red the desulfurizer. This design was proposed by SINTEF as member of CACHET-II.

As for the Zn case, the hot raw syngas is supposed to fluidize the absorption reactor where sulfur is removed according to reaction (5-48). Solid particles are separated by a cyclone and ducted to the regeneration section, while the syngas exiting from the top of the cyclone is cleaned from fines in a hot gas filter. The sulfur-laden solids pass through the regenerator section. In the first regenerator reactor, the solid mixture interacts with diluted air (4% O_2) and $CuSO_4$ and CuO are formed (reaction (5-49)); then in the second bed the solid mixture is completely regenerated thanks to the reaction with hydrogen (reaction (5-50)). The SO_2 rich gas released after the cyclone and the hot filter is expanded and sent to the FGD.

- *Sulfur removal*

$$2Cu(s) + H_2S(g) \leftrightarrow H_2(g) + Cu_2S(g) \quad (5\text{-}48)$$

- *Regeneration*

$$Cu_2S(s) + 2.5O_2(g) \leftrightarrow CuSO_4(s) + CuO(s) \quad (5\text{-}49)$$

$$CuSO_4(s) + CuO + 3H_2(g) \leftrightarrow 2Cu(s) + SO_2(g) + 3H_2O \quad (5\text{-}50)$$

5.5.1 MODELING AND KINETICS

The model features the same equations presented in chapter 5.3 but for the stoichiometric coefficient and the equilibrium constant, which refers to a new equation.

- Desulfurization:

$$2\dot{N}_{sulfur} \cdot \eta_{S-conversion} = \dot{N}_{Cu} \cdot \frac{dX_{Cu}}{dt} \tag{5-51}$$

$$\frac{n_{sorb} rate_{sorb}}{2n_{gas,in}} = \frac{M + X_{H2S,equil}}{M+1} ln\left(\frac{X_{H2S,equil}}{X_{H2S,equil} + X_{H2S,out}}\right) \tag{5-52}$$

$$y_{H2S,out} = y_{H2S,in}\left[1 - X_{H2S,equil}\left(1 - e^{\frac{-n_{sorb} rate_{sorb}}{2n_{gas,in}\beta}}\right)\right] \tag{5-53}$$

Where:

$$M = \frac{y_{H_2,in}}{y_{H2S,in}} \quad X_{H2S,equil} = 1 - \frac{M}{k_{equil}} \tag{5-54}$$

$$\beta = \frac{M + X_{H2S,equil}}{k_{equil} M + 1} \approx 1 \quad rate_{sorb} = \frac{C_{H2S,in}}{dF/dX} \tag{5-55}$$

TG testing of the sulphur sorbent was performed in a high pressure TGA apparatus at SINTEF. The gas speed and H_2S concentration were varied in order to make sure that the sorption was the limiting step. Results showed that the reaction is limited only by the kinetic parameter τ_{USC}. The data fitting of the kinetic expression $(1-(1-X)^{1/3})$ vs. time is reported in Figure 5-19, while the resulting fitting equation is shown in (5-56). A kinetic of the first order is assumed also in this case as for the Zn sorbent.

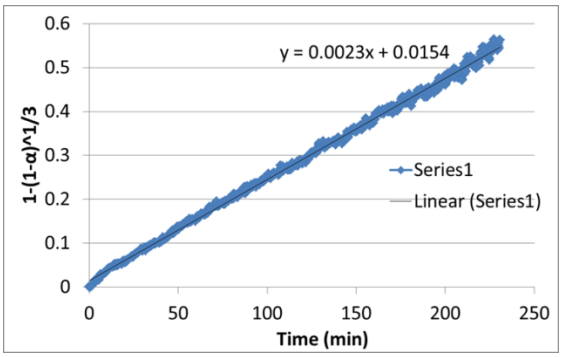

Figure 5-19: kinetic conversion vs time.

$$\tau_{KIN} = 3850/C_{H2S} \cdot e^{(-20000/RT)} \tag{5-56}$$

5.5.2 RESULTS

Thanks to the kinetic model of the desulfurizer, different data can be obtained and transferred to the process simulation.

Figure 5-20 reports a general picture of the Cu-based desulfurization process: the H_2S slip is lower when the sorbent is more active for a given number of solid inventory. For an IGCC application (>100kg/s of syngas to be treated) there is the need of at least 4000 mol of Cu.

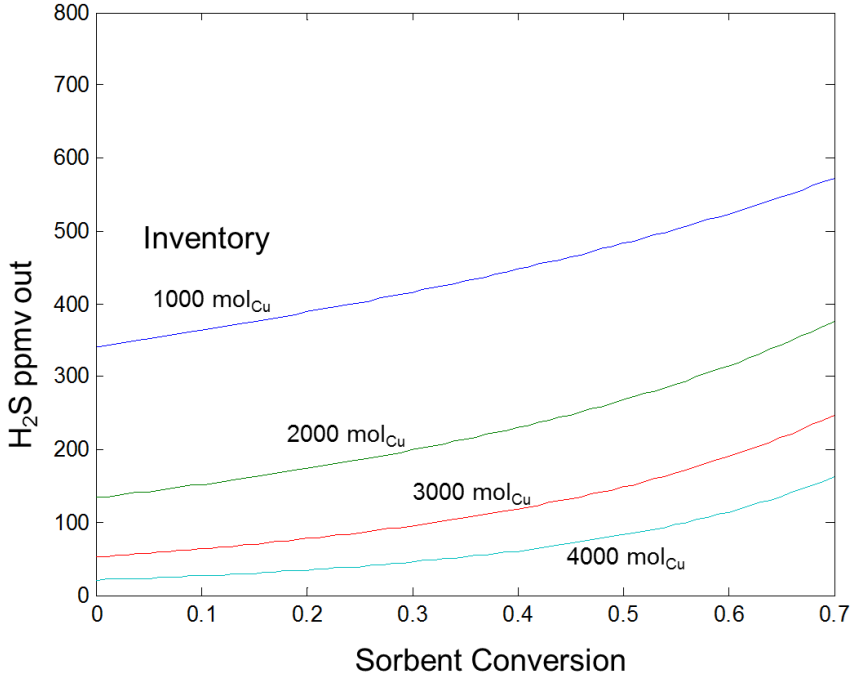

Figure 5-20: H_2S at the desulfurizer exit as function of the sorbent conversion through the reactor (x axis) and the amount of solid inside the reactor

Figure 5-21 and Figure 5-22 report different reactor design conditions required to have 5 ppm of H_2S in the released syngas. The sorbent inventory increases at higher sulfidation level inside the bed (X_{des}) because the sorbent is less active and this must be encompassed by a higher number of sorbent moles. Similarly, lower reactor temperature makes the kinetic slower with an inventory increase.

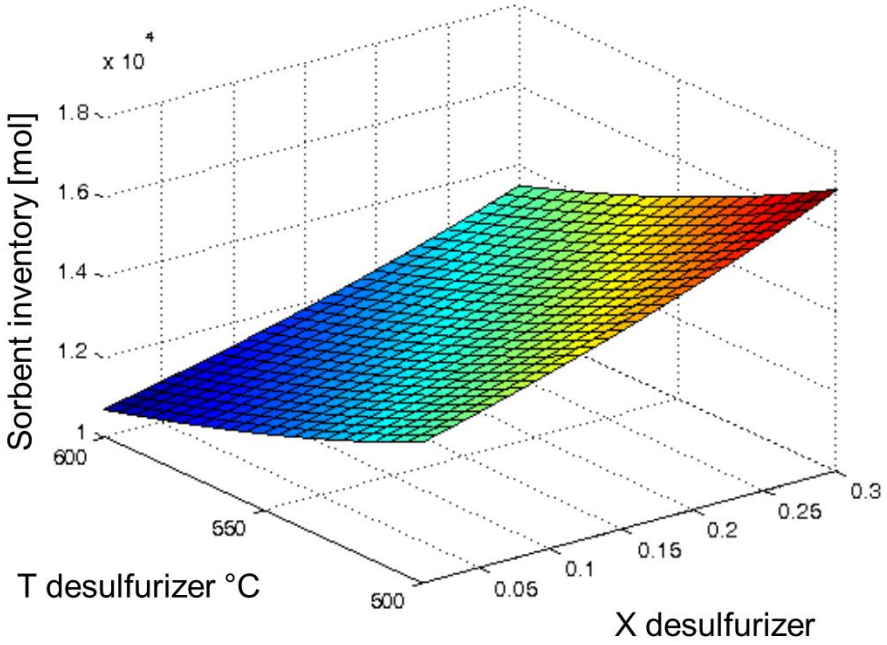

Figure 5-21: sorbent inventory as function of the desulfurizer temperature and the solid composition inside the reactor

The reactor cost is directly proportional to the reactor volume which once again is linked to the required inventory; therefore the 3D curve reported in Figure 5-22 presents the same shape of Figure 5-21. The desulfurizer cost can be easily kept below 4 M€ by working at 550 °C and between 0.1-0.2 solid conversion. Design parameters and costs are reported in Table 5-7 for different desulfurizer conversion and temperature.

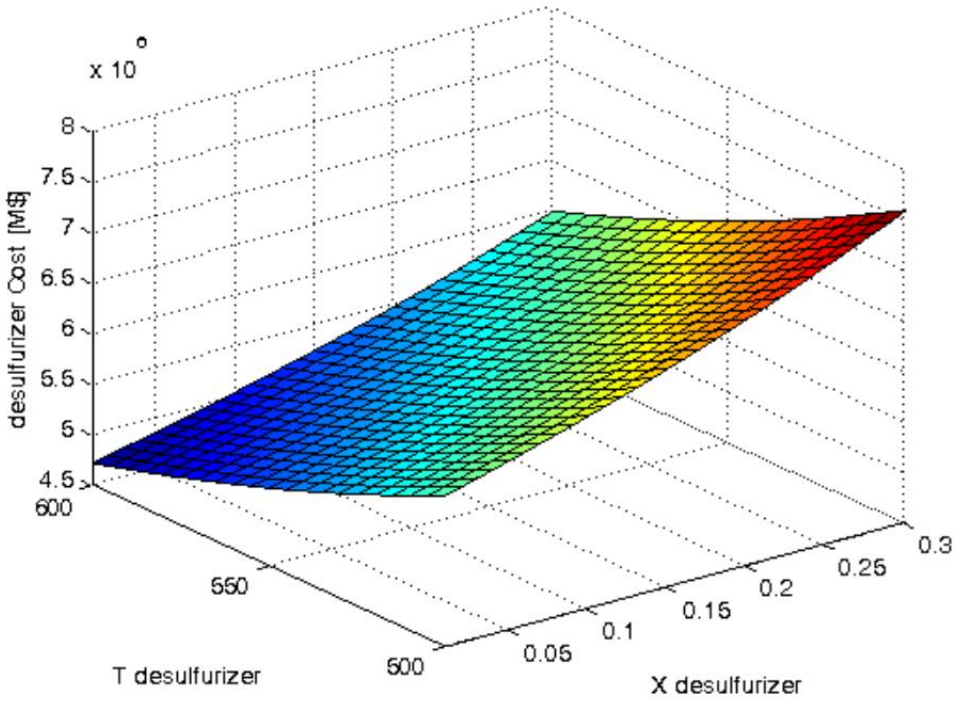

Figure 5-22: desulfurizer cost as function of the desulfurizer temperature and the desulfurizer solid conversion

Table 5-7: Inventory, height, diameter, volume and cost as function of desulfurizer temperature and conversion

T [°C]	X	Inventory [mol]	H [m]	D [m]	V [m^3]	Cost [M€]
500	0.1	1.44E+04	3.85	0.95	2.75	4.9
500	0.2	1.56E+04	3.96	0.98	2.98	5.3
500	0.3	1.70E+04	4.08	1.01	3.25	5.8
525	0.1	1.35E+04	3.78	0.93	2.58	4.6
525	0.2	1.46E+04	3.85	0.96	2.79	4.9
525	0.3	1.59E+04	3.97	0.99	3.05	5.4
550	0.1	1.27E+04	3.70	0.91	2.42	4.3
550	0.2	1.37E+04	3.77	0.94	2.62	4.7
550	0.3	1.50E+04	3.88	0.97	2.87	5.1
575	0.1	1.20E+04	3.60	0.90	2.29	4.1
575	0.2	1.30E+04	3.71	0.92	2.48	4.4
575	0.3	1.42E+04	3.82	0.95	2.71	4.8
600	0.1	1.14E+04	3.56	0.88	2.17	3.9
600	0.2	1.23E+04	3.67	0.90	2.35	4.2
600	0.3	1.34E+04	3.77	0.93	2.57	4.6

REFERENCES

[1] **Kohl, Arthur and Nielsen, Richard.** *Gas Purification.* Fifth Edition. s.l. : Gulf Publishing Company.

[2] **Meng, Xiangmei, et al.** In bed and downstream hot gas desulphurization during solid fuel gasification: a review. *Fuel Processing Technology.* s.l. : Elsevier, 2010. Vol. 91, pp. 964-981. 10.1016/j.fuproc.2010.02.005.

[3] **Gupta, R. and Gangwal, S.K.** Enahnced Durability of Desulfurization Sorbents for Fluidized Ved Applications. *Report, Research Triangle Institute.* 1992.

[4] **Mojtahedi, Wahab.** H2S Removal from Coal Gas at Elevated Temperature and Pressure in Fluidized Bed with Zinc Titanate Sorbents. 1. Cyclic Tests. *Energy & Fuels.* s.l. : ACS, 1995. Vol. 9, pp. 429-434.

[5] **Konttinen, J.T., Zevenhoven, A.P. and Hupa, M.M.** Hot Gas Desulfurization with Zinc Titanate Sorbents in a Fluidized Bed. 1. Determination of Sorbent Particle Conversion Rate Model Parameters. *Ind.Eng.Chem.Res.* s.l. : ACS, 1997. 36, pp. 2332-2339.

[6] **Konttinen, J.T., et al.** Modeling of Sulfided Zinc Titanate Regeneration in a Fluidized-Bed Reactor. 1. Determination of the Solid Conversion Rate Model Parameters. *Ing.Eng.Chem.Res.* s.l. : ACS, 1997. 36, pp. 5432-5438. S0888-5885(97)00035-3.

[7] **Park, J. et al.** Simultaneous removal of H2S and COS using Zn-based solid sorbents in the bench scale continuous hot gas desulfurization system integrated with a coal gasifier. *Korean J.Chem. Eng.* 2012. Vol. 29, 12, pp. 1812-1816.

[8] **DOE/NETL.** *Pinon Pine IGCC Power Project Assessment.* 2002. 2003/1183.

[9] **Sughrue, Edward L., et al.** *Desulfurization and Sorbents for same. 6,656,877 B2* United States, Dec 2, 2003. Conocophillips.

[10] **Bagajewicz, M.J.** Studies on hot gas hydrogen sulfide removal sorbents in fixed-bed reactors at high temperatures. *PhD Thesis.* s.l., USA : California Institute of Technology, 1988.

[11] **Jothimurugesan, K and Gangwal, S.K.** Regeneration of zinc titanate H2S sorbents. s.l. : Ind.Eng.Chem.Res, 1998. 37, pp. 1929-1933.

[12] **Woods, M.C., et al.** Reaction between H2S and Zinc Oxyde-Titanium Oxyde Sorbents. 1. Single Pellet Kinetic Studies. *Ind.Eng.Chem.Res.* s.l. : ACS, 1990. 29, pp. 1160-1167.

[13] **Barin, I., Knacke, O. and Kubaschewski, O.** *Thermodynamic Properties of Inorganic Substances-Supplement.* New York - Berlin : Springer-Verlag, 1977.

[14] **Kunii, Daizo and Levenspiel, Octave.** Fluidized Reactor Models. 1. For Bubbling Beds of Fine, Intermediate, and Large Particles. 2. For the Lean Phase: Freeboard and Fast Fluidization. s.l. : Ind. Eng. Chem. Res., 1990. Vol. 29, 7, pp. 1226-1234.

[15] —. The K-L reactor model for circulating fluidized beds. s.l. : Chemical Engineering Science, 2000. Vol. 55, pp. 4563-4570.

[16] **Konttinen, J.T., Zevenhoven, C.A.P. and Hupa, M.M.** Hot Gas Desulfurization with Zinc Titanate Sorbents in a Fluidized Bed. 2. Reactor Model. *Ind.Eng.Chem.Res.* 1997. 36, pp. 2340-2345.

[17] **Kunii, Daizo and Levenspiel, Octave.** *Fluidization Engineering.* s.l. : Butterworth-Heinemann. 0-409-90233-0.

[18] **Lew, Susan, Sarofim, Adel F. and Flytzani-Stephanopoulos, Maria.** Modeling of the Sulfidation of Zinc-Titanium Oxide Sorbents with Hydrogen Sulfide. s.l. : AIChE Journal, 1992. Vol. 38, 8, pp. 1161-1169.

[19] **Zevenhoven, Cornelis A.P., Yrajas, K. Patrik and Hupa, Mikko M.** Hydrogen Sulfide Capture by Limestone and Dolomite at Elevated Pressure. 2. Sorbent Particle Conversion Modeling. s.l. : Ind.Eng.Chem.Res., 1996. 35, pp. 943-949. 0888-5885/96/2635-0943$12.00/0.

[20] **Levenspiel, Octave.** *Chemical Reaction Engineering.* s.l. : John Wiley & Sons. 0-471-25424-X.

[21] **Konttinen, J.T., Zevenhoven, C.A.P. and Hupa, M.M.** Modeling of Sulfided Zinc Titanate Regeneration in a Fluidized-Bed Reactor. 2. Scale-Up of the Solid Conversion Model. *Ind.Eng.Chem.Res.* s.l. : ACS, 1997. 36, pp. 5439-5446.

[22] **Basu, Prabir.** *Combustion and Gasification in Fluidized Beds.* s.l. : Taylor & Francis, 2006. 0-8493-3396-2.

[23] **Grace, J.R.** *Can. J. Chem. Eng.* 1986. Vol. 64, p. 353.

[24] **Yi, Chang-Keun, et al.** Simultaneous Experiments of Sulfidation and Regeneration in Two Pressurized Fluidized-bed Reactors for Hot Gas Desulfurization of IGCC. *Korean Journal of Chemical Engineering.* 2001. 18, pp. 1005-1009.

6 USING HYDROGEN AS GAS TURBINE FUEL

Nomenclature and Acronyms

ASU: Air Separation Unit
CC: Combined Cycle
EBC: Environmental Barrier Coating
EINOX: NO_X emission index, ppmvd @15% O2
GT: Gas Turbine
G: Mass flow rate, kg/s
h: Average gas-to-blade heat transfer coefficient, W/m2K
HRSC: Heat Recovery Steam Cycle
HRSG: Heat Recovery Steam Generator
IGCC: Integrated Gasification Combined Cycle
LHV: Low Heating Value, MJ/kg
NGCC: Natural Gas Combined Cycle
$p_{C,IN}$: combustor inlet pressure, bar
ppmvd: part per million volume dry
STFT: SToichiometric Flame Temperature
T: Temperature, °C or K
$T_{C,IN}$: combustor inlet temperature, °C or K
TFL: flame temperature, K
TPZ: temperature in combustor primary zone, K
TBC: Thermal Barrier Coating
TIT: Turbine Inlet Temperature, °C or K
TITISO: Turbine Inlet Temperature ISO, °C or K
TOT: Turbine Outlet Temperature, °C or K
Φ: Equivalence ratio

The following chapter aims to establish the performance of a gas turbine when using hydrogen rich mixture. This work was carried out thanks to a research agreement with ENEL S.p.a.

Gas turbine equipped with diffusive or premixed flame combustor has been compared. Slightly different assumptions about the machine were considered in order to reproduce the average ENEL electric park.

6.1 INTRODUCTION

Large scale power plants with pre-combustion CO_2 capture, e.g. Integrated Gasification Combined Cycles and Integrated Reforming Combined Cycles, convert the primary fuel into a hydrogen rich syngas then burned in a combined cycle to achieve the maximum conversion efficiency into electricity. However, the use of hydrogen rich syngas in gas turbines poses a number of issues already addressed by several authors [1-3]. The most important issue to be tackled concerns the mitigation of NO_X emissions which becomes critical because of the very high hydrogen flame temperature. This issue is relevant not only for adapting machines originally designed for natural gas but also for developing from scratch machines for hydrogen rich fuels. In diffusive flame combustors, the flame tends to be close to the stoichiometric conditions and hence its temperature must be mitigated by diluting the fuel with inert species, such as steam and nitrogen. This dilution causes a significant decrease of the plant efficiency. On the other hand, in lean premixed combustors the flame temperature is directly limited by the large excess of air and no dilution is required. However, realizing a stable premixed hydrogen flame is not straightforward because of its high flame speed demanding high air velocities to obtain short mixing times and high turbulence rates. As a drawback, premixed combustors may suffer from high pressure drops. For this reason gas turbine manufacturers [4-6] are currently

investigating different combustor geometries in order to obtain the same NO_X emissions and combustor pressure drops achieved in natural gas fueled lean premixed combustors.

This work aims at estimating the efficiency gain attained in a combined cycle by substituting inert diluted diffusive flame combustors with lean premixed combustors.

6.2 ISSUES RELATED TO THE USE OF HYDROGEN

With respect to natural gas, hydrogen combustion causes a variation of the flame properties, mainly temperature, speed and geometry and a higher water concentration in the product gases. All these variations, along with the change of the fuel flow rate due to a change in the LHV, bring about a modification of the machine design specifications. Current market of syngas/hydrogen fired gas turbines is minor and therefore these models are actually derived from machines originally designed to run on natural gas. As a consequence, some variations of the operating parameters are required in order to comply with the compressor-turbine matching and to guarantee an adequate blade lifetime and NO_X emissions. Such variations typically imply a change of the TIT with respect to the nominal point of the natural gas fired engine. A description of such a scenario is reported in [1]. Differently, in this work we focus on machines specifically designed for hydrogen rich fuels. For this reason, in the following analysis we assume that the compressor geometry and size are adjusted to match the expander performance map at the specified pressure ratio and air to fuel mass flow rates ratio.

When switching from natural gas to hydrogen, one of the main concerns is limiting the NO_X emissions provided that: i) lean premixed (a.k.a. Dry Low NO_X) combustors used with natural gas, at present are not commercially available for hydrogen because of technical hurdles posed by the very high reactivity of hydrogen; ii) the flame temperature of hydrogen is significantly higher than natural gas. The current industrial practice to burn H_2 in a gas turbine consists in employing diffusive flame combustors and preventing NO_X formation by diluting the fuel with steam or nitrogen, made available from the steam cycle or an ASU respectively.

For instance, according to [8], steam dilution (where steam is either extracted from the steam cycle or supplied by a saturator) is adopted in the Wabash River IGCC and in the Fusina pilot plant of Enel [9], while nitrogen dilution in the Tampa plant, and in the Ashtabula IGCC project. Typically, if an ASU is available at the plant site, nitrogen is preferred to steam because it implies a lower efficiency penalty, as it will be shown in Section 6.6.

However, the use of fuel dilution penalizes plant efficiency, operation flexibility and costs for the following reasons:

- If nitrogen is used, a nitrogen compressor is necessary to pressurize the gas from the ASU delivery pressure up to the minimum combustor inlet pressure. Not only does the additional compressor imply an economic penalty due to its cost, but also a decrease of the net plant efficiency due to its electric consumption. Provided that in a combustion the diluting nitrogen takes the place of an equivalent excess air flow rate, the electric, mechanical and polytropic efficiencies of the nitrogen compressor are significantly lower than the GT air compressor. Moreover discharge pressure must be 5-10 bar higher because combustors require a fuel injection pressure which may be significantly higher

than the air pressure. Thus, even if pure nitrogen is an energy "free" by-product of the ASU, nitrogen dilution implies an efficiency penalty.

- If steam is extracted from the heat recovery steam cycle and used for dilution, the plant efficiency is penalized for two reasons: (i) the exergetic loss arising when mixing steam and fuel, (ii) the decrease of the turbine inlet temperature necessary to cope with the higher H_2O content in the flue gases. If steam is extracted from the steam turbine and mixed with fuel, the decrease of the steam turbine power output is not compensated by the increase of the gas turbine power because a large exergetic loss occurring when steam irreversibly flashes from its extraction pressure to the H_2O partial pressure of the fuel stream. Moreover, as an additional drawback, the higher H_2O content of the flue gases increases the hot gas-blade heat transfer coefficient resulting in an increase of the blade metal temperature, as pointed out in [1-3]. As a result, the TIT must be lowered to preserve the blade integrity and expected lifetime.
- The operation of the GT is strictly constrained by the matching with the ASU or the steam cycle if N_2 or steam are used. This affects the operational flexibility of the plant. In addition, the operation of the stand-alone gas turbine (i.e., without an HRSG or the supply of N_2) is not possible.
- Last but not least, even if large mass flow rates of diluents are employed, diffusive flame combustors cannot meet the increasingly demanding targets on NO_X emission [5].

To overcome the above mentioned limitations, gas turbine manufacturers are currently developing premixed hydrogen combustors [4-6]. However, the task is challenging because: i) due to the larger flammability limits of hydrogen and the lower ignition temperatures of hydrogen with respect to natural gas, it is difficult to mix fuel and air without ignition, ii) the very high flame speed may cause unstable operation, specially at partial load, due to the flash-back phenomena, iii) despite the high gas speed imposed by the fuel properties, it is necessary to design a combustor geometry with limited pressure drops and, iv) low sensitivity to the minor constituents, which may be present in the fuel stream (i.e., CO, CO_2, CH_4), is required. Regarding the first issue, Alstom researchers showed in [4] that the auto-ignition delay time for a hydrogen rich mixture (H_2/N_2 = 70/30 by volume) is ten times shorter than natural gas. This event highlights not only possible auto-ignition issues in the mixing zone, but also the necessity of creating a turbulent flow which promptly mixes hydrogen and air. Indeed, to limit NO_X emissions, it is mandatory to obtain a perfect mixing of air and fuel before the combustion takes place. Thus, turbulent vortices and air velocity must be considerably intensified to obtain an uniform fuel/air distribution and such expedients may considerably increase the combustor pressure drop. Thus, high gas velocities are imposed not only by the flash-back risks but also the turbulence required by the fuel/air mixing step. It has been noted that adding some nitrogen to the fuel can facilitate fuel/air mixing [4, 6] and, for this reason, current research projects consider H_2-N_2 mixtures and not pure H_2.

Several approaches to premixed hydrogen combustors have been studied:

- Swirl premixers, similar to DLN combustors for natural gas [10]
- Lean Direct Injection [11]
- Micro-mixers [6, 12]

For example, GE researchers presented in [6] their test procedures and experimental facilities used to develop a very promising multi-tube mixer design with limited pressure drops, about 3.5% air side, and quite low NO_X emissions, 6 ppm at 15% O_2, 1900K of flame temperature, 17 bar, and 60/40 H_2/N_2 (volume basis) as fuel. Such design has been tested in a full-can rig with high hydrogen mixtures. Also Siemens researchers are developing an advanced combustion system capable of operating at firing temperatures of H-class GTs with less than 10 ppm of NO_x at 15% O_2 [5].

Firing hydrogen instead of methane implies a number of effects which involve also the design of the turbine. More specifically, assuming that the compressor pressure ratio and the TIT are kept at the same values of the natural gas fired case, the increase of the H_2O content in the product gases caused by the higher H/C ratio of the fuel, leads to:

- Increment of the product gas to inlet air volumetric flows ratio;
- Increment of the turbine enthalpy drop;
- Increment of the turbine outlet temperature (TOT);
- Increment of the heat-transfer coefficient on the outer side of the turbine blades;
- Faster degradation of Environmental Barrier Coatings (EBC) and Thermal Barrier Coatings (TBC).

Figure 6-1 shows the influence of hydrogen combustion at different steam or nitrogen dilution rates on: i) the isentropic enthalpy drop and, ii) the gas turbine combustor outlet to inlet volumetric flow rates ratio with outlet temperature = 1400°C, pressure = 17.0 bar and diluents at 27.1 bar, 300°C. The figure represents the percentage variation with respect to the natural gas operation.

Compared to natural gas, the simple hydrogen combustion increases the enthalpy drop by about 5%. Such variation remains roughly constant with respect to the nitrogen flow added for dilution while increases appreciably with the steam flow rate. Indeed, assuming the working fluid as an ideal gas and observing that the steam specific heat capacity (c_p) approximately doubles that of N_2, it is possible to prove that the isentropic expansion enthalpy drop rises as a consequence of the increased flue gases c_p. For instance, adding steam to reach a stoichiometric flame temperature equal to 2300 K implies a 10 % increase of the turbine enthalpy drop with respect to the natural gas case. Such variation must be considered when designing the turbine stages and carefully evaluated with respect to the maximum allowed stage load. Regarding this issue, three stage turbines, which turn out to be competitive for natural gas, may not be suitable for fulfilling a so large enthalpy drop, as pointed out in [13].

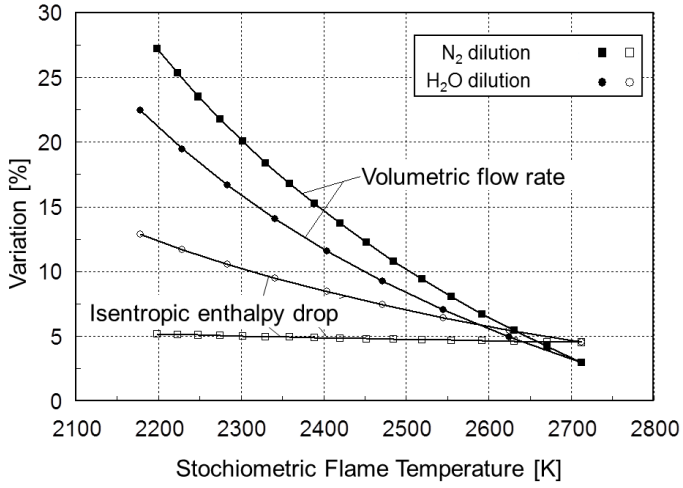

Figure 6-1: variation of the isentropic expansion enthalpy drop and turbine inlet volumetric flow due to the use of hydrogen with/without diluents with respect to natural gas operation (for fixed TIT and pressure ratio). The variation is plotted as a function of the stoichiometric flame temperature when diluting hydrogen with nitrogen and steam.

Despite the appreciable increase of the expansion enthalpy drop, the increase of H_2O fraction causes an increase of the turbine outlet temperature (TOT) with respect to natural gas operation, for a given pressure ratio and TIT. This effect can be motivated by recalling that (i) H_2O is characterized by a lower c_p/c_v ratio (specific heat at constant pressure / specific heat at constant volume) than N_2, and (ii) the isoentropic outlet temperature is dependent on the c_p/c_v ratio according to:

$$TOT_{ISO} = TIT \cdot \beta_{EXP}^{-\vartheta} \tag{6-1}$$

$$\vartheta = {(c_p/c_v - 1)}\Big/{c_p/c_v} \tag{6-2}$$

Where β_{EXP} denotes the expansion pressure ratio and ϑ is related to the c_P/c_V ratio.

According to equation (6-1) and (6-2), a decrease of the c_P/c_V ratio leads to an increase of the TOT.

Figure 6-1 shows also that the flue gases/air volumetric flow ratio increases by about 3.5% if pure hydrogen is fired, and up to 20% or 16% if respectively nitrogen or steam is added to keep the flame temperature at 2300 K. Such variation is not negligible and implies a major resizing of either the compressor or the turbine cross sectional area. Notice that in the case of no dilution, the flue gas/air volumetric ratio increases by about 3% because of the decrease of product gas molecular weight, even if the flue gas/air mass ratio reduces by about 2%.

In addition to the above mentioned macroscopic effects, the higher concentration of H_2O in the product gases aggravates the design specifications of the blade cooling system. Since the steam concentration improves the heat transfer coefficient on the flue gas side, a more efficient cooling system, with larger cooling flow rates, is required in order to operate the GT with the same TIT of natural gas while maintaining the blade wall temperatures below the allowed limits [1, 3]. For instance, according to [1], if the GT is resized to maintain the same air inlet mass flow

rate of NG operation, the total air mass flow rate extracted for blade cooling must be increased by about 3% if pure hydrogen is burned, and by about 21% if steam is added for dilution.

If the turbine cooling system can be properly designed, the increase of heat flux from the flue gases to the cooling flows is not problematic. However, there are additional issues related to the coating lifetime which arise when the through thickness thermal gradient increases. Indeed, it appears that high through thickness thermal gradients accelerate some modes of cracking and degradation of TBCs and EBCs, as pointed out in [13]. Moreover, it is proven that the presence of water vapour in the flue gases speeds up the oxidation mechanism of the bond coating, shortening the TBC lifetime [14]. As a consequence of these degradation mechanisms of the protective coatings (also accelerated because of the presence of particulate and gaseous metals deriving from the feedstock in syngas from coal), it may be necessary to decrease the TIT with respect to the NG operation in order to preserve the turbine lifetime.

6.3 PREDICTION OF NO_X EMISSIONS

Nitrogen oxides are by far the most important pollutant emission from a natural gas fired gas turbine. Such an issue becomes even more important for hydrogen fired machines because in those cases the other regulated pollutants (carbon monoxide, unburned hydrocarbons, soot and, with a different connotation, CO_2) simply cannot form due to the lack of carbon atoms in the fuel while control of NO_X emissions is made difficult by the reasons previously mentioned.

In general, two different methods can be proposed to control NO_X emissions from gas turbines [1]:

- premixed lean combustion;
- diffusive flame dilution with inert species (mainly steam, water or nitrogen).

The aim of this chapter is setting up a comparative analysis of the effects these two combustion concepts have on the performance of a combined cycle. A tool for quantitative prediction of the NO_X emissions is therefore fundamental to fix the level of dilution to be considered in the investigation.

The analysis carried out by Tsalavoutas et al. [15] showed that different correlations for evaluation of NO_X emissions available in the public literature lead to predictions which may differ by orders of magnitude when the correlations are applied exactly in the form they were originally proposed. This is due to the fact that correlations are based on parameters highly dependent on the design of both the engine and the combustor chamber. Moreover coefficients may have been calibrated to correctly predict NO_X emissions of a specific gas turbine model but they lead to drastically wrong estimation under different conditions. However paper [15] showed also that predictive ability of correlations can be hugely improved by their adaptation to the experimental data by means of numerical optimization methods. In particular it proved that, once it has been adapted to fit data available from instrumental measurements, the correlation

[1] In addition, a selective catalytic removal process can be adopted for NO_X abatement from exhaust gases of turbine power plants. This technique can be applied to H_2-fueled gas turbines, as well as for conventional units, but it does not at all affect the combustion process and gas turbine operations and therefore it will be totally neglected in this analysis.

proposed by Döpelheuer and Lecht [16] is particularly suitable to predict NO_X emissions of a heavy duty gas turbine equipped with diffusion flame combustors at full and partial load.

A similar approach was followed here to give a tentative estimation of NO_X emissions achievable by dilution. A significant amount of data was available to authors from the experimental activities carried over a prototypical combustor installed on a test rig at ENEL's experimental facility [9][17] in Sesta (Italy). They refer to a single can, silos-type diffusive flame combustion system configured to burn natural gas and hydrogen mixtures in any proportion and featuring steam injection for inhibition of NO_X formation.

Reference is made to the correlation format expressing the NO_X emission index ($EINO_X$) as absolute value (eq. 2 in [16]):

$$EINO_X = A\left(\frac{p_{C,in}}{T_{C,in}}\right)^B T_{PZ}^C \cdot e^{D/T_{FL}} \tag{6-3}$$

where T_{PZ} is the combustor primary zone temperature calculated as:

$$T_{PZ} = 0.5 \cdot (T_{FL} + T_{C,IN}) \tag{6-4}$$

while T_{FL} is the flame temperature given by:

$$T_{FL} = 0.75 \cdot STFT + 0.25 \cdot T(\Phi) \tag{6-5}$$

STFT is the temperature reached in a homogenous stoichiometric (i.e. $\Phi = 1$) fuel / diluent /air mixture, while $T(\Phi)$ is the temperature at a homogeneous equivalence ratio of Φ (≤ 1), in the primary zone.

Döpelheuer and Lecht [16] provide values for coefficients B, C and D in equation (**6-5**) (equal to 0.5, –1.5 and –38000 respectively) and recommend to set the coefficient A with reference to a known emission value specific for the given gas turbine in a given operating conditions.

According to the procedure suggested in [15], we tried to improve the correlation predicting capability by fitting all the coefficients on emission data collected in an extended test campaign on a H_2 fired combustor [9][17]. Data cover steam to H_2 dilution mass ratios ranging from 0 to 5.5 and served for calibration of the coefficients A, C and D which result equal to 1.462×10^{12}, –0.6667, and –40211 respectively. Conditions at the combustor inlet were hardly influenced by dilution meaning that $p_{C,IN}$ and $T_{C,IN}$ are approximately the same for all the conditions tested. Accordingly, coefficient B resulted completely insensible to the regression on such data set and it was therefore kept at the original value indicated in [16] (B=0.5). The resulting correlation can approximate the experimental values within a 5% average absolute deviation and a 12.3% maximum error. It has been applied to evaluate NO_X emissions reported in the table of section 6. For cases with the highest TIT (resulting in a combustor outlet temperature ~ 1400°C) $\Phi = 1$ has been adopted for calculation of T_{FL} in equation (**6-5**), in agreement with the indication in [16] for

the full load condition. Cases at lower TIT have been treated by considering a temperature T(Φ) resulting from the equivalence ratio required to decrease the combustor outlet temperature to the corresponding value.

6.4 DESIGN APPROACH FOR HYDROGEN FUELLED GAS TURBINE

The study carried out in the following is based on the assumption that gas turbines specifically designed for burning hydrogen will be available. Therefore the performance analysis does not take into account possible constraints related to adapting machines originally designed for natural gas operations. We acknowledge that currently the GT manufacturers supply hydrogen/syngas fuelled gas turbine modifying the existing natural gas based machines; indeed, this is a reasonable market-driven approach. Nevertheless, in this work we decided to move further and try to compartmentalize the analysis to the real technology limitations which arise in hydrogen based gas turbine. Consistently, this requires considering re-engineered gas turbine. This perspective, which is common among energy utilities, allows evaluating clearly the hydrogen GT potentialities in a future market.

On the contrary all the gas turbine components are re-designed because the market demand will justify it. Therefore, a reference, average 50 Hz F-class large-scale gas turbine has been defined with reference to the characteristics of the most recent natural gas fired combined cycles of the Enel fleet. The reference plant is based on a single gas turbine, triple pressure level and reheat Heat Recovery Steam Generator and one steam turbine. Its heat balance and performance are summarized in Table 6-1. The calculation code described in the chapter 4 has then been tuned to reproduce the performance of the reference unit by adjusting the most significant design specs (TIT, efficiency of the turbomachines, operating blade metal temperature, etc.). Once the model has been calibrated, it is applied to the evaluation of the different hydrogen fired plants considered in the analysis.

Even if the described procedure allowed to set a large number of design parameters, more of these are actually arbitrary. To keep the design of the hydrogen fired machine as much as possible close to the reference plant design, these additional assumptions have been adopted:

- compressor pressure ratio and the geometry of the expander (number of stages, mean diameter of the rows, blade height) are the same of the reference gas turbine;
- in presence of an additional diluent flow, the compressor-turbine fluid dynamic matching is set by modifying the compressor inlet airflow rate;
- variation of the enthalpy drop are compensated by adjusting the load coefficients of the stages.
- TIT (defined as the total temperature at 1st rotor inlet) is the same of the reference case, meaning that an increase in the gas-blade heat transfer coefficient (essentially due to steam dilution) can be compensated by slightly increasing the coolant mass flow rate, being this possible in the "re-design" approach.

According to these assumptions, the mentioned computer code is able to estimate the efficiency of the stages, the cooling flow rate and finally the overall plant performance.

However the discussion in chapter 2, pointed out some aspects whose effects cannot be precisely quantified and therefore should be taken into account by using a precautionary "de-rating" strategy. As long as hydrogen combustion is concerned, the following two aspects can be cited:

- a faster degradation of TBC and EBC;
- a more uneven distribution of temperature on the turbine admission arc due to the fuel characteristics and combustion modality (diffusive vs. premixed flame) leading to higher pattern factor.

Table 6-1: heat balance and performance of the reference, natural gas fueled combined cycle.

LHV thermal input, MW	723.5
Gas turbine gross power, MW	282.0
Gas turbine gross electric efficiency, %	38.98
Steam turbine gross power, MW	141.4
Combined cycle net electric power, MW	419.5
Combined cycle net efficiency, %	57.98
Compressor outlet temperature, °C	406.6
Turbine outlet temperature, °C	578.1

These issues could affect the operating conditions of the blades, eventually resulting in a lifetime reduction, or alternatively, in a reduction of the blade metal operating temperature to mitigate their effects. Since we cannot provide a realistic estimate of such effects, a sensitivity analysis was carried out assuming more conservative blade temperatures than those resulting from the "state-of-the-art" definition. Therefore TIT has been reduced to meet the more stringent condition for the assigned technological level of the cooling system [2]. Even if in the re-engineering approach a blade temperature decrease could be accomplished by increasing the cooling flow rate at constant TIT, this strategy (that actually could lead to a better performance) was not taken into consideration to avoid investigating: i) unfeasible cooling circuit geometries because of manufacturing and technological limitations not contemplated by the calculation model and ii) cooling circuit operating conditions far from those used to calibrate the model.

[2] In the calculation model, this technological level is indentified by the cross sectional area of the spent coolant ejecting holes. Hence, TIT is reduced as long as the resulting cooling flow can be ejected through the stipulated area in the most critical row of the expander (which always turned out to be the first rotor).

Table 6-2: main assumptions: fuel and ambient air conditions, gas turbine and HRSG parameters, diluent for diffusive flame combustor application

Fuel	
Natural gas molar composition, %: CH_4 90.0; CO_2 = 1.3; C_2H_6 = 4.3; C_3H_8 = 0.1; N_2 = 4.3	
LHV fuel, MJ/kg	44.752
Fuel Temperature, °C	40
Ambient Air	
Temperature, °C	15
Relative humidity, %	60
Pressure, kPa	101.3
Gas Turbine	
Combustor pressure loss (nominal), %	3.0
Inlet filter pressure loss, mbar	7
Compressor pressure ratio	17
HRSG	
Evaporation pressure (HP-IP-LP), bar	130 / 36 / 4
ΔT pinch point, °C	10
ΔT approach point, °C	25
Condensing pressure, bar	0.04
Maximum steam turbine inlet temperature, °C	565
Gas side pressure losses, mbar	30
DILUENT FOR DIFFUSIVE FLAME H_2 COMBUSTOR	
Steam diffusive flame combustor	
Fuel-air overpressure at combustor, bar	10
Steam temperature at the fuel mixer, °C	300
Nitrogen diffusive flame combustor	
Nitrogen pressure at the fuel mixer, bar	27.1
Fuel-air overpressure at combustor, bar	10
Nitrogen temperature at the fuel mixer, °C	300
Number of inter-refrigerators	2
Number of compressor groups	3
Isentropic efficiency for each compressor group	0.82
Intercooler exit temperature, °C	35

6.5 CALCULATION METHODOLOGY AND ASSUMPTIONS

Heat and mass balance and overall performance of all the cases considered in this work have been evaluated by a computer code developed by the authors' research group at Politecnico di Milano and thoroughly described in [7]. The code is conceived for prediction of gas turbine performance at the design point and includes the one-dimensional design of the turbine, functional to establish all the aerodynamic, thermodynamic, and geometric characteristics of each blade row required for an accurate estimation of the cooling flows and the evolution of the cooled expansion. The model accounts for convective cooling in multi-passage internal channels with enhanced heat transfer surfaces, as well as film and TBC cooling.

The present model was already applied to investigate the behavior of a hydrogen fired gas turbine [1]. In that paper a comprehensive explanation was carried out about the effects of changing the flue gas composition (due to H_2 combustion and optionally adding a diluent) on the performance of the cooling circuit and the other operating characteristics of a turbine expander.

So in this work we don't recall that discussion but just present the new results obtained, while making reference to that paper for the theoretical fundamentals.

The main assumptions considered for the simulations are reported in Table 6-2. As mentioned above, the gas turbine "state-of-the-art" is set with reference to a machine (featuring 17 compressor stages, 4 turbine stages, 3 cooled stages, 2 TBC cooled rows and film cooled nozzle) representing the average of large size, 50 Hz F-class units in the Enel fleet. Design specs used to calibrate the gas turbine model according to values of Table 6-1are listed in Table 6-3 while all the other parameters required in the calculation are taken at the same values of [7].

Table 6-3: design parameters resulting from model calibration.

Inlet air mass flow rate, kg/s	672.6
Combustor Outlet Temperature, °C	1400.0
Turbine Inlet Temperature, °C	1337.0
Polytropic compressor efficiency	0.922
Turbine cooled stages efficiency	0.933
Maximum metal temperature, first nozzle, °C	865
Maximum metal temperature, first rotor, °C	835
Maximum metal temperature, downstream stators, °C	840
Maximum metal temperature, downstream rotors, °C	810

6.6 RESULTS

Figure 6-2 summarizes all the possible layouts of H_2 fired plant. For all the cases considered, hydrogen is supposed to be available at the required pressure, at least the compressor outlet pressure plus 10 bar.

When the premixed combustor is adopted (Figure 6-2a), there are no process modifications compared with the NGCC; after being preheated to 40°C by an external source, the fuel is sent to the GT. The bottoming steam cycle layout does not show any change compared to the natural gas case.

As far as the diffusive flame combustor with N_2 dilution is concerned (Figure 6-2b), hydrogen is heated up to 40°C and then mixed with nitrogen coming from the intercooled compressor, whose features are reported in Table 6-2. The nitrogen pressure at the inlet of the last compressor group is set in order to obtain 300°C and 27 bar at the outlet, which guarantees 10 bar of overpressure compared to the air. The pressure ratio for the first and second group is then divided minimizing the power requirement. Nitrogen is supposed to be available on site at no cost (as in an IGCC) at ambient conditions. In this case too, the HRSC is the same of the natural gas case.

Finally, when diffusive flame combustor with steam dilution is considered (Figure 6-2c), hydrogen at 40°C and steam at 300°C, 27 bar are mixed before entering the combustion chamber. Steam is bled at 36 bar from the HRSC steam turbine, corresponding to about 370°C, and it is attempered to 300°C with saturated water from IP drum.

In diffusive flame cases, dilution levels were varied over a wide range to provide a significant sensitivity analysis of the gas turbine performances. Highest diluent to H_2 ratio was fixed to get a

STFT equal to 2200K, leading to NO_x emissions below 20 ppmvd (a typical value for commercial plants) according to methodology exposed in chapter 3.

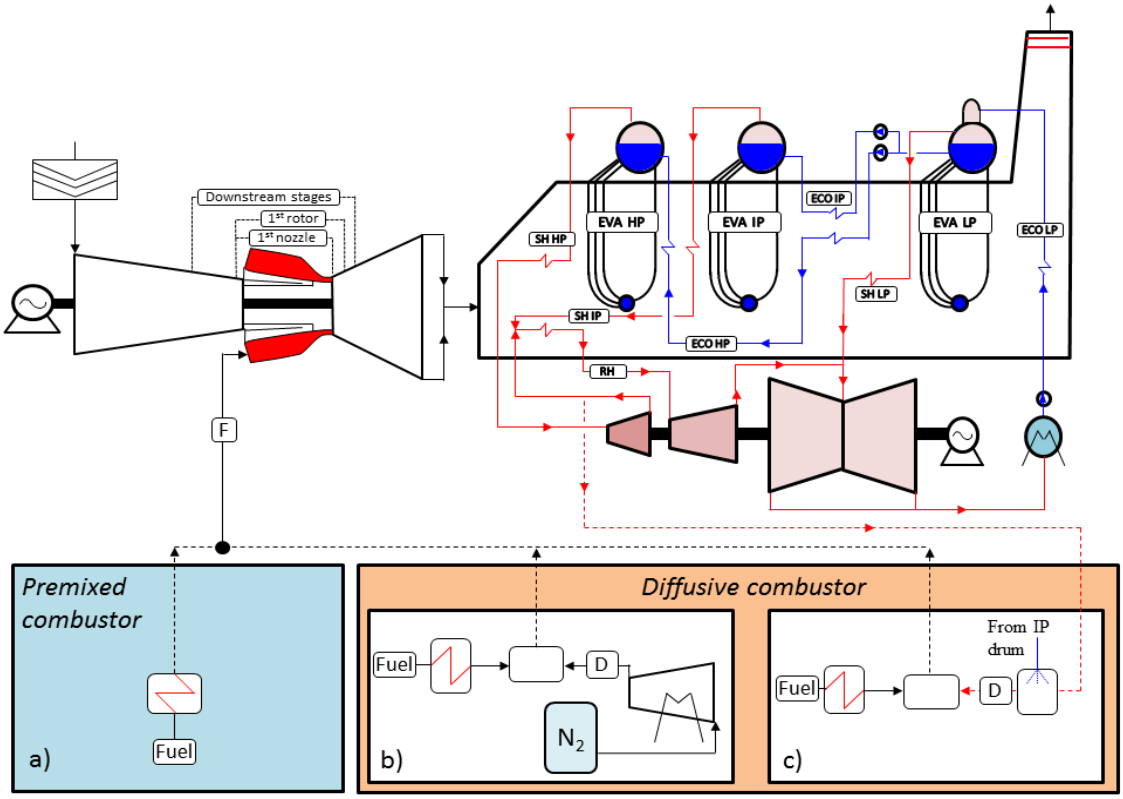

Figure 6-2: the combined cycle plant layout for hydrogen fueled cases; in the upper part of the figure the GT and HRSG are represented. The bottom part of the figure reports the plant features for the three scenarios considered: a) premixed flame combustor, b) diffusive flame combustor with nitrogen dilution and c) diffusive flame combustor with steam dilution.

6.6.1 *DIFFUSIVE FLAME COMBUSTOR AND STEAM DILUTION*

Thermodynamic results for the diffusive flame combustor and steam dilution are shown in Table 6-4.

All the cases at nominal TIT feature a higher GT power thanks to the lower air mass flow rate from the compressor; at STFT = 2200K, the power reaches 325.4 MW_E, about 15% more than the reference gas turbine. On the contrary, the steam turbine power decreases by 27% and 7% for STFT = 2200K and 2575K respectively, due to the diluent bleeding. The combined cycle overall power is almost unchanged (~1%) while the plant efficiency lowers steeply at higher steam to hydrogen ratio because of the irreversibilities related to the steam/gas mixing.

The GT cooling flows rate increases as steam dilution rises and the H_2O concentration in the flue gas increases bringing about a higher external convective heat transfer coefficient. Looking at the nozzle and first rotor (the most critical rows as far as cooling is concerned), cooling flows rate rises by about 2.8% at STFT=2575K, 3.8% at 2500K, 6.4% at 2350K and 9.8% at 2200K compared to the reference case (ref-values: 42.85 kg/s and 24.66 kg/s for the nozzle and first rotor, respectively). Such an increase of cooling flow rate is quite limited and probably within

the tuning capability of a gas turbine for all the range of dilution considered. Even more, from the point of view of completely "re-engineering" the gas turbine, it should not be a problem to cope with such a small cooling flow increase. The right columns of Table 6-4 analyzes the turbine behavior when the maximum blade temperature is lowered by 20 and 40°C respectively compared to the nominal value, while the cooling flow rate is kept virtually unchanged (with the meaning illustrated in the previous footnote 2). When reducing the blade temperature, the most evident effect is that the associated TIT decrease is approximately twice. This behavior can be explained by neglecting the real gas turbine cooling circuits including film and TBC cooling and multi-pass channels and assimilating the blade to a cross-flow heat exchanger where heat capacity of the outer stream (flue gas) is infinitely larger than the one of the inner stream (coolant). Thanks to this simplification, the main temperature profiles along the blade longitudinal coordinate can be easily drawn as in Figure 6-3, where the solid lines refer to the nominal conditions.

When considering an equal decrease (ΔT) of TIT and maximum blade metal temperature, the temperature profiles modify as shown by the dashed lines of Figure 6-3. Since the heat flux on the blade external wall is maintained at the same value of the nominal point, the inner blade wall temperature profile equally translates of ΔT too. Looking at the coolant side, provided that the heat power from the outer side is the same of the nominal condition, the coolant would experience the same temperature profile (with a ΔT_C temperature increase) as the incoming coolant temperature is constant. This situation is actually unfeasible because this would cause a ΔT reduction of the inner wall blade – coolant temperature difference at the channel exit (ΔT_{IN-C}) that, in turn, would imply a mismatch between the external and internal heat flux. In order to keep the system in thermal equilibrium is therefore required to increase the cooling flow in order to reduce ΔT_C, as illustrated in Figure 6-3. Similarly, for a given cooling flow rate (i.e. at fixed cooling system technology), it is straightforward that a larger TIT decrease is required to cope with a reduction of the blade metal temperature in order to keep the balance of the cooling system.

Looking at the cases with same steam/hydrogen ratio but lower blade metal temperature, it can be noted that the resulting decrease of TIT causes a significant efficiency decay: 0.6 or 1.3 percentage points for the −20°C and −40°C cases, respectively.

Finally, the volumetric heating value of the hydrogen mixture varies in the range of 6000-9000 kJ/Nm^3, which is fairly equivalent to syngas typically burned in refinery plants [18].

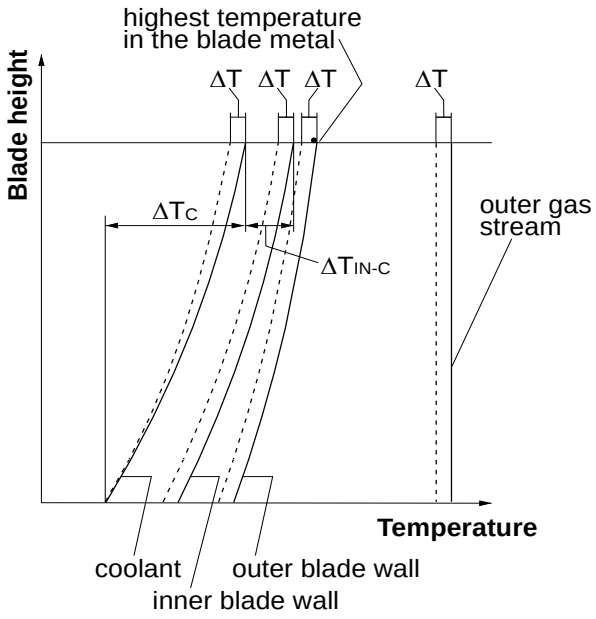

Figure 6-3: comparison between blade temperature profiles of the reference case (solid line) and a modified case (dashed line) where a reduction ΔT is applied to the gas stream and to the blade material.

Table 6-4: results for the hydrogen fueled combined cycle with diffusive flame combustor and steam dilution. Nomenclature. H_2O: steam dilution; NO_X1-2-3-4: ordered with decreasing STFT (2575, 2500, 2350, 2200 K); TIT1-2-3: ordered with decreasing TIT (or blade metal temperature), 1 is the nominal temperature, 2 and 3 correspond to a metal temperature decrease of 20 or 40°C respectively.

CASES		H_2O NO_x1 TIT1	H_2O NO_x2 TIT1	H_2O NO_x3 TIT1	H_2O NO_x4 TIT1	H_2O NO_x1 TIT2	H_2O NO_x2 TIT2	H_2O NO_x3 TIT2	H_2O NO_x4 TIT2	H_2O NO_x1 TIT3	H_2O NO_x2 TIT3	H_2O NO_x3 TIT3	H_2O NO_x4 TIT3
G compressor inlet, kg/s		647.1	638.0	616.8	590.7	661.4	652.4	631.7	607.0	676.2	667.4	647.1	623.1
Pressure ratio		17				17				17			
G hydrogen fuel, kg/s		6.10	6.14	6.24	6.37	5.95	5.99	6.09	6.17	5.80	5.84	5.93	6.00
G diluent / G hydrogen		1.62	2.60	4.86	7.56	1.61	2.60	4.85	7.56	1.61	2.60	4.85	7.56
G at turbine inlet, kg/s		531.9	527.6	517.4	504.8	546.8	542.4	532.4	524.8	562.4	557.9	548.1	540.6
H_2O mol% at turbine inlet		18.84	20.65	24.88	30.17	18.00	19.73	23.76	28.40	17.17	18.82	22.64	27.06
T at compressor outlet, °C		406.7				406.6				406.6			
STFT, K		2575	2500	2350	2200	2575	2500	2350	2200	2575	2500	2350	2200
Temperature, °C	COT	1400.0	1400.0	1401.0	1401.9	1358.0	1359.0	1360.0	1349.9	1316.0	1317.0	1319.0	1308.9
	TIT	1337.0				1298.9	1299.4	1299.7	1290.9	1260.6	1261.2	1261.9	1254.0
	TIT_{ISO}	1230	1230	1228	1225.9	1199.0	1199.0	1198.0	1190.9	1168.0	1168.0	1167.0	1160.9
NO_X, ppmvd 15% O_2		250.3	159.3	58.9	19.0	241.3	153.3	56.6	18.0	232.2	147.4	54.3	17.1
TOT, °C		578.2	580.0	584.4	589.7	557.8	559.6	563.7	564.8	537.5	539.2	543.1	544.1
T of blade metal		Nominal				Nominal –20°C				Nominal –40°C			
Cooling mass flow rate, kg/s	Nozzle	44.0	44.4	45.5	46.9	44.1	44.5	45.6	45.6	44.1	44.6	45.6	45.7
	Rotor 1	25.4	25.7	26.3	27.2	25.4	25.7	26.4	26.4	25.5	25.8	26.5	26.5
	Stages	61.7	62.4	64.1	66.3	60.6	61.3	63.0	63.0	59.3	60.1	61.7	61.7
h, W/m^2K	Nozzle	2.55	2.57	2.63	2.69	2.54	2.56	2.61	2.66	2.53	2.55	2.59	2.64
	Rotor 1	1.84	1.86	1.89	1.94	1.83	1.84	1.88	1.92	1.82	1.83	1.86	1.90
G at ST inlet, kg/s		73.3	74.1	75.9	78.3	69.4	70.2	71.9	73.1	65.2	65.9	67.6	68.6
Diluted fuel LHV, kJ/Nm^3		9054.7	8270.9	6916.0	5786.6	9057.4	8269.5	6916.3	5786.6	9056.8	8269.9	6916.7	5786.4
LHV thermal input, MW		731.6	736.7	748.7	763.9	713.9	719.0	730.4	739.7	695.7	700.5	711.4	720.2
Gas turbine gross power, MW		296.5	301.2	312.0	325.4	288.3	293.0	303.6	314.9	279.7	284.2	294.6	305.7
Steam turbine gross power		130.9	126.5	116.4	103.8	124.1	119.9	110.0	96.1	117.5	113.4	103.5	90.0
Combined cycle net power		423.6	424.0	424.9	425.9	408.8	409.3	410.2	407.9	393.7	394.2	394.9	392.6
Combined cycle net efficiency, %		57.91	57.56	56.75	55.76	57.27	56.93	56.15	55.13	56.59	56.27	55.51	54.51

6.6.2 RESULTS WITH DIFFUSIVE FLAME COMBUSTOR AND NITROGEN DILUTION

Thermodynamic results for the diffusive flame combustor and nitrogen dilution are shown in Table 6-5.

The GT power increases with respect to the reference natural gas fired case in all the nominal-TIT simulations: at STFT=2200K, the power output is 330 MW, about 17% more than the reference. The power augmentation is consistent with the steam dilution cases. The steam cycle power output is not affected by the diluents flow rate because actually the nitrogen replaces the equivalent excess air in the combustor. The steam cycle power output turns out to be slightly lower than the reference case because of the lower flue gas mass flow rate at the GT outlet which decreases from 688 kg/s to 666 kg/s. Such a decrease of the flue gas mass flow rate is due to the fact that, on one hand, the volumetric flow rate is constant (about 166 m^3/s) as the first stator geometry is fixed for the natural gas and hydrogen cases (i.e. same mean rotor diameter and blade height), and on the other hand, the specific volume of the working fluid increases, as discussed in Figure 6-1. The increase in the flue gas specific heat (due to the higher H_2O content) and the cooling flow rates do not balance the previous effects, so that the steam power output decreases.

Provided that H_2O concentration is not affected by N_2 dilution, the cooling flow rates does not vary for the cases at fixed TIT. Compared to the corresponding steam dilution cases (i.e., same STFT), the cooling mass flow rates are lower in a range from 2 to 8%. Compared to the reference natural gas fired case, the coolant flow rates rises by about 1.5%.

The plant efficiency reduces as the nitrogen compressor consumption increases: at STFT=2575K the efficiency is slightly higher than the reference, whilst at STFT=2200K there is a drop of 1.5 percentage points (p.p.).

As far as the reduction of the blade temperature is concerned, the TIT decreases by about 40°C or 80°C, similarly to the steam dilution cases. Compared to the nominal TIT plant, the efficiency reduction is 0.7 p.p. and 1.3 p.p. for –20 and –40°C on the blade respectively.

The hydrogen rich syngas features a LHV in the range of 5000-8700 kJ/Nm^3; these values are lower than the steam dilution cases because of the larger nitrogen mass flow rate required to achieve a desired STFT.

Table 6-5: results for the hydrogen fueled combined cycle with diffusive flame combustor and nitrogen dilution. Nomenclature. *N_2*: nitrogen dilution; *NO_x1-2-3-4*: ordered with decreasing STFT (2575, 2500, 2350, 2200 K); *TIT1-2-3*: ordered with decreasing TIT (or metal blade temperature), 1 is the nominal temperature, 2 and 3 correspond to a decrease of 20 or 40°C on the metal respectively.

CASES		N_2 NO_x1 TIT1	N_2 NO_x2 TIT1	N_2 NO_x3 TIT1	N_2 NO_x4 TIT1	N_2 NO_x1 TIT2	N_2 NO_x2 TIT2	N_2 NO_x3 TIT2	N_2 NO_x4 TIT2	N_2 NO_x1 TIT3	N_2 NO_x2 TIT3	N_2 NO_x3 TIT3	N_2 NO_x4 TIT3
G compressor inlet, kg/s		640.0	626.8	596.7	560.5	654.5	641.5	612.1	576.8	669.5	656.9	628.2	593.7
Pressure ratio		17				17				17			
G hydrogen fuel, kg/s		6.05	6.06	6.09	6.13	5.91	5.92	5.95	5.98	5.76	5.77	5.80	5.83
G diluent / G hydrogen		3.46	5.55	10.30	15.93	3.45	5.55	10.29	15.93	3.45	5.55	10.29	15.93
G at turbine inlet, kg/s		538.3	537.9	537.1	536.0	553.0	552.6	551.7	550.7	568.4	568.1	567.2	566.2
H_2O mol% at turbine inlet		15.95	15.95	15.96	15.98	15.25	15.26	15.27	15.28	14.56	14.56	14.58	14.59
T at compressor outlet, °C		406.6				406.6				406.6			
STFT, K		2575	2500	2350	2200	2575	2500	2350	2200	2575	2500	2350	2200
Temperature, °C	COT	1400.0	1400.0	1400.0	1400.0	1358.0	1358.0	1358.0	1358.0	1316.0	1316.0	1316.0	1315.9
	TIT	1337.0				1298.9	1299.0	1299.0	1298.9	1260.0	1260.0	1260.0	1260.4
	TIT_{ISO}	1231.0	1231.0	1231.0		1200.0	1200.0	1200.0	1200.0	1168.0	1168.0	1168.0	1167.9
NO_X, ppmvd 15% O_2		250.4	159.5	58.9	19.0	241.6	153.4	56.6	18.1	232.6	147.5	54.2	17.3
TOT, °C		575.0	574.9	574.7	574.4	554.8	554.7	554.5	554.2	534.7	534.6	534.4	534.2
T of blade metal, °C		Nominal				Nominal –20°C				Nominal –40°C			
Cooling mass flow rate, kg/s	Nozzle	43.3	43.3	43.3	43.3	43.4	43.4	43.4	43.4	43.5	43.5	43.5	43.5
	Rotor 1	25.0	25.0	25.0	25.0	25.0	25.0	25.0	25.0	25.1	25.1	25.1	25.1
	Stages	60.5	60.4	60.2	59.9	59.4	59.3	59.1	58.8	58.1	58.0	57.8	57.6
h, W/m^2K	Nozzle	2.51	2.51	2.51	2.51	2.50	2.50	2.50	2.50	2.49	2.49	2.49	2.49
	Rotor 1	1.82	1.82	1.82	1.82	1.81	1.81	1.81	1.81	1.80	1.80	1.80	1.80
G at ST inlet, kg/s		72.0	72.0	71.9	71.8	68.2	68.1	68.0	67.9	64.0	64.0	63.9	63.8
Diluted fuel LHV, kJ/Nm^3		8639.9	7709.0	6197.3	5025.9	8642.2	7709.3	6198.0	5026.7	8642.8	7710.2	6198.2	5026.8
LHV thermal input, MW		725.8	727.3	730.8	734.8	708.6	710.0	713.3	717.2	690.6	692.0	695.2	699.1
Gas turbine gross power, MW		297.8	303.1	315.3	329.9	289.6	294.8	306.6	320.9	280.9	285.9	297.5	311.4
Steam turbine gross power, MW		137.7	137.6	137.5	137.3	130.9	130.8	130.7	130.5	124.1	124.1	123.9	123.8
Nitrogen compressor power, MW		-10.3	-16.6	-31.0	-48.2	-10.1	-16.2	-30.2	-47.1	-9.8	-15.8	-29.5	-45.9
Combined cycle net power, MW		421.3	420.2	417.9	415.1	406.6	405.6	403.3	400.5	391.5	390.6	388.3	385.6
Combined cycle net efficiency, %		58.04	57.78	57.19	56.49	57.38	57.12	56.54	55.84	56.69	56.44	55.86	55.16

6.6.3 RESULTS WITH PREMIXED COMBUSTOR

Thermodynamic results for the premixed combustor are shown in Table 6-6. The hydrogen fired GT with premixed combustor at nominal TIT and combustor pressure drop ($\Delta p/p_{combustor}$ = 3%), features the same power output of the reference natural gas case. An increase in the combustor pressure losses from 3% to 10% makes the power output to fall down to 261 MW as a result of two concurrent effects: (i) the reduction of the turbine pressure ratio and thus enthalpy drop, (ii) the reduction of the turbine inlet density which results in a decrease of the mass flow rate as the turbine geometry is fixed. The latter effect also brings about a reduction of the steam power output.

The cooling flow rates for $\Delta p/p_{combustor}$ = 3% are exactly the same as in the nitrogen diluted case for all the TITs considered. As the $\Delta p/p_{combustor}$ increases, the required cooling mass flow rates decreases as a consequence of the reduced flue gas densities that results in a lower gas-blade heat transfer coefficient.

When comparing with the natural gas fired plant, the combined cycle efficiency turns out to be 0.5 p.p. higher due to the different properties of the fluids. As the pressure drop increases, the efficiency decay of the GT, which is quite relevant (i.e., 1.2 p.p. as pressure drop increases from 3% to 10%), is partially compensated by an improvement of the HRSC efficiency due to the higher TOT. Accordingly, the combined cycle efficiency reduces by just 0.6 p.p.

Consistently with the diffusive flame combustor results, the TIT reduction is about two times the maximum blade temperature decrease. Comparing the lower TIT with the nominal TIT cases, the efficiency penalty is in the range of 0.7 p.p. and 1.4 p.p. when the blade temperature is decreased by 20°C and 40°C, respectively.

Table 6-6: results for the hydrogen fueled combined cycle with premixed combustor. Nomenclature. *Prem*: premixed combustor; *Δp 1-2-3*: ordered with increasing combustor pressure loss (3.0, 6.5, 10.0); *TIT1-2-3*: ordered with decreasing TIT (or metal blade temperature), 1 is the nominal temperature, 2 and 3 correspond to a decrease of 20 or 40°C on the metal respectively.

CASES		Prem Δp1 TIT1	Prem Δp2 TIT1	Prem Δp3 TIT1	Prem Δp1 TIT2	Prem Δp2 TIT2	Prem Δp3 TIT2	Prem Δp1 TIT3	Prem Δp2 TIT3	Prem Δp3 TIT3
G compressor inlet, kg/s		661.8	640.7	619.4	675.7	654.2	632.7	690.1	668.3	646.3
Pressure ratio			17			17			17	
G hydrogen fuel, kg/s		6.03	5.83	5.63	5.89	5.69	5.48	5.74	5.54	5.34
G at turbine inlet, kg/s		539.0	521.2	503.3	553.6	536.3	518.9	569.1	551.3	533.4
H_2O mol% at turbine inlet		15.94	15.94	15.95	15.24	15.20	15.16	14.55	14.51	14.47
T at compressor outlet, °C			406.6			406.6			406.6	
Combustor pressure loss, %		3.0	6.5	10.0	3.0	6.5	10.0	3.0	6.5	10.0
STFT, K			2712			2712			2712	
Temperature, °C	COT	1400.0	1400.0	1400.0	1358.0	1355.0	1353.0	1316.0	1313.0	1311.0
	TIT		1337.0		1298.9	1296.8	1294.5	1260.3	1258.3	1256.2
	TIT_{ISO}	1231.0	1230.0	1229.0	1200.0	1198.0	1196.0	1168.0	1166.0	1164.0
TOT, °C		575.1	580.3	585.7	555.0	559.1	563.5	534.8	538.9	543.2
T of blade metal, °C			Nominal			Nominal –20°C			Nominal –40°C	
Cooling mass flow rate, kg/s	Nozzle	43.3	42.0	40.7	43.4	41.8	40.3	43.5	41.9	40.4
	Rotor 1	25.0	24.3	23.6	25.0	24.2	23.4	25.1	24.3	23.4
	Stages 2+3	60.6	59.0	57.4	59.5	57.5	55.6	58.2	56.3	54.4
h, W/m^2K	Nozzle	2.52	2.46	2.39	2.51	2.44	2.38	2.50	2.44	2.37
	Rotor 1	1.82	1.78	1.73	1.81	1.77	1.72	1.80	1.76	1.71
G at ST inlet, kg/s		72.1	71.0	69.9	68.2	67.1	65.9	64.1	63.1	62.1
Diluted fuel LHV, kJ/Nm^3			107789			10789			10789	
LHV thermal input, MW		723.6	699.8	675.9	706.2	682.0	657.7	688.3	664.7	641.0
Gas turbine gross power, MW		289.1	275.4	261.7	281.0	267.3	253.5	272.5	259.1	245.6
Steam turbine gross power, MW		137.8	135.6	133.4	131.0	128.6	126.2	124.3	122.0	119.8
Combined cycle net power, MW		423.1	407.2	391.4	408.3	392.2	376.1	393.1	377.6	362.0
Combined cycle net efficiency, %		58.47	58.19	57.9	57.81	57.51	57.18	57.12	56.8	56.46

6.6.4 GENERAL COMMENT TO THE RESULTS

Final results are summarized in Figure 6-4a) and b). Figure 6-4a) reports the comparison among all the cases at nominal TIT. It can be noted that: i) considering the diffusive flame combustion at the same STFT, the efficiency of nitrogen diluted plants is always higher than steam, ii) the slope of the efficiency-STFT curve is greater for steam than nitrogen diluent, which makes the steam based cases more penalized at low STFT and, iii) the GT with premixed combustor always achieves higher performances than the diffusive flame combustor but for Δp/p=10% and diffusive STFT > 2500 K.

Figure 6-4b) reports the efficiency as a function of the metal blade temperature for the three considered scenarios. Results substantially confirm the trend observed at nominal TIT, i.e., the premixed combustor achieves the highest performance and the nitrogen diluted combustor has higher efficiency than the corresponding steam case.

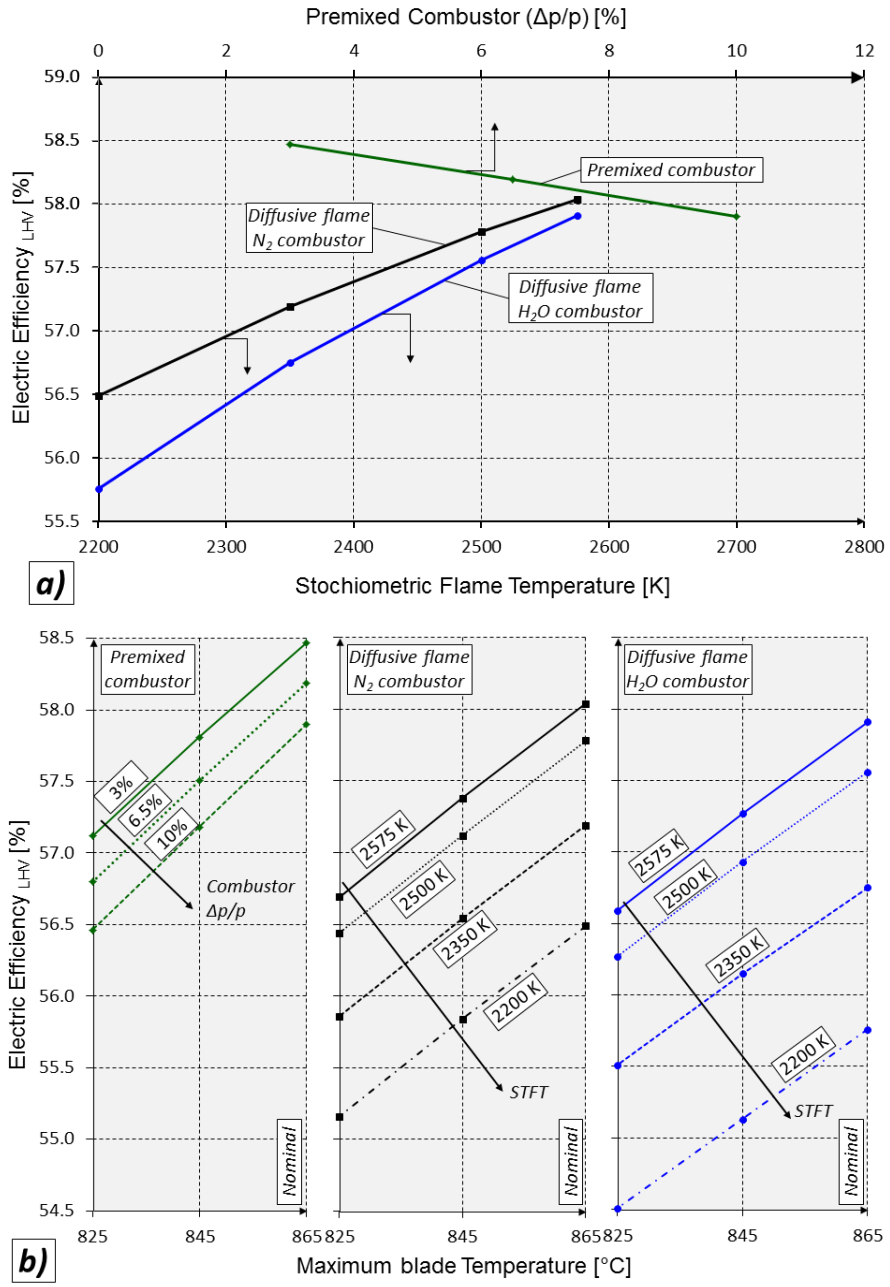

Figure 6-4: a) Combined cycle electric efficiency for all the cases at nominal TIT: the efficiency for steam and nitrogen diluted combustors is plotted as function of the STFT (bottom x-axis) while the efficiency for the premixed combustor is plotted as function of the combustor relative pressure loss (upper x-axis). b) Electric efficiency for all the simulated cases as a function of the maximum blade metal temperature; moving left to right: premixed combustor, nitrogen diluted combustor and steam diluted combustor.

6.7 CONCLUSIONS

In this chapter, a comparison between hydrogen fueled gas turbine with diffusive and premixed flame combustor was carried out on the basis of homogeneous assumptions. First, the combined cycle model was calibrated with reference to a natural gas fueled F-class GT followed by a triple pressure level HRSC. Then, different hydrogen fuelled cases have been investigated: (i) diffusive flame combustor with steam dilution, (ii) diffusive flame combustor with nitrogen dilution and, (iii) premixed combustor.

The analysis showed that:

- In order to achieve STFT=2200K, the diluent to hydrogen ratio must be equal to 7.6 and 16 for steam and nitrogen dilution respectively.
- Dilution always negatively affects the combined cycle efficiency: the higher the diluent to hydrogen ratio the lower the CC efficiency. Comparing the two diffusive flame cases, nitrogen always achieves higher efficiency than steam at equal stoichiometric flame temperature.
- The CC efficiency penalty due to inert dilution is limited as far as the TIT and the blade metal temperature are kept at the nominal values. A decrease of the allowed blade metal temperature reflects into a twice reduction of the TIT with a noticeable efficiency decay.
- The efficiency of the simple cycle GT engine is remarkably affected by an increase of the pressure drop in the combustor. However, because of the simultaneous TOT increase, the efficiency decay of the CC is much less sensible. On other hand, at fixed expander geometry and compressor pressure ratio, the combustor pressure drop causes a significant mass flow rate decrease which results in a proportional reduction of the power output.

REFERENCES

[1] **Chiesa, P, Lozza, G.,** 2005, "Using Hydrogen as a Gas Turbine Fuel", Journal of Engineering for Gas Turbines and Power, 127(1), pp- 73–81.

[2] **Oluyede, EO, Phillips, JN.,** 2007, "Fundamental Impact of Firing Syngas in Gas Turbines", Proceedings of ASME Turbo Expo 2007.

[3] **Sabau, A. S., Wright, I. G.,** 2009, "The Effects of Changing Fuels on Hot Gas Path Conditions in Syngas Turbines", Journal of Engineering for Gas Turbines and Power, 131(4), 044501.

[4] **Poyyapakkam, M. et al,** 2012, "Hydrogen Combustion within a Gas Turbine Reheat Combustor", Proceedings of ASME Turbo Expo 2012.

[5] **Bradley, T., Marra, J.,** 2012, "Advanced Hydrogen Turbine Development Update", Proceedings of ASME Turbo Expo 2012.

[6] **York, W. D., Zimibsky, W. S., Yilmaz, E.,** 2012, "Development and Testing of a Low NOX Hydro-gen Combustion System for Heavy Duty Gas Turbines", Proceedings of ASME Turbo Expo 2012.

[7] **Chiesa, P, Macchi, E.,** 2004, "A Thermodynamic Analysis of Different Options to Break 60% Electric Efficiency in Combined Cycle Power Plants", Journal of Engineering for Gas Turbines and Power, 126(4), pp. 770–785.

[8] **Dennis, R. D., Shelton, W. W., Le, P.,** 2007, "Development of Baseline Performance values for Turbines in Existing IGCC Applications", Proceedings of the ASME Turbo Expo 2007.

[9] **Cocchi, S., Sigali, S**.: "Development of a Low-NO_X Hydrogen-Fuelled Combustor for 10 MW Class Gas Turbines", proc. of ASME Turbo Expo 2010, paper GT2010-23348, DOI: 10.1115/GT2010-23348, June 2010.

[10] **Cheng, R.**, 2008, "Adaption of the Low-Swirl Burner Technology for Syngas and H_2 Gas Turbines", Proceedings of the Future of Gas Turbine Technology: 4th International Conference.

[11] **Weiland, N., Sidwell, T., Strakey, P**., 2011, "Testing of a Hydrogen Dilute Diffusion Array Injector at Gas Turbine Conditions", Proceedings of ASME Turbo Expo 2011.

[12] **Lee, H., Hernandez, S., McDonnell, V., Steinthorsoon, E., Mansour, A., Hollon, B.,** 2009, "Development of Flashback Resistant Low-Emission Micro-Mixing Fuel Injector for 100% Hydrogen and Syngas Fuels", Proceedings of ASME Turbo Expo 2009.

[13**] GE Energy,** 2006, "Advanced IGCC/Hydrogen Gas Turbine Development. Technical progress Report for Quarterly Period April – June 2006", report downloaded from www.netl.doe.gov on October 29th 2012.

[14] **Zhou, C., Yu., J., Gong, S., Xu, H.,** 2003, "Influence of Water Vapor on the High Temperature Oxidation Behavior of Thermal Barrier Coatings", Materials Science and Engineering, A348 (2003), pp. 327-332.

[15] **Tsalavoutas A., Kelaidis M., Thoma N., Mathioudakis K.,** "Correlations Adaptation for Optimal Emissions Prediction", proc. of ASME Turbo Expo 2007, paper GT2007-27060, DOI: 10.1115/GT2007-27060, May 2007.

[16] **Döpelheuer A., Lecht M.,** "Influence of Engine performance on Emissions Characteristics", proc. of RTO AVT Symposium on "Gas Turbine Engine Combustion, Emissions and Alternative Fuels", Lisbon, Portugal, October 1998.

[17] **Cocchi S., Provenzale M., Cinti V., Carrai L., Sigali S., Cappetti D.,** "Experimental Characterization of a Hydrogen Fuelled Combustor With Reduced NOx Emissions for a 10 MW Class Gas Turbine", proc. of ASME Turbo Expo 2008, paper GT2008-51271, DOI: 10.1115/GT2008-51271, June 2008.

[18] **Jones R., Goldmeer J., Monatti B.,** 2011, "Addressing Gas Turbine Fuel Flexibility". GE Energy Report GER4601 rev. B, downloaded from www.ge-energy.com on October 29th 2012.

7 SEWGS INTEGRATION IN CO_2 CAPTURE PLANTS

Nomenclature and Acronyms

ATR: Auto Thermal Reformer
CAESAR:CArbon-free Electricity by SEWGS: Advanced Materials, Reactor and process design
CCR: Carbon Capture Ratio
CCS: Carbon Capture and Storage
COT: Combustor Outlet Temperature
E: CO_2 specific emission rate
EXP: Expansion
GHR: Gas Heated Reformer
HDS: Hydro De-Sulphurization Reactor
HR: Heat Rate
HRSC: Heat Recovery Steam Cycle
HRSG: Heat Recovery Steam Generator
HTS: High Temperature Shift reactor
LP: Low Pressure
NG: Natural Gas
NGCC: Natural Gas Combined Cycle
PSA: Pressure Swing Adsorption
SEWGS: Sorption Enhanced Water Gas Shift
SPECCA: Specific Primary Energy Consumption for CO2 Avoided
TIT: Turbine Inlet Temperature
TITiso: Turbine Inlet Temperature (defined according to ISO standard)
TOT: Turbine Outlet Temperature
WGS: Water Gas Shift
η: Efficiency

7.1 SORPTION ENHANCED WATER GAS SHIFT REACTOR

7.1.1 THE PRINCIPLE OF THE SEWGS PROCESS

The combination of high temperature equilibrium reactions with pressure swing adsorption (PSA) processes was investigated in the 1990s by Air Products and Chemicals Inc. From this work, SEWGS evolved and has since been studied further within the CO_2 Capture Project (CCP) [1] and in Cachet Framework Programme 6 (FP6) [2]. It was further developed in CAESAR FP7 project [3] for natural gas, coal and blast furnace applications.

SEWGS comprises of multiple fixed beds operating in parallel that adsorb CO_2 at high temperature and pressure, and release it at low pressure. The combination of CO_2 conversion and removal enhances the H_2 production and the purity of the stream feeding the Gas Turbine (GT) combustor, whilst a separate CO_2 by-product can be recovered from the adsorbent by regenerating the bed [4]. This stream can then be compressed and sequestered with further clean-up.

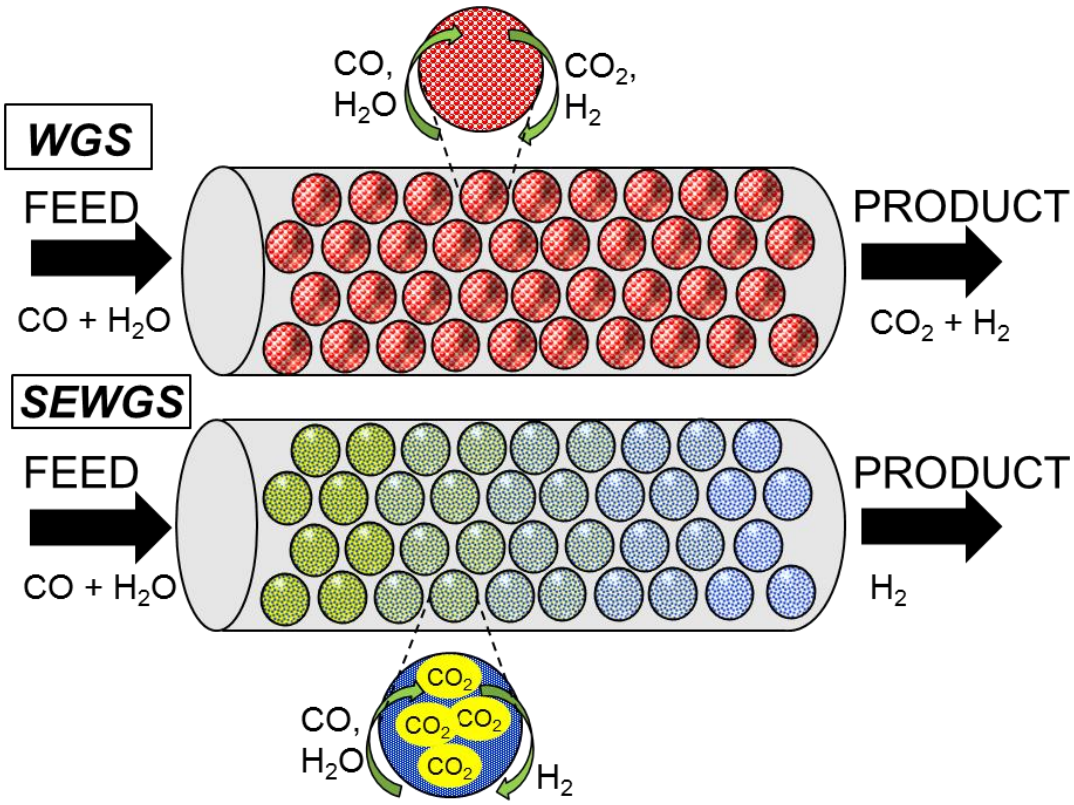

Figure 7-1: Shift scheme reaction into (top) ordinary water gas shift reactor and (bottom) SEWGS reactor.

The advantages of combining the water gas shift reaction with separation of CO_2 are:

- Process simplification: CO_2 conversion and separation at high temperature removes the need for low temperature shift reactor and potentially reduces the size or eliminates the high temperature shift reactor as well.
- High hydrogen and CO_2 recovery: in conventional pre combustion CO_2 capture, the WGS section leaves part of the CO unconverted, which results in lower hydrogen and CO_2 recovery. In SEWGS, all the CO is converted and hydrogen recovery is maximized.
- Better heat integration: CO_2 is captured at high temperature, while in conventional pre-combustion systems the capture is performed at ambient or even sub-ambient temperatures with thermodynamic disadvantages.
- Lower steam usage in HTS/LTS: removal of CO_2 in SEWGS requires lower steam usage than conventional HTS/LTS because equilibrium is moved towards products thanks to product subtraction rather than reactant concentration.

7.1.2 DESCRIPTION OF THE SEWGS PROCESS

The SEWGS process is based around a multi-bed PSA unit with each vessel filled with CO_2 adsorbent and WGS catalyst. These vessels are then subjected to a sequence of process steps, i.e. a process cycle that produces a decarbonized hydrogen stream during the sorption/reaction step which ends at a predeterminated level of CO_2 breakthrough, and a CO_2 rich stream during sorbent regeneration [5] [6]. A pressure swing cycle that reduces the gas phase partial pressure of CO_2 is employed to regenerate the adsorbent and to produce a low-pressure stream rich in

CO_2. This process is hence similar to pressure swing adsorption units commonly used for air separation, hydrogen purification, and other gas separations. The SEWGS cycle contains several different steps and is illustrated in Figure 7-2.

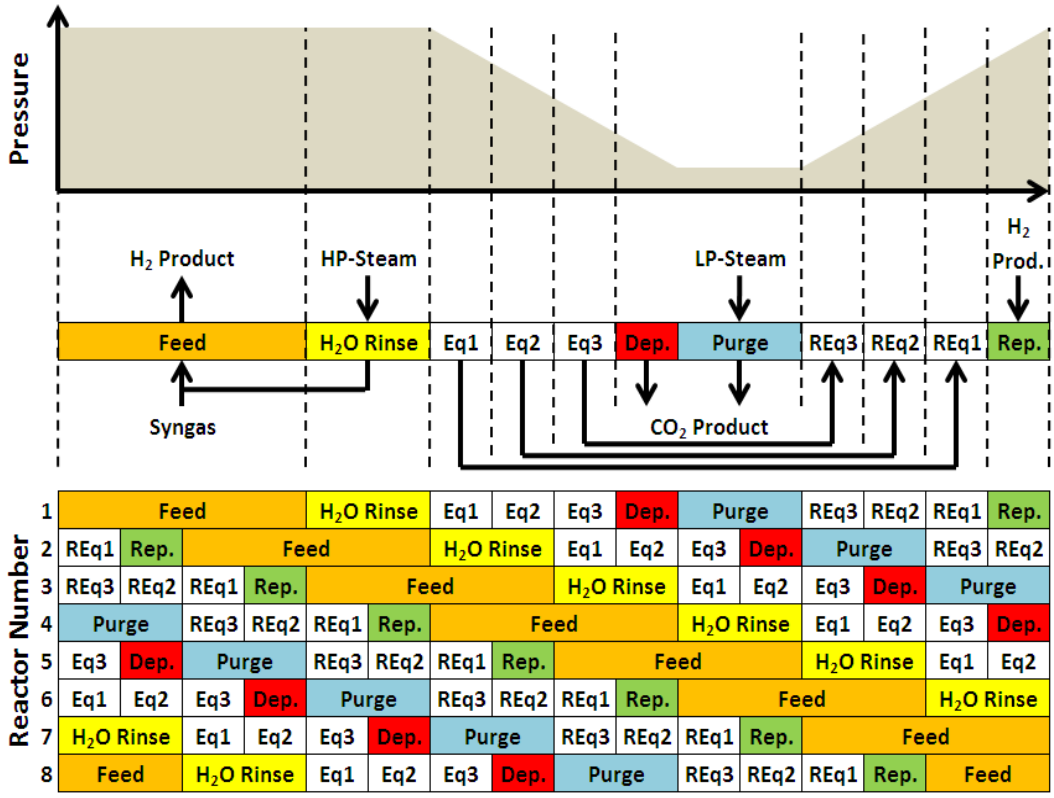

Figure 7-2: Pressure variation at each different operation step into the SEWGS reactor (top) and process occurring in each vessel (bottom).

The process starts with the feed, where the syngas at high pressure and temperature (i.e. about 30 bara and 400°C) goes through the SEWGS reactor, the CO_2 is captured and a hydrogen-rich stream is produced. This yields a hydrogen-rich product at essentially feed pressure and higher temperature because of the WGS reaction taking place (450°C). When the sorbent is saturated by CO_2, the feed gas is directed to another vessel while regeneration starts in the current vessel. The first step of regeneration is a rinse step, where steam is sent to the SEWGS reactor to sweep the hydrogen still present in the reactor and send it to feed of another vessel. Without this step, a significant quantity of fuel gas would end up in the CO_2 product, reducing its purity and negatively affecting the system efficiency. The steam usage for the rinse step is a trade-off between the necessity to recover as much as H_2-rich gas possible and the efficiency penalty for steam extraction. A different rinse gas such as nitrogen or CO_2 itself can be adopted, but steam is preferred because of its availability and guarantees high CO_2 purity. After rinse, co- or counter-current pressure equalizations (EQ2-EQ3) start in order to limit the compression work. At the end of the last equalization step, the vessel contains only a mixture of CO_2 and steam.

Recovery of CO_2 is achieved in the next two steps named depress and purge. The depressurization step is carried out counter-currently down to the pressure of CO_2 recovery, then steam is used to counter-currently purge the bed. The purge steam pressure must be high enough to overcome the pressure drop of the adsorber/reactor; the steam can be either bled from the turbine or produced with a dedicated level in the HRSG. The effluent gas is a low pressure CO_2

/steam mixture at around 400 °C. The final step of the process consists of vessel re-pressurization, first by accepting gas from other vessels undergoing the pressure equalization EQ3, EQ2 and EQ1, and later by receiving counter-current product gas. Multiple beds are necessary in order to produce a continuous stream of hydrogen and CO_2; the optimal number of beds is usually between six to eight reactors, all connected with valves, which is a good compromise between installed cost and efficiency.

7.1.3 SORBENT CHARACTERIZATION

The solid-phase high-temperature CO_2 adsorbent is the heart of the SEWGS process. The material must efficiently adsorb and desorb CO_2 via pressure swing cycles (between ~30 and ~1.0 bar) at operating temperatures in the range of 350-550 °C. Sorbent must be characterized by some important features concerning the following aspects:

- High CO_2 capacity and selectivity over H_2
- Low H_2O adsorption
- Low specific cost
- Mechanical stability under pressure and temperature variation
- Chemical stability in the presence of impurities
- Easily regenerated by steam (CAESAR target, 2 mol steam/ mol CO_2)

In particular, CO_2 adsorption capacity is the key parameter to develop an efficient capture system with low efficiency penalties. By increasing the CO_2 adsorption capacity, more CO_2 can be captured in the same volume reducing the steam usage for rinse and purge with further benefits from energy perspective.

The reference sorbent considered in this work for the SEWGS process was developed within CAESAR project and was named for simplicity *Sorbent Alfa*; *Sorbent Alfa* is a potassium carbonate hydrotalcite-based material and it was considered as reference [7]. This sorbent was tested under thousands of cycles in the multicolumn facility at ECN, showing similar performances but improved mechanical stability compared to the previous sorbent used in the CACHET project [8]. Finally, *Sorbent Alfa* showed the capability to adsorb H_2S together with CO_2; H_2S is also desorbed during purge step. Hence, sulphur separation from the syngas is performed by SEWGS, and an additional purification process is required downstream to separate sulphur from carbon dioxide [9]. Section 7.6.2 is dedicated to solve this issue

In addition to the cases developed for *Sorbent Alfa*, a more advanced solution based upon an improved sorbent (named *Sorbent Beta*) capable of enhancing the system performance was evaluated. Compared to *Sorbent Alfa*, the new sorbent showed a more advantageous isotherm shape and an adsorption capacity about 60% or 100% higher than the reference material, at design feed conditions for natural gas and coal respectively (CO_2 partial pressure equal to 2.8 bara for NG and 6 bara for coal). This performance reflects the behavior of a new type of sorbent recently tested in ECN laboratories based on different composition than S*orbent Alfa*.

Depending on the adsorbent features, the SEWGS reactor may require the adoption of a common HTS catalyst which would be mixed with the adsorbent. Experiments at ECN demonstrated that the developed sorbent promotes WGS reaction making the catalyst pointless. Therefore, in this work, SEWGS is considered to be filled only with adsorbent.

7.2 MODELING THE SEWGS PROCESS

The SEWGS modeling activity was carried out exclusively by Air Products as part of the CAESAR project framework and is extensively discussed in [10]. Therefore, only a brief summary of [10] is here reported in order to facilitate the understanding of the following process modeling.

The SEWGS model is based on PSA simulators already described in literature [11] with some additional complexity in the inclusion of WGS reaction terms. Assumptions made in the model include:

(1) Radial gradients within the vessel are zero, so a one-dimensional model is acceptable.
(2) The adsorbent bed can be treated as homogeneous with constant physical and geometric properties along its length.
(3) Axial dispersion and pressure gradients are negligible.
(4) Mass transfer can be described by linear driving force (LDF) with a single lumped coefficient.
(5) Gas and solid are in local thermal equilibrium.
(6) Ideal gas behavior.
(7) The water-gas-shift reaction rate depends on the gas phase compositions.

The SEWGS model is based on partial differential equations which resolve: i) the material balance of each individual component, ii) the energy balance for combined gas and sorbent and, iii) the wall energy balance. These equations were spatially discretised using a finite volume method and then solved in time using an implicit integration technique. Grid sizing was refined until negligible numerical errors were obtained.

The breakthrough test data were used to fit the parameters for the SEWGS model. With the model matched reasonably well with the experimental data, the tool was used to predict the performance of commercial size units to allow an estimate of sizing and operating cost.

Figure 7-3 a) and b) show an example of what happens inside the SEWGS reactor: the CO_2 loaded on the sorbent in a) and the H_2O molar fraction in b). The highest CO_2 loading is not found during the feed stage, but at the end of rinsing. This is because CO_2 is still at high pressure during this step and the sorbent is slowly taking it out of the gas phase as it reaches equilibrium. As the pressure is reduced through the equalisation and depressurisation steps, then the amount of CO_2 on the sorbent is reduced. This drops further during the purge step when low pressure steam is used to enhance desorption. Due to the highly favorable shape of the isotherm, the H_2-product end of the bed always has a high loading, but this relates to only a small slip of CO_2 from the sorbent.

Figure 7-3 b) shows how the molar fraction of steam varies over the course of the cycle. During the feed step there is a rise in steam concentration along the length of the bed as CO_2 is

adsorbed, although this is countered in part as H_2O is lost as it reacts with CO. During the rinse step, steam is introduced at the product end of the bed, but this does not need to pass through the entire sorbent. Instead, the equalisation steps are used to reduce the pressure causing the steam at the H_2-product end of the bed to expand and push out void gas into a vessel being repressurised. At the end of the equalisation steps, steam and CO_2 alone are present in the voids.

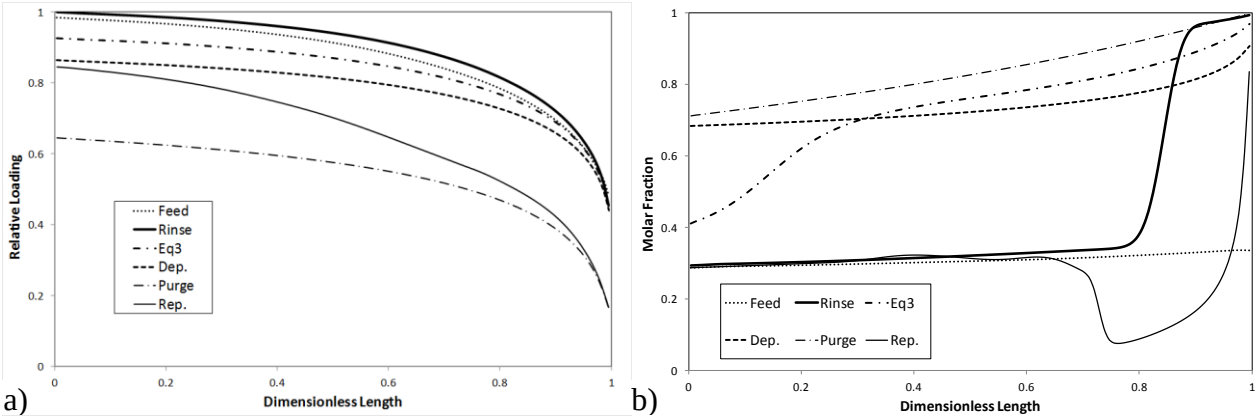

Figure 7-3: a) CO_2 loading over the course of a counter-current steam rinse cycle; b) H_2O molar fraction over the course of a counter-current steam rinse cycle. From [10]

7.3 APPROACH TO SEWGS INTEGRATION WITHIN POWER PLANTS

As common to all pre-combustion systems, the SEWGS process significantly modifies the power plant layout. From a macroscopic point of view, both in natural gas, coal and blast furnace applications, the resulting overall plant can be ideally divided into three sections:

- Section 1: syngas production island. It consists of the chemical reactors and all the equipment required to convert the initial fuel feedstock into a CO rich syngas. In natural gas fired plants it comprises the GHR-ATR; in the coal plants it consists in the coal gasifier and air separation unit. Finally in steelworks it is represented by all the reactors which produce the blast furnace mixture.
- Section 2: CO_2 separation and hydrogen rich mixture production island. In all the considered plants it is identified by: i) the WGS, ii) the SEWGS itself, iii) the CO_2 compression train and iv) all the heat exchangers following the syngas production.
- Section 3: power island. It comprises the gas turbine (GT) and all the equipment of the heat recovery steam cycle (HRSC).

In a previous work [12] the level of integration between the three sections in case of natural gas plant was extensively studied. From a qualitative point of view, a tight integration between the syngas, hydrogen and power island reduces the efficiency penalty, but may lead to higher investment costs and lower operational flexibility.

Three different levels of integration between the hydrogen and power islands were considered:

- <u>Level of integration 0</u>
  1. No interactions exist between the three areas: all the steam required by the SEWGS is produced inside sections 1 and 2.

2. Air for the ATR is taken from an electrically driven air compressor.

- Level of integration 1
  1. Syngas and hydrogen islands are close linked with the power island.
  2. Air for the ATR is taken from an electrically driven air compressor.
- Level of integration 2
  1. Syngas and hydrogen islands are close linked with the power island.
  2. Air for the ATR is taken from GT air compressor and sent to a blower (required to overcome the pressure drops).

The integration between syngas, hydrogen and power islands enhances the heat recovery; the cooling of the GT exhausts contributes to meet the steam demand as much efficiently as possible. In particular, two different utilizations of the CO_2-steam stream were investigated: in the first, the stream was cooled to ambient temperature recovering heat for the NG saturator and pre-heating, while in the second a sub-atmospheric expander was adopted to produce power while limiting heat rejection.

The three different levels of integration were extensively discussed and compared at constant sorbent performances in [12]. The best case arisen featured the tighter integration between the different sections with the expansion of the CO_2-steam stream. Therefore all the cases further developed and reported in this work are always based on tight integration of the sections.

7.4 PROCESS PARAMETERS AND INVESTIGATED CASES

The number of operating parameters that can be varied with respect to the SEWGS technology and the optimization of such a process is a complex task. In order to establish which SEWGS working conditions maximize the plant efficiency (and the economics), the following parameters were investigated:

- **CO_2 purity**: it was found that the CO_2-product purity is a strong function of the amount of rinse steam introduced to the vessel [10]. The more steam that is added, the more voids gas is flushed out and the purer the CO_2-product. As the penalty of losing H_2 from the process into the CO_2-product is significant and justifies the use of a high rinse quantity, a CO_2 purity in the 98-99% were considered.
- **SEWGS CCR**: it accounts for the carbon recovery in the SEWGS (captured CO_2 to total carbon input ratio). Even though carbon capture rates of 100% can be achieved in the SEWGS, the penalty in terms of purge steam requirement and/or adsorbent quantity pushes the carbon capture rate lower. Three values have been considered: 90, 95 and 98%.
- **Purge Pressure**: the purge pressure fix the pressure of the tail gas released from the SEWGS. Differently from the common PSA, the tail gas must always be recompressed up to the CO_2 capture pressure. Therefore the choice of purge pressure is not straightforward. Modelling showed that decreasing the purge pressure results in a reduction in the purge gas quantity as the equilibrium driving force for desorption is increased [10]. On the other hand, a lower purge pressure requires more power to compress the CO_2 product. It was found from the SEWGS modelling that an additional penalty for operating at very low pressure is that it causes steam to desorb

from the sorbent [10]. This would be replaced by the steam content of the feed gas reducing the inert fraction in the hydrogen rich syngas and therefore requiring more N_2 as diluent. Moreover, operating below atmospheric pressure also causes safety concerns on hydrogen plants. Taking into account all considerations, the optimum purge pressure for this sorbent material was found to be around atmospheric pressure.

- **Size and quantity of vessels required**: it is determined by the amount of sorbent used for the SEWGS process. Larger amounts of sorbent mean lower cyclic capacities can be used, so less purge steam is required [10]. On the other hand, the amount of rinse steam required increases as more void gas is present that must be flushed out. A vice-versa result is found when the sorbent quantity is decreased. Optimization of vessel size-quantity is also linked to the cycle time for the SEWGS process: short cycle times result in lower purge requirements as the cyclic capacity of the sorbent can be reduced due to the smaller quantity of CO_2 introduced each cycle. However, the vessel must be rinsed and the voids flushed out more often, increasing the amount of rinse steam required. When varying the sorbent quantity and the cycle time there is the need to cope with the fluidization limits: it constrains the smallest cycle time and the largest vessel size that can be adopted. This limitation can be worked out by using more trains of SEWGS units with smaller vessels and shorter cycles, but with capital cost penalty.

All the aforesaid parameters affect not only the SEWGS but also the power plant performance (first of all the purge/rinse steam demand). It results that the SEWGS optimization must be done together with the overall power plant simulation.

The following paragraphs report therefore all the cases considered for the SEWGS optimization within a power plant either natural gas, coal or blast furnace fuelled.

7.4.1 SEWGS Working Conditions for Natural Gas Plants

Table 7-1 summarizes the cases investigated in this work for natural gas plant and *Sorbent Alfa*. The investigated values range between 90 and 98% for CCR, fixing CO_2 purity either equal to 98 or 99%. Other parameters that affect steam usage, such as number of trains, number of vessels per train and purge pressure, are kept constant at values of 8 x 9 and 1.1 bara respectively; all these parameters were deeply investigated within CAESAR project and the values adopted in this work are the best trade-off between efficiency-economics and feasibility of the SEWGS reactor. Vessel length is fixed at 34 ft (10.36 m) since shorter vessel would require too high steam flow-rate. In terms of purge pressure, sub-atmospheric conditions are challenging because of fluidization limits inside the bed (fluidization depends on volumetric flow and consequently, low pressure enhances fluidization phenomena). Cases with 99% CO_2 purity and 98% CO_2 capture were not considered to avoid exceedingly high steam usage.

The overall steam usage adopted in the previous work [12] was significantly lower (both 0.9 for a carbon capture ratio of 98% and CO_2 purity of 99%) than the values reported in Table 7-1, leading to different and more optimistic thermodynamic performances.

Table 7-1: SEWGS working conditions investigated and steam demand (as Steam to Carbon ratio) for *Sorbent Alfa.*

	Case 1	Case 2	Case 3	Case 4	Case 5
Purity (%)	98	98	98	99	99
Carbon capture ratio (%)	90	95	98	90	95
Rinse flow (S/C ratio)	0.73	0.74	0.75	0.85	0.86
Purge flow (S/C ratio)	1.41	2.13	3.08	1.45	2.16

The cases analyzed with *Beta Sorbent* are summarized in Table 7-2. Only the 99% purity cases were considered, since it resulted as the more interesting one. Moreover, the higher capacity allowed investigating also additional cases as 98% CCR and 99% purity, and different vessel numbers (six trains instead of eight); for reference sorbent, these cases were not allowed due to a fluidization constraint, and too high steam usage. When the vessel volume is the same as for *Sorbent Alfa* cases, the improved capacity of *Sorbent Beta* reduces significantly the amount of purge steam required (about 90%), and only slightly that of rinse steam. This is because the rinse steam mainly depends on total sorbent volume and target CO_2 purity, while purge steam is a function of sorbent capacity.

When a lower number of vessels is considered, thus reducing total sorbent volume, rinse steam reduction occurs with penalties in terms of purge steam usage. It must be outlined that efficiency penalties related to rinse are significantly higher than purge ones (rinse is at about 30 bara instead of 1.1 bara of purge).

Table 7-2: SEWGS working conditions with *Sorbent Alfa* and *Sorbent Beta.*

Vessel n°	8 x 9						6 x 9					
Vessel length	34 ft						34 ft					
Purity, (%)	99		99		99		99		99		99	
CCR, (%)	90		95		98		90		95		98	
	Rinse	Purge	Rinse	Purge	Rinse	Purge	Rinse	Purge	Rinse	Purge	Rinse	Purge
Alfa Sorbent	0.85	1.45	0.86	2.16	-	-	-	-	-	-	-	-
Beta Sorbent	0.80	0.14	0.82	0.31	0.85	0.55	0.57	0.35	0.60	0.64	0.62	1.21
Delta steam, (%)	-6	-90	-5	-86	-	-	-	-	-	-	-	-

7.4.2 SEWGS Working Conditions for Coal Plants

Table 7-3 summarizes the cases investigated in this work for coal plant and *Sorbent Alfa*. Investigated values range between 90 and 98% for CCR, while CO_2 purity is equal to 98%, 99% and 99.5%. Other parameters that affect steam usage, such as number of trains, number of vessels per train and purge pressure, were kept constant at values of 6x9 and 1.1 bar respectively; vessel length is fixed at 40 ft (12.2 m) since shorter vessel would require too high steam flowrate.

It can be noted that the amount of rinse affects the CO_2 purity, while purge influence CCR. In the previous work [13], rinse and purge S/C ratio were assumed equal to 0.65 for a carbon

capture ratio of 98% and CO_2 purity of 99%, thus purge flows were significantly different compared to steam usages measured recently.

Finally, a case with five trains instead of six, CO_2 purity 99% and CCR 90%, was investigated. Resulting S/C ratio are equal to 0.35 and 1.49 for rinse and purge step respectively. Higher CCR cannot be considered because of the too large steam flow rate.

Table 7-3: SEWGS working conditions investigated for coal plant and *Sorbent Alfa.*

Purity (%)		**98.0**			**99.0**			**99.5**	
CASE	A,1	A,2	A,3	B,1	B,2	B,3	C,1	C,2	C,3
Carbon capture ratio (%)	90	95	98	90	95	98	90	95	98
Rinse flow (S/C ratio)	0.33	0.34	0.34	0.43	0.44	0.44	0.49	0.49	0.49
Purge flow (S/C ratio)	0.60	0.96	1.40	0.68	1.06	1.49	0.72	1.11	1.54

The cases analyzed with *Sorbent Beta* are summarized in Table 7-4 and are quite different from *Sorbent Alfa* ones since the higher capacity leads to: (i) more flexible solutions and, (ii) no fluidization constraints. For this reason, no direct comparison between these two sorbents is presented. As far as *Sorbent Beta* is concerned, only 99% CO_2 purity cases was considered, since it resulted as the most interesting one. About CCR, 95% and 98% cases were investigated. Case at 90% CCR was not taken into account because for bed length of 34 ft, even with zero purge flow, the resulting CCR was higher and equal to 92%.

Table 7-4: SEWGS working conditions investigated for coal plant and *Sorbent Beta.*

Vessel n°		**5 x 9**			**5 x 9**	
CCR (%)		95			98	
Purity (%)		99			99	
Vessel length (ft/m)	22/6.7	28/8.5	34/10.4	22/6.7	28/8.5	34/10.4
Rinse (S/C ratio)	0.23	0.29	0.36	0.24	0.30	0.38
Purge (S/C ratio)	0.85	0.27	0.08	1.43	0.47	0.20

Rinse steam increases with vessel length, but it is not significantly affected by CCR. On the contrary, purge flow depends on vessel length as well as total sorbent volume. This is because rinse is required to flush the syngas out of the bed once it is saturated by CO_2, so it is a function of sorbent volume to be swept, while purge depends on sorbent capacity: higher CCR and lower sorbent volumes require a higher sorbent regeneration, hence steam flow. The same analysis could be carried out reducing vessel numbers instead of length. However, it will not change thermodynamic performances of the plant.

7.4.3 SEWGS Working Conditions for SteelWorks Plants

SEWGS operating conditions adopted in this case are reported in Table 7-5; values are presented in terms of the required kmols of steam relative to the kmols of total carbon in the feed. Values are reported for the two different sorbents, *Alpha* and *Beta*. The number of trains, vessels per train, the purge pressure and the CO_2 purity were kept constant.

Table 7-5: SEWGS working conditions investigated for steel plant with *Sorbent Alpha* and *Sorbent Beta*.

Sorbent type	**Sorbent Alpha**		**Sorbent Beta**	
SEWGS CCR %	95		95	
Train number	6 trains x 9 vessels		6 trains x 9 vessels	
Purge pressure [bar]	1.1		1.1	
CO_2 purity [%]	99		99	
Steam demand	Rinse	Purge	Rinse	Purge
[mol_{H2O}/mol_{Carbon}]	0.52	0.89	0.20	0.26
Temperature [°C]	400		400	
Pressure [bar]	28.0	1.25	28.0	1.25

7.5 NATURAL GAS PLANT

7.5.1 PLANT LAY-OUT

The SEWGS lay-out, shown in Figure 7-4, is based on the advanced configuration developed in [12] which featured the tighter integration among the different sections and with CO_2-steam stream expansion (formerly named Integration 2 EXP). It was selected in order to limit exergy losses, with advantages from an efficiency point of view, adding some interconnections between the hydrogen island and the HRSG. Moreover, air for the reforming is taken at the GT air compressor outlet: this solution enhances the compression efficiency as the air flow rate at the compressor inlet is close to the design conditions: no Variable Guide Vanes (VGV) control is necessary with increased surge margin and control range. The main drawback is the more complex start-up. Steam for reforming and SEWGS operation is taken from the HRSG allowing optimized heat management. Methane reforming and rinse steam demand is met by bleeding from cold reheat (RH) at 28 bara, while the purge steam is produced in a dedicated loop at 400°C and 1.10 bara in the HRSG. Following the fuel feeding: NG, which is available at 70 bara and 10°C from the pipeline, is mixed with a small amount of hydrogen[1] and preheated to 380°C, as required by the Hydro DeSulphurization reactor (HDS), through a recuperative and a syngas heat exchanger. The HDS process is assumed to be at about 29 bara which is set by the minimum fuel overpressure at the GT combustor inlet (NG throttling is considered as in the reference case [14]). NG is then saturated, heated to 300°C and mixed with steam bled from the steam turbine to reach the 1.1 Steam-to-Carbon (S/C) ratio required by the GHR-ATR reactor. Modeling of the GHR-ATR is calibrated using data available in open literature [15] [16] [17] and already discussed in chapter 3. After additional pre-heating, the NG-steam mixture enters the GHR-ATR reactor together with air; between the GT compressor and GHR-ATR, an electrically driven compressor is added to achieve the reforming pressure. The air flow rate is selected to achieve an equilibrium temperature of 950°C inside the reformer.

After the GHR-ATR, the syngas is cooled down to about 410 °C producing HP saturated steam in a waste heat boiler: the saturated water is taken from the HP drum, evaporated and sent back to the HRSG. Adoption of a waste heat boiler instead of SH or RH heat exchangers prevents metal dusting as that maximum metal temperature is limited to 400 °C, which is considered the starting value of this phenomenon [18]. Then, syngas enters a preliminary high

[1]The hydrogen content is set at 2% in the stream as required by the desulphurization process.

temperature shift (HTS) reactor whose inlet and outlet temperatures are about 310 °C and 400 °C respectively. HTS is followed by SEWGS. The preliminary shift step upstream of the SEWGS is required to reduce the temperature rise inside the multiple beds which can be detrimental for sorbent capacity and stability. Indeed, this is a conservative solution which aims to preserve the sorbent integrity limiting at the same time the SEWGS reactor complexity, i.e. the cost.

The hydrogen rich stream produced by SEWGS is sent to the GT combustor after cooling to 350°C producing HP steam for the HRSG.

The CO_2-steam stream regenerated from the SEWGS unit superheats rinse steam, and is then expanded in a multi-stage axial turbine, similar to the LP stages of a steam turbine, but without liquid phase issues. The expander outlet pressure and temperature depend on the steam content in the stream (a sensitivity analysis on this parameter is discussed in the results section). Then the stream is cooled, producing hot water for the saturator and NG pre-heating.

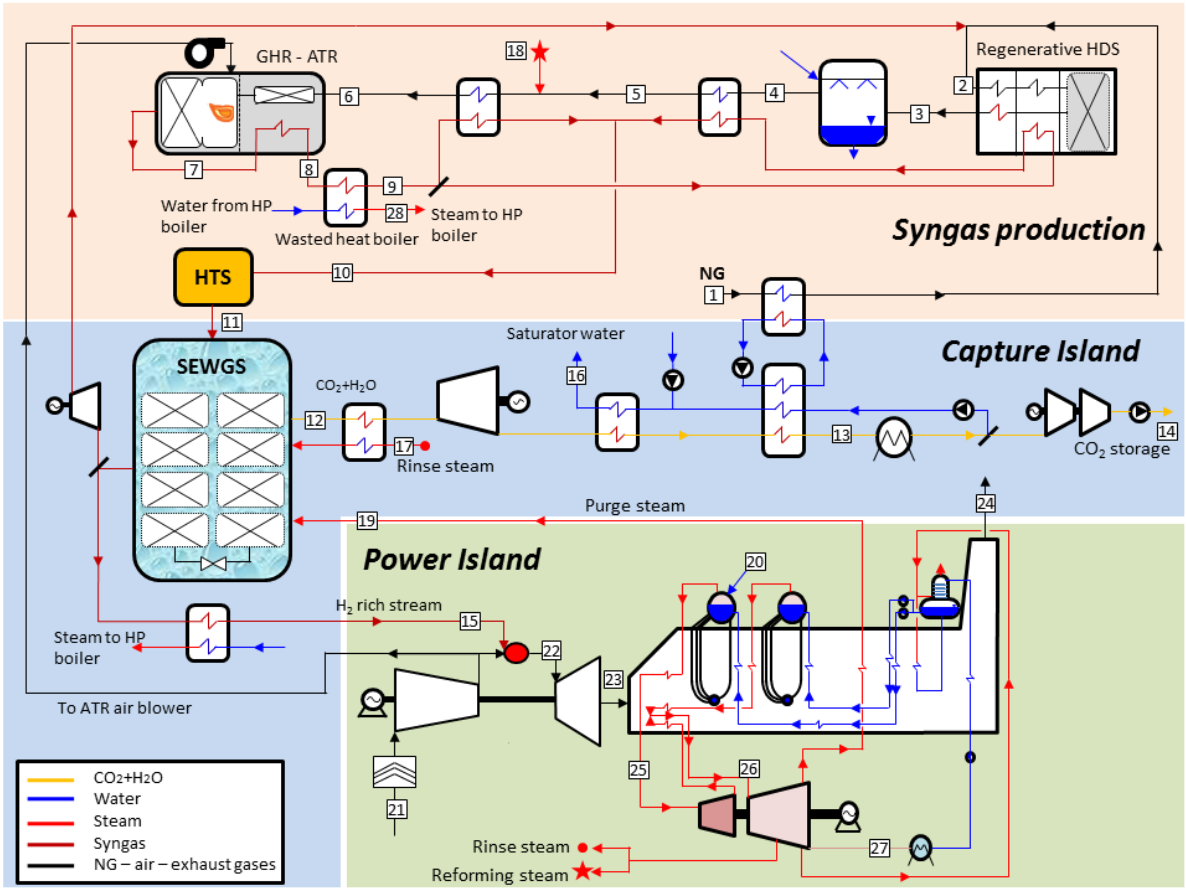

Figure 7-4: layout of investigated natural gas fuelled SEWGS case

Table 7-6: mass flow rate, temperature, pressure and composition of the main fluxes reported in Figure 7-4.

Point	G	T	p	Composition, %mol.								
	kg/s	°C	bara	CH_4	C_2H_6+C_3H_8	CO	CO_2	H_2	H_2O	Ar	N_2	O_2
1	16.7	10.0	70.0	Natural Gas as reported in chapter 3								
2	17.2	382.0	28.95	85.9	7.8	.02	1.9	2.00	0.1	.02	0.9	-
3	17.2	123.2	28.66	85.9	7.8	.02	1.9	2.00	0.1	.02	0.9	-
4	21.9	159.3	28.09	67.4	6.1	.02	1.5	1.6	21.6	.01	1.7	-
5	21.9	300.0	27.53	67.4	6.1	.02	1.5	1.6	21.6	.01	1.7	-
6	37.1	302.1	27.53	40.0	3.6	.01	.9	.9	53.5	.01	1.0	-
7	105.3	950.0	25.64	0.5	-	12.7	4.0	34.7	16.1	0.4	31.60	-
8	105.3	646.1	25.38	0.5	-	12.7	4.0	34.7	16.1	0.4	31.60	-
9	105.3	409.8	25.13	0.5	-	12.7	4.0	34.7	16.1	0.4	31.60	-
10	105.3	311.9	24.63	0.5	-	12.7	4.0	34.7	16.1	0.4	31.60	-
11	105.3	402.4	23.64	0.5	-	5.0	11.6	42.4	8.4	0.4	31.60	-
12	94.7	430.8	1.05	-	-	-	23.6	.1	76.1	-	.1	-
13	94.7	79.1	0.15	-	-	-	23.6	.1	76.1	-	.1	-
14	40.9	25.0	110.0	-	-	-	99.0	.6	-	-	.4	-
15	63.1	350.0	23.17	0.6	-	.7	.3	56.2	3.8	0.4	37.9	-
16	33.7	190.0	110.3	-	-	-	-	-	100.0	-	-	-
17	15.1	400.0	27.0	-	-	-	-	-	100.0	-	-	-
18	15.2	335.5	27.5	-	-	-	-	-	100.0	-	-	-
19	37.9	400.0	1.25	-	-	-	-	-	100.0	-	-	-
20	46.7	337.1	130.0	-	-	-	-	-	100.0	-	-	-
21	650.0	15.0	1.01	Air as reported in chapter 3								
22	514.6	COT 1440.0 TIT 1360.1 TIT_{ISO} 1258.8	17.61	-	-	-	.4	-	16.3	.9	72.9	9.5
23	644.8	595.2	1.04	-	-	-	0.4	-	13.4	0.9	73.7	11.6
24	644.8	70.0	1.01	-	-	-	0.4	-	13.4	0.9	73.7	11.6
25	198.9	559.5	120.9	-	-	-	-	-	100.0	-	-	-
26	151.1	561.0	22.55	-	-	-	-	-	100.0	-	-	-
27	92.6	32.2	0.048	-	-	-	-	-	100.0	-	-	-
28	37.2	338.0	131.3	-	-	-	-	-	100.0	-	-	-
Net Power Output					**425.20**	**MW**		**Net Electric Efficiency**				**47.68**

7.5.2 RESULTS

Figure 7-5 shows the influence of the CO_2 avoided on plant net electrical efficiency and SPECCA. It can be seen that increasing CO_2 capture above 90%[2] leads to significant efficiency penalties because of the exponential increase of steam usage (see Table 7-1). The best compromise in terms of SPECCA leads to CO_2 avoided values between 85-90%, however only the economic assessment discussed in chapter 9 will be able to confirm it.

The curves in the figure demonstrate that there is negligible impact of CO_2 purity on system performance (outlet expander pressure is set at 0.15 bara): the higher steam usage for rinsing (2 kg/s out of 15.05 kg/s) is balanced by the lower amount of hydrogen captured with the CO_2 and, consequently, lost (0.7 MW_{LHV} for 99% purity vs 1.4 MW_{LHV} for 98% purity).

[2] Corresponding SEWGS CCR are lower, due to unconverted CH_4

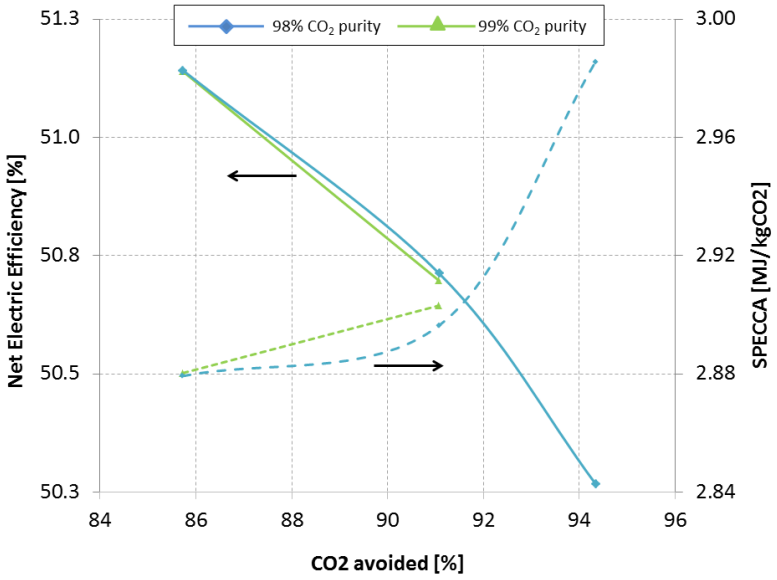

Figure 7-5: net electric efficiency (solid lines) and SPECCA (dotted lines) for different SEWGS CCR

CO_2-steam expander outlet pressure is another parameter to be optimized both in term of efficiency and economic point of view: lower exiting pressure might increase the power output and efficiency, but penalizes the economics due to the higher volumetric flow rate. The optimization was carried out for 99% of CO_2 purity and CO_2 capture ratio of 95%. (case5 according to definition in Table 7-1).

As shown in Figure 7-6, the highest efficiency (and lower SPECCA) is achieved for expander outlet pressure in the range of 0.15 bara. The optimal condition is a compromise between recovered condensation heat by the expander and higher CO_2 compression work. It must be outlined that for higher outlet pressure, expander and CO_2 compression work decrease together with investment costs.

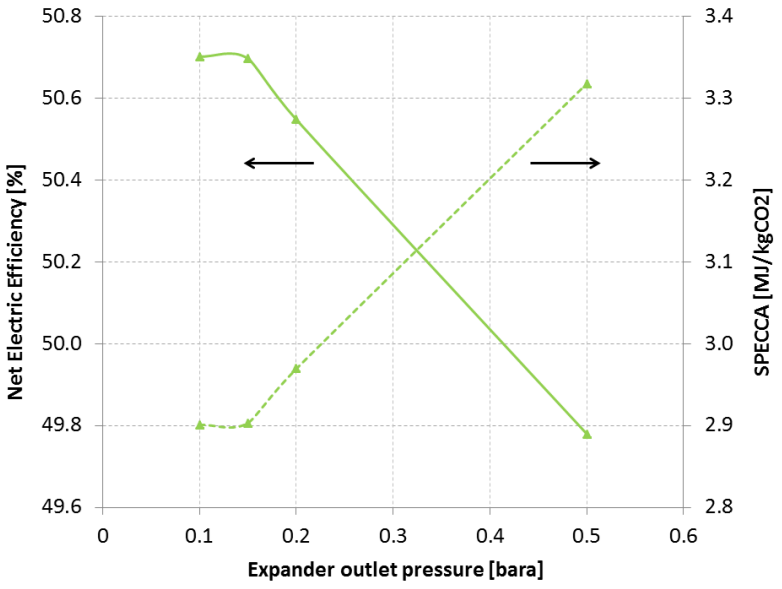

Figure 7-6: net electric efficiency (solid lines) and SPECCA (dotted lines) for different expander outlet pressure (Case 5).

Performances and power balances of the most promising cases are presented in Table 7-7 together with reference cases [14] [19] [20].

Net electric efficiency obtained for SEWGS case 5 is about 0.8% points higher than reference case with CO_2 capture carried out by MEA, with an efficiency penalty compared to the no-capture case of 7.6% point. SEWGS CO_2 avoidance is in the range of 86% and 91%, while reference MEA is in between.

The resulting SPECCA is in the range of 2.9 MJ/kg_{CO2} which is about 12% and 6% lower than the reference cases MEA and MDEA, respectively, suggesting the thermodynamic advantages of SEWGS towards competitive solutions. Focusing on power balances, CO_2 compression work in SEWGS cases is significantly higher than MEA and MDEA, because compression starts at 0.15 bara instead of 1.2 bara: the higher compression work is positively balanced by the CO_2-steam expander power output.

Finally, net power output reduction for SEWGS compared to no-capture case, is smaller than the MEA one and is in the order of 40 MW. Pre-combustion capture brings about higher thermal power input consequent of the constant size of the gas turbine and reforming reaction heat duty, whilst post-combustion capture works at constant fuel input modifying only the bottoming steam cycle (i.e. smaller steam turbine power). On the contrary, MDEA case has a slightly higher power output than reference NGCC.

Summarizing, thermodynamic performances of SEWGS in NGCC are promising.

Table 7-7: NGCC with carbon capture by SEWGS (reference NGCC and NGCC with capture via amine scrubbing and MDEA are also shown).

	NGCC	NGCC with MEA	NGCC with MDEA	SEWGS Case 4	SEWGS Case 5
N° of gas turbine	2	2	2	2	2
Gas Turbine Electric Net Power [MW]	272.1	272.1	294.5	277.4	276.1
CO_2-steam Expander [MW]	-	-	-	51.2	63.7
Steam Cycle Electric Gross Power, [MW]	292.8	215.7	305.1	253.9	237.6
Steam Cycle Auxiliaries, [MW]	-3.5	-3.4	-35.2	-4.2	-4.1
CO_2 compressor, [MW]	-	-22.6	-29.0	-42.5	-44.7
GHR-ATR air compressor [MW]	-	-	-18.7	-13.1	-13.1
Auxiliaries for heat rejection, [MW]	-3.7	-4.4	-3.1	-4.4	-4.4
BOP capture section, [MW]	-	-19.8	-8.1	-0.3	-0.3
Net Power Output, [MW]	**829.9**	**709.7**	**830.0**	**795.5**	**786.9**
Thermal Power Input$_{LHV}$, [MW]	**1422.6**	**1422.6**	**1651.0**	**1555.5**	**1552.1**
Thermal Power Input$_{HHV}$, [MW]	1575.5	1575.5	1828.4	1722.7	1719.0
Net Electric Efficiency$_{LHV}$, [%]	**58.34**	**49.90**	**50.30**	**51.14**	**50.70**
Net Electric Efficiency$_{HHV}$, [%]	52.67	45.06	45.39	46.18	45.78
Emissions [g_{CO2}/kWh_{el}]	351.8	41.1	29.8	50.2	31.4
CO_2 avoided, [%]	-	88.3	91.5	85.7	91.1
CO_2 purity, [%]	-	-	-	99.0	99.0
SPECCA, [MJ_{LHV}/kg_{CO2}]	**-**	**3.36**	**3.07**	**2.88**	**2.90**

7.5.3 ADVANCED SOLUTION: SORBENT BETA

Comparison of the overall plant performance with *Sorbent Alfa* and *Sorbent Beta* and equal sorbent volume is reported in Figure 7-7.

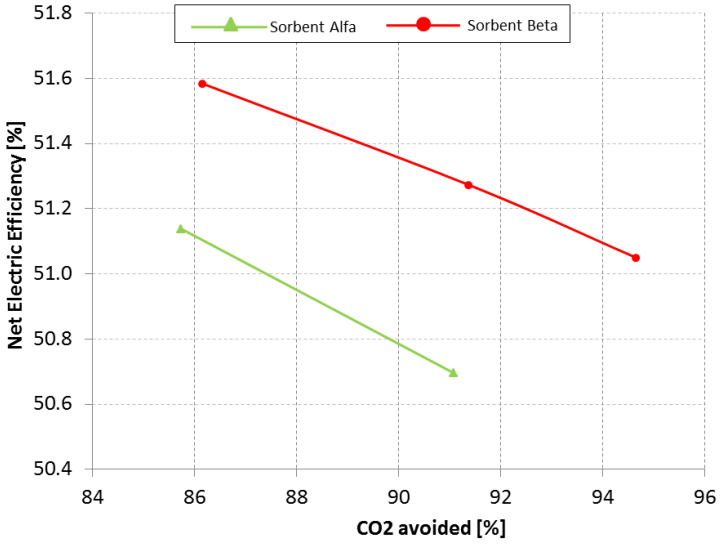

Figure 7-7: net electric efficiency for *Sorbent Alfa* and *Sorbent Beta* in NG plant.

Results presented for *Sorbent Beta* were calculated with an optimized expander outlet pressure of 0.3 bara: the lower amount of steam in the CO_2 increases optimal expansion pressure (see Figure 7-8). Results show that improved sorbent capacity reduces efficiency penalty of about 0.5% points and allows SEWGS CCR to increase up to 98% with an overall net electric efficiency of 51%. Moreover, the higher capacity reduces the steam consumption at high CCR and consequently the efficiency penalties: the negative slope of the efficiency as a function of CCR (see Figure 7-7) is lower for *Sorbent Beta* than *Sorbent Alfa*.

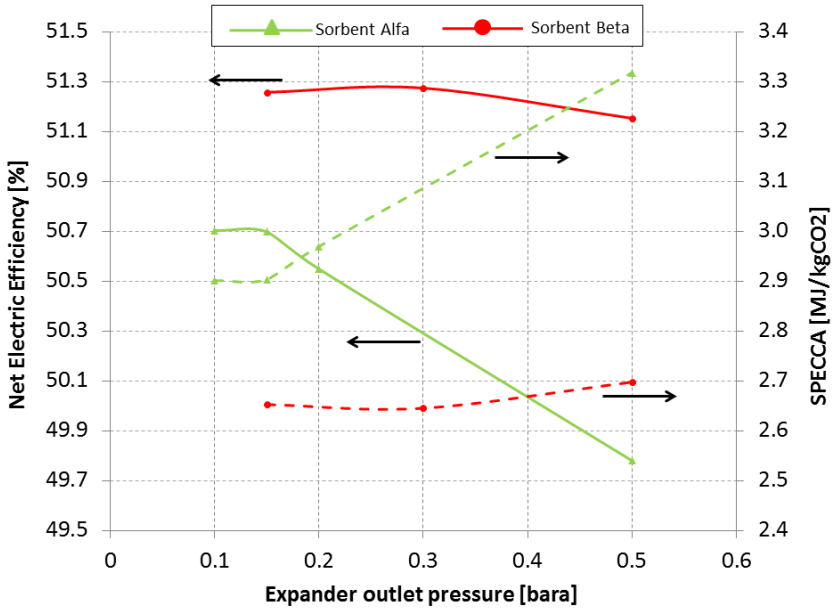

Figure 7-8: net electric efficiency as a function of expander outlet pressure for Sorbent Alfa and Sorbent Beta for CCR 95% and purity 99%; dashed lines refer to SPECCA values, continuous lines to net electric efficiency.

The comparison in terms of different SEWGS vessels or sorbent volume (see Figure 7-9) suggests that the lower the vessel numbers, the lower the efficiency penalty and the energy consumption for CO_2 avoided. The advantages are significant at 90% and 95% CCR, while they disappear at 98% CCR when purge flow-rate to regenerate the sorbent rises significantly. The adoption of a lower number of vessels and consequently sorbent volume requires an exponential increase of purge steam for regeneration, because the required capacity of the sorbent is significantly higher.

Moreover, it can be outlined that the minimum SPECCA as a function of CCR depends on the number of vessel considered: it occurs at 98% for 72 vessels, and it decreases to 90% CCR for 54 vessels.

Finally, it must be reminded that economic advantages of lower number of vessels appear only when cost of CO_2 avoided is assessed.

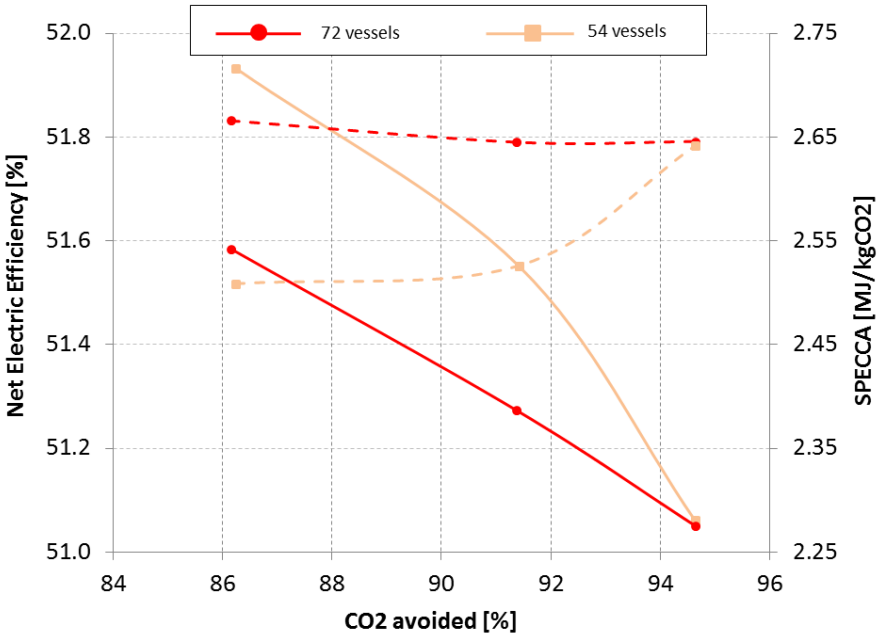

Figure 7-9: net electric efficiency for different vessel numbers with Beta Sorbent; dashed lines refer to SPECCA values, continuous lines to net electric efficiency

Table 7-8 reports the power balances for the considered cases with *Sorbent Beta*; it can be seen that the different steam consumption due to the change in vessel number affects only the expander and the steam cycle power output, whilst all the other parameters are constant. Consistently, the adoption of 54 vessels reduces the rinse flow and increases the steam cycle power output when 90% and 95% CCR are considered; given the small change in the expander power output, the overall efficiency increases. This is not the case for 98% CCR as the decrease of rinse steam is balanced by the high increase of purge steam; globally, the sum of the CO_2-steam expander and the steam cycle power outputs is constant, leading to equal efficiency.

The adoption of an improved sorbent capacity reduces efficiency penalty up to 0.8% points when compared to *Sorbent Alfa* performances. This results in a SPECCA of 2.5 MJ/kg_{CO2} (reference cases were above 3 MJ/kg_{CO2}).

Table 7-8: comparison of SEWGS performances for different vessel volume with *Sorbent Beta*.

Vessel number	**72 (8 x 9)**			**54 (6 x 9)**		
CCR	90	95	98	90	95	98
N° of gas turbine	2	2	2	2	2	2
Gas Turbine [MW]	276.0	274.9	274.5	276.1	274.9	274.5
CO_2-steam Expander [MW]	20.9	23.4	26.6	19.8	24.0	31.0
Steam Cycle Electric Gross Power, [MW]	284.4	279.6	274.8	290.7	283.4	270.6
Steam Cycle Auxiliaries, [MW]	-4.2	-4.2	-4.2	-4.1	-4.1	-4.1
CO_2 compressor, [MW]	-35.2	-37.0	-38.1	-35.2	-37.0	-38.1
GHR-ATR air compressor [MW]	-13.1	-13.1	-13.1	-13.1	-13.1	-13.1
Auxiliaries for heat rejection, [MW]	-0.5	-0.5	-0.6	-0.5	-0.6	-0.6
BOP capture section, [MW]	-4.4	-4.4	-4.4	-4.1	-4.1	-4.1
Net Power Output, [MW]	**799.95**	**793.65**	**790.06**	**805.35**	**797.95**	**790.21**
Thermal Power Input$_{LHV}$, [MW]	1550.8	1547.9	1547.6	1550.8	1547.9	1547.6
Thermal Power Input$_{HHV}$, [MW]	1717.4	1714.3	1713.9	1717.4	1714.3	1713.9
Net Electric Efficiency$_{LHV}$, [%]	**51.58**	**51.27**	**51.05**	**51.93**	**51.55**	**51.06**
Net Electric Efficiency$_{HHV}$, [%]	46.58	46.30	46.10	46.89	46.55	46.10
Emissions [g_{CO2}/kWh_{el}]	48.7	30.3	18.8	48.40	30.18	18.85
CO_2 avoided, [%]	86.2	91.4	94.6	86.24	91.42	94.64
SPECCA, [MJ_{LHV}/kg_{CO2}]	**2.67**	**2.65**	**2.65**	**2.51**	**2.53**	**2.64**

To summarize, SEWGS is a promising technology which reduces efficiency penalties related to CO_2 capture compared to reference cases: the optimum SPECCA found for SEWGS is 2.51 MJ/kg_{CO2}, while it is 3.4 MJ/kg_{CO2} and 3.1 MJ/kg_{CO2} for MEA and MDEA respectively.

The key parameter for the success of SEWGS technology is the sorbent cyclic capacity. However, the improved performances of 60% leads to a net electric efficiency gain of only 12%, since efficiency penalties is related also to CO_2 compression (about 4.5%points) and, in second order, to reforming section (about 1% points).

7.5.4 CONCLUSIONS: SEWGS IN NATURAL GAS FUELLED PLANT

This work investigated optimal working of SEWGS which is a promising CO_2 capture process for pre-combustion technology. The assumed power plant layout was the result of previous work which showed advantages of a tight integration between hydrogen and power islands. SEWGS working conditions were optimized in terms of CO_2 purity and Carbon Capture Ratio; moreover, the impact of sorbent capacity was also investigated. Results showed similar values for efficiency penalty and SPECCA for CO_2 purity of 98% and 99%. Thus, 99% can be indicated as optimal working conditions for advantages during transport and storage.

As far as Carbon Capture Ratio is concerned, higher CO_2 avoidance increases efficiency penalties as consequence of the increased steam usage in SEWGS. However, SPECCA, which represents the specific energy consumption for CO_2 avoided, is almost constant. A higher sorbent capacity has significant impact on system performances reducing SPECCA from 2.9

MJ/kg_{CO2} down to 2.5 MJ/kg_{CO2}. Compared to reference capture technology via amine scrubbing, the SPECCA decrease ranges from a minimum of 15% to a maximum of 25%.

In chapter 9, an economic assessment will be carried out for the most interesting SEWGS cases and for the reference case to determine the cost of CO_2 avoided.

7.6 COAL PLANT

7.6.1 PLANT LAYOUT

Integration of SEWGS in IGCC is presented in this section. A previous work determined thermodynamic advantages of applying SEWGS for H_2S and CO_2 co-capture compared to a more conventional solution where it is integrated downstream of a commercial acid gas removal (AGR) process [13]. By avoiding syngas cooling/preheating sections, simultaneous CO_2 and H_2S capture allows (i) exergy losses reduction and (ii) lay-out simplification. Hence, considering the reliable performances of the sorbent towards sulphur [9], the adoption of a conventional AGR process upstream SEWGS is considered not attractive, and will not be discussed in this work.

Heat&Mass balances of the gasification island are equal to the reference cases presented in chapter 3: this allows making consistent comparison with the state-of-the-art technologies with and without CO_2 capture, stressing advantages and disadvantages of innovative solutions towards conventional ones.

The amount of syngas at combustor inlet is determined in order to have the same GT dimensions, i.e. keeping same diameter and blades height in the last stage as reported in chapter 3 and extensively discussed in chapter 6. This assumption requires in first approximation a fixed exhaust gases mass flow at outlet.

After the gasification section, steam is added to the syngas to achieve a Steam/CO ratio of 1.9 before entering the water gas shift reactor (WGSR). The adoption of an adiabatic WGSR before the SEWGS is required in order to control the temperature rise inside SEWGS reactors. The adoption of cooled vessels in the SEWGS process is not considered economically attractive. Because of sulphur presence in the syngas, catalyst is CrMo type. The catalyst converts also COS into H_2S, so there is no interest in investigating the sorbent behavior towards COS. After WGS, a waste heat boiler is adopted to recover the heat released by CO conversion and to reduce syngas temperature at SEWGS inlet. After CO_2 and sulphur separation in the SEWGS unit, the hydrogen rich syngas produced at about 450°C can feed the gas turbine. However, because of fuel temperature limit assumed equal to 350°C, a cooling step between SEWGS and combustor is introduced. During the desorption process, CO_2 and sulphur are released at the same pressure and a further separation step must be adopted.

SEWGS layout, compared to the reference IGCC with CO_2 capture has the significant advantage of avoiding syngas cooling to ambient temperature leading to equipment savings not outlined in thermodynamic balances, but only in the economic assessment in chapter 9 of this work.

CO_2-steam stream is expanded at sub-atmospheric pressure in order to exploit part of the steam condensation heat. This practice is common in geothermal plants: the power gain obtained

by the additional expansion of the whole steam+gas flow rate is larger than the power required by the incondensable gas compressor [21]. Advantage of expansion solution was already outlined in the natural gas case. Hence, after the SEWGS, CO_2-steam stream superheats steam for rinse step and is then expanded in a single-stage axial turbine, similar to the LP stages of a steam turbine, but without liquid phase issues. The optimum expanding pressure depends on the steam concentration in the stream, thus depending on the SEWGS CCR and CO_2 purity set as target, but it is limited at 0.5 bar. De facto, being the unique large low temperature heat source in the plant, the expansion pressure must be high enough to guarantee high pressure water economization.

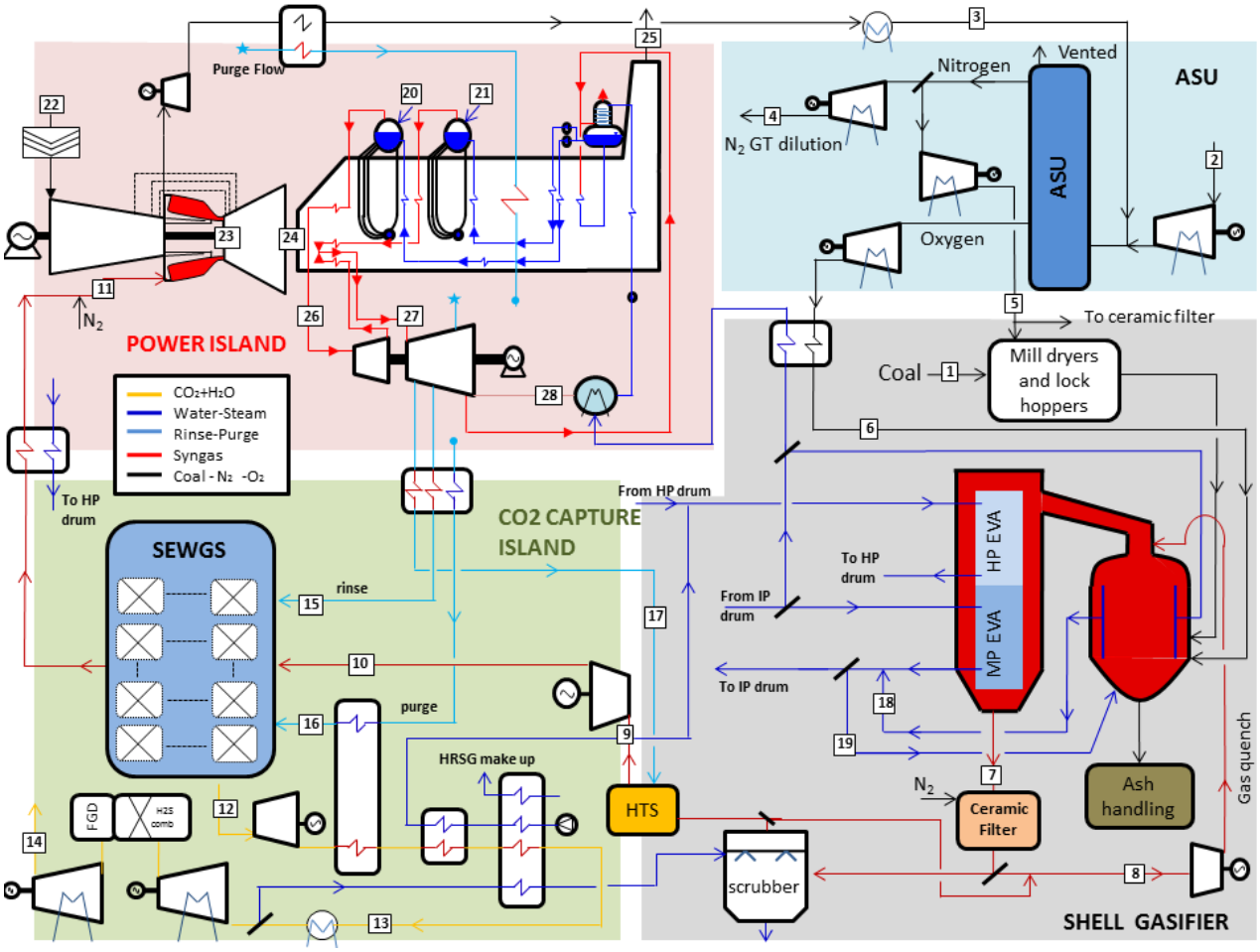

Figure 7-10: Layout of the IGCC power plant with CO_2 capture by SEWGS (54 trains).

Table 7-9: mass flow rate, pressure, temperature and composition of the main fluxes of IGCC with carbon capture by SEWGS; CCR 95%, CO2 purity 99% and 54 trains. (Numbers refer to Figure 7-10).

Point	G	T	p	Composition, %mol.								
	kg/s	°C	bar	CH_4	CO	CO_2	H_2	H_2O	Ar	N_2	O_2	H_2S
1	37.6	15.0	-	Dry Coal 2%, coal composition as in chapter 3								
2	70.0	15.0	1.01	Air as in chapter 3								
3	70.0	30.0	5.76									
4	31.5	260.6	27.2	-	-	-	-	-	-	100.0	-	-
5	10.5	133.8	88.0	-	-	-	-	-	-	100.0	-	-
6	33.1	180.0	48.0	-	-	-	-	-	3.1	1.9	95.0	-
7	130.7	300.0	41.0	-	56.5	2.9	26.2	5.4	.9	8.0	-	.2
8	55.8	200.0	41.0	-	51.7	2.7	24.0	12.5	.8	8.2	-	.2
9	148.7	484.3	40.2	-	5.0	24.3	35.7	30.1	0.4	4.4	-	.1
10	148.7	411.8	24.1	-	5.0	24.3	35.7	30.1	0.4	4.4	-	.1
11	79.7	350.0	23.2	-	.4	1.4	49.5	24.4	0.5	23.7	-	-
12	160.5	431.1	1.1	-	-	35.6	.3	64.0	-	.04	-	-
13	160.5	67.6	0.5	-	-	35.6	.3	64.0	-	.04	-	-
14	92.6	25.0	110.0	-	0.01	98.8	0.94	-	0.02	0.11	0.08	-
15	17.7	400.0	23.8	-	-	-	-	100.0	-	-	-	-
16	42.6	400.0	1.1	-	-	-	-	100.0	-	-	-	-
17	60.5	364.0	53.6	-	-	-	-	100.0	-	-	-	-
18	11.9	300.0	54.0	-	-	-	-	100.0	-	-	-	-
19	3.4	300.0	54.0	-	-	-	-	100.0	-	-	-	-
20	94.9	340.0	144.0	-	-	-	-	100.0	-	-	-	-
21	18.2	269.0	54.0	-	-	-	-	100.0	-	-	-	-
22	655.3	15.0	1.01	Air, as in chapter 3								
23	524.4	COT: 1440	17.6	-	-	0.58	-	23.45	0.87	66.78	8.32	-
		TIT: 1360		-	-	-	-	-	-	-	-	-
		TIT_{ISO}:1257		-	-	-	-	-	-	-	-	-
24	665.0	603.9	1.04	-	-	0.47	-	19.06	0.88	68.84	10.75	-
25	665.0	100.0	1.01	-	-	0.47	-	19.06	0.88	68.84	10.75	-
26	142.3	551.0	133.9	-	-	-	-	100.0	-	-	-	-
27	104.7	559.0	44.2	-	-	-	-	100.0	-	-	-	-
28	58.9	32.2	0.048	-	-	-	-	100.0	-	-	-	-
Net Power Output				**393.14**		**MW**	**Net Electric Eficiency**				**38.52**	**%**

Resulting T-Q diagram is presented in Figure 7-11. CO_2+steam mixture cooling supplies heat to HP and IP feed-water, so purge heating is carried out partly in the HRSG and partly cooling rinse steam.

Considering that the stream is mainly composed by CO_2 and steam, no safety issues caused by negative relative pressure as air leaking should occur; the only drawback can be a reduced CO_2 purity. Similar results were achieved also in NGCC application. Sub-atmospheric CO_2 stream pressure slightly affects sulphur removal systems in term of power required.

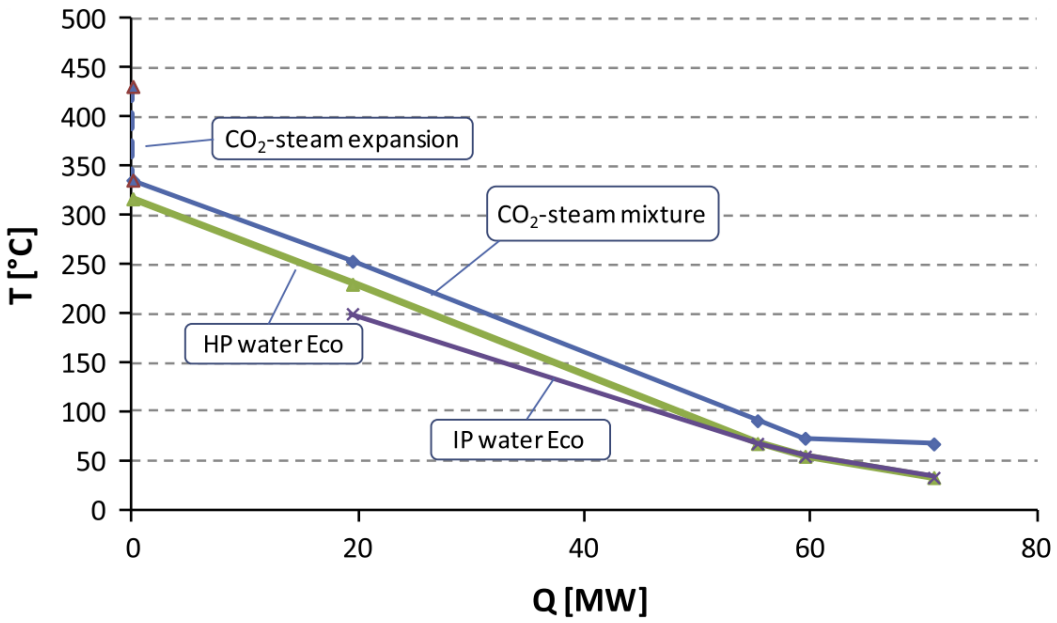

Figure 7-11: CO_2–steam mixture cooling for IGCC with SEWGS; 99% purity and 95% CCR.

7.6.2 $H_2S - CO_2$ SEPARATION

As recommended in [19], H_2S concentration in sequestered CO_2 must be below 200 ppm. In order to remove H_2S from CO_2 rich stream without penalizing both efficiency and environmental performances, an H_2S selective non energy-intensive process must be selected. After a thorough bibliography research, H_2S catalytic combustion has been identified as the most suitable solution. CO_2-H_2S stream pass through a catalytic bed where H_2S is oxidized to SO_2, suitable temperature for oxidation includes from about 190°C to about 480°C, preferably in the range 200-370 °C. Suitable pressure includes between 0.5 bar and about 150 bar. As far as the sub-atmospheric expander is concerned, there is the need to match suitable pressure and temperature ranges (preferably $p > p_{atm}$ and $T > 200$ °C). This issue can be addressed through limited plant layout modifications: the first CO_2 compressor stage can be used to increase the CO_2-H_2S pressure (point 1 in Figure 7-12). Subsequently, the incoming oxygen (point 2 in Figure 7-12) can be extracted after the first stage of the intercooled oxygen compressor at the desired pressure. Achieved hydrogen sulfide conversion is very close to 100%. SO_2 produced is then converted to gypsum in a commercial wet FGD. An alternative solution implies the adoption of Claus-Scott reactors obtaining elemental sulfur; in this case the H_2S catalytic combustion must oxidize one third of the incoming H_2S. The small amount of oxygen required is supplied by the ASU without any significant penalty, the CO_2 stream will result in high purity flow with a little higher O_2 concentration that does not affect the compression. Two different commercially ready applications have almost the same operating conditions of the SEWGS sour case. The first one has been applied to EOR [22]; concentrations and temperature range of the CO_2 stream mixture are perfectly aligned with SEWGS application. Lay out of the process is reported in Figure 7-12 and thermodynamic properties and chemical composition of the relevant streams are shown in Table 7-10.

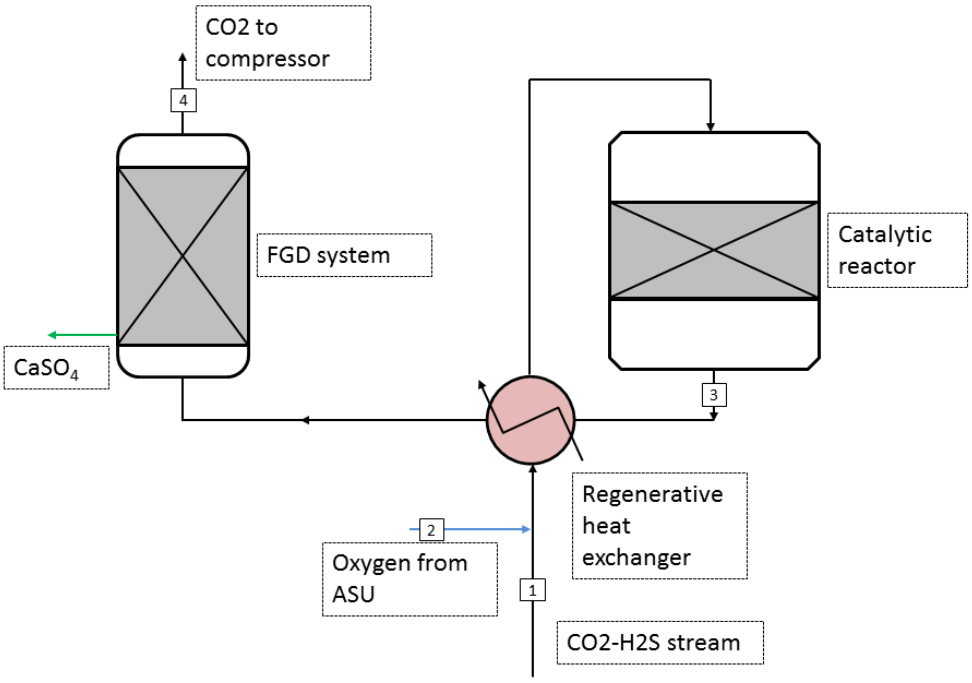

Figure 7-12: catalytic H_2S combustion and SO_2 removal – data refers to Sour SEWGS.

Table 7-10: mass flow rate, pressure, temperature and composition of CO_2 in H_2S separation section. (Numbers refer to Figure 7-12).

Point	G	T	p	Composition, %mol.									
	kg/s	°C	bar	CH_4	CO	CO_2	H_2	H_2O	Ar	N_2	O_2	H_2S	SO_2
1	95.1	30	1.01	-	0.01	93.05	0.89	5.66	-	0.09	-	0.31	-
2	0.4	82.6	4.09	-	-	-	-	-	3.09	1.91	95	-	
3	95.5	200-400	1.01	-	0.01	92.67	0.88	5.94	0.02	0.10	0.08	-	0.30
4	95.1	30	1.01	-	0.01	92.94	0.88	5.96	0.02	0.10	0.08	-	90 ppm
storage	92.6	30	110	-	0.01	98.8	0.94	-	0.02	0.11	0.08	-	90 ppm

The second considered application for H_2S catalytic combustion has been tested and adopted in several geothermal power plants [23]; basically, it can be chosen because SEWGS off-gas results to be similar to geothermal fluids. Compared to the solutions reported in the cited reference applications, an FGD system has been preferred for the SO_2 conversion as it guarantees high efficiency and good availability for the power plant although it introduces higher costs.

Efficiency penalty for this additional separation step of H_2S removal accounts for about 0.2% points on the overall efficiency, thus significantly lower than conventional systems.

Finally, sulfur separation can be achieved through biochemical conversion as described by Paques™ [24]. This advanced solution permits equipment costs reduction of about 50% compared to Claus system although it requires an Acid Gas Enrichment Unit because of the low concentration of sulphur at the inlet.

7.6.3 ASSUMPTIONS

The only new assumption compared to chapter 3 concerns the CO_2-steam expander: the isentropic efficiency can be assumed equal to 92% because of expansion similarity to the last stages of a steam turbine both in terms of working conditions and volume flows (400 m^3/s and 1 bar at the inlet and 780 m^3/s at the outlet). Moreover, the higher exhaust pressure significantly reduces leaving losses, and the CO_2 presence limits moisture formation during expansion with benefits from efficiency and wear point of view. Expander and CO_2 compressor are not connected on the same shaft with advantages from flexibility point of view, but loosing 0.15% points of overall efficiency.

7.6.4 RESULTS

Two different SPECCA values are presented in Table 7-11 as a consequence of the adoption of two difference reference cases: ASC and IGCC. This is because the latter was adopted as base for SEWGS, while the former is the state-of-the-art technology in power plant based on coal. The SPECCA presented in all the figures refers to IGCC reference case.

The influence of the CO_2 avoided and CO_2 purity on plant net electrical efficiency and SPECCA is shown in Figure 7-13. Efficiency significantly decreases with CO_2 avoided and a slope variation can be noted at 93%; this is a consequence of the exponential increase of the purge flow rate. As far as CO_2 purity is concerned, no significant difference can be noted from 98% to 99.5% indicating that the increase of rinse demand from 6.45 kg/s to 19.68 kg/s, is balanced by the lower amount of hydrogen captured together with CO_2 (1.2 MW_{LHV} for 99.5% CO_2 purity vs. 4.8 MW_{LHV} for 98% CO_2 purity); lower purity means that more hydrogen is lost in liquid CO_2.

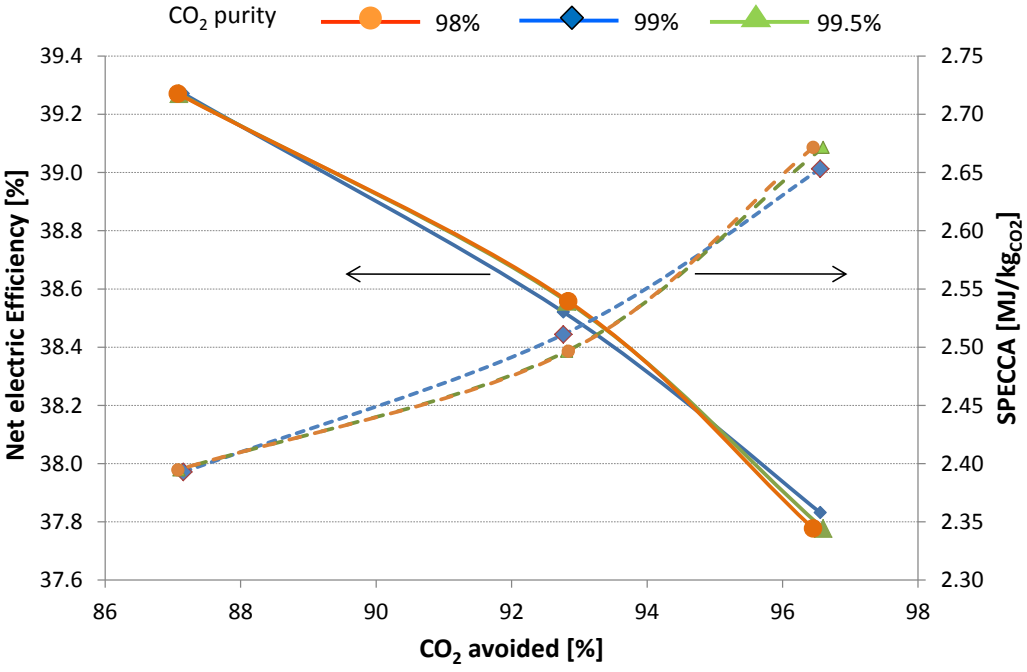

Figure 7-13: net electric efficiency (solid lines) and SPECCA (dotted lines) for different SEWGS CCR.

Expander outlet pressure is another parameter to be optimized both in term of efficiency and economic point of view. The optimization was carried out for 99% of CO_2 purity and CO_2 capture ratio of 95% (case B2 according to definition in Table 7-3). Expander outlet pressure is in the range of 0.5 bara and 1.1 bara; a minimum temperature of the CO_2-steam at expander outlet is required in order to supply heat for scrubber and water pre-heating.

The highest efficiency (and lower SPECCA) is achieved for expander outlet pressure of 0.5 bara. The optimal condition is a compromise between recovered condensation heat by the expander and higher CO_2 compression work. It must be outlined that for higher outlet pressure, expander and CO_2 compression work decrease together with investment costs.

When the number of vessels is reduced from 54 to 45 (5 SEWGS trains instead of 6), the amount of steam usage in SEWGS rises significantly with penalties from efficiency point of view (no cases with 95% and 98% CCR could be carried out because of too large steam usage in the SEWGS). Results for SEWGS with 99% CO_2 purity and 90% CCR (see Figure 7-14) show that the net electric efficiency reduces of 0.5% points and SPECCA increases of 0.3 MJ/kg_{CO2}, that corresponds to a relative rise of 10%. Advantages of a lower number of vessel can be outlined only by a detailed economic assessment (see chapter 9 of this work), since investment costs and sorbent replacement can be reduced.

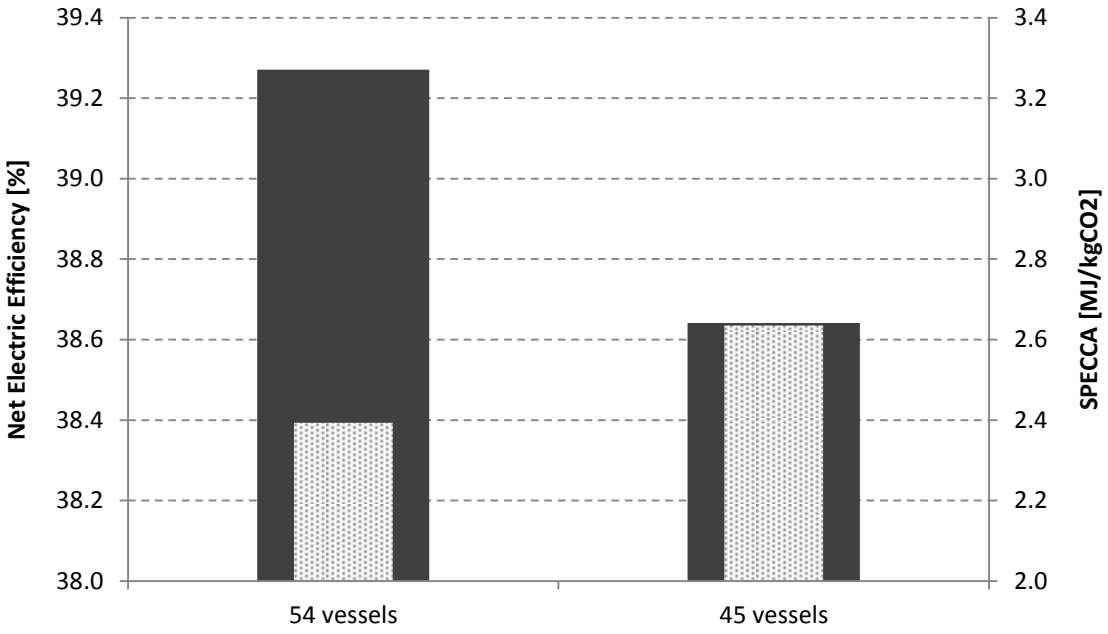

Figure 7-14: net electric efficiency (background bars) and SPECCA (front bars) for different SEWGS number of vessels for 99% CO_2 purity and 90% CCR.

The performance of the SEWGS cases with 99% CO_2 purity together with reference IGCC with and without capture is summarized in Table 7-11.

Table 7-11: IGCC with carbon capture by SEWGS – Simulation results for different cases.

	IGCC	SELEXOL	SEWGS			
Trains			54	54	54	45
CCR/CO_2 purity (%)			90/99	95/99	98/99	90/99
Gas Turbine, [MW]	290.2	305.0	305.2	304.6	304.1	306.11
Expanders, [MW]	8.5	10.2	49.0	52.6	56.1	54.30
Steam Cycle Gross Power, [MW]	197.7	179.2	145.6	137.9	129.2	133.7
Steam Cycle auxiliaries, [MW]	-3.1	-3.21	-2.8	-2.6	-2.4	-2.5
Coal and ash handling [MW]	-2.2	-2.53	-2.5	-2.5	-2.5	-2.4
ASU + O_2 compression [MW]	-22.7	-26.6	-26.0	-26.0	-26.0	-26.0
N_2 comp. for fuel dilution, [MW]	-32.1	-24.0	-15.4	-15.4	-15.4	-15.4
N_2 compression for LH., [MW]	-9.2	-11.1	-10.5	-10.5	-10.5	-10.5
CO_2 compressor, [MW]	--	-22.9	-35.6	-37.6	-38.9	-35.7
Aux. for heat rejection, [MW]	-2.5	-2.53	-2.8	-2.9	-2.9	-2.8
BOP, [MW]	-2.2	-21.8	-4.2	-4.4	-4.5	-4.4
Net Power Output, [MW]	**422.4**	**379.6**	**400.0**	**393.1**	**386.2**	**394.3**
Thermal Power Input$_{LHV}$, [MW]	896.5	1053.5	1018.6	1020.6	1020.9	1020.3
Net Electric Efficiency$_{LHV}$, [%]	**47.12**	**36.03**	**39.27**	**38.52**	**37.83**	**38.64**
Net Electric Efficiency$_{HHV}$, [%]	45.21	34.58	37.68	36.96	36.30	37.08
Efficiency penalty, [%points]	--	-11.1	-7.8	-8.6	-9.3	-8.5
Cold gas efficiency, [%]	81.8	73.7	74.3	74.1	73.8	74.2
Emissions, [g_{CO2}/kWh_{el}]	732	98.5	94.0	53.0	25.2	95.8
CO_2 avoided, [%]	--	86.5	87.2	92.8	96.6	86.9
SPECCA (ASC), (MJ_{LHV}/kg_{CO2})	--	3.02	1.79	1.93	2.09	2.01
SPECCA (IGCC), (MJ_{LHV}/kg_{CO2})	--	**3.71**	**2.39**	**2.51**	**2.65**	**2.63**

All SEWGS cases have the same thermal power input because of the similar hydrogen rich stream produced, and the fixed mass flow at turbine outlet. For this reason, the net power output and the efficiency difference among all cases depends on heat management and auxiliaries power consumption.

Gas turbine power output is significantly higher than reference gas turbine designed for natural gas application which has a net power output of 276 MW. This is because decarbonized fuel has lower heating value leading to reduced amount of air compression work. For this reason, the installation of a properly sized generator must be taken into account. The higher GT power output of SEWGS than IGCC is because of the steam content in the fuel; steam added and not converted in the WGSR goes directly to the GT, while in IGCC it is condensed before the AGR section. Expanders power output increases with CCR because of the higher mass flow rate of the CO_2-steam stream. This increase is partly balanced by the higher CO_2 compression work.

Three different expanders are adopted in the plant: the first is common to the reference IGCC and expands air from the GT to the ASU, about 10 MW, the second for syngas expansion upstream SEWGS of about 20 MW (this expander allows to reduce the amount of rinse steam for SEWGS) and the last is CO_2+steam expander which produces from 19 to 26 MW. The CO_2+steam expander partly balance the lower steam turbine gross power output expanding the

steam bled from the steam turbine. It must be pointed out that the outlet pressure is 0.5 bara, which is significantly higher than that of HRSC condenser.

SEWGS efficiencies are in the range of 37.8% and 39.3% with a CO_2 avoided in the range of 96.6% and 87.2%. SPECCA increases with CCR because of higher (i) steam usage in SEWGS and (ii) CO_2 compression work moves from 2.4 MJ/kg_{CO2} to 2.6 MJ/kg_{CO2}.

As term of comparison, reference IGCC with CO_2 capture, Selexol, has a net electric efficiency of 36.0% with a CO_2 avoidance of 87% and SPECCA of 3.7 MJ_{LHV}/kg_{CO2}, which is about 30% higher than SEWGS cases. ASC efficiency penalties are even higher as shown in the final table of chapter 3.

7.6.5 *Advanced solution: Sorbent Beta*

The application of *Sorbent Beta* to SEWGS process is discussed in this section. As abovementioned *Sorbent Beta* has an average improved capacity of 100% compared to *Sorbent Alfa* at feed SEWGS conditions (CO_2 partial pressure equal to 6 bara).

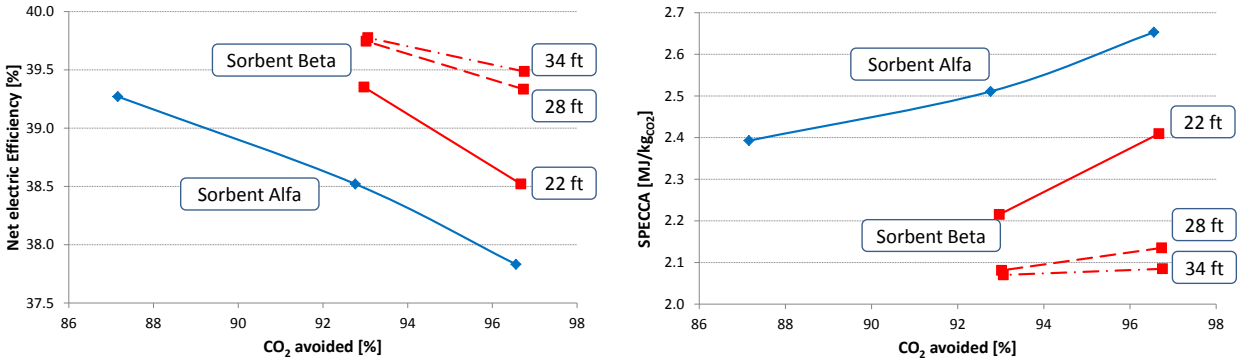

Figure 7-15: net electric efficiency and SPECCA for *Sorbent Alfa* and different vessel length with *Sorbent Beta.*

Results (see Figure 7-15) show that improved sorbent capacity can reduce efficiency penalty up to 1.2% points. Increasing sorbent volume has a significant impact on electric efficiency (about 0.4% points at 95% CCR and 0.8% points at 98% CCR) increasing the bed length from 22ft to 28ft, while the effect is negligible moving from 28ft to 34ft as a consequence of the limited variation of purge flow. Concerning SPECCA, the adoption of an improved sorbent leads to specific energy consumption for CO_2 avoided below 2.1 MJ/kg_{CO2}.

Table 7-12: performances of *Sorbent Beta* for different vessel volumes and CCR.

CCR [%]	95			98		
Vessel lenght [ft/m]	22/6.7	28/8.5	34/10.4	22/6.7	28/8.5	34/10.4
Gas Turbine, [MW]	304.4	302.6	300.7	304.2	302.8	304.2
Expanders, [MW]	49.1	45.4	45.0	53.8	47.3	45.6
Steam Cycle Gross Power, [MW]	149.8	157.7	158.7	138.4	153.5	156.5
Steam Cycle auxiliaries, [MW]	-2.8	-2.9	-3.0	-2.5	-2.9	-3.0
Coal and ash handling [MW]	-2.5	-2.4	-2.4	-2.5	-2.5	-2.5
ASU + O_2 compression [MW]	-26.0	-25.9	-25.8	-26.0	-26.0	-26.0
N_2 comp. for fuel dilution, [MW]	-15.4	-15.4	-15.3	-15.4	-15.4	-15.4
N_2 compression for LH., [MW]	-10.5	-10.5	-10.4	-10.5	-10.5	-10.5
CO_2 compressor, [MW]	-37.6	-37.5	-37.4	-38.9	-38.8	-38.9
Aux. for heat rejection, [MW]	-2.7	-2.7	-2.7	-2.7	-2.7	-2.7
BOP, [MW]	-4.3	-4.1	-4.1	-4.4	-4.2	-4.1
Net Power Output, [MW]	**401.5**	**404.2**	**403.3**	**393.3**	**400.7**	**403.2**
Thermal Power Input$_{LHV}$, [MW]	1020.3	1017.0	1013.9	1021.1	1018.8	1021.1
Net Electric Efficiency$_{LHV}$, [%]	**39.35**	**39.75**	**39.78**	**38.52**	**39.33**	**39.49**
Net Electric Efficiency$_{HHV}$, [%]	37.76	38.14	38.17	36.96	37.74	37.89
Efficiency penalty, [%points]	-7.77	-7.37	-7.34	-8.60	-7.78	-7.63
Cold gas efficiency, [%]	73.2	73.2	73.2	73.2	73.2	73.2
Emissions, [g_{CO2}/kWh_{el}]	51.5	51.1	50.8	24.4	23.9	23.8
CO_2 avoided, [%]	**93.0**	**93.0**	**93.1**	**96.7**	**96.7**	**96.8**
SPECCA (ASC), (MJ_{LHV}/kg_{CO2})	1.65	1.53	1.52	1.86	1.60	1.55
SPECCA (IGCC), (MJ_{LHV}/kg_{CO2})	**2.22**	**2.08**	**2.07**	**2.41**	**2.14**	**2.08**

Power balances, summarized in Table 7-12, show that CCR and sorbent volume affect steam turbine and expanders power output, while other parameters are almost constant.

Number of vessels and rinse flow reduction rise the steam cycle power output for 90% and 95% CCR with significant efficiency advantages. Simultaneously, expander power output and CO_2 compressor consumption reduce, leading to a positive balance. At 98% CCR, the sum of expander and HRSG power output is equal between 54 and 72 vessels; hence the net electric efficiency is constant.

Compared to *Sorbent Alfa*, the adoption of an improved sorbent capacity reduces efficiency penalty up to 0.8% points, leading to a SPECCA of 2.1 MJ/kg_{CO2} (reference cases were well above 3 MJ/kg_{CO2}) and allows adopting different process configuration with thermodynamic and economic advantages.

As a term of comparison, the liquefied CO_2 captured accounts for about 4% point of the overall exergy at system inlet. The remaining exergy losses of capture section are about 3.5% meaning that SEWGS process is very efficient and adds few penalty points.

7.6.6 CONCLUSIONS

SEWGS is a promising CO_2 capture process for pre-combustion technology. In particular, SEWGS stands out in coal based plants, since experimental results showed that sorbent simultaneously captures H_2S and CO_2 with thermodynamic advantages (no thermal swing) and

equipment savings. Down-stream process to separate CO_2 and H_2S is required since co-capture option was not considered. After presenting thermodynamic performances of the reference cases based on dry-feed Shell gasifier and pulverized coal plants, optimal SEWGS working conditions were evaluated in order to minimize efficiency penalties and CO_2 emissions. The first sorbent considered in SEWGS, named *Sorbent Alfa*, achieved a net electric efficiency between 38% and 39% with CO_2 avoidance between 96% and 86% respectively. The resulting SPECCA is about 2.5 MJ/kg_{CO2}, which is considerable lower than reference IGCC with capture via Selexol (3.7 MJ/kg_{CO2}) and ASC with amine scrubbing (4.2 MJ/kg_{CO2}). Results showed that CO_2 purity (investigated from 98% to 99%) has limited impact on efficiency penalty and SPECCA. Thus, 99% can be suggested as optimal working conditions because of advantages during transport and storage. The adoption of a new sorbent with 100% higher cyclic capacity than *Sorbent Alfa*, named *Sorbent Beta,* allowed adopting different SEWGS configurations reducing the number of vessels from 54 to 45 as well as the steam usage. SPECCA can be reduced down to 2.0 MJ/kg_{CO2}. The optimum Carbon Capture Ratio seems to be in the range of 90% to 95%, however only the economic assessment carried out in chapter 9 will confirm it assessing the cost of CO_2 avoided.

7.7 BLAST FURNACES PLANT

The SEWGS integration in steel plants is a CO_2 capture application to an industrial process. Therefore, several differences arise if compared with previous cases on natural gas and coal cases. This section of chapter 7 is organized in order to make a comprehensive analysis of the considered industrial application. In paragraph 7.7.1 an introduction on steel plant and carbon capture in steelworks is presented. In paragraph 7.7.2 the reference cases with and without carbon capture are defined; in paragraph 7.7.5 SEWGS is described together with its integration in the overall plant; in section 7.7.6 new assumptions are reported whilst sections 7.7.7 and 7.7.8 are dedicated to results and conclusions.

7.7.1 INTRODUCTION ON STEEL PLANT

Steel industry is the most energy-intensive manufacturing sector accounting for 10-15% of total industrial energy consumption [25]. Being based on fossil fuels and electricity utilization, it accounts for large anthropogenic CO_2 emission, estimated at 1500-1600 MtonneCO_2 year. During last 10 years, steel industry has experienced a large production increase almost doubling the year yield reaching about 1400 Mtonne; developing countries like China, India and Brazil played the main role in this sharp growth. Assuming that the steel demand will continuously rise in the next years, carbon mitigation has to be applied to steel industry as well as power plant.

Specific CO_2 emission depends on several parameters whose most important are: type of steel production process, energy efficiency of the considered process, country base electric energy system and type of fuel adopted for iron conversion. World steel production is based on two main processes: blast furnace and electric arc furnace. The first accounts for around 60% of the market while the second provides around 35%; the remaining 5% is based on alternative processes.

As far as integrated steelworks are concerned, the energy interdependency of the different process is complex; example of the input and output flows is shown in Figure 7-16. Therefore, it results that several CO_2 capture solutions can be investigated and applied with different levels of integration with the plant. Early CO_2 capture opportunities are based on blast furnace redesign such as i) CO-rich top gas recycling in the furnace and ii) direct reduction of iron ore through hydrogen. Both these processes aims at reducing the CO_2 produced directly in the iron making process. Another option, which is investigated in this section, is to mitigate CO_2 emissions by applying carbon capture to the bottoming power cycle which is typically included in integrated steelworks. This solution would allow reducing the CO_2 emission to almost half of the base case without requiring changes in the steel production process. Moreover it could better harness the know-how being developed in the power production area.

Blast furnace steel plant is characterized by the production of process-gases that can be recovered and adopted as energy source both for the plant demand and for grid power production. As shown in Figure 7-16, the enriched gas mixture comes from three different processes: i) the blast furnace itself, which is the main gas producer, ii) the coke oven plant and iii) the basic oxygen furnace. Power plants play an important role in integrated steelworks as they consume the excess process gases and provide the necessary steam and power to all the key processes. The gas mixture burnt in the power plant accounts for about 50% of the total gas production.

Historically, blast furnace steel plants have been integrated with conventional steam cycle power plants where the steam generated from burning off-gas was expanded in a steam turbine. The steam generator in such a configuration is generally fed also with other fuels like natural gas or oil; internal steam demand is met with turbine bleedings. The relatively simple arrangement can achieve a high level of availability and is designed to use process gases with low calorific value, mainly BF gas. Recently, this plant layout has been discarded in favour of a more efficient combined cycle.

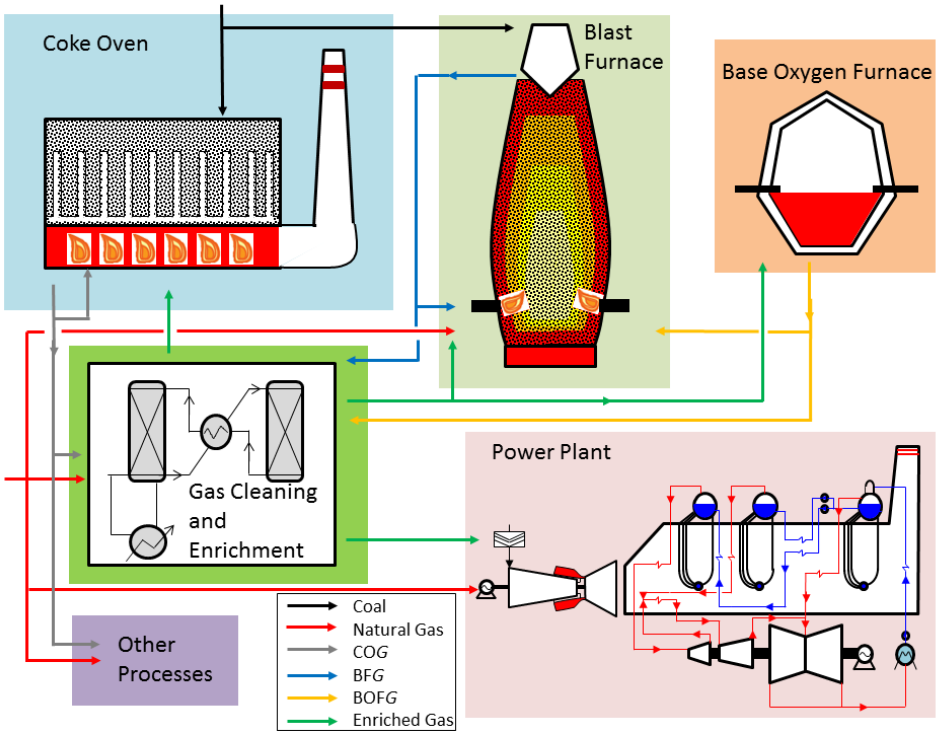

Figure 7-16: Overall layout of an integrated steel plant with the main gas streams exchanged.

7.7.2 Reference Cases With And Without Capture For Steelworks Application

In order to evaluate SEWGS in steel plants, two reference cases with and without capture have been developed. Reference cases are based on pure blast furnace feeding and combined cycle performances derived from data of commercial plants. In order to simplify the final comparison and to avoid misleading interpretations of the performance of the different configurations assessed, no blending with natural gas is considered before combustion. It has been assumed to adopt one GT and one HRSG as the steel-off gas production cannot feed two large size combined plants. BF gas cleaning is carried out inside the steel plant battery limit where the gas is available at ambient conditions. The considered GT is a generic F class with no TIT de-rating due to the low LHV of the fuel; this hypothesis, even though significant for performances calculations, is applied to all the considered plant, with and without capture, in order not to affect the comparison.

7.7.3 NGCC no capture

A commercial plant for blast furnace application based on EBTF [19] was modelled (named NGCC REF). Gas turbine is fuelled with steel mill off-gas. Compared to pure NG fuelled plant, a significant amount of power is required for the steel-off gas compression as gas is available at ambient pressure; no further significant penalties have been applied.

Steel mill off-gas mass flow and composition have been derived from a large, state-of–the-art integrated steel plant. It has been supposed to keep a constant steel mill off-gas production. HRSG and steam turbine data refer to chapter 3 assumptions. Stack temperature has been set at 80°C. The condensing pressure is set at 0.048 bar, assuming the use of a cooling tower. The

resulting net power output is 319.2 MW with a net electric efficiency of 52.3% and specific CO_2 emission of 1338 g/kWh.

7.7.4 NGCC WITH MEA POST COMBUSTION CAPTURE

As far as carbon capture is concerned, a reference case with post combustion capture was developed (named *MEA CAP*): CO_2 capture is based on amine technology which represents the commercial ready technology for carbon capture. Ancillary consumptions for the absorption cycle have been specifically calculated and optimized by varying the L/G ratio: the high CO_2 content in the exhaust gas slightly reduces the specific heat duty for MEA regeneration than fossil fuel plants. The CO_2 capture section is simulated as described in chapter 3. The resulting MEA-solvent regeneration energy is about 3.5 MJ/kg_{CO2} which is also consistent with recent work on post-combustion capture from steel mill [26].

It has been found that, because of the large CO_2 mass flow compared to the heating value, the steam produced in the HRSG does not allow reaching high carbon capture values even with the adoption of a back pressure turbine configuration, where all the steam expanded is condensed in the MEA stripper reboiler. Therefore, part of exhaust gases after the HRSG are directly sent to the stack, bypassing the CO_2 capture section. Size (or number) of the absorber of the MEA plant is hence reduced with respect to a case where all the flue gases are treated. With the considered bypass configuration, 90% of carbon is removed from 45% of the total flue gases, the remaining 55% being directly sent to the stack. Although other configurations have been considered where the entire flue gases are treated, the selected configuration seems to be the best compromise between performances and capital costs. The resulting net power output is 235.9 MW with a net electric efficiency of 38.7% and CO_2 emissions of 870.4 g/kWh.

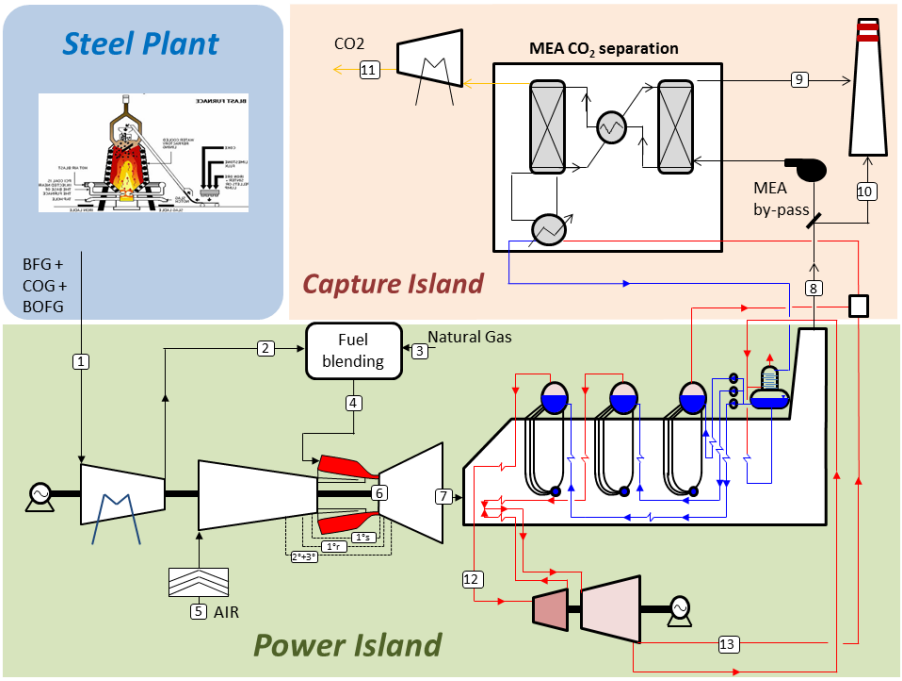

Figure 7-17: plant layout of the reference case with CO2 capture by MEA.

7.7.5 SEWGS PLANT LAYOUT

Two different plant layouts have been investigated:

- SEWGS with intercooled gas compression and saturator (SEWGS SAT), shown in Figure 7-18: steel mill off-gas is compressed with intercooling stages with benefits on the compression work; steam bleedings for shift are substantially reduced adopting a saturator whose water is heated by recovering heat from intercooled compressor, CO_2 cooling and off-gas exiting the compressor. The main drawbacks of this configuration are represented by: i) the temperature swing between the gas compressor and the shift and ii) the stream exiting the SEWGS is not expanded as in natural gas and coal cases above mentioned in order to increase the heat to the saturator water. High pressure steam is produced by cooling the hydrogen rich syngas exiting the SEWGS and the rinse steam withdrawn from the hot RH.
- SEWGS with intercooler compressor and expander (SEWGS EXP): steel mill off-gas is compressed in an intercooled compressor modifying the last stage pressure ratio in order to make the gas available at 320°C, suitable for the high temperature shift. The CO_2-steam mixture exiting the SEWGS is expanded till 0.5 bar and cooled by producing IP and LP steam. HP steam is produced in a dedicated section by cooling: i) the syngas leaving the WGS, ii) the H_2-rich stream exiting the SEWGS and iii) the rinse steam withdrawn from the hot RH. This configuration allows a better harness of the sensible energy inside the capture island but requires a higher steam bleed for the WGS process.

All the SEWGS cases are calculated with almost atmospheric purge pressure and 95% of CO_2 recovery from the total amount adsorbed in the bed.

7.7.6 EXTRA ASSUMPTIONS

The SEWGS application to steel-mill requires extra assumptions compared to the natural gas or coal case and generally presented in chapter 3. The new assumptions, reported in Table 7-13, concern the steel off-gas composition and the intercooled compressor of the blast furnace gas.

Table 7-13: assumptions for SEWGS integration in steelworks factory.

Rich Blast Furnace Gas				
(BFG + COG)	CH_4	2.10 %	C_2H_4	0.20 %
	CO	21.29 %	C_2H_6	0.07 %
	CO_2	19.57 %	H_2	7.22 %
	C_2H_2	0.01 %	N_2	49.53 %
	O_2	0.02 %		
LHV		3.386 MJ/kg		
Steel gas compressor				
Compressor ratio		28		
Number of intercoolers		2		
Organic efficiency		99.8 %		

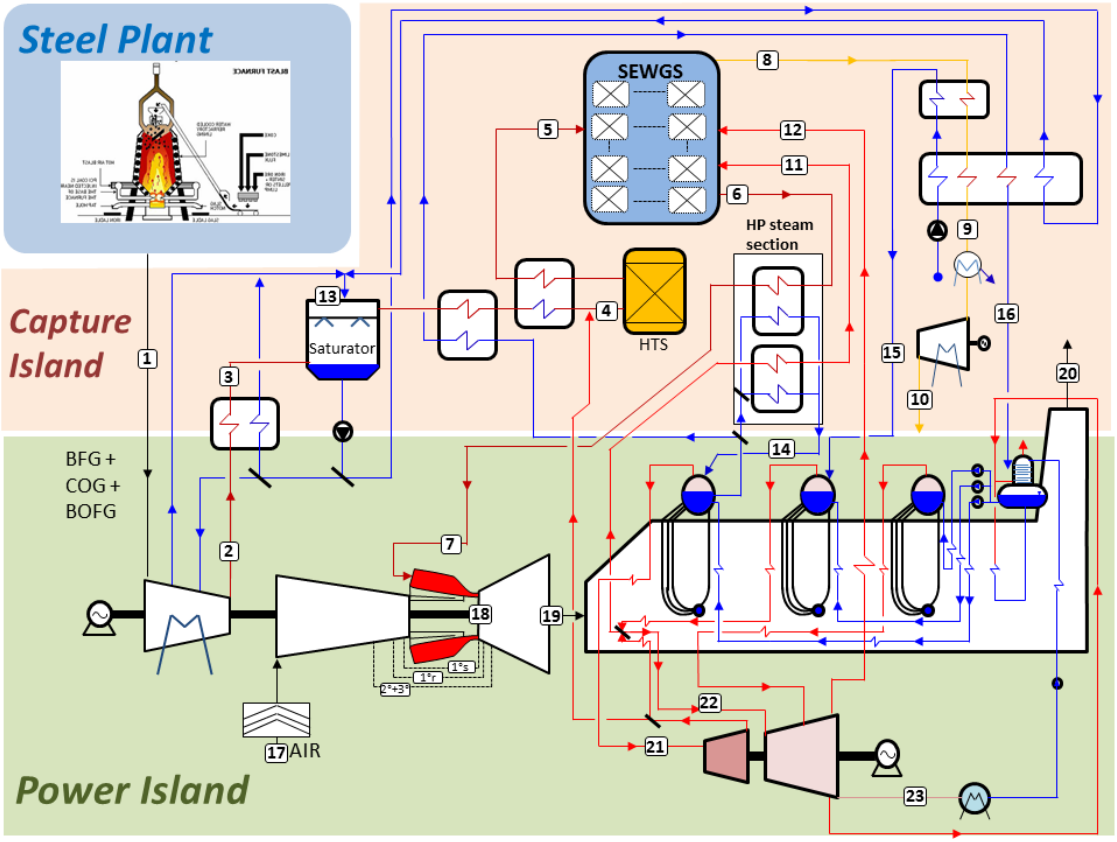

Figure 7-18: plant layout of SEWGS SAT configuration, with intercooled compressor and saturator.

7.7.7 RESULTS

The results of the investigated plants are shown in Table 7-14. The reference case without capture has a net electric efficiency of 52.3% and specific emissions of 1338 g_{CO2}/kWh_{el} which is almost twice the specific emission of an USC plant. This is due to the high CO_2 content of the fuel gas. The post-combustion capture case is largely affected by steam bleeding for solvent amine regeneration leading to about 50% reduction of steam turbine power output. The resulting net electric efficiency is 38.7% with a limited penalization considering the low value of the fuel gas, but with a low CO_2 avoided of only 35%. This is also consistent with the results presented in [26] where the CO_2 capture ratio is below 50%.

The SEWGS case with Sorbent Alpha achieves a good trade-off between thermodynamic and capture performances. This is stressed by the SPECCA which is considerably below the post-combustion case (3 MJ/kg_{CO2} of SEWGS vs. 5 MJ/kg_{CO2} of MEA). The adoption of *Sorbent Beta*, which has twice the capacity of *Sorbent Alfa*, sharply increases the efficiency with a gain of about four percentage points at almost constant carbon avoidance; a higher sorbent capacity reduces the SEWGS steam demand increasing the steam cycle power output of 27 MW. When saturator is adopted the calculated efficiency is 39.3% whilst with the expander it slightly increases to 39.9%. Accordingly, the SPECCA value lowers to 2.0 and 1.9 MJ/kg_{CO2} for *SEWGS SAT* and *SEWGS EXP* respectively. The difference between the two SEWGS layouts is set by: i) the steam cycle, whose power output is higher when the saturator is adopted, ii) the expander, which adds 12 MW to the power production, and iii) the intercooled compressor which increases by 2 MW more when the saturator is not used. In addition to the better efficiency, equipment

savings may also be anticipated for the SEWGS EXP case, due to the lack of the saturator and the reduced heat transfer surface.

Table 7-14: Performances of all the considered cases; moving from left to right: NGCC without capture, NGCC with postcombustion capture by MEA, SEWGS with saturator and *Sorbent Alpha*, SEWGS with saturator and *Sorbent Beta*, SEWGS with expander and *Sorbent Beta*.

		NGCC ref	MEA	SEWGS SAT alpha	SEWGS SAT beta	SEWGS EXP beta
Gas input	[kg/s]	180	180	180	180	180
Thermal input LHV	$[MW]_{LHV}$	609.5	609.5	609.5	609.5	609.5
POWER PRODUCTION						
Gas Turbine net power	$[MW]_{el}$	199.0	199.0	192.1	189.1	187.3
Steam Cycle gross power	$[MW]_{el}$	123.3	66.6	62.6	90.3	83.4
Expander	$[MW]_{el}$	--	--	--	--	12.6
CONSUMPTIONS						
HRSC pumps	$[MW]_{el}$	1.5	1.5	2.1	2.2	1.7
CO_2 compressor	$[MW]_{el}$	--	19.5	36.0	36.0	37.0
MEA auxiliaries	$[MW]_{el}$	--	8.5	--	--	--
Heat Rejections	$[MW]_{el}$	1.6	0.2	1.5	1.4	1.3
BOP	$[MW]_{el}$	--	--	0.22	0.18	0.05
OVERALL BALANCES						
Net Power Output	$[MW]_{el}$	319.2	235.9	215.0	239.6	242.9
$\eta_{electric}$	**[%]**	**52.3**	**38.7**	**35.3**	**39.3**	**39.9**
$\Delta\eta$	[%points]	--	-13.7	-17.1	-13.0	-12.5
CO_2 emissions	[g/kWh]	1338.0	870.4	215.6	193.4	190.8
CO_2Avoided	[%]	--	34.9	83.9	85.5	85.7
SPECCA	**$[MJ/kg_{CO2}]$**	**--**	**5.2**	**3.0**	**2.0**	**1.9**

7.7.8 CONCLUSIONS: SEWGS IN STEEL MILL PLANT

Different plant layouts with and without carbon capture were considered and performance of SEWGS-based plants was compared to post-combustion carbon capture with MEA one. It was found that SEWGS reaches good performances with around 85% CO_2 avoidance. On the other hand, MEA post combustion configuration does not seem a valuable solution to significantly decrease the CO_2 emissions, due to a carbon capture rate lower than 50%. Among the different SEWGS layouts investigated, the adoption of an intercooled compressor and a CO_2-steam expander featured the best performances.

REFERENCES

[1] **Carbon Capture Project.** *http://www.co2captureproject.org/ccp2_capture.html.* [Online]

[2] Cachet FP6 Project. *http://www.cachetco2.eu/.* [Online]

[3] Caesar FP7 Project. *http://caesar.ecn.nl.* [Online] 2008.

[4] **Allam T, Chiang R, Hufton J, Middleton P, Weist E, White V.** developmnent of sorption Enhanced water gas shift process. [aut. libro] Thomas D and Benson S. *Carbon Dioxide Capture for Storage in Deep Geologic Formations –Results from the CO2 Capture Project.* Oxford : Elsevier Editor, 2005.

[5] **Wright A, White V, Hufton G, Selow E, Hinderink P.** Reduction in the cost of pre-combustion CO2 capture through. 2009, Vol. 1.

[6] **Van Selow E, Cobden P, Van den Brink R, Hufton J, Wright A.** Performance of sorption-enhanced water-gas shift as a pre-combustion CO2 capture technology. 2009, Vol. 1.

[7] **van Selow ER, Cobden PD, Wright AD, van Der Brink RW, Jansen D.** Improved sorbent for the sorption-enhanced water-gas shift process. *Energy Porcedia.* 2011. Vol. 4, 1090-1095.

[8] **Van Selow, E.R., et al.** Carbon Capture by Sorption-Enhanced-Water-Gas-Shift Reaction Process using Hydrotalcite-Based Material. s.l. : Ind.Eng.Chem.Res, 2009. Vol. 48, 9, p. 4184-4193.

[9] **van Dijk E, Walspurger S, Cobden P, van den Brink R.** Testing of hydrotalcite based sorbents for CO2 and H2S capture for use in sorption enhanced water gas shift. *Proceeding of GHGT-10 International conference , Amsterdam 2010.*

[10] **Wright, Andrew.** *D2.3 - public report/ peer reviewed publication on reactor modeling.* 2012.

[11] **Kumar, R., et al.** A versatile process simulator for adsorptive separations. *Chem.Eng.Sci.* 1994. Vol. 18. 3115-25.

[12] **Manzolini G, Macchi E, Binotti M, Gazzani M.** Integration of SEWGS for carbon capture in natural gas combined cycle. Part A: Thermodynamic performances;. *International Journal of Green-house Gas Control.* 2011. Vol. 5, 2, pag 200-213.

[13] **Gazzani M, Macchi E, Manzolini G.** CAESAR:SEWGS integration into an IGCC plant. *Energy Procedia* . 2011. Vol. 4, 1096-1103.

[14] **Manzolini G, Macchi E, Binotti M, Gazzani M.** Integration of SEWGS for carbon capture in Natural Gas Combined Cycle. Part B: Reference case comparison. *International Journal of Greenhouse Gas Control.* 2011. Vol. 5, 2, Pag 214-225.

[15] **Abbott et al.** *Process for the production of Hydrocarbons. US 7,087,652 B2* United States, 8 August 2006.

[16] **Johnson Mattey.** *http://www.jmcatalysts.com/ptd/site.asp?siteid=694&pageid=705.* [Online] Johnson Mattey.

[17] **Abbott et al.** *Production of hydrocarbons by steam reforming and fisher-tropsch reaction. US 7,323,497 B2* USA, 29 January 2008.

[18] **Dean Jr, Sheldon W.** Estimating Metal Dusting Attack on Stainless Steel Alloys in Syngas Environments. *Corrosion 2001.* 2001, 01384.

[19] **European Benchmark Task Force.** European best practice guide for assessment of CO2 capture technologies. 2011. Vol. http://www.energia.polimi.it/news/D%204_9%20best%20practice%20guide.pdf.

[20] **Romano, M C, Chiesa, P e Lozza, G.** Pre-combustion CO2 capture from natural gas power plants, with ATR and MDEA processes. *International Journal of Greenhouse Gas Control.* s.l. : Elsevier, 2010. 4, p. 785-797. doi:10.1016/j.ijggc.2010.04.015.

[21] **Santini Paolo.** Modular Geothermal Plants in Italy: Technical Characteristics and Operation results. *Proceedings of World Geothermal conference.* Antalya, Turkey, 24-29 April 2005.

[22] **Madgavakar et Al.** *Selective combusting of hydrogen sulfide in carbon dioxide injection gas. 4,389,912* United States, 10 may 1983.

[23] **Enel SPA, Roma.** *Processo per la rimozione dell'idrogeno solforato da gas non condensabili di un impianto geotermico. FI/012190/IN* Italy.

[24] **http://www.paques.nl/.**

[25] **IPCC.** *Carbon Dioxide Capture and Storage.* s.l. : Cambridge Unversity Press, 2005.

[26] **Arasto, A, et al.** Post-combustion capture of CO2 at an integrated steel mill - Part I: Technical concept analysis. *International Journal of Greenhouse Gas Control.* 2012.

[27] **Franco F et al.,.** Common framework and test cases for transparent and comparable techno-economic evaluations of CO2 capture technologies - the work of the European Benchmark task Force. *Proceedings of GHGT-10 international conference, Amsterdam 2010.*

[28] **Manzolini G, Macchi E, Binotti M, Gazzani M.** Integration of SEWGS for carbon capture in natural gas combined cycle. Part A: Thermodynamic performances;. *International Journal of Green-house Gas Control.* 2011. Vol. 5, 2, pag 200-213.

[29] **Franco F, Anantharaman R, Bolland O, Booth N, et al.** Common framework and test cases for transparent and comparable techno-economic evaluations of CO2 capture technologies - the work of the European Benchmark task Force. *Proceedings of GHGT-10 international conference, Amsterdam 2010.*

[30] **Politecnico di Milano.** Software presentation: GS (Gas-Steam Cyckes). *http://www.gecos.polimi.it/software/gs.html.* [Online] 2009.

[31] **Consonni S, Lozza G, Macchi E, Chiesa P, Bombarda P.** Gas turbine-based cycles for power generation. Part A: calculation model. 1991.

[32] **Lozza, G.** Bottoming steam cycles for combined gas-steam power plants: a theoretical estimation of steam turbine performance and cycle analysis. New Orleans, USA : ASME Cogen-Turbo, 1990.

[33] **Manzolini G, Dijkstra JW, Macchi E, Jansen D.** Technical Economic Evaluation of a system for electricity production with CO2 capture using membrane reformer with permeate side combustion. 2006.

[34] **Chiesa P, Macchi E.** A thermodynamic analysis of different options to break 60% electric efficiency in combined cycle power plants. 2004, Vol. 126, 770-785.

[35] **Aspentech Documentation.** Aspen Physical Property System. *V 7.2.*

[36] **Gross, J e Sadowski, G.** *Perturbed-Chain SAFT: An Equation of State Based on a Perturbation Theory for Chain Molecules.* s.l. : Res. Ind. Eng. Chem. American Chemical Society, 18 01 2001. Vol. 40, 4, p. 1244-1260. 10.1021/ie0003887.

[37] **Phiong HS, Cooper C, Adesina A, Lucien FP.** Kinetic Modelling of the catalytic hydrogeneation of CO2-expanded alfa-methylstyrene. s.l. : Journal of Supercritical Fluids, 2008. Vol. 46 (40-46). doi:10.1016/j.supflu.2008.03.006.

[38] **Zhang H, Liu Z, Han B.** Critical points and phase behavior of toluene-CO2 and toluene-H2-CO2 mixture in CO2-rich region. s.l. : Journal of Supercritical Fluids, 2000. Vol. 18 (185-192).

[39] **Campanari S, Chiesa P, Manzolini G.** CO2 capture from combined cycles integrated with Molten carbonate Fuel Cells. s.l. : International Journal of Greenhouse Gas Control, 2010. Vol. 4, 3. 441-451.

[40] **Chiesa P, Campanari S, Manzolini G.** CO2 cryogenic separation from combined cycle integrated with molten carbonate fuel cells. s.l. : Internatonal Journal of Hydrogen Energy . Vol. 2011, In press. DOI: 10.1016/j.ijhydene.2010.09.068.

8 HYDROGEN SEPARATION MEMBRANES INTEGRATION IN CO_2 CAPTURE PLANTS

Nomenclature and Acronyms

CACHET: CArbon Capture and Hydrogen production with membranes
CCR: Carbon Capture Ratio
CCS: Carbon Capture and Storage
COT: Combustor Outlet Temperature
E: CO_2 specific emission rate
HGD: Hot Gas Desulgurization
HGCU: Hot Gas Clean Up
HP: High Pressure
HRF: Hydrogen Recovery Factor
HR: Heat Rate
HRSC: Heat Recovery Steam Cycle
HRSG: Heat Recovery Steam Generator
HTS: High Temperature Shift reactor
IGCC: Integrated Gasification Combined Cycle
LP: Low Pressure
SPECCA: Specific Primary Energy Consumption for CO2 Avoided
TIT: Turbine Inlet Temperature
TITiso: Turbine Inlet Temperature (defined according to ISO standard
TOT: Turbine Outlet Temperature
WGS: Water Gas Shift
WP: Work Package
η: Efficiency

This chapter presents the technical assessment of hydrogen selective membranes application in coal based IGCC plant for CO_2 capture. The objective of this analysis was the optimization of membrane modules operation both in term of cycle efficiency and cost of CO_2 avoided.

After a short introduction on membrane fundamentals, this chapter is composed of:

- Definition of membrane type and membrane module layout
- Issues related to use of membrane in dry fed IGCC
- Introduction to the membrane area computation tool
- Layout of the investigated cases
- Results

8.1 MEMBRANE FUNDAMENTALS

A very simplified layout of a membrane for gas separation is shown in Figure 8-1: the feed gas is separated into the permeate and the retentate through the membrane layer. The first large membrane application was used to separate U^{235} from U^{238} but membranes became economically feasible only in the 80's with some application for the separation of H_2, acid gases CO_2/CH_4 and N_2 production from air.

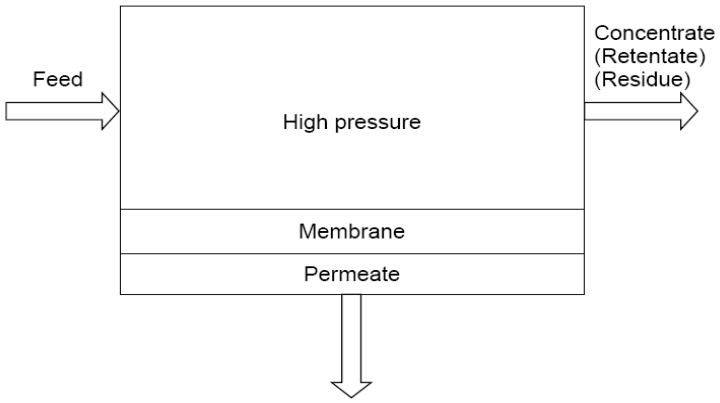

Figure 8-1: simplified membrane lay out.

All the processes involved in a membrane are supported by a wide background of mass transfer theory. Substances move through membranes by several mechanisms such as viscous flow (microfiltration) or electrical potential (fuel cell or electrolysis). For all membranes, Fick diffusion law is somehow important and it is dominant in gas permeation and reverse osmosis. The driving force for Fick transport of a substance is a gradient in chemical potential:

$$N_i = -D_i \cdot \frac{dC_i}{dx} \tag{8-1}$$

Where N_i is the mass of component i transported, [kmol/m^{2}s], D_i is diffusivity of component i, [m^2/s], C_i is concentration, [kmol/m^3], and x is distance, [m].

Assuming D_i is constant, and in particular that it is independent of C_i and that the concentrations in the liquid phase are in equilibrium with the membrane, Fick's law may be written as:

$$N_i = D_i \frac{\Delta C}{z} \tag{8-2}$$

Where z is the thickness of the membrane active layer and ΔC are the concentration differences between feed and permeate. The concentration of a component in the membrane phase will be quite different than its concentration in the fluid phase even though they are in equilibrium. The diffusivity in the membrane phase will always be much different than it is in the fluid phases. The diffusivity of a gas in a membrane is found to be inversely proportional to its kinetic diameter. Partial pressure is proportional to chemical potential and can be used as the variable design calculations for most gases of interest. Frictional losses on the permeate side will affect the permeate pressure. Permeation rate is a point function dependent on the difference in partial pressures at a point on a membrane. Many variables affect point partial pressures, among them are membrane structure, module design, and permeate gas-sweep rates.

All the transport mechanisms which take place in membrane are reported in Table 8-1.

Table 8-1: segregative properties of the various transport regimes; λ is the mean free path, d_p is the pore size.

Conditions	Regime or mechanism	Nonsegregative	Segregative
λ<<dp, ΔP	Viscous	X	
λ<<dp	Molecular		X
λ>>dp	Knudsen	X	X
Molecular size ≈ d_p	Configurational		X
T<T; adsorption	Surface diffusion		X
$T<T_c$ e $P<P_c$,	Capillary condensation		X

8.2 HYDROGEN SEPARATION MEMBRANES AND CACHET II APPROACH

Hydrogen selective membranes are recognized as a promising technology for reducing efficiency penalty in power plants with CO_2 capture [1]. Among different membrane technologies [2], the hydrogen selective one perfectly fits in the precombustion decarbonization concept [3] [4]. In particular, Pd-based membranes are one of the most investigated in the laboratories thanks to their high selectivity and good hydrogen fluxes. Moreover, hydrogen separation is performed at medium temperature (350°C-500°C) allowing the direct use of the separated hydrogen as fuel for the gas turbines [5] [6]. Weak points that have to be improved are (i) the intolerance to sulphur and (ii) the stability.

Two different kind of membranes were developed in CACHET-II project and both were considered in this work: the first is a pure Pd membrane showing a high H_2 permeance, but no tolerance towards sulphur [7] and the second is a Pd-alloy based membrane which has a reduced permeance but can support sulphur content up to 1-2 ppm without reducing the flux to a large extent [8]. Since the sulphur content in the syngas is in the range of 5000-10000 ppm, a sulphur removal system upstream the membrane is required. Pure Pd membranes were developed in Work Package 1 (WP1) of CACHET-II, while Pd-alloy were investigated in WP2.

Usually, when hydrogen selective membranes are considered for CO_2 capture in power plants, the membrane reactor concept is presented. Membrane reactor consists of simultaneous hydrogen conversion and separation; in the IGCC plant case, membranes are integrated with the Water Gas Shift reaction. The CACHET-II project decided to develop membrane separator modules instead of membrane reactors (no WGS reaction is performed together with hydrogen separation) [9] [10]. This decision was mainly driven by techno-economics assessment and operationability issues: membrane substitution would be a lot easier if the membrane are not filled with catalyst.

The adopted separation concept is based on membrane modules, which can be either two or three, with adiabatic high temperature shift (HTS) reactor in between to increase the CO conversion. The number of HTS depends on the amount of hydrogen that is separated, also known as Hydrogen Recovery Factor (HRF). When 90% HRF is considered, only one HTS can be adopted, while for higher HRF (>90% or 95%) additional HTS are required in order to convert as much CO as possible. The adoption of membrane modules instead of membrane reactors reduces temperature variation issues inside the reactor and along the membranes; inside the reactor, significant temperature gradients (>50-100°C) can occur being detrimental for the

membrane as consequence of the differential thermal expansion between the membrane layer and the porous support. The membrane module layout is shown in Figure 8-2a. In order to limit the membrane area, different values of working pressure were investigated. As the gasification pressure cannot be changed, compression of the feed stream was adopted as shown in Figure 8-2b.

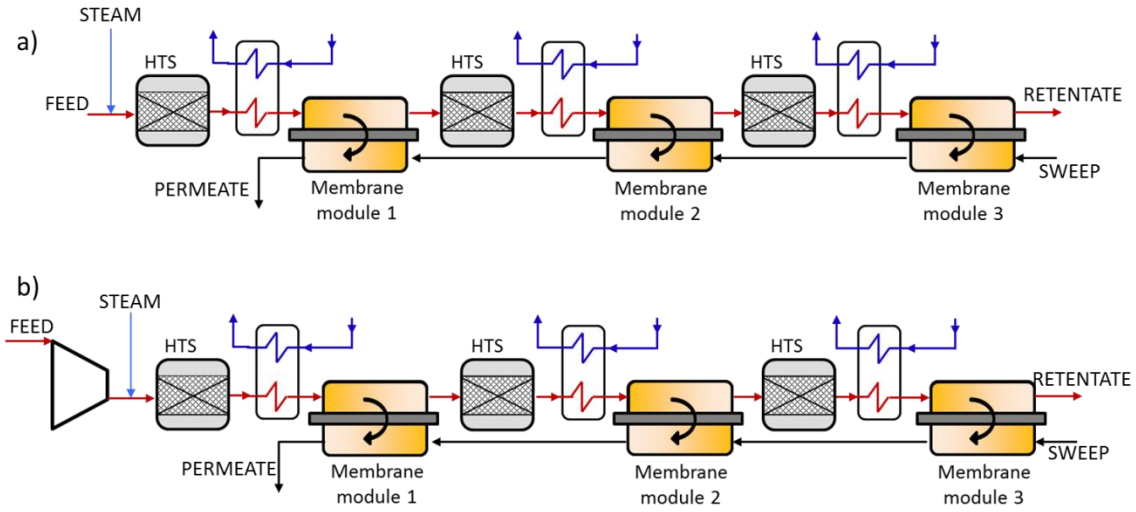

Figure 8-2: membrane module configurations considered: a) three membrane modules, pressure is defined by the gasification island; b) three membrane modules with compression of the feed stream

8.2.1 EFFECT OF GASIFICATION PROCESS ON MEMBRANE INTEGRATION

Among coal based power plants, Integrated Gasification Combined Cycle was selected for membrane application because of high pressure syngas which is fundamental for hydrogen permeation across the membrane. After a preliminary comparison of different gasification technologies [11], the Shell dry feed process was selected. Comprehensive description is reported in chapter 3 and 4.

The adoption of a dry feed gasifier with high carbon conversion (>99%) leads to higher gasifier efficiency (measured in terms of cold gas efficiency) and higher plant efficiency, when compared to slurry fed gasifiers. The main drawback of this technology when applied to a membrane-integrated process is the significant inert concentration in the syngas, mostly nitrogen used as fuel carrier. This leads to: i) lower H_2 partial pressure in the membrane feed and consequently lower H_2 fluxes through the membrane and ii) lower CO_2 purity after the hydrogen separation. If the CO_2 concentration limits before sequestration are not satisfied, an additional purification step must be introduced. According to EBTF guidelines [12] the inert limit value is set to 4% which can be hardly met when lock-hopper feeding process is adopted (e.g. like in the Shell gasifier).

These issues can be encompassed in two ways:

- Enhancing the efficiency of the retentate downstream purification step. This is the most conservative solution as it does not affect the gasification island. Nevertheless it does not cope with the decrease of the hydrogen partial pressure.

- Modifying the coal feeding system of the gasifier preventing nitrogen dilution. This solution allows improving both the hydrogen partial pressure and the retentate purity. As drawback, it requires modifications of the gasification process which can be critical.

The first solution leads to the adoption of cryogenic system. Such a process can reduce the energy consumption for purification of CO_2-rich streams when the initial CO_2 concentration is higher than about 60% [13].

The second solution leads to the adoption of CO_2 as coal feeding carrier inside the lock hopper. As abovementioned, this is not a commercial solution and it requires making some assumptions in order to evaluate the potentiality. The kinetic simulation described in chapter 4 (paragraph 4.10.3) was used to compute the new syngas composition. Also in this case a purification step is required to recovery the hydrogen remaining in the retentate. Thanks to the negligible amount of inert, an oxycombustion of the retentate can be carried out.

Both the solutions were investigated in this work. Anyway, the advanced solutions presented in the following paragraphs (post-firing and hot gas desulfurization) were applied only to the standard nitrogen-based gasification process because of the higher potentiality of the latter. The two configurations described are reported in Figure 8-3.

Finally, a further configuration with hybrid nitrogen/CO_2 as coal feeding is proposed.

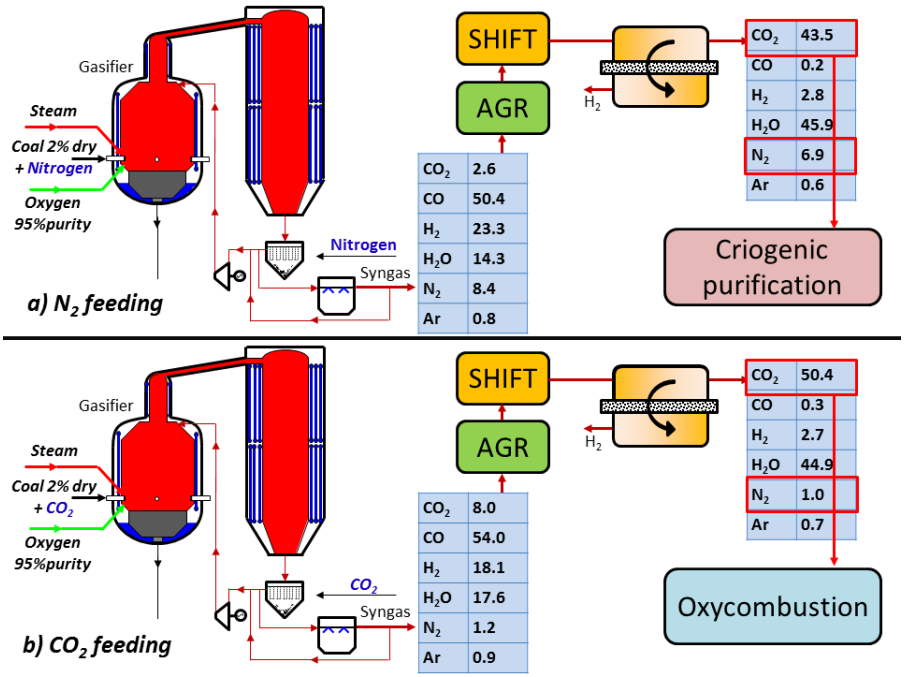

Figure 8-3: macro representation of the gasification and hydrogen separation section; a) gasifier with nitrogen as coal carrier and b) gasifier with CO_2 as coal carrier.

In addition to the gasifier configuration, the plant layout depends on the type of membrane considered: as far as not sulfur tolerant membranes are concerned, Rectisol® process is adopted for syngas purification. On the contrary, when membranes are slightly sulfur tolerant, Selexol® process is considered. Figure 8-4 shows an overall view of the investigated cases depending on:

i) the gasifier system, ii) the coal feeding process, iii) the CO_2-rich gas purification, iv) the H_2S membrane tolerance and, v) the desulfurization system adopted.

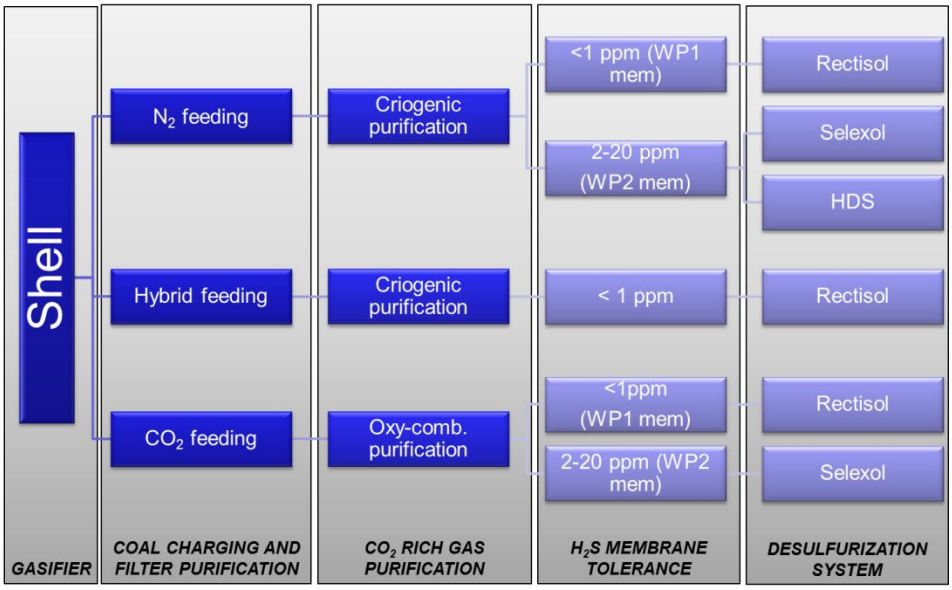

Figure 8-4: summary of the investigate cases for membrane application in IGCC plant.

8.2.1.1 Cryogenic separation

This section describes the cryogenic separation process considered for CO_2 purification. This process was already introduced in previous works applied to molten carbonate fuel cells [13] [14]. However, considering the different boundary conditions, both lay-out and operating parameters were optimized for retentate composition and pressure.

Provided that: i) CO_2 concentration of the stream at the membrane outlet is about 80% (v.d.), ii) CO_2 purity must be above 96% and, iii) hydrogen and carbon monoxide in the stream must be recovered to minimize efficiency penalties, the cryogenic separation is the most suitable process. Cryogenic techniques are the least energy consuming system to perform CO_2 separation from fuel incondensable gases included in the mixture. In such a process the treated stream is cooled approaching the triple point temperature of the CO_2 (–56.6 °C), so that most of it condenses and can be separated from other species which have much lower boiling point, and therefore remains in the gaseous phase.

As discussed before, different feed pressures were considered to increase the hydrogen flux, hence reducing the membrane surface area. However, the feed pressure affects also the operating conditions of the cryogenic separation process: the CO_2 capture ratio of the cryogenic separation process increases with the inlet stream pressure, but the purity reduces. For this reason, a compromise between membrane permeation and cryogenic process performances must be determined.

The cooling source for retentate condensation can be supplied adopting two different approaches: (i) the closed/internal system where cooling is accomplished by throttling the separated CO_2 stream in a self-refrigerated loop or (ii) the external heat removal with multi-evaporation compression chiller.

Although the industrial application is still limited, the internal refrigerating configuration seems to offer simple equipment and plant layout, with lower investment and make-up costs than the external chillers. For this reason, the adoption of a self-refrigerated cycle was selected. The main drawback is the higher energy requirement compared to the external cycle, about 10% vs. ethane and 4% vs. ethylene; however, the energy consumption of the entire section is below 10 MW making the difference between the two options (1MW) negligible in the overall plant power balance. This decision was supported by industrial partner of CACHET-II consortium.

The internal cryogenic separation consists of a self-refrigerated system which uses the CO_2 separated in the circuit as cooling source (see Figure 8-5). It is based on two-steps flash separation which reduces the compression power required to overcome the process pressure losses. In the adopted configuration, the CO_2-rich stream is first dehydrated with a circulating triethylene glycol desiccant and/or molecular sieve to prevent plugging due to ice formation in the cold section. The stream is then cooled and partially condensed in the multi-flow heat exchanger, HE1. The temperature at the hot side outlet of HE1 is an important parameter in operating the process. Lowering this temperature reduces the mass flow rate sent to knockout drum 2 and hence the mass flow rate of the second-stage condensate circulated to the CO_2 re-booster and the associated power. On the other hand, lowering the temperature increases the duty of heat exchanger HE1, requiring a higher pressure drop in the throttling valve TV1 to keep a given minimum temperature difference inside HE1; this lowers the pressure of the combined stream entering the CO_2 HP compressor, increasing its duty. In order to strike a compromise between these opposing effects, the temperature has been set around –30 °C, a value that minimizes the overall compression power. Note also that the extent to which incondensable gases can be recovered is almost independent of the temperature.

The liquid separated in the first knockout drum is throttled through valve TV1 and introduced to the cold side of heat exchanger HE1, in which it is heated and evaporated. The pressure drop in TV1 (11.7 bar) is set to ensure a 3°C minimum approach inside HE1. Since the separation efficiency increases monotonically with decreasing temperature, the vapor fraction exiting the first knockout drum is further cooled down to –53°C through the exchangers HE2 and HE3. This value has been selected to ensure that the temperature of the stream entering the cold side of HE3 remains slightly above (+0.6°C) the CO_2 freezing point. The pressure drop introduced by the throttling valve TV2 (18.4 bar) and the particular arrangement of HE3 have again been selected to insure a 3°C temperature difference within HE3. The liquid streams separated in the drums and evaporated in the heat exchangers are finally mixed, compressed in an intercooled compression train up to 80 bar and then pumped in liquid phase to 110 bar for long range transportation. According to calculation carried out, the CO_2 separation efficiency ranges between 95%-98% whilst the CO_2 stream purity is in between 96-98% (mol basis).

The vapor fraction exiting drum 2 is heated up in HE2 and HE1, and then sent to the gas turbine along with natural gas. Stream 10 contains almost 96% of the original LHV value of the input stream (1) and represents about 9% of the total fuel input to the gas turbine (LHV basis).

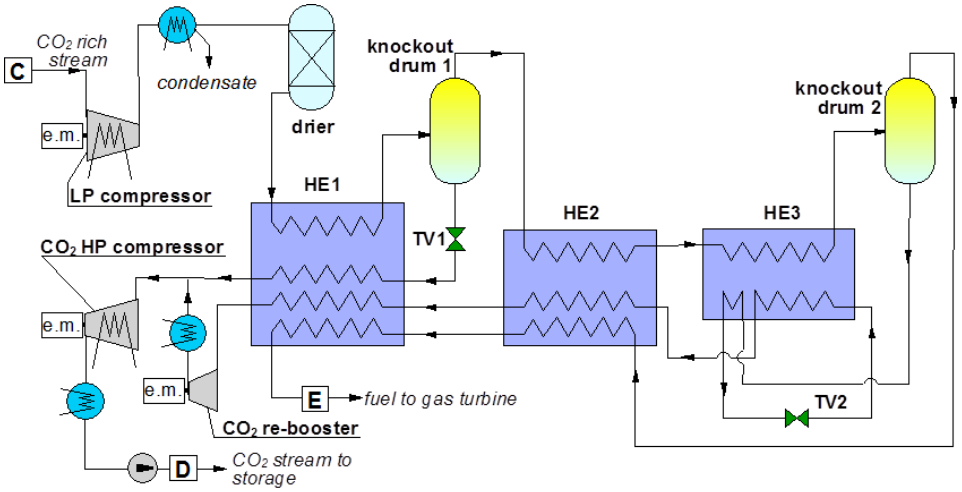

Figure 8-5: layout of the cryogenic CO_2 separation and compression section.

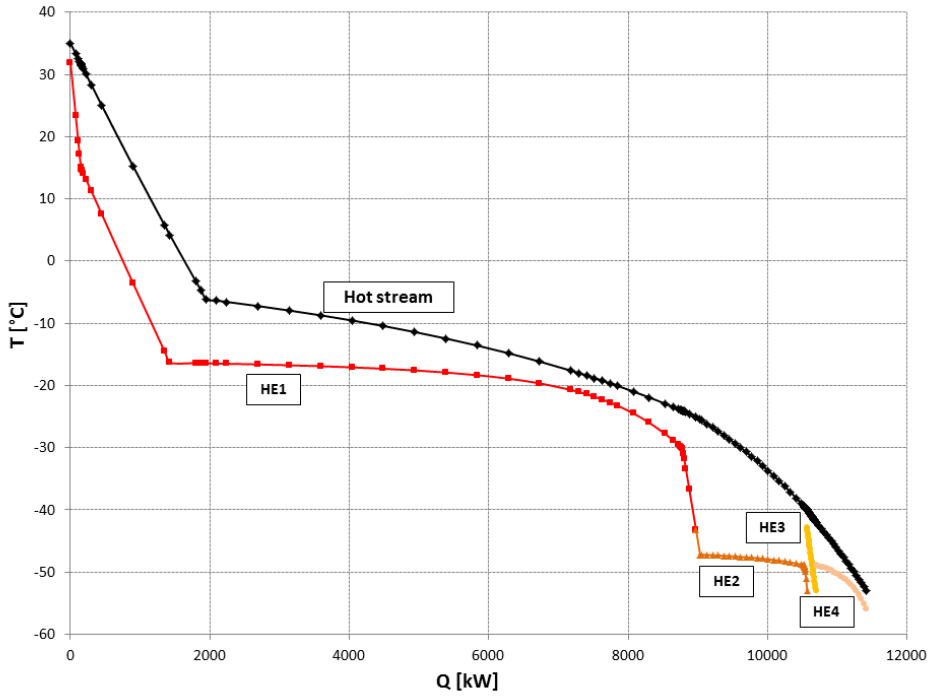

Figure 8-6: aggregate temperature-heat duty diagram for the heat exchangers included in the cryogenic process of Figure 8-5.

8.3 SIMULATION OF THE MEMBRANE SEPARATION PROCESS

The membrane modeling has significant impact on the results presented in this work. The membrane surface area was determined with a two-dimensional model developed by SINTEF within the CACHET-II project. Mass and energy balances for the feed side are discretized using a finite volume method. Thus, the radial profiles of temperature and chemical species concentration are determined. The sweep flow is modeled as a plug parameter.

The mass transfer across the membrane is calculated using a corrected Sieverts law, while mass transfer through the support is calculated using a Dusty Gas model. A schematic of the H_2 flux across the membrane is represented in Figure 8-7.

The simulation tool accounts for bulk-phase feed side mass transfer characteristics ($P_{H2,bulk}$ → $P_{H2,interface}$), permeability and mass transfer resistance associated with the membrane deposition layer $P_{H2,interface}$ → $P_{H2,wall}$), mass transfer characteristics through the ceramic support tubing ($P_{H2,wall}$ → $P_{H2,support}$) and at the bulk-phase permeate side of the membrane ($P_{H2,support}$ →$P_{H2,sweep}$).

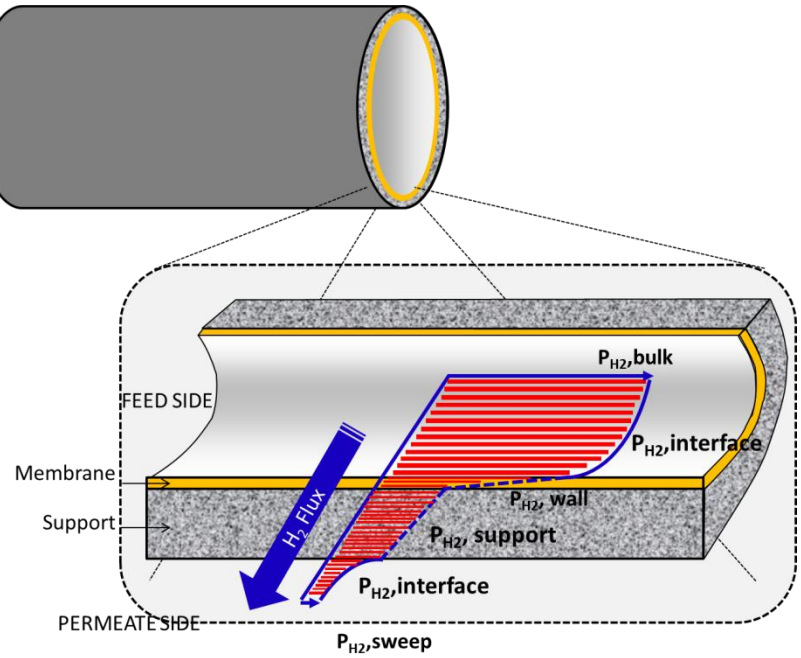

Figure 8-7: qualitative representation of the driving force (partial pressure) for the hydrogen mass transfer across a tubular membrane.

Transport parameters are calculated as function of membrane operating conditions as temperature, pressure, velocity, etc.. The mass transfer model has been validated against experimental data performed at DICP and ECN laboratories. The resulting parameters of the model for the pure Pd membrane are: thickness equal to 7.266×10^{-6} m, permeability at reference conditions (T=400 °C) equal to 9.592×10^{-13} kmol m/m^2 s Pa^n, activation energy of 12.8 kJ/kmol and n equal to 0.676 [9] [10]. When a sulphur tolerant membrane is considered, the permeability is assumed reduced by 60% [8]. With the calibrated parameters, the model showed that some parameters affect more than other the hydrogen flux. However, it can be stated that there is no

rate-limiting step in the hydrogen permeation across the membrane outlining the importance of including all the hydrogen permeation resistance. The optimum configuration is composed by three membrane modules in series because the mass transfer limitation from bulk phase to membrane interface was found to be the most important parameter. With one and two membrane modules, the flow in the feed side is laminar type. Moving to three membrane modules, the flow becomes turbulent reducing the bulk to interface resistance. Higher number of membranes will increase the pressure drops, hence reducing the driving force, as well as plant complexity

8.4 MEMBRANE INTEGRATION IN NITROGEN-BASED IGCC

This section presents the plant layouts when membranes are applied to nitrogen-fed gasifier. Three different cases are reported.

- *Base case*: membranes are conventionally applied to IGCC consistently with module in Figure 8-2; all the separated hydrogen is fed to the Gas Turbine (paragraph 8.4.1)
- *Advanded case 1*: the membrane module is rearranged in order to produce a small amount of ambient pressure hydrogen for HRSG post-firing (paragraph 8.4.2)
- *Advanced case 2*: the layout is the same of the advanced case 1 but for the sulphur removal system which is based on the hot gas clean-up process reported in chapter 5 (paragraph 8.4.3).

8.4.1 MEMBRANE AND N_2FEEDING: BASE CASE

As already anticipated, the gasification technology is based on Shell-Prenflo dry feed gasifier. The power and mass balances of the gasifier is reported in chapter 3. Besides membrane module, the power plant includes only conventional components. The process is equal to the reference case without CO_2 capture until the AGR. CO shift conversion is carried out after the sulphur removal section reducing CO_2 venting in AGR and steam condensation exergy losses.

Considering the sulphur tolerance of the two membranes, two acid gas removal (AGR) process up-stream have been considered: Rectisol for pure Pd membrane and Selexol for the Pd-alloy based membranes which can tolerate H_2S up to 5 ppm. The Selexol process is based on a mixture of dimethyl ethers of polyethylene glycol, while Rectisol is based on chilled methanol [15]. Lay-out of investigated cases is shown in Figure 8-8. The only difference between Rectisol and Selexol lay-out is in COS hydrolizer: Rectisol is selective to H_2S and COS, while Selexol is more selective to H_2S requiring the conversion of COS upstream[1].

The power plant size is based upon one gasification train generating syngas for one gas turbine combined cycle. Oxygen is produced in an ASU partially integrated to the gas turbine compressor: 50% of the air at the ASU distillation column comes from the GT compressor. An expander between the gas turbine compressor and the ASU is adopted to decouple the pressures and recover part of the compression work. N_2 produced in the ASU is compressed and partly used in lock hoppers for coal feeding, and partly sent to the membrane modules as sweep gas

[1] Selexol can capture COS as well, but the CO_2 co-captured would be significant with penalties for the CO_2 emissions.

reducing the hydrogen partial pressure leading to a decrease in membrane surface area required. Moreover, nitrogen dilution reduces the stoichiometric flame temperature to 2200 K limiting the NO_x formation, as described in chapter 6. Syngas exits the scrubber at about 170°C and then is further cooled to ambient temperature. In the Selexol case, gas is treated in the COS hydrolyser before being cool down. Low temperature heat is recovered producing hot water for the saturator. Syngas is then further cooled with water and sent to acid gas removal (AGR) unit after condensate separation.

Both in Rectisol and Selexol, separated H_2S is sent to the sulphur recovery unit. Zero net steam is assumed from the sulphur recovery unit, i.e. the steam raised by H_2S combustion in the Claus plant is balanced by the heat required to keep S molten and to regenerate the SCOT solvent. The energy consumptions for the Selexol AGR reboiler is estimated to be 5.82 kWh/kg_{H2S} while the power consumption for pumps etc. in the AGR is 0.5382 kWh/kg_{H2S} (assumptions taken from EBTF [12]). About Rectisol, no indications from EBTF have been provided, so a detailed simulation with ASPEN was carried out, although it is not shown for brevity. Rectisol requires a higher electric demand because of the low temperature working conditions (absorber column work between -10°C and -20°C), leading to a stripper column heat duty at 70°C of 15 kWh/kg_{H2S} and a power consumption of 5.4 kWh/kg_{H2S}. Moreover the amount of CO_2 separated together with CO_2 is equal to 6.62 mol_{CO2}/mol_{H2S}. This is about 6 times the Selexol venting and is a further drawback from CO_2 capture and CO_2 avoided point of view. An advanced configuration where CO_2 is separated from H_2S can be eventually considered to reduce CO_2 emissions; however this is beyond the scope of this work. Heat duty from the LP steam is also required for sour water stripper, where NH_3, SO_2 and other impurities from the scrubber are removed.

After the AGR unit, syngas is saturated and additional steam is added in order to achieve 1.9 S/CO ratio at WGS. Saturator allows increasing water content in the syngas, which is generated by recovering low-temperature heat and reducing the amount of steam to add. The additional steam required to achieve 1.9 S/CO is partially bled from the steam turbine at the high pressure section outlet (usually named cold RH) and partially produced in the plant waste heat boilers. The further syngas compression from 40 bar to about 60 bar before the saturator is also evaluated: higher the syngas total pressure, higher the H_2 permeation driving force and lower the membrane surface area.

In the Rectisol case, where membranes are pure Pd and not sulphur tolerant, the maximum temperature inside membrane is set at 400°C. In the Selexol case, where Pd-Cu membranes are adopted, the maximum membrane temperature is 450°C. Since no reactions occur in the module, the maximum temperature is located at the feed inlet, while at the outlet, the temperature is slightly lower because of the cooling effect of the sweep gas. This assumption affects mainly the membrane surface area rather than system efficiency since the fuel temperature at combustor inlet is set at 350°C requiring the retentate cooling.

Three different HRF (90%, 95% and 98%) were assumed in order to outline its influence over electric efficiency and CO_2 capture ratio.

Nitrogen released from the ASU and compressed up to 25[2] bar is used as sweep gas. An intercooled compressor is adopted to limit the power consumption. The amount of sweep gas is set in order to have a H_2 concentration of 40% at reactor outlet. The lower this value the lower the membrane surface area required. Nevertheless a limit on hydrogen concentration is defined by the GT combustor (fuel LHV > 4000 kJ/Nm^3). After hydrogen separation the retentate stream, which mainly consists of CO_2, H_2O and unconverted H_2 and CO, is cooled down to ambient temperature producing HP steam for the HRSG and IP water economization. Because of the high steam content and pressure, a part of condensation heat can be recovered for water economization (dew point is at about 200°C).

As anticipated in paragraph 8.2.1, the inert content in the CO_2 is significant. The high inert content consequence of dry feeding gasifier makes ineffective the retentate oxy-combustion as purification process. At 35°C, CO_2 molar concentration, volume dry, is 76% and 82% at 90% and 98% of HRF respectively. The cryogenic process has a CO_2 separation efficiency in the range of 90-95%, depending on the CO_2 purity at the inlet of the process, which is function of HRF.

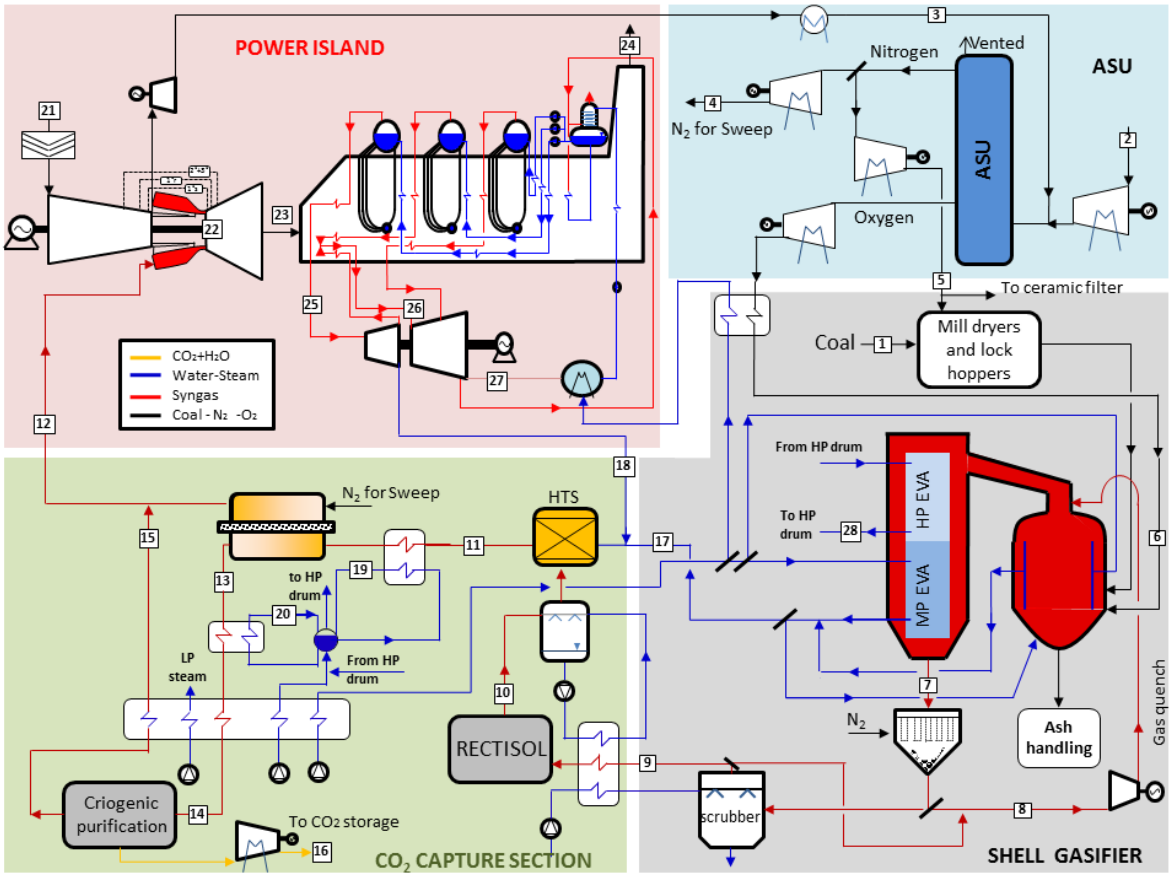

Figure 8-8: layout for the Shell with membrane and low temperature AGR.

[2] It is important to outline that permeate pressure drops are a fundamental parameter. In order to keep a significant driving force inside the membrane reactor, permeate pressure drops should be below 1 bar, otherwise HRF can be limited and the amount of membrane surface area significantly increases.

Heat and mass balance of the main points in Figure 8-8 are shown in Table 8-2.

Table 8-2: flows, conditions and compositions for Shell with membrane and low temperature AGR (Rectisol, 95% HRF).

	G	T	p	Composition, %mol								
#	[kg/s]	[°C]	[bar]	CH4	CO	CO2	H2	H2O	Ar	N2	O2	H2S
1	38.7	15.0	44.0	Dry Coal, 2% moisture as in chapter 3								
2	70.8	15.0	1.0	Air as in chapter 3								
3	70.8	30.0	5.8	Air as in chapte 3								
4	83.6	252.8	25.0	-	-	-	-	-	-	100.0	-	-
5	8.8	80.0	48.0	-	-	-	-	-	-	100.0	-	-
6	33.9	180.0	48.0	-	-	-	-	-	3.1	1.9	95.0	-
7	134.1	300.0	41.1	-	56.7	2.9	26.2	5.0	0.9	8.2	-	0.2
8	57.4	200.0	41.1	-	52.1	2.7	24.1	11.5	0.8	8.6	-	0.2
9	89.9	158.1	41.1	-	50.4	2.6	23.3	14.3	0.8	8.4	-	0.2
10	78.2	35.0	37.1	-	59.1	2.7	27.4	0.2	0.9	9.8	-	1ppm
11	159.5	494.0	36.4	-	4.5	23.2	34.2	33.3	0.4	4.4	-	-
12	142.0	325.0	25.0	-	0.1	1.9	36.7	21.9	0.3	39.1	-	-
13	153.4	400.0	36.0	-	0.2	43.5	2.8	45.9	0.6	6.9	-	-
14	153.5	50.0	34.6	-	0.2	43.5	2.8	0.2	0.6	6.9	-	-
15	25.0	186.8	34.2	-	1.0	15.0	13.4	34.2	2.4	34.0	-	-
16												
17	12.5	300.0	54.0	-	-	-	-	100.0	-	-	-	-
18	57.5	417.5	55.9	-	-	-	-	100.0	-	-	-	-
19	33.7	339.0	144.0	-	-	-	-	100.0	-	-	-	-
20	5.6	343.0	144.0	-	-	-	-	100.0	-	-	-	-
21	594.8	15.0	1.0	Air as in chapter 3								
22	522.1	COT 1440.5 TIT 1360.0 TIT_{ISO} 1257.0	17.6	-	-	0.9	-	25.6	0.7	67.1	5.7	-
23	665.0	606.7	1.0	-	-	0.7	-	20.7	0.8	69.1	8.7	-
24	665.0	115.0	1.0	-	-	0.7	-	20.7	0.8	69.1	8.7	-
25	167.2	559.2	133.9	-	-	-	-	100.0	-	-	-	-
26	111.6	559.1	44.3	-	-	-	-	100.0	-	-	-	-
27	112.1	559.1	44.3	-	-	-	-	100.0	-	-	-	-
28	97.7	32.2	0.0	-	-	-	-	100.0	-	-	-	-

8.4.2 MEMBRANE AND N_2FEEDING: ADVANCED CASE 1 (POST-FIRING)

In addition to the previous configuration, where all the hydrogen separated in the membranes is burned in the GT combustor, a second lay-out was implemented. This new concept was realized at the end of the PhD work as solution to the unpromising economic results obtained for all the layouts developed in the CACHET-II framework (see chapter 9).

In this new configuration, shown in Figure 8-9 the overall membrane section is divided into two macro areas. In the first zone, which is composed by three membrane modules, hydrogen is separated at the pressure required by the GT combustor while in the second zone, hydrogen is separated at ambient pressure and used to post-fire the Heat Recovery Steam Generator. The most part of H_2, 90% of the total separated, is still sent to the GT combustor; this value was decided using a rule of thumb, but performance confirmed it was a good guess. The rationales behind this second configuration are: i) the membrane surface area can be extremely large if all

the hydrogen is separated at high pressure and ii) the integration of the heat available from the gasification island and the HRSG makes the heat recovery not efficient. In particular, the gasification island produces a large mass flow of saturated steam (both at high and medium pressure) which has to be pre-heated and super-heated in the HRSG. This penalizes the heat transfer because there is lack of heat available at low and high temperature.

It is important to stress that this new configuration does not feature any technology barrier: post-firing is widely adopted in combined cycle and CACHET-II membrane can stand up to 100 bar of absolute pressure difference [10].

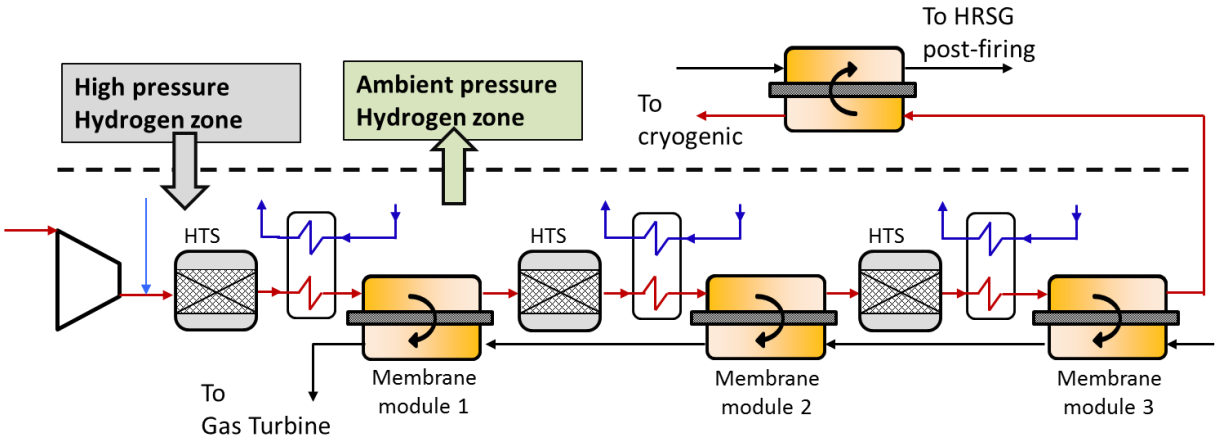

Figure 8-9: membrane module layout for combined GT and HRSG post-firing hydrogen production.

The resulting plant lay-out is presented in Figure 8-10. The only difference with the previous one is that there are two different hydrogen streams produced: 90% of the separated hydrogen is diluted with nitrogen at 25 bar and sent to the gas turbine. The remaining, slightly diluted with nitrogen, is at 1.1 bar and it is used to post-fire the heat recovery steam generator.

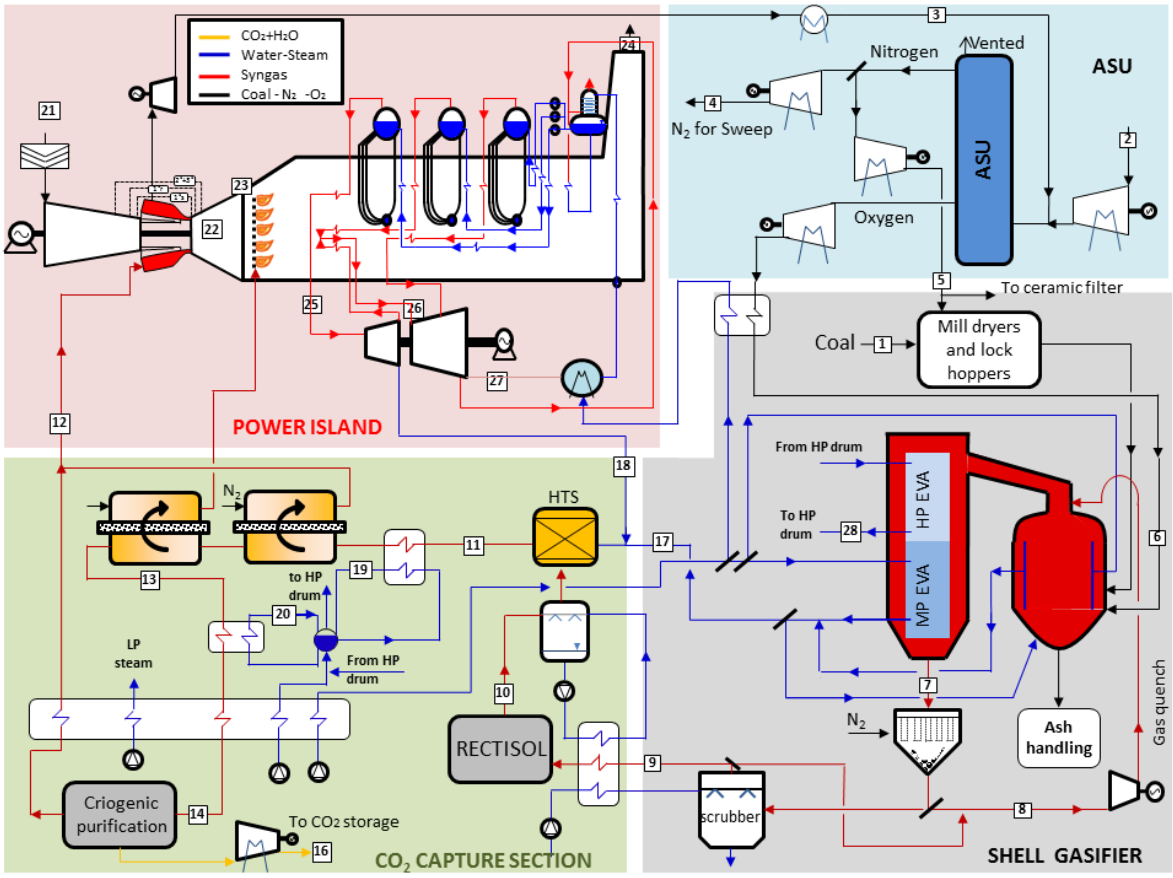

Figure 8-10: layout for the IGCC with membrane and Rectisol as AGR, CO_2 purification via cryogenic process and HRSG post-firing.

8.4.3 MEMBRANE AND N_2FEEDING: ADVANCED CASE 2 (HGD)

The second advanced plant is very similar to the previous case 1 but for the desulfurization process, which is now a hot gas clean up system, and the membrane type, which is now Pd-alloy type.

The high temperature sulphur removal system was integrated in the latest membrane lay-out with post-firing considered for the CACHET-II Project. This configuration showed the larger economic benefits thanks to the minimization of the membrane surface area. The analysis performed must be considered a preliminary assessment since both HGD and membrane sulphur tolerant are still at an early stage of development. As operating conditions of the HGD, it is assumed a desulfurizer temperature of 450°C as indicated for Sintef sorbent in chapter 5. As well the size of the reactor and sorbent inventory were presented in chapter 5. They were calculated to have an H_2S slip equal to 5 ppm, a compromise between cost of the HGD and membrane permeance decay. Moreover, more complex configurations featuring fixed bed reactor downstream the HGD to completely separate the sulphur can be adopted with advantages for the membrane, but at higher complexity.

The plant configuration with the HGD is equal to the abovementioned reference case up to the scrubbing. Then, the syngas is mixed with steam bled from the steam turbine in order to achieve a S/C ratio of 1.90 and sent to the water gas shift reactor. The HGD takes place after the WGS; this allows keeping the gasification island fixed and converting the COS directly in the

WGS. In fact the sorbent developed by Sintef was tested only for H_2S selectivity and not toward COS. Shifted syngas at about 500 °C is therefore desulphurized; a schematic of the HGD is shown in Figure 8-11 together with thermodynamic properties and mass flow rate for the main points in Table 8-3. It must be reminded that being the desulphurizer a fluidized bed, the temperature of the reactor depends more on solids than on the syngas. For this reason, the syngas can enter at 500°C, while the reactor is at 450°C.

The sulphur removal system is modelled with input from the kinetic model described in chapter 5. The stream for regeneration is depleted air with an oxygen content of 4%. Dilution is performed adding nitrogen from the ASU, which is subtracted to the sweep gas with penalties from membrane surface area. The second penalty of the HGD is the hydrogen required for the $CuSO_4$ reduction (this step is performed in R2). The amount of hydrogen necessary corresponds to about 5 MW thermal power. There are two outputs of the sulphur removal system: the sweet syngas (9) and the SO_2 with N_2. The latter is expanded to ambient pressure balancing part of the depleted air compressor consumptions.

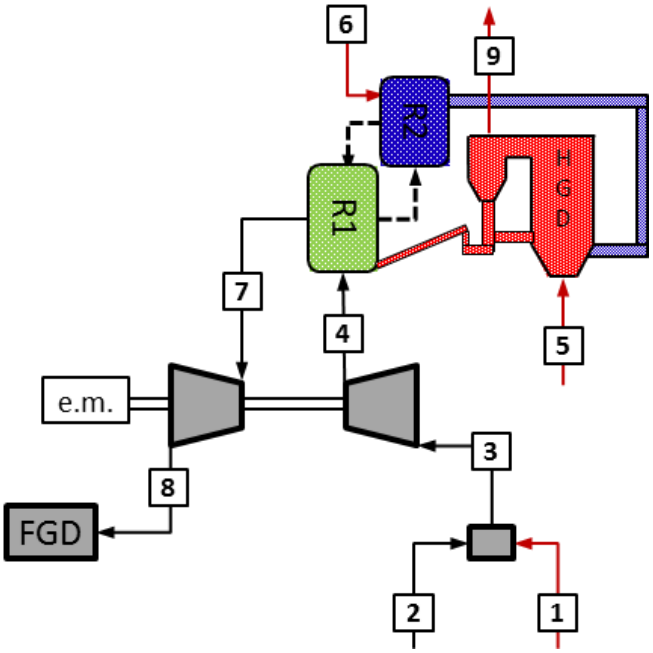

Figure 8-11: schematic of a potential lay-out of the high temperature sulphur removal process.

Table 8-3: mass flow rate, temperature, pressure and composition of the main fluxes reported in Figure 8-11.

	T	P	G	Molar concentrations (%)								
	°C	bar	kg/s	Ar	CO	CO_2	H_2	H_2O	H_2S	N_2	O_2	SO_2
1	15.0	1.0	2.4	0.9	0.0	0.0	0.0	1.0	0.0	77.3	20.7	-
2	22.0	1.2	9.8	-	-	-	-	-	-	100.0	-	-
3	20.6	1.0	12.2	0.2	-	0.0	-	0.2	0.0	95.6	4.0	-
4	450.0	53.5	12.2	0.2	-	0.0	-	0.2	0.0	95.6	4.0	-
5	515.5	53.5	155.2	0.4	5.9	22.8	35.8	30.3	0.1	4.7	-	-
6	113.4	53.5	0.1	-	-	-	89.0		-	11.0	-	-
7	451.4	53.5	12.4	0.2	-	0.0	5.0	0.2	-	94.1	-	1.6
8	43.2	1.0	12.4	0.2	-	0.0	5.0	0.2	-	94.1	-	1.6
9	515.2	53.5	154.9	0.4	5.9	22.8	35.9	30.3	-	4.7	-	-

After desulphurization, the syngas is cooled down to 450°C, and then sent to the membrane separation section. The membrane separation section consists of four membrane modules in series with three water gas shift sections in-between. Membranes are the sulphur tolerant kind developed in WP2; compared to no-sulphur tolerant membranes developed in WP1, they show a lower permeance. The first three modules separate hydrogen at high pressure for the gas turbine combustor while in the last module, the hydrogen is separated at ambient pressure for the post-firing, like in advanced case 1. Part of the ambient pressure hydrogen separated (about 0.3 kg/s) is sent to the high temperature sulphur removal section for the reduction of $CuSO_4$.

Retentate stream, which mainly consists of CO_2, H_2O, unconverted H_2 and CO is cooled down to ambient temperature producing high pressure steam for HRSG and IP water economization. The schematic of this configuration is shown in Figure 8-12.

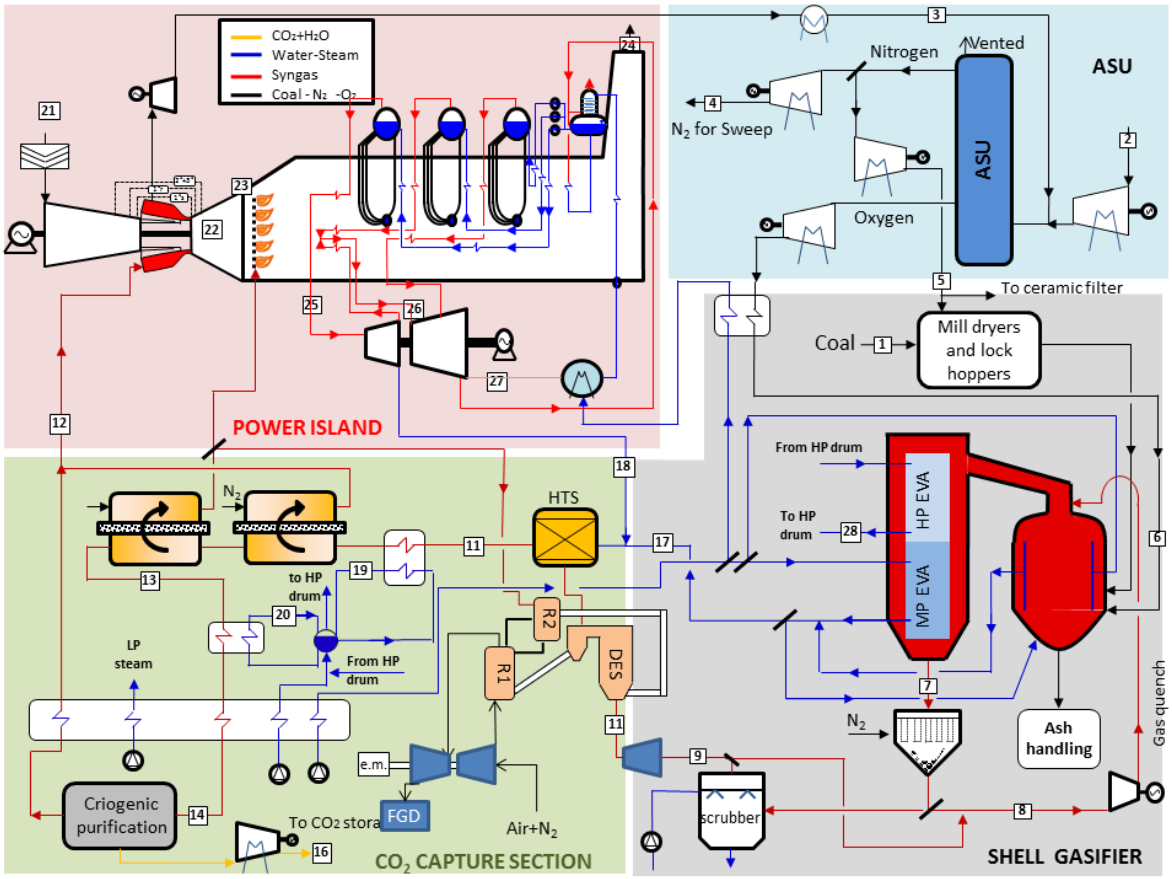

Figure 8-12: lay-out for the high temperature sulphur removal process integrated in an IGCC.

8.4.4 MEMBRANE AND N2FEEDING: RESULTS

Results of the base case layout with nitrogen lock hoppers are presented in Table 8-4. Generally, comparing membrane plants with no capture IGCC, it can be noted that: i) the thermal power input increases in order to keep the same GT dimensions, ii) the GT power increases because of the lower LHV of the decarbonized syngas, iii) the steam cycle power decreases due to the WGS steam demand, iv) the gasifier auxiliaries and ASU consumptions raises proportionally to the fuel feedstock and v) the nitrogen dilution compressor consumption increases because almost all the nitrogen produced is compressed and adopted as sweep gas.

The advantage of high pressure CO_2 separation is stressed by the limited consumption of the CO_2 compressor (e.g. one third of the required power in SEWGS plants). Results show that efficiency penalty for all cases is between 7% and 8% with Selexol cases achieving the highest efficiencies; advantages of "sulphur" tolerant membranes can be quantified in 0.5% points.

The detailed comparison between WP1 membrane (Pd, not sulfur tolerant) and WP2 membrane (Pd-alloy, slightly sulfur tolerant) as function of the HRF is shown in Figure 8-13. Both cases are calculated assuming a feed pressure of 37 bar.

It can be noted that the two configurations are similar from a thermodynamic point of view. Small differences arise because of the AGR process adopted: compared to Selexol, Rectisol has a slightly higher energy consumption for separating sulphur (4 MW more), together with a higher amount of CO_2 vented. However, Rectisol is active towards COS which makes the hydrolysis reactor pointless and avoids the associated inefficient temperature swing. This makes the heat recovery more efficient. As consequence of the lower efficiency and higher specific emissions the SPECCA of Rectisol is about 0.35 MJ/kg_{CO2} higher than the Selexol cases. Indeed, both the values are promising.

On the other hand there is a significant difference in terms of membrane surface area: Pd-alloy membranes require an almost double area. This is because of the lower permeance for sulfur tolerant membrane compared to the no-tolerant. Provided that membrane cost is proportionally linked to the surface area, the Pd-alloy solution seems non-attractive for conventional AGR processes. Consistently, Pd-alloy and Selexol plants are not considered in the further cases presented but when HGD is considered. Indeed, sulphur tolerant membranes can fully exploit their potentiality when applied downstream a warm gas clean-up.

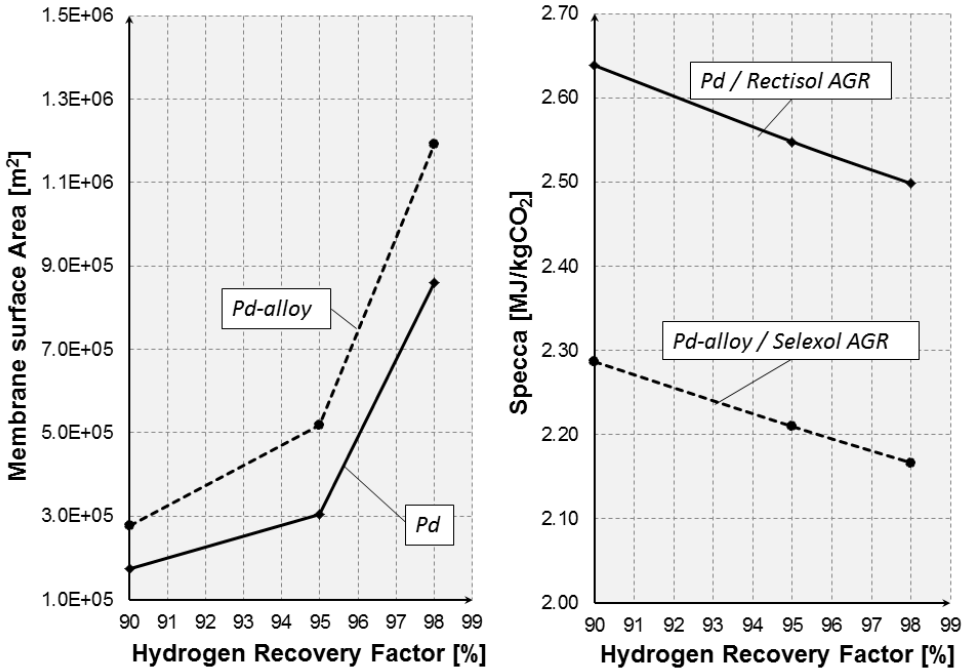

Figure 8-13: comparison between WP1 membranes (Pd, not sulfur tolerant) and WP2 membranes (Pd-alloy, slightly sulfur tolerant). On the left hand side the total membrane area for different HRF values; on the right hand side the efficiency variations as consequence of the AGR process required.

As shown in Figure 8-14a the HRF has a significant impact on plant efficiency, CO_2 avoided and membrane surface area. Higher HRF brings about: i) higher plant efficiency because more hydrogen is sent to the gas turbine, ii) lower CO_2 emissions thanks to the higher CO_2 selectivity of the cryogenic purification process and iii) larger membrane surface area. Since the thermodynamic advantages are limited compared to the membrane surface area increase (see Figure 8-14b), the optimum HRF should be 90%. However, it will be confirmed by the economic assessment.

The feed side pressure has a significant impact on membrane surface area, thanks to the higher partial pressure difference between feed and permeate side. On the efficiency, the impact of feed pressure is limited: the higher compression work is partly balanced by a more efficient heat recovery of the retentate thermal power. Moreover, the steam for WGS is at 54 bar in all cases (equal to the cold RH pressure), hence there are no additional penalties from this point of view. The increase in the steam cycle power is more important than the feed compression power moving from 37 to 47 bar; this is not any longer true when the feed pressure is 54 bar. Finally, it must be stressed that the feed pressure can't be higher than 54 bar because of the CO_2 purity constraints; above 54 bar, the cryogenic purification section cannot provide a CO_2 purity above 96%.

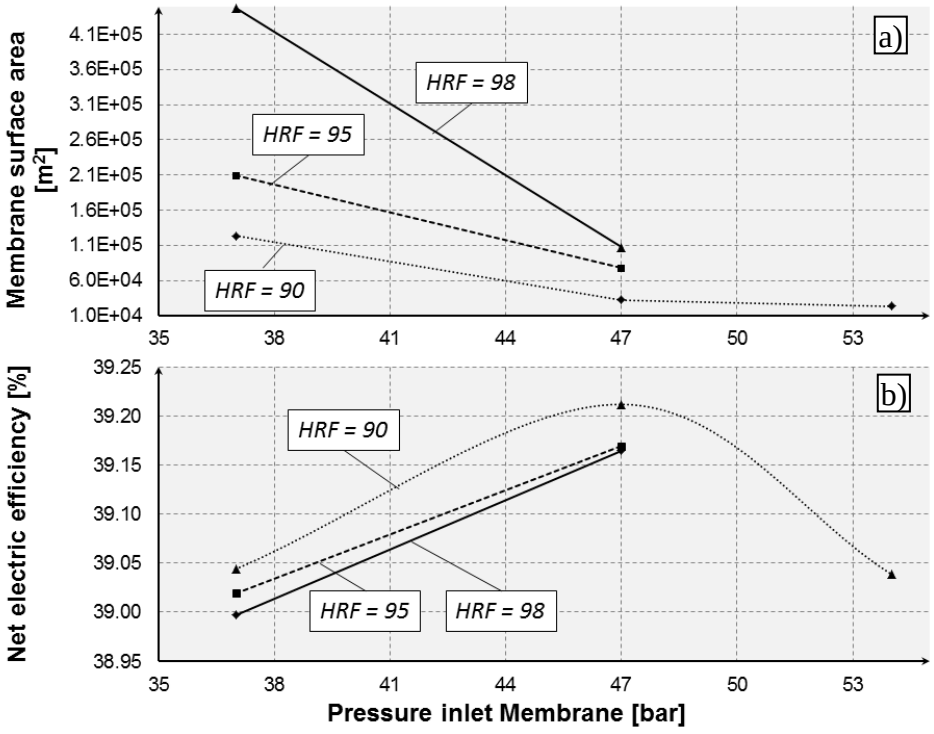

Figure 8-14: a) membrane area as function of different feed pressure for HRF equal to 90, 95 and 98%. b) Net electric efficiency of the overall plant as function of the feed pressure and for HRF equal to 90, 95 and 98%. All cases are based on Pd/Rectisol configuration.

Another significant result is the negligible efficiency variation with HRF: this is because the cryogenic separation allows the CO_2 to be purified and compressed with limited energy consumption, exploiting unconverted CO and H_2 in the combined cycle thus minimizing efficiency penalties. As far as CO_2 capture is concerned, the impact is more important because at

higher HRF, CO_2 concentration increases leading to a more selective cryogenic process, and consequent 5% points avoidance variation.

As far as the advanced case with post-firing is concerned, performance results are reported in Table 8-5 while membrane areas are shown in Figure 8-15. The advanced layout with post-firing achieves very good results: i) the required membrane area sharply decreases from 23300 to 14300 at 54 bar feed and ii) the efficiency increases from 39.0 up to 39.7% at the same time. The plant efficiency is very sensitive towards the HRSG maximum steam cycle; compared to the reference conservative case (565°C) two other values were considered: i) 585°C, which is the state-of-the-art for an H-class GT and, ii) 620°C, which is feasible with minor boiler modifications. Only the case with steam maximum temperature of 565 °C, the efficiency is equal to the case without post-firing at 39.0%. The efficiency increase compared to the base case is due to the steam production optimization which leads to a higher heat recovery cycle efficiency. Lower feed pressure (i.e. 47 bar) has slightly higher efficiency, around 39.7%. The membrane surface area reduction is due to the lower permeate pressure in the last module which keeps a high driving force, even with low hydrogen partial pressure at feed side. This is outlined in Figure 8-15b, showing the area for each module, where the last module contributes for less than 10% of the overall surface area.

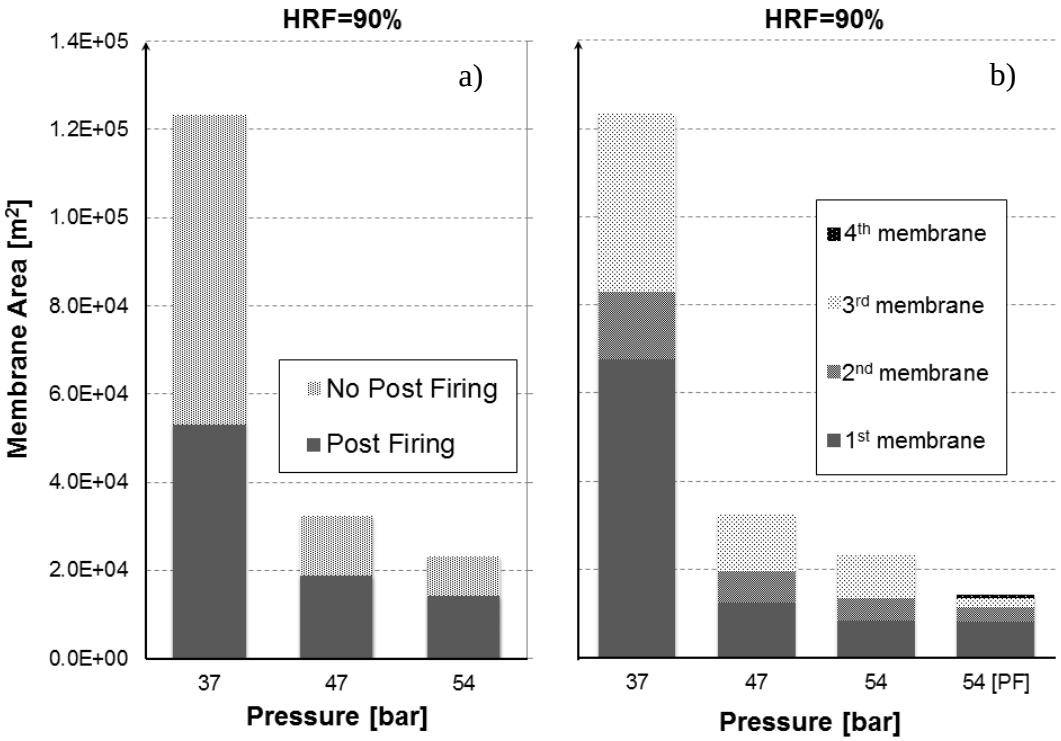

Figure 8-15: comparison of the total membrane area as function of the feed pressure and the plant layout: a) in light gray the base case, in dark gray the advanced case 1 with adoption of post firing. b) total membrane area distribution among the different membrane as function of the feed pressure and configuration.

Concerning the advanced case 2 with HGD and Pd-alloy membranes, results are reported in Table 8-5. Only cases with overall HRF=90% was considered as results of the base case analysis. About thermodynamics, HGD increases the net electric efficiency by 1% point. This is due to: i) lower consumptions of the sulphur removal, ii) better heat integration with a higher net

power output of the steam cycle and, iii) reduced pressure losses thanks to the equipment savings. Another advantage in terms of power balances is the lower consumption of the sweep gas compressor, which however penalizes the membrane surface area. The hydrogen required for $CuSO_4$ reduction accounts for 5 MW_{th} which corresponds to less than 0.2% point efficiency penalty. The drawback of this sulphur abatement system is in the 5ppm sulphur content in the syngas feeding the membrane which results in a 50% increase of the membrane area compared to not-sulphur tolerant membranes. A temperature of 450°C was assumed at membrane reactor, in order to have the highest possible permeance, however, this configuration penalizes the CO conversion in CO_2, leading to a lower CO_2 avoidance than Rectisol case.

Table 8-4: energy balances for membrane integration in the base case nitrogen fed gasifier. Data are reported for different membranes (Pd-alloy/selexol and Pd/Rectisol), different HRF (90, 95, 98 %) and different feed pressure (37, 47, 54).

		IGCC	Pd-alloy			Pd						
AGR			**Selexol**			**Rectisol**						
HRF	[%]		90	95	98	90	95	98	90	90	95	98
Feed pressure	[bar]		37	37	37	37	37	37	47	54	47	47
Gas Turbine	[MW]	290.2	331.6	334.4	335.9	332.2	335.0	336.5	323.5	323.1	327.2	329.2
HRSC gross power	[MW]	197.7	168.2	165.1	163.0	169.8	166.9	164.9	173.8	174.2	170.9	169.1
Expander ASU	[MW]	8.5	9.9	9.9	9.9	9.9	9.9	9.9	9.8	9.8	9.8	9.8
Coal handling	[MW]	-1.7	-1.9	-1.9	-1.9	-1.9	-1.9	-1.9	-1.9	-1.9	-1.9	-1.9
Ash handling	[MW]	-0.5	-0.6	-0.6	-0.6	-0.6	-0.6	-0.6	-0.6	-0.6	-0.6	-0.6
AGR sulphur adsorption	[MW]	-0.4	-0.4	-0.4	-0.4	-4.6	-4.6	-4.6	-4.5	-4.5	-4.5	-4.5
N_2 compression LH	[MW]	-9.2	-12.1	-12.1	-12.1	-12.2	-12.2	-12.2	-12.0	-12.0	-12.0	-12.0
N_2 sweep compressor	[MW]	-32.1	-39.2	-39.2	-39.2	-39.5	-39.5	-39.5	-38.8	-38.9	-39.0	-39.0
ASU + O_2 compression	[MW]	-22.7	-26.2	-26.2	-26.2	-26.4	-26.4	-26.4	-26.0	-26.0	-26.1	-26.1
HRSC auxiliaries	[MW]	-3.1	-2.9	-2.8	-2.8	-2.9	-2.9	-2.8	-3.1	-3.1	-3.1	-3.0
Blower	[MW]	-1.1	-1.2	-1.2	-1.2	-1.2	-1.2	-1.2	-1.2	-1.2	-1.2	-1.2
CO_2 compressor	[MW]	-0.0	-10.6	-10.2	-10.0	-10.7	-10.3	-10.0	-9.9	-9.6	-9.6	-9.5
Feed Compressor	[MW]	-0.0	-0.0	-0.0	-0.0	-0.0	-0.0	-0.0	-2.2	-4.0	-2.2	-2.2
BOP	[MW]	-0.7	-2.0	-2.1	-2.1	-2.0	-2.1	-2.1	-1.2	-1.2	-1.3	-1.4
Aux. for heat rejection	[MW]	-2.5	-2.2	-2.1	-2.1	-2.2	-2.2	-2.1	-2.3	-2.4	-2.3	-2.2
Net Power output	**[MW]**	**422.4**	**410.3**	**410.4**	**410.1**	**407.7**	**407.9**	**407.7**	**403.2**	**401.7**	**404.1**	**404.4**
Thermal Power Input$_{LHV}$	[MW]	896.6	1037.1	1038.1	1037.8	1044.1	1045.5	1045.5	1028.3	1028.9	1031.6	1032.6
Efficiency	**[%]**	**47.1**	**39.57**	**39.5**	**39.5**	**39.04**	**39.0**	**39.0**	**39.2**	**39.0**	**39.2**	**39.2**
Specific emission	[g/kWh]	732.1	94.5	69.6	54.0	133.5	109.8	95.4	113.4	105.3	94.1	82.0
CO_2 avoided	[%]	0.0	87.1	90.5	92.6	81.8	85.0	87.0	84.5	85.6	87.1	88.8
SPECCA	**[MJ/kg$_{CO2}$]**	**0.000**	**2.29**	**2.21**	**2.17**	**2.64**	**2.55**	**2.50**	**2.49**	**2.52**	**2.43**	**2.39**

Table 8-5: energy balances for membrane integration in advanced case with post firing and with Hot Gas Desulfurization and nitrogen fed gasifier. Data are reported for different HRF (90, 95, 98 %), different feed pressure (37, 47, 54) and different maximum steam temperature in the HRSG (565, 585, 620 °C).

		Post Firing cases							
AGR		**Rectisol, Pd membrane**						**HGD, Pd-alloy**	
HRF	[%]	90	90	90	90	95	98	90	90
Feed pressure	[bar]	47	54	54	54	54	54	47	54
Max steam T	[°C]	620	565	585	620	565	565	565	565
Gas Turbine	[MW]	315.2	315.8	315.6	315.2	319.1	321.8	316.1	315.9
HRSC gross power	[MW]	227.1	223.0	224.7	227.7	222.7	219.6	224.4	226.2
Expander ASU	[MW]	10.6	10.6	10.6	10.6	10.7	10.6	10.5	10.5
Coal handling	[MW]	-2.1	-2.1	-2.1	-2.1	-2.1	-2.1	-2.0	-2.0
Ash handling	[MW]	-0.6	-0.6	0.6	-0.6	-0.6	-0.6	-0.6	-0.6
AGR sulphur adsorption	[MW]	-4.9	-4.9	4.9	-4.9	-4.9	-4.9	-3.4	-3.5
N_2 compression LH	[MW]	-12.9	-13.0	13.0	-12.9	-13.1	-13.1	-12.9	-12.9
N_2 sweep compressor	[MW]	-41.5	-41.6	41.6	-41.5	-41.9	-41.9	-36.6	-36.6
ASU + O_2 compression	[MW]	-28.1	-28.1	28.1	-28.1	-28.3	-28.3	-28.0	-28.0
HRSC auxiliaries	[MW]	-3.6	-3.8	3.7	-3.6	-3.8	-3.8	-3.7	-3.8
Blower	[MW]	-1.3	-1.3	1.3	-1.3	-1.3	-1.3	-1.3	-1.3
CO_2 compressor	[MW]	-10.3	-10.3	10.3	-10.3	-10.4	-10.5	-10.3	-10.3
Feed Compressor	[MW]	-2.5	-4.5	4.5	-4.5	-5.6	-5.6	-2.9	-6.0
BOP	[MW]	-1.2	-1.1	1.1	-1.1	-0.0	-0.0	-1.0	-1.0
Aux. for heat rejection	[MW]	-2.7	-2.8	2.8	-2.7	-2.8	-2.7	-2.8	-2.9
Net Power output	**[MW]**	**441.2**	**435.2**	**436.9**	**439.7**	**437.5**	**437.2**	**445.6**	**443.8**
Thermal Power $Input_{LHV}$	[MW]	1110.4	1113.2	1112.2	1110.4	1120.7	1119.8	1105.7	1105.5
Efficiency	**[%]**	**39.7**	**39.1**	**39.3**	**39.6**	**39.0**	**39.0**	**40.3**	**40.2**
Specific emission	[g/kWh]	100.9	102.3	102.0	101.5	100.8	98.6	123.9	124.7
CO_2 avoided	[%]	86.2	86.0	86.1	86.1	86.2	86.5	83.1	83.0
SPECCA	**[MJ/kg_{CO2}]**	**2.25**	**2.49**	**2.42**	**2.30**	**2.50**	**2.49**	**2.13**	**2.18**

8.5 MEMBRANE INTEGRATION IN CO_2 –BASED IGCC

This section presents power plant lay-out based on Shell gasification technology with CO_2 feeding and hydrogen membranes. Two different cases are presented:

- *Base case*: membranes are applied to an IGCC plant where coal is charged using CO_2 instead of nitrogen.
- *Advanced case 3 – hybrid*: this case was developed to cope with the inert dilution issue and limiting the modifications inside the gasification island

8.5.1 MEMBRANE AND CO_2 FEEDING: BASE CASE

Provided the limited benefits of sulphur tolerant membranes in terms of efficiency and cost of CO_2 avoided (as reported in chapter 9), only WP1 membranes were considered in the following cases. Consistently, the AGR process adopted is based on Rectisol technology. The HGD was not investigated in order to limit the number of critical technologies.

The hydrogen separation is performed in different membrane modules in series as shown in Figure 8-2. Membrane modules are applied to IGCC adopting all conventional components in the rest of the plant. The main difference compared to the nitrogen case previously reported is the coal feeding technology. The adoption of CO_2 as coal feeding strongly reduces inert concentration in the produced syngas. This allows: i) increasing the hydrogen partial pressure at the entrance of the membrane modules and ii) simplifying the retentate purification step. In fact, the low inert amount in the resulting syngas (N_2 is introduced only with coal; the N_2 amount in 95% pure oxygen is negligible) makes oxy-combustion feasible for retentate purification.

The amount of CO_2 considered for coal feeding is determined keeping the same volumetric flow of nitrogen case, hence doubling the mass flowrate [12] (this is because the molecular mass of CO_2 is higher than N_2 and at feeding conditions, CO_2 is supercritical). Figure 8-16a shows the gasifier island layout for the abovementioned plant.

With the current lock hopper system, about 50% of the fuel carrier is vented in atmosphere during charging process. This is because nitrogen venting has neither economic nor environmental drawbacks and it is the easiest option. If the fuel carrier adopted is CO_2, venting reduces the CO_2 capture ratio with significant thermodynamic and economic penalties. It is expected that the feeding technology can be improved reducing venting, if necessary, although not all the CO_2 could be recovered. In order to determine the impact of this assumption, two different CO_2 venting related to fuel feeding were assumed: i) no CO_2 is vented and ii) CO_2 is vented according to the nitrogen feeding case (the vented ratio is kept fixed). Probably, the real value is in-between.

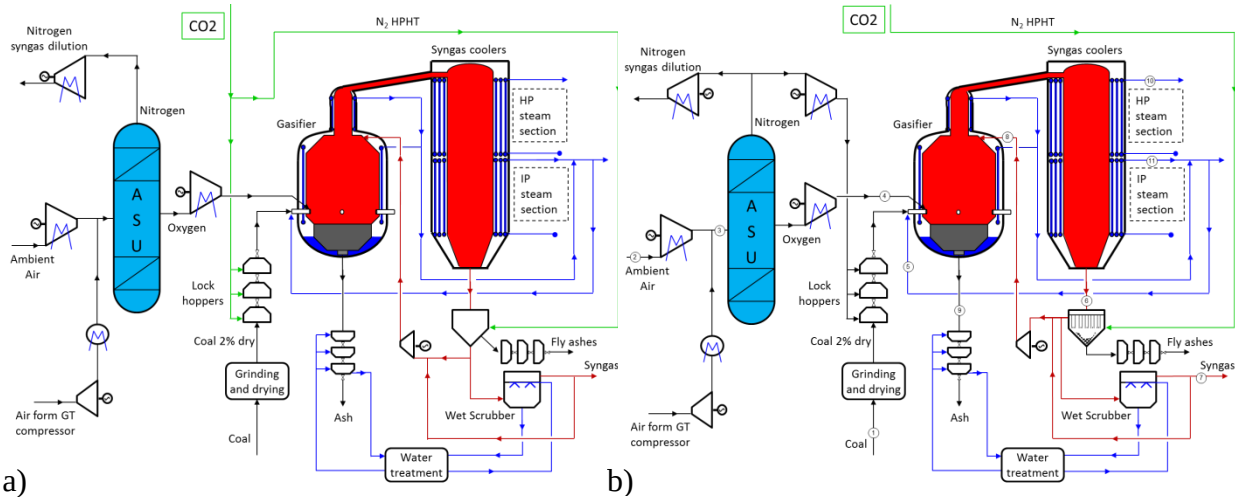

Figure 8-16: gasifier island layout for: a) only CO2 is adopted as fuel carrier and candle filters purge and, b) nitrogen is used to charge the coal while CO2 purifies the candle filters.

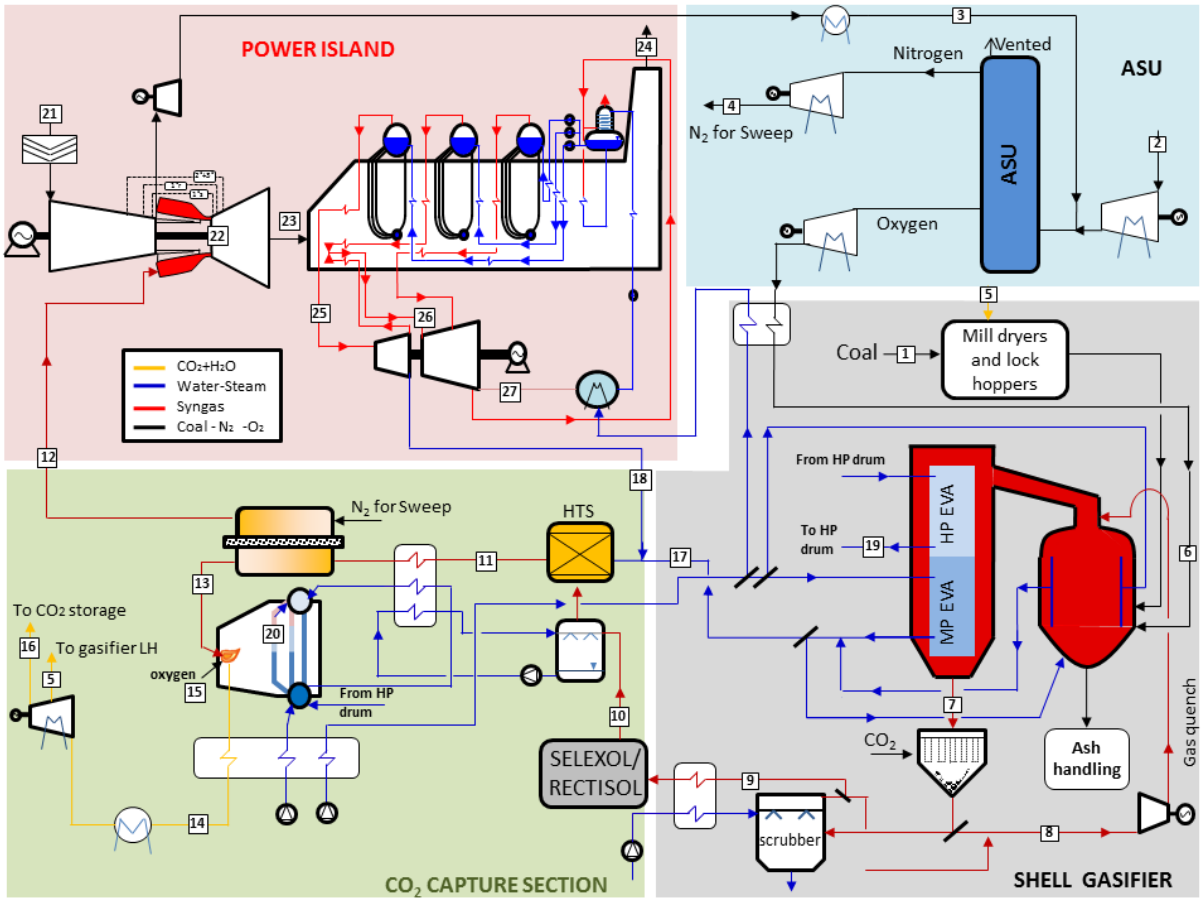

Figure 8-17: plant layout of the IGCC with CO_2 feed and hydrogen separation membranes.

The overall plant layout, shown in Figure 8-17, is equal to the nitrogen case but for: i) the lock hopper charging system, ii) the nitrogen compressor for the lock hoppers is no more required since the CO_2 for fuel feeding is compressed together with the CO_2 captured and ii) the CO_2 purification process which is now an oxy-combustor boiler.

Retentate stream mainly consists of CO_2, H_2O and unconverted H_2 and CO which are burned with oxygen. Hot gases are cooled in an integrated drum for HP steam production. The oxygen is taken from the ASU. Cases with membrane feed pressure above gasification conditions require an additional compression in order to achieve the desired pressure.

The calculated syngas composition was determined with the reduced order model described in chapter 4. The temperature and compositions at gasifier outlet have been determined accordingly.

Table 8-6: flows, conditions and compositions for Shell with membrane and low temperature AGR (Rectisol, 95% HRF).

	G	T	p	Composition, %mol.								
#	kg/s	°C	bar	CH_4	CO	CO_2	H_2	H_2O	Ar	N_2	O_2	H_2S
1	39	15	44	Dry Coal, 2% moisture as in chapter 3								
2	78	15	1	Air as in chapter 3								
3	78	30	6									
4	113	253	25	--	--	--	--	--	--	100.0	--	--
5	44	80	44	--	--	96.6	--	--	1.5	1.9	--	--
6	34	180	48	--	--	0.0	--	--	3.1	1.9	95.0	--
7	135	300	41	--	61.5	6.0	20.6	9.4	1.0	1.3	--	0.2
8	52	200	41	--	55.5	8.2	18.6	15.4	0.9	1.2	--	0.2
9	102	166	41	--	54.0	8.0	18.1	17.6	0.9	1.2	--	0.2
10	86	80	37	--	66.2	8.9	22.2	0.2	1.1	1.5	--	--
11	173	503	36	--	5.3	27.1	32.8	33.8	0.5	0.6	--	--
12	129	315	25	--	--	--	40.0	6.9	0.0	53.1	--	--
13	167	400	36	--	0.3	50.4	2.7	44.9	0.7	1.0	--	--
14	169	88	34	--	--	50.6	--	47.6	0.8	1.0	--	--
15	3	123	35	--	--	--	--	--	3.7	1.4	95.0	
16	123	25	110	--	--	96.6	--	--	1.5	1.9	--	--
17	21	300	54	--	--	--	--	100.0	--	--	--	--
18	42	416	56	--	--	--	--	100.0	--	--	--	--
19	88	339	144	--	--	--	--	100.0	--	--	--	--
20	44.4	339	144	--	--	--	--	100.0	--	--	--	--
21	614	15	1.01	Air as in chapter 3								
22	529.63	COT 1439.4	17.61	--	--	0.02	--	18.6	0.64	73.9	6.78	--
		TIT 1633.2		--	--	--	--	--	--	--	--	--
		TIT_{iso}1532.2		--	--	--	--	--	--	--	--	--
23	665	597	1	--	--	--	--	15.3	0.7	74.6	9.4	--
24	665	115	1	--	--	--	--	15.3	0.7	74.6	9.4	--
25	170.4	557.4	133.9	--	--	--	--	100	--	--	--	--
26	130.3	559.1	44.28	--	--	--	--	100	--	--	--	--
27	117.6	32.17	0.048	--	--	--	--	100	--	--	--	--

8.5.2 MEMBRANE AND CO_2 FEEDING: HYBRID CASE

As aforesaid, the hybrid feeding does not imply any substantial modification to the lay-out. The main difference compared to the previously discussed case is in the feeding and filter cleaning for the gasification section: in this case, N_2 is the fuel carrier while candle filters are cleaned with CO_2. This configuration allows reducing the inert concentration in the syngas and simultaneously keeping unchanged the feeding system. There are no technology

limits and CO_2 venting during the charging process. The resulting amount of nitrogen for lock-hoppers is 0.444 kg_{N2}/kg_{coal} while the CO_2 for filters is 0.234 kg_{CO2}/kg_{coal}.

The calculated syngas composition at scrubber outlet was determined keeping the results composition at the outlet of the syngas cooler (see chapter 4), then assuming that all the CO_2 for candle filters ends in the syngas.

The adoption of CO_2 for candle filters increases the CO_2 purity at membrane outlet from 75.7% to 80.8% (on dry basis). The CO_2 purity is not high enough to perform an oxy-combustion; the cryogenic separation system is therefore adopted. Because of the lower diluent concentration, the CO_2 purity and CO_2 capture increase compared to the pure N_2 feeding: 98.0 and 93.3% vs. 97.4 and 90.1 respectively.

The hybrid feeding configuration has significant impact on the membrane module working conditions, since feeding composition is different from both cases with conventional feeding and CO_2 feeding.

Only the case with 90% HRF was investigated because it was the optimum for the two previous configurations; different feed pressures were also evaluated.

8.5.3 MEMBRANE AND CO_2 FEEDING: RESULTS

Similarly to the nitrogen feeding case, several sensitivity analyses on main membrane operating conditions were performed in order to optimize the plant. Three different hydrogen recovery factor (HRF) were investigated to outline its influence over electric efficiency and CO_2 capture ratio. The feed pressure was varied from 37 bar to 54 bar. Overall results are reported in Table 8-7. The same considerations reported for nitrogen case comparing the membrane plants with no capture IGCC can be applied to CO_2 feeding cases. Anyway, it can be stressed that: i) the steam cycle power increases, most of all at low HRF, because of the oxy-combustion steam boiler and ii) all nitrogen is adopted as sweep gas increasing the sweep compressor consumption.

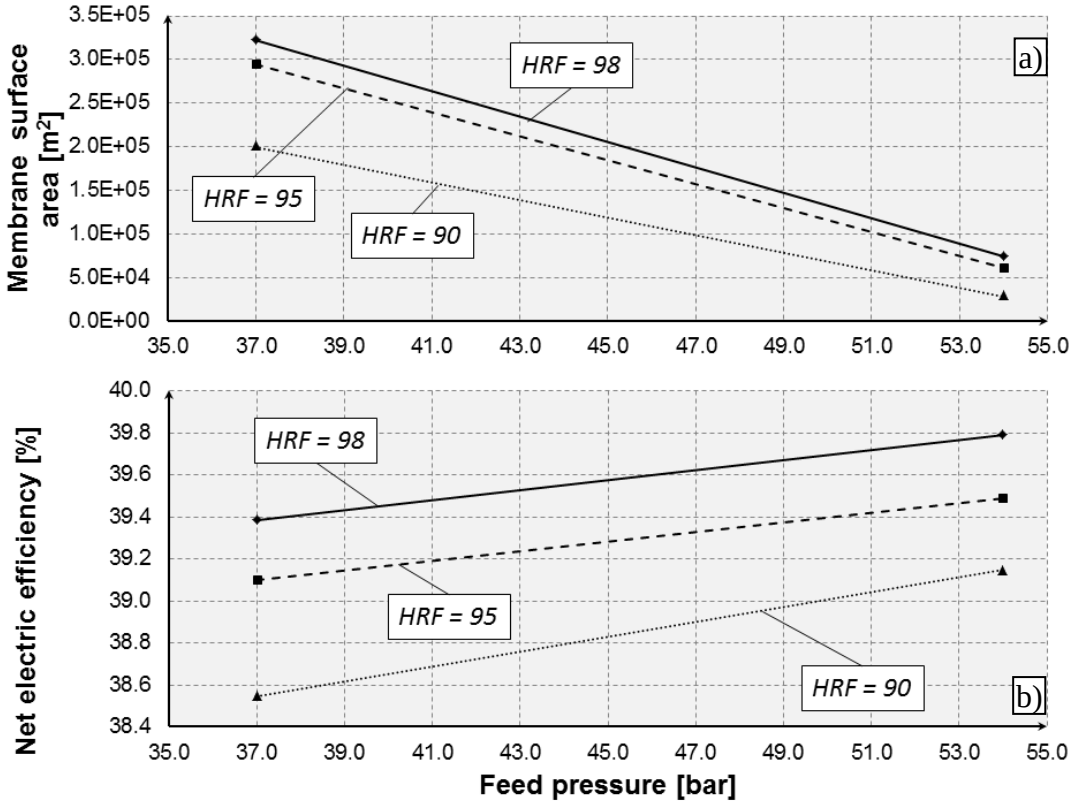

Figure 8-18: a) membrane area as function of different feed pressure for HRF equal to 90, 95 and 98%. b) Net electric efficiency of the overall plant as function of the feed pressure and for HRF equal to 90, 95 and 98%. All cases are based on Pd/Rectisol configuration and CO_2 fed gasifier.

Results show that efficiency penalty for membrane cases is between 7% and 8% with lowest penalties at higher HRF and higher feed pressure. HRF positively affects system efficiency because more hydrogen is converted in a combined cycle rather than in a steam cycle. On the other side, the membrane surface area moving from 90% to 98% increases of more than 200% with economic penalties. At higher feed pressure, the heat recovery after retentate combustion is more efficient, boosting system performances, and the membrane area can be reduced of about 75%. Efficiency and membrane surface area trends are shown in Figure 8-18.

Higher pressure than 54 bar was not considered since it would have required major plant variations. Moreover, the WGS steam would have to be bled before the HP turbine outlet strongly penalizing the plant efficiency. As for the previous case, the adoption of three membranes in series reduces the membrane surface area (membrane surface area reduces by 60% assuming three membranes in series instead of two). For this reason, only this configuration is discussed. The surface reduction depends on the higher H_2 partial pressure and higher turbulence in the tubes. However, in this case, the additional WGS has higher benefits from H_2 partial pressure point of view because of the higher CO content at membrane inlet compared to nitrogen feeding case (5.25% vs 4.45%).

Hence, in this case the adoption of three membrane modules in series has significant benefits with the only drawback of additional pressure drops of about 1 bar at feed side; this will slightly increase the CO_2 compression work; the resulting net electric efficiency is only

0.03% lower than the case with two membrane modules. Sintef model predicts permeate pressure drops below 1kPa, so they can be neglected.

Focusing on CO_2 emissions and CO_2 avoidance, it can be noted that the improvement of the coal feeding technology is necessary. At current feeding performances, the CO_2 avoidance is in the range of 70%: this result does not fulfil capture target which is usually above 85%-90%. On the contrary, an optimal feeding situation where all the CO_2 adopted as fuel carrier is recovered would result in CO_2 avoidance close to 100%. Considering the very high capture ratio which can be achieved, this option must be considered.

Compared to reference case for CO_2 capture (Selexol), membrane achieves a higher efficiency (up to 3% points), while for the CO_2, Selexol achieves 87% which is exactly in the middle of the membrane case.

About CO_2 purity, it increases with the HRF (96.1% at 90% HRF vs.96.4% at 98% HRF): at higher HRF, less oxygen is required for retentate purification, thus less amount of inert is mixed with the CO_2.

Compared to the conventional case with nitrogen feeding, where the SPECCA was in the range of 2.5-2.6 MJ/kg_{CO2}, the case with hybrid configuration guarantees a high efficiency but it is penalized for the CO_2 avoidance. This is because the CO_2 content in the feed is higher, hence a larger amount is vented in the AGR process and in the cryogenic separation process as well. At higher pressure, the difference reduces, because of the higher CO_2 recovery in the cryogenic separation systems. From these results, it can be noted that the hybrid configuration would have very limited advantages compared to the conventional nitrogen feeding.

Table 8-7: energy balances for membrane integration in CO_2 and hybrid fed gasifier. Data are reported for different HRF (90, 95, 98%) and feed pressure (37, 47, 54 bar).

			CO_2 feed						**Hybrid feed**	
AGR			Rectisol						Rectisol	
HRF			90		95		98		90	
Feed pressure		[bar]	37	54	37	54	37	54	37	54
Gas Turbine		[MW]	308.6	308.3	315.7	315.7	319.7	319.9	320.7	320.5
HRSC gross power		[MW]	228.9	235.1	198.0	202.3	180.3	184.4	172.7	174.6
Expander ASU		[MW]	12.3	12.3	10.9	10.9	10.2	10.2	9.7	9.8
Coal handling		[MW]	-2.1	-2.1	-2.0	-2.0	-1.9	-1.9	-1.9	-1.9
Ash handling		[MW]	-0.6	-0.6	-0.6	-0.6	-0.6	-0.6	-0.6	-0.6
AGR sulfur adsorption		[MW]	-4.9	-4.9	-4.6	-4.6	-4.5	-4.5	-4.4	-4.4
N_2 compression LH		[MW]	--	--	--	--	--	--	-9.5	-9.5
N_2 sweep compressor		[MW]	-60.0	-59.8	-53.6	-53.6	-49.7	-49.7	-40.6	-40.6
ASU + O_2 compression		[MW]	-32.7	-32.7	-29.2	-29.2	-27.2	-27.2	-25.9	-26.0
HRSC auxiliaries		[MW]	-3.4	-2.0	-3.1	-1.9	-2.9	-1.8	-2.7	-2.1
Blower		[MW]	-1.1	-1.1	-1.0	-1.0	-1.0	-1.0	-1.2	-1.2
CO_2 compressor		[MW]	-8.5	-3.7	-8.1	-3.6	-7.9	-3.4	-10.3	-10.1
Feed compression		[MW]	--	-5.6	--	-5.3	--	-5.2	-2.2	-4.1
BOP		[MW]	-2.6	-2.9	-2.4	-2.3	-2.3	-2.4	-1.6	-2.1
Aux. for heat rejection		[MW]	-3.7	-3.7	-3.3	-3.3	-3.0	-3.1	-2.4	-2.4
Net Power Output		[MW]	430.1	436.7	416.8	421.4	409.1	400.0	400.0	400.0
Thermal Power Input$_{LHV}$		[MW]	1111.2	1111.2	1062.0	1062.0	1035.0	1025.1	1026.6	1025.1
Efficiency$_{LHV}$		**[%]**	**38.6**	**39.2**	**39.2**	**39.5**	**39.4**	**39.3**	**39.0**	**39.0**
Optimistic	Emissions	[g_{CO2}/kWh_{el}]	20.1	20.6	20.7	20.5	20.5	20.6	184.4	177.9
	CO_2 avoided	[%]	97.1	97.19	97.18	97.21	97.23	97.18	74.8	75.7
	SPECCA	[MJ_{LHV}/kg_{CO2}]	**2.50**	**2.19**	**2.20**	**2.07**	**2.11**	**2.19**	**2.90**	**2.89**
Actual	Emissions	[g_{CO2}/kWh_{el}]	219.9	216.5	216.8	214.7	215.2	216.6	--	--
	CO_2 avoided	[%]	70.0	70.43	70.39	70.68	70.60	70.41	--	--
	SPECCA	[MJ_{LHV}/kg_{CO2}]	**3.3**	**3.02**	**3.04**	**2.85**	**2.90**	**3.03**	--	--

8.6 CONCLUSIONS

From thermodynamic point of view, hydrogen membranes are a promising solution for CO_2 capture plant in IGCC plants. The computed efficiency and SPECCA are very high in each developed configuration. Carbon capture avoided ranges between 85-95% depending on the feeding technology and the efficiency of the purification process. Provided the good thermodynamic performances, the membrane area become the most effective evaluating parameters. It was found that membrane area features huge variations depending on the type of membrane and the operating conditions adopted. Pd-alloy membrane does not harness its sulfur tolerance in conventional Selexol process. Both in nitrogen- or CO_2-based gasifier, the pure Pd membrane requires low HRF and high feed pressure in order to limit as much as possible the surface. Nevertheless, the required area is still large.

The new configuration developed with post-firing results to be the most promising because of the higher efficiency and lower membrane area. Economic figures in chapter 9 will confirm this.

Pd-alloy and HGD is a promising solution for long-term application because both the technologies requires more R&D.

Finally, CO_2-based gasifier can be an innovative solution, most of all if combined with HRSG post-firing as for the nitrogen case. This will be addressed in future works.

REFERENCES

[1] **Beavis, R.** The EU FP6 Cachet Project - Final results. *Energy Procedia 4.* 2011. pp. 1074-1081. 10.1016/j.egypro.2011.01.157.

[2] **Bredesen, R., Jordal, K. and Bolland, O.** High-temperature membranes in power generation with CO2 capture. *Chemical Engineering and Processing: Process Intensification.* 2003. Vol. 43, 9, pp. 1129-1158. 10.106/j.cep.2003.11.011.

[3] **Jordal, K., et al.** Integration of H2-separating membrane technology in gas turbine process for CO2 capture. *Energy.* 2004. Vol. 29, pp. 1269-1278. 10.1016/j.energy.2004.03.086.

[4] **Mejdell, A.L., et al.** Performance and application of thin Pd-alloy hydrogen separation membranes in different configurations. *Journal of the Taiwan Institute of Chemical Engineers.* 2008. Vol. 3, 40, pp. 253-259. 10.1016/j.jtice.2008.12.013.

[5] **Manzolini G, Dijkstra JW, Macchi E, Jansen D.** Technical Economic Evaluation of a system for electricity production with CO2 capture using membrane reformer with permeate side combustion. 2006.

[6] **Manzolini, G. and Viganò, F.** Co-production of hydrogen and electricity from autothermal reforming of natural gas by means of Pd-Ag membranes. *Energy Procedia.* 2009. Vol. 1, pp. 319-326. 10.1016/j.egypro.2009.01.044.

[7] **Kulprathipanja, A., et al.** Pd and Pd-Cu membranes: inhibition of H2 permeation by H2S. *Journal of Membrane Science.* 2005. Vol. 254, pp. 49-62.

[8] **Peters, T.A., Kaleta, T. and Bredesen, R.** Inhibition of hydrogen transport through a selection of thin Pd-alloy membranes by H2S: membrane stability and flux recovery in H2/N2 and WGS feed mixtures. *Catalysis Today.* 2012. 193, pp. 8-19.

[9] **Song, B. and Forsyth, J.A.** Cachet II: Carbon capture and hydrogen production with membranes. *Energy Procedia, proceedings of the GHGT 11.* Kyoto : s.n., 2012.

[10] **van Berkel, F., et al.** Pd-membranes on their way towards application for CO2 capture. *Energy Procedia, proceeding of the GHGT 11.* Kyoto : s.n., 2012.

[11] **Manzolini, G., et al.** *Cachet2: Deliverable 4.2 - Base case report.* 2011.

[12] **European Benchmark Task Force.** European best practice guide for assessment of CO2 capture technologies. 2011. Vol. http://www.energia.polimi.it/news/D%204_9%20best%20practice%20guide.pdf.

[13] **Chiesa P, Campanari S, Manzolini G.** CO2 cryogenic separation from combined cycle integrated with molten carbonate fuel cells. s.l. : Internatonal Journal of Hydrogen Energy . Vol. 2011, In press. DOI: 10.1016/j.ijhydene.2010.09.068.

[14] **Manzolini G, Campanari S, Chiesa P, Giannotti A, et. al.** CO2 separation from combined cycle using molten carbonate fuel cells. *Submitted to ASME Fuel Cell Science, Engineering and Technology conference 2011.*

[15] **Korens, N., Simbeck, D. and Wilhelm, D.** *Process screening analysis of alternative gas treating and sulfur removal for gasification.* s.l. : SFA Pacific, 2002. prepared for US Department of Energy.

[16] **Politecnico di Milano.** D4.2 Base case report. *CACHET II Project.*

[17] **Mark Prins, Shell employee, personnal communication, March 2010.**

[18] **Politecnico di Milano.** Software presentation: GS (Gas-Steam Cyckes). *http://www.gecos.polimi.it/software/gs.html.* [Online] 2009. [Riportato: 8 January 2010.]

[19] **Aspentech Documentation.** Aspen Physical Property System. *V 7.2.*

[20] **Gazzani M, Manzolini G, Macchi E, Ghoniem A.F.** Reduced order modeling of the Shell-Prenflo entrained flow gasifier. *Fuel, in press.* 2012.

9 ECONOMICS OF SEWGS AND H_2 MEMBRANES

Nomenclature and Acronyms

ATR: Autothermal Reformer
CAESAR:CArbon-free Electricity by SEWGS: Advanced materials, reactor and process design
CCR: CO_2 Capture Ratio
COE: Cost of Electricit
EBTF: European Benchmarking Task Force
EPC: Engineering, Procurement and Construction cost
GHR: Gas Heated Reformer
GT: Gas Turbine
HRSG: Heat Recovery Steam Generator
HTS/LTS: High Temperature Shift/Low Temperature Shift
MDEA: N-Methyldiethanolamine
MEA: Monoethanolamine
NG: Natural Gas
NGCC: Natural Gas Combined Cycle
NOAK: N^{th} Of A Kind
O&M: Operation and Maintenance
SEWGS: Sorption Enhanced Water Gas Shift
SPECCA: Specific Primary Energy Consumption for CO2 Avoided
TDPC: Total Direct Plant Cost
TEC: Total Equipment Cost
TIT: Turbine Inlet Temperature
TITiso: Turbine Inlet Temperature (defined according to ISO standard)
TOT: Turbine Outlet Temperature
TOP: Turbine Outlet Pressur
WGS: Water Gas Shift reactor
η: Efficiency

9.1 ECONOMIC ASSESSMENT METHODOLOGY

The template for the economic assessment methodology is the EBTF work [1]. Transport and storage costs are not taken into account in this analysis since they do not depend on the capture technique. For the considered plant sizes, that are relatively large (the flow rates of captured CO_2 are about 250 t/h), reference costs for transport and storage are in the range of 1-4 $/t$_{CO2}$ and 6-13 $/t$_{CO2}$, respectively. The variation depends on power plant distance from the storage site and the considered storage site [2].

The Cost of Electricity (COE) is calculated using IEA models by setting the net present value (NPV) of the power plant to zero [3] [4]. This can be achieved by varying the plant COE until the revenues balance the cost over the whole life time of the power plant.

An economic analysis will be also presented for all the reference cases with and without carbon capture discussed in a Chapter 3.

The required investment including fixed and variable O&M costs are derived from various references: most of the data are taken from EBTF work and they are consistent with the reference cases. Components which are not part of the EBTF assessment (e.g. SEWGS) are taken from literature or calculated by dedicated software (ThermoFlow™ [5] and Aspen™ [6]). Pre-combustion technology cases have fewer references, mainly because of higher uncertainties in component costs.

9.1.1 TOTAL PLANT COST ASSESSMENT

Total plant costs are calculated with the so-called Bottom-Up Approach (BUA) which consists of breaking down the power plant into basic components or equipment, and adding installation and indirect costs. This approach is a general one since it can be applied to any power plant but requires a reference equipment cost for each considered item. The reference can come from the supplier, literature or can be calculated through dedicated tools.

The first step consists of calculating the Total Direct Plant Costs (TDPC) which are the sum of the bare equipment costs and the corresponding installation costs such as piping, erection, outside battery limits, etc.. TDPC plus the Indirect Costs (IC), calculated as a percentage of the direct plant costs, leads to Engineering, Procurement and Construction costs (EPC). Finally, the Total Plant Cost (TPC), which results from EPC plus owner's cost and contingencies, is calculated.

The individual installation costs are calculated as a percentage of the corresponding equipment one. A rigorous methodology usually implies the adoption of dedicated coefficients for each item and plant component. However, this approach would require many arbitrary assumptions and could cause misleading results when applied to different, unconventional power plants. For this reason, only two coefficients for installation costs are applied depending on plant component: CO_2 capture section/hydrogen island and power section. This is because the formers are more similar to chemical plants requiring higher installation costs, while power section installation costs are typical of NGCC and equal to 68% of the TDPC. This number is calculated as a weighted average from coefficients adopted in [7]. For installation costs in CO_2 capture section/hydrogen islands, they are increased and assumed equal to 80% of the TDPC.

Total plant costs aggregate and other coefficient adopted are shown in Table 9-1.

Table 9-1: total plant costs assessment methodology.

Plant Component		Example
XXXXXXX		A
WWWWW		B
YYYYYYY		C
ZZZZZZZ		D
TOTAL EQUIPMENT COST [TEC]		A+B+C+D
Direct costs as percentage of the total equipment costs (TEC)		
Piping/valves, Civil Works, Instrumentation, steel-structure, Erection, etc.	XY%	XY% TEC
Total Installation Costs [TIC]	**XY%**	XY% TEC
TOTAL DIRECT PLANT COSTS [TDPC]		TEC + TIC
Indirect costs [IC]	14%	14% TDPC
Engineering Procurement and Construction [EPC]		**TDCP+IC**
Contingencies and owner's costs (C&OC)		
Contingency	10%	10% EPC
Owner's cost	5%	5%EPC
TOTAL CONTINGENCIES&OC [C&OC]	**15%**	**15% EPC**
TOTAL PLANT COST [TPC]		**EPC+C&OC**

For each component/subsystem, a scaling parameter was selected and the actual erected cost C was derived from the cost C_0 of a reference component of size S_0 by the relationship:

$$C = nC_0 \left[{}^{S}/_{nS_0} \right]^f \tag{9-1}$$

Where S is the actual size and f is the scale factor. The coefficient n refers to the number of components for the base case.

Contingencies equal to 10% are representative of a mature technology or a n^{th}-of-a-kind plant (NOAK). The cost of electricity of a first-of-a-kind plant is usually significantly higher as a consequence of additional contingency costs which are in the range of 30-40%. The aim of this chapter is to compare SEWGS and membranes when they are mature technologies and see whether they are competitive or not, thus as NOAK.

The conversion factor (€/US$) adopted for values originally given in US$ was 1.25 and currency refers to 2008 value, on grounds of IHS CERA Power capital cost (recommended by

Gas Turbine World for power plant cost assessment, [8]) as reported in [9]. Economic assessment is dated 2008 as agreed within EBTF.

Bottom-Up-Approach (BUA) is adopted for all cases, even ASC, in order to have a consistent comparison. It must be outlined that in preliminary studies, the resulting specific costs of ASC determined with BUA was lower than Top-Down-Approach (TDA) [1]. The Total Plant Cost assessment for ASC will not be presented in detail: further details can be found in [1].

9.1.2 COAL O&M AND CONSUMABLE COSTS

Cost assumptions about fuel, Operation and Maintenance (O&M) and consumables are summarized in Table 9-2.

Table 9-2: O&M and consumable costs [1].

Natural Gas Costs	€/GJ_{LHV}	6.5
Coal Costs	€/GJ_{LHV}	3
O&M Natural Gas		
Labour costs, no capture case	M€	6
Labour costs, capture case	M€	9
Maintenance costs	% of Total plant cost	2.5
Insurance	% of Total plant cost	2
O&M Coal		
Labour costs, ASC case w/o capture	M€	8
Labour costs, ASC case with capture	M€	12
Labour costs for IGCC cases	M€	8.9
Maintenance	% of Total plant cost	1
Insurance	% of Total plant cost	1
Consumables		
Evaporative tower blow-off	% of evaporated water	100
Cooling water make-up costs	€/m^3	0.35
HRSG water blow-off	% of steam produced	1
Process water costs	€/m^3	2
MEA make-up,	kg_{MEA}/t_{CO2}	1.5
MEA make-up costs,	€/t_{MEA}	1042
Catalyst replacement		
Reforming catalyst lifetime	Years	5
Reforming catalyst cost	k€/m^3	50
Water Gas Shift lifetime	Years	5
Water Gas Shift cost	k€/m^3	14

Labor costs refer to an average European social environment. For maintenance and insurance costs, the approach was taken from IEA [3] [4] and coefficients were corrected according to EBTF figures.

9.1.3 EQUIPMENT COSTS DATABASE

The specific gas turbine equipment cost for the NGCC reference plant is calculated as an average of PG9351 (FA) and SGT5-4000F models price per kW given in Gas Turbine World Handbook [10]. For the scale up factor, considering the assumption of constant mass flow rate exhaust gases, all the gas turbines investigated in this work have the same size; the only difference is related to the generator power output. For this reason, a relatively low scale factor of 0.3 is assumed. Costs related to combustor modifications required by syngas compositions are neglected.

Most of the other data used for power section total investment cost calculation are derived from results presented by DOE [7], recently updated adopting a cost index variation and are consistent with EBTF public report on economic assessment [1]. The equipment costs database is summarized in Table 9-3.

Table 9-3: costs of the reference equipments

Plant Component	Scaling Parameter	Reference Erected Cost C_0 (M€)	Reference Size, S_0	Scale factor f	N
Power Plant Components					
Gas turbine, generator and auxiliaries, [7] [10]	$GT_{\text{Net Power}}$ [MW]	49.4	272.12	0.3	2
HRSG, ducting and stack, [7] [10]	U*S [MW/K]	32.6	12.9	0.67	2
Steam turbine, generator and auxiliaries, [7] [10]	$ST_{\text{Gross Power}}$ [MW]	33.7	200.0	0.67	1
Cooling water system and BOP, [7]	Q_rejected [MW]	49.6	470.0	0.67	1
Gasification Components					
Gasifier, [1]	Thermal input [MW]	90.0	828.0	0.67	1
Syngas cleaning and auxiliaries [1]	Thermal input [MW]	3.84	828.0	0.67	1
Air separation Unit (ASU) [1]	Oxygen produced [kg/s]	26.6	28.9	0.7	1
Ash handling [1]	Ash flow rate [kg/s]	4.7	9.7	0.6	1
Coal handling, [1]	Coal input [kg/s]	27.5	32.9	0.67	1
Water treatment [1]	Coal input [kg/s]	10.7	32.9	0.67	1
Desulfurization and gas treating					
NG Zinc Oxide desulfurization process	Thermal input LHV [MW]	0.66	413.82	0.67	4
Acid Gas Removal (Selexol) [1]	Coal input [kg/s]	12.0	32.9	0.67	1
Acid Gas Removal (Rectisol)	Coal input [kg/s]	13.2	32.9	0.67	1
H_2S catalytic combustion/Flue Gas Desulphurization (FGD)	Volumetric Flowrate [m^3/s]	48.6	745	1	1
Claus [1]	Sulphur flow rate [kg/s]	8.0	0.2	0.67	1
Oxycombustor	Thermal power [MW]	1.29	3	1	1
GHR-ATR and Water Gas Shift					
Gas Heated Reformer- Auto Thermal Reformer (GHR-ATR)	Thermal input LHV [MW]	As described in [11]			
Sour water gas shift reactors [1]	Thermal input [MW]	11.7	954.1	0.67	2

High Temperature shift + Low Temperature Shift (HTS+LTS)	Thermal power input LHV	3.71	815.2	0.67	2
High Temperature Shift (HTS)	Thermal power input LHV	3.33	827.6	0.67	2
CO_2 separation					
MEA CO_2 separation system, [12]	CO_2 captured [kg/s]	29.0	38.4	0.8	2[a]
MDEA CO_2 separation system	CO_2 captured [kg/s]	68.2	46.14	0.8	2
Selexol CO_2 separation system [1]	CO_2 captured [kg/s]	28.1	69.4	0.8	1
Sorption Enhanced Water gas Shift (SEWGS)	N° of trains	8.74	1	1	-
Membranes	Membrane area, m^2	5.8	1000	1	1
Heat recovery and Heat exchangers					
Waste heat boiler	Heat exchanged [MW]	1.8	57.2	0.9	2
High temperature HE	Heat exchanged [MW]	1.0	10.0	0.8	1
Low temperature heat recovery (LTHR) [1]	Thermal input [MW]	6.1	828.0	0.67	1
Saturator	Thermal input [MW]	0.20	828.0	0.7	1
Low temperature HE	Heat exchanged [MW]	1.0	10.0	0.8	1
Turbo-machineries					
CO_2 intercooled compressor and condenser, [12]	Compressor power [MW]	9.9	13.0	0.67	1
Nitrogen compressor for dilution [1]	Compressor power [MW]	14.8	47.6	0.67	1
Air blower [7] [10]	Compressor Power [MW]	14.77	47.61	0.67	1
Expander [7]	Expander power	33.7	200	0.67	2

[a] The adoption of two GT and two HRSG requires two separated carbon capture system, one for each HRSG.

SEWGS and membranes costs were set in CAESAR and CACHET-II projects, respectively; the large experience in energy-chemical plants of the industrial partner makes the estimates reliable.

For the air compressor, a conservative specific cost of an axial air compressor was assumed even if, considering the low pressure ratio and volumetric flow, it would probably be a radial type, and consequently less expensive.

The expander specific cost was set equal to the steam turbine, because of the similar working conditions in terms of pressure and temperature.

9.1.4 COST OF ELECTRICITY AND CO_2 AVOIDED CALCULATION

As anticipated, the aim of the economic assessment is to make an estimation of the final cost of electricity (COE).

The time required for power plant construction, also for carbon capture cases, is assumed to be 3 years for NG plant and 4 years for coal plant.

The main economic assumptions for natural gas and coal are reported in Table 9-4 and Table 9-5, respectively.

Table 9-4: main economic assumptions for Natural Gas economic assessment [1]

Discount rate, %	8
First year operating hours, h	5700
Rest of lifetime operating hours, h	7500
Operating lifetime, years	25
Construction time, years	3

Table 9-5: main economic assumptions for coal economic assessment [1]

Discount rate, %	8
First year operating hours, h	3500
Second year operating hours, h	5700
Rest of lifetime operating hours, h	7500
Operating lifetime ASC, years	40
Operating lifetime IGCC, years	25
Construction time, years	4

The assumed operating hours per annum are typical of early 2000, where large scale fossil fuel power plant worked predominantly at base load, with hydro-power and small scale plants as peak-load. Recently, because of the increasing penetration of non-dispatchable renewable energy generation, this value has significantly decreased. However, it is difficult to predict what the future will be and if power plant with CO_2 capture will be assimilated to green-energy sources or not[1].

The cost of CO_2 avoided is defined as:

$$Cost\ of\ CO_2\ avoided = \frac{(COE)_{CO2\ cap} - (COE)_{ref}}{(CO_2 kWh^{-1})_{ref} - (CO_2 kWh^{-1})_{CO2\ cap}} \quad (9\text{-}2)$$

Where Ref is the power plant without carbon capture and CO_2 cap is the plant with carbon capture.

[1] Plants with CO_2 capture have limited emissions and reduced impact on the environment; for this reason, they are closer to renewable energy rather than conventional fossil fuel power stations. However, at present time, no plant has ever been built and there is no directive and/or law on this subject.

9.2 SEWGS ECONOMIC ANALYSIS

9.2.1 NATURAL GAS PLANT

This section presents the economic assessment of SEWGS integrated in natural gas plants previously presented. As done in chapter 7, firstly *Sorbent Alfa* cases are discussed, then *Sorbent Beta* is considered.

Estimated cost of a SEWGS train, which is composed of 9 vessels, is 8.7 M€ based on previous studies carried out in CCP [13]. For the adopted configuration with two GT, eight trains are necessary for the Sorbent Alfa, while it can be reduced to six for Sorbent Beta (a detailed description of these sorbents and explanation on the number of vessel are given in chapter 7). The resulting total capital requirement and specific cost is summarized in Table 9-6.

Table 9-6: total capital requirement (M€) calculation for reference and SEWGS cases in natural gas plant

	NGCC reference	NGCC MEA	NGCC MDEA	SEWGS Case 1	SEWGS Case 2	SEWGS Case 3	SEWGS Case 4	SEWGS Case 5
				Cost [M€]				
Desulfurizer	-	2.4	2.6	2.5	2.5	2.5	2.5	2.5
GHR-ATR/ATR	-	-	29.3	27.7	27.7	27.7	27.7	27.7
WGS HTS+LTS	-	-	11.2	-	-	-	-	-
HTS	-	-	-	6.4	6.4	6.4	6.4	6.4
MEA	-	56.7	-	-	-	-	-	-
MDEA	-	-	132.2	-	-	-	-	-
SEWGS	-	-	-	69.6	69.6	69.6	69.6	69.6
Gas Turbine	98.8	98.8	101.2	99.3	99.1	99.0	99.4	99.2
HRSG	45.7	44.8	59.7	51.4	51.6	52.8	51.5	52.1
Steam Turbine	43.2	35.1	44.2	39.9	38.2	36.0	39.5	37.8
Heat rejection	49.4	54.9	55.1	54.8	52.8	55.4	54.8	55.1
CO_2 compressor	-	14.4	17.0	22.1	22.8	23.3	22.0	22.8
Air Blower	-	-	7.9	6.2	6.2	6.2	6.2	6.2
CO_2+Steam Exp.	-	-	-	16.7	19.4	22.5	17.0	19.7
Heat Exchangers	0.3	0.3	6.0	5.6	5.8	5.7	5.9	5.9
BOP	0.1	0.1	4.5	1.7	1.7	1.7	1.8	1.8
TEC, [M€]	**237.5**	**307.4**	**468.3**	**404.1**	**406.3**	**409.0**	**404.6**	**407.0**
TIC, [M€]	161.5	217.8	342.5	292.9	294.9	297.1	293.3	295.3
TDPC, [M€]	**399.0**	**525.2**	**810.7**	**697.0**	**701.2**	**706.2**	**697.8**	**702.3**
Indirect cost, [M€]	55.9	73.5	113.5	97.6	98.1	98.9	97.7	98.3
EPC, [M€]	**454.9**	**598.7**	**924.2**	**794.6**	**799.4**	**805.0**	**795.5**	**800.6**
C&OC, [M€]	68.2	89.8	138.6	119.2	119.9	120.8	119.3	120.1
Total plant cost, [M€]	**523.1**	**688.5**	**1062.9**	**913.8**	**919.3**	**925.8**	**914.9**	**920.7**
Net power Output, [MW]	829.9	709.92	830.0	795.41	786.99	779.20	795.47	786.9
Specific costs, [€/kW]	**630.4**	**969.9**	**1280.6**	**1148.7**	**1168.1**	**1188.1**	**1150.1**	**1170.1**

Specific investment costs for capture plant are significantly higher than reference NGCC without capture. In particular, they range from 54% of MEA and 100% of MDEA; SEWGS

cases are between these two figures. Higher investment costs of MEA than NGCC are mainly due to CO_2 capture island (80%) and to CO_2 compressor (20%). It must be outlined that assumed cost for MEA, taken from EBTF work, seems to be on the optimistic side compared to other references (e.g. another EU project named DEMOYS indicated a specific investment cost of 1100 €/kW compared to 970 €/kW given here). Most of the MDEA reference case additional costs are due to the capture section which accounts for 28% of the total plant cost.

In SEWGS cases, TEC increases about 80% compared to NGCC, half of which depends on SEWGS process costs. This assessment shows that SEWGS equipment cost in NG applications looks as expensive as amine scrubbing, thus reducing advantages of this technology from an investment point of view.

Finally, the adoption of CO_2-steam expansion accounts for 20 M€ plus 5 M€ for a larger CO_2 compressor. Cost of Electricity will indicate if these additional costs are more than balanced by the higher efficiency and consequently lower fuel costs. Calculated cost of electricity for SEWGS and reference cases are summarized in Table 9-7.

Table 9-7: Cost of Electricity and Cost of CO_2 avoided for SEWGS and reference cases in natural gas plant

Plant Component	NGCC ref	NGCC MEA	NGCC MDEA	SEWGS Case 1	SEWGS Case 2	SEWGS Case 3	SEWGS Case 4	SEWGS Case 5
SEWGS CCR/CO_2 purity	-	-	-	90/98	95/98	98/98	90/99	95/99
Net Power Output, [MW]	829.9	709.7	830.0	795.4	787.0	779.2	795.5	791.3
Thermal Power Input$_{LHV}$, [MW]	1422.6	1422.6	1651.0	1555.3	1551.9	1550.1	1555.5	1552.1
Net Electric Efficiency$_{LHV}$ [%]	58.34	49.90	50.30	51.14	50.72	50.27	51.14	50.70
CO_2 avoided, [%]	-	88.3	91.5	85.7	91.1	94.3	85.7	91.1
SPECCA [MJ_{LHV}/kg_{CO2}]	**-**	**3.36**	**3.07**	**2.88**	**2.90**	**2.99**	**2.88**	**2.90**
Investment cost, [€/MWh]	9.55	15.59	19. 89	17.68	18.05	18.42	17.70	18.08
Fixed O&M costs, [€/MWh]	3.85	5.24	7.31	6.49	6.52	6.55	6.49	6.52
Consumables, [€/MWh]	0.59	1.38	1.39	2.08	2.11	2.14	2.08	2.11
Fuel costs, [€/MWh]	40.11	46.89	46.55	45.76	46.14	46.55	45.76	46.16
COE, [€/MWh]	**54.10**	**69.10**	**74.63**	**72.01**	**72.82**	**73.66**	**72.03**	**72.87**
Cost of CO_2 avoided [€/t_{CO2}]	**N/A**	**47.5**	**63.8**	**59.4**	**58.4**	**59.0**	**59.5**	**58.6**

The resulting levelized cost of electricity for NGCC without CO_2 capture is 54.10 €/MWh. As shown in Table 9-7, most of COE depends on fuel costs (as typical of NG based power plants), while the sum of fixed and variable costs accounts for less than 10%. In CO_2 capture case, COE increases by 15-20 €/MWh as a consequence of the higher investment costs and lower efficiency which leads to higher specific fuel consumption. The calculated cost of CO_2 avoided for MEA and MDEA cases are 47.5 €/t_{CO2} and 63.8 €/t_{CO2} respectively. The cost of CO_2 avoided for the MEA case is lower than similar studies in literature [2] [14] [15] [16], however it can represent amine scrubbing with advanced solution.

Among all investigated SEWGS cases, COE is almost constant and higher than reference NGCC of about 33%. The lowest cost of CO_2 avoided is achieved for Case 2 and Case 5 which have a CO_2 avoidance of about 90% (95% CCR of SEWGS). The reason is that Case 3, which has a higher CO_2 avoidance, is penalized by system efficiency (a higher energy is required to

regenerate the sorbent) which is not balance by the lower emissions. While Case 1 and Case 4 have a lower CO_2 avoidance which is penalized by investment costs: the SEWGS system cost is not influenced by CCR, so its specific costs for CO_2 captured is higher. Since the difference in terms of CO_2 avoided between Case 2 and Case 5 is negligible (0.2 €/t_{CO2}), Case 5, which features 99% CO_2 purity, is the preferred option because of the lower resulting transport and storage costs.

Compared to NGCC with MDEA, SEWGS cases have a lower investment, fixed operating and fuel cost thanks to the higher efficiency; only consumables costs, which are mainly related to sorbent replacement, are higher than MDEA. The resulting cost of CO_2 avoided is about 59 €/t_{CO2}, which is about 7% lower than MDEA. Compared to MEA, SEWGS higher efficiency cannot balance the penalties arising from higher investment costs rising the CO_2 avoidance costs by 12 €/t_{CO2}.

One of the optimization parameters investigated in chapter 7 was the CO_2-steam expander outlet pressure. This analysis is here proposed in terms of COE and cost of CO_2 avoided (see Figure 9-1) showing that the optimal condition occurs for 0.15 bara which coincides with the thermodynamic assessment. Additional investment costs are balanced by the higher efficiency and consequently lower fuel costs.

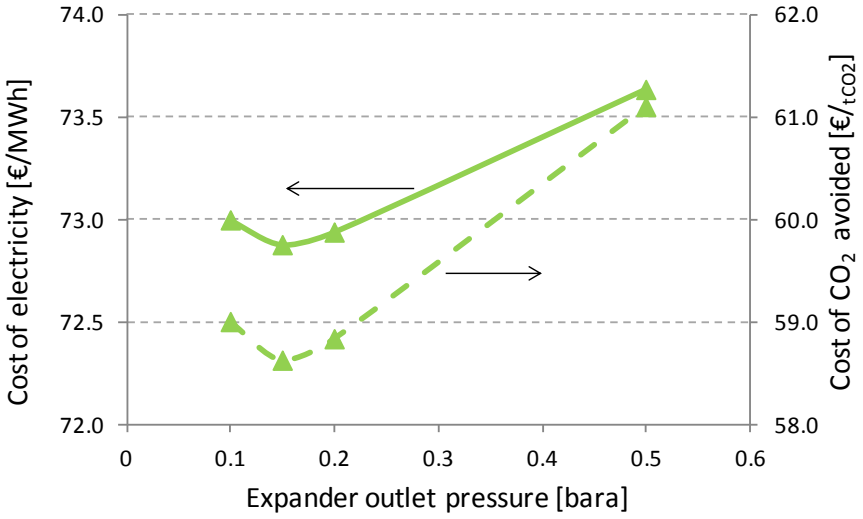

Figure 9-1 – Cost of electricity and Cost of CO_2 avoided as a function of expander outlet pressure for *Sorbent Alfa* with CCR 95% and CO_2 purity 99%; natural gas plant.

To summarize, the assessment of SEWGS in NGCC showed that *Sorbent Alfa* performances has a lower cost of CO_2 avoided than MDEA which belongs to the same capture route. However, *Sorbent Alfa* performances are not competitive with the amine scrubbing technology; higher efficiency of SEWGS configuration is not enough to balance 20% additional investment costs.

For this reason, SEWGS economic assessment was also performed for *Sorbent Beta* which has an improved capacity of 60% more than *Sorbent Alfa* (at 2.7 bara CO_2 partial pressure). First, the same cases as *Sorbent Alfa* are presented to evaluate the impact of thermodynamic advantages on COE (number of vessels equal to 72 and CO_2 purity 99%). Considering the higher capacity, the overall steam usage is reduced by about 80%, thus optimal expander outlet pressure increases from 0.15 bara to 0.3 bara. The calculated results, summarized in Figure 9-2 and Table

9-8, show that the improved capacity of the sorbent can reduce COE and the cost of CO_2 avoided by 1 €/MWh and 5 €/t_{CO2} respectively. These costs are determined keeping the same SEWGS vessel number of *Sorbent Alfa* case, and consequently equipment costs, hence they are only due to the higher efficiency (about 1% points).

Lower specific investment costs result mainly from higher efficiency, but also on lower cost of the CO_2 compressor and CO_2-expander as a consequence of the reduced steam flow-rate and higher pressure at expander outlet and consequently at compressor inlet.

Focusing on the cost of CO_2 avoided, *Sorbent Beta* shows the lowest value for 98% CCR in SEWGS; for *Sorbent Alfa*, the optimum occurred at 95%.

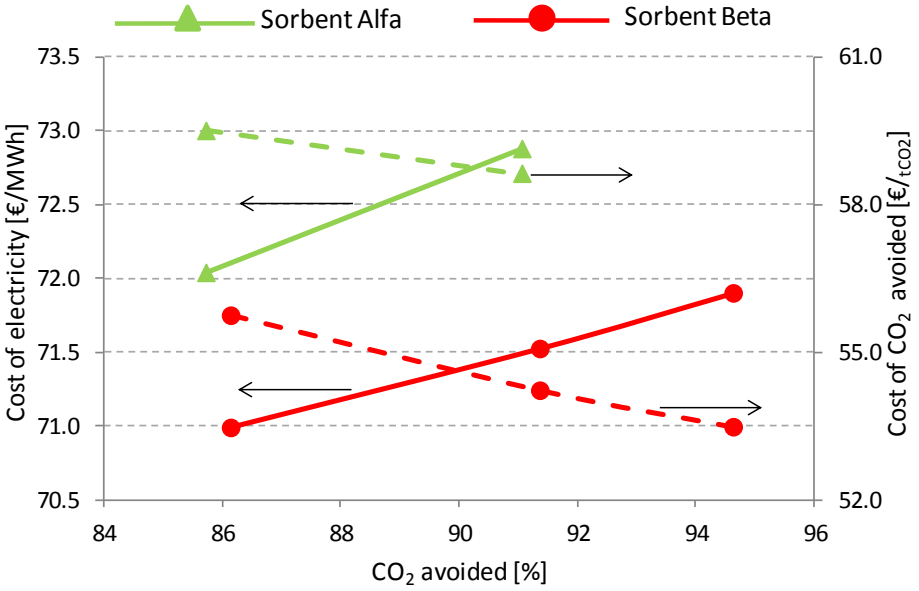

Figure 9-2 – Comparison between *Sorbent Alfa* and *Sorbent Beta* in terms of cost of electricity and cost of CO_2 avoided (CO_2 purity 99%) with 72 vessels; natural gas plant.

A lower number of SEWGS trains (6 vs. 8) was also investigated to determine investment cost reduction on COE. The adoption of a higher capacity allows investigating fewer number of vessels, 6 trains instead of 8, which means 54 vessels vs. 72 with advantages both in terms of efficiency, and investment costs. Results, summarized in Table 9-8, show that a reduced number of vessels allows to achieve a CO_2 avoidance costs of 49 €/t_{CO2} with 95% CCR; this result is very similar to MEA case. Main advantages of 54 vessels compare to 72 vessels case are in terms of investment and consumables cost; these two costs only depend on the SEWGS volume. Another consideration is that the optimum CCR is not 98% as in cases with 72 vessels, but occurs at 95%. This is because the number of vessel reduction requires an exponential increase of the steam to regenerate the sorbent causing higher efficiency penalties. It can be noted that optimum CCR is not easily predictable, since it depends on several parameters.

Table 9-8: comparison between different SEWGS numbers with *Sorbent Beta* in terms of Cost of Electricity and Cost of CO_2 avoided; natural gas plant.

N° of vessels		72			54	
CCR/CO_2 purity	90/99	95/99	98/99	90/99	95/99	98/99
Net Power Output, [MW]	800.0	793.6	790.1	805.3	797.9	790.2
Net electric Efficiency, [%]	51.58	51.27	51.05	51.93	51.55	51.06
CO_2 avoided, [%]	86.2	91.4	94.6	85.7	91.1	94.6
SEWGS costs [M€]	**69.6**	**69.6**	**69.6**	**52.2**	**52.2**	**52.2**
Total equipment costs [M€]	**395.9**	**396.8**	**397.8**	**378.4**	**379.4**	**382.2**
Total Plant Costs [M€]	895.2	895.5	897.8	852.8	855.4	861.9
Specific Investment costs [€/kW]	**1119.0**	**1128.3**	**1136.4**	**1058.9**	**1072.0**	**1090.8**
Investment cost, [€/MWh]	17.17	17.40	17.56	16.23	16.49	16.84
Fixed O&M costs, [€/MWh]	6.38	6.39	6.40	6.15	6.16	6.20
Consumables, [€/MWh]	2.07	2.09	2.10	1.79	1.81	1.84
Fuel costs, [€/MWh]	45.36	45.64	45.84	45.06	45.39	45.83
COE, [€/MWh]	**70.98**	**71.52**	**71.90**	**69.23**	**69.85**	**70.70**
Cost of CO_2 avoided [€/t_{CO2}]	**55.7**	**54.2**	**53.5**	**49.9**	**49.0**	**49.9**

From these results, it can be deduced that SEWGS technology can be competitive vs. MEA only if *Sorbent Beta* demonstrates its reliability, performances and mechanical stability in long run tests.

Finally, a sensitivity analysis on fuel and SEWGS costs is shown in Figure 9-3 together with reference MEA. A reduction of SEWGS costs of 50% leads to a lower cost of CO_2 avoided by "only" 5 €/t_{CO2}, which corresponds to a 10% reduction. This is because the impact of SEWGS costs on total equipment costs, when 54 vessels configuration is adopted, is less than 15%, while other components cost such as GHR-ATR, CO_2 compressor, etc., remain constant and account for more than 20%. Therefore, the cost of SEWGS is not the critical part of this application, but it is the overall cost of the pre-combustion section.

A variation of fuel costs from 4 to 9 €/GJ_{LHV} increases the cost of CO_2 avoided about 12 €/t_{CO2}; efficiency penalties are more significant for high fuel costs.

For fuel costs of 8.5 €/GJ_{LHV}, SEWGS cost of CO_2 avoided matches MEA, since the efficiency becomes more important than investment costs.

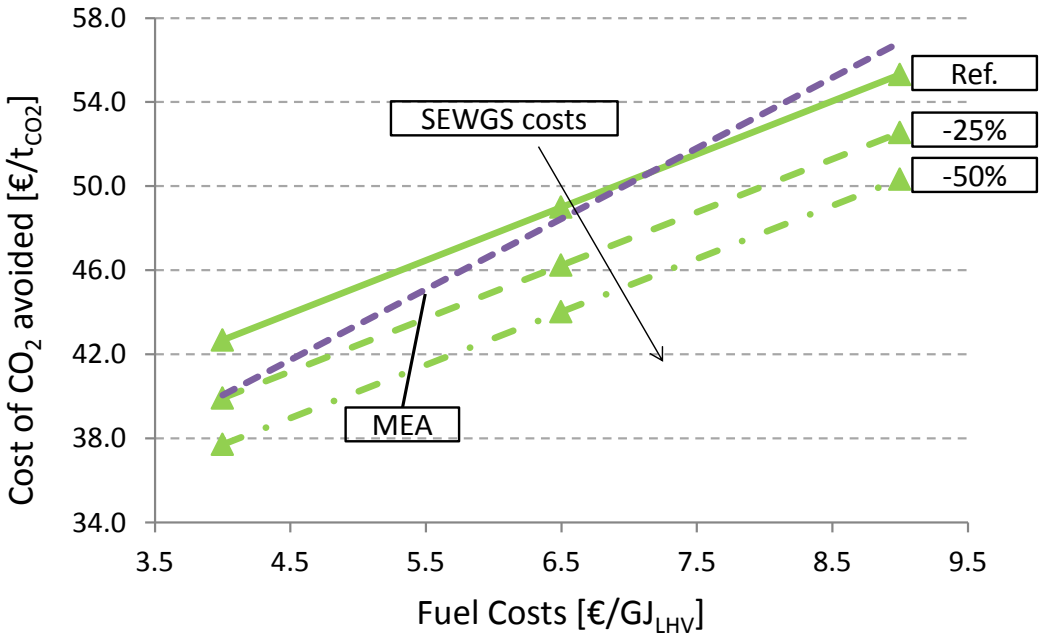

Figure 9-3 – Cost of CO_2 avoided for different fuel and SEWGS prices (SEWGS 95% CCR and 54 vessels); natural gas plant.

Finally, the impact on COE and cost of CO_2 avoided of financial support for CCS development from government/institution is evaluated. In particular, the proposal of European Community to finance 15% of the overall investment costs [17] is considered. This support reduces the COE from 70.7 €/MWh (SEWGS case with 54 vessels and 95% CCR) to 67.5 €/MWh, which is still 13 €/MWh above the reference NGCC without capture. The cost of CO_2 avoided will reduce to 41.5 €/t_{CO2} from 49.0 €/t_{CO2}. Actually, the financial support can help the CCS development, but it cannot balance additional costs since the increase of COE is mostly related to higher fuel costs.

9.2.1.1 Conclusions

The economic assessment of an innovative CO_2 capture system based on the SEWGS technology (Sorption Enhanced Water Gas Shift) was investigated and compared with a number of selected reference cases. In particular, a post-combustion scheme based on amine scrubbing and a pre-combustion lay-out with MDEA are taken as reference: the first one is closer to commercialization, while the second one is more similar to SEWGS schemes. Two different SEWGS sorbents, named *Sorbent Alfa* and *Sorbent Beta*, were compared together from an economic point of view in order to determine whether the reference sorbent performances (*Sorbent Alfa*) are competitive with those of the reference cases or an improvement is necessary. Results showed that SEWGS with Sorbent Alfa has a significantly lower cost of CO_2 avoided than the reference pre-combustion technology MDEA (58.6 €/t_{CO2} vs. 63.8 €/t_{CO2}), but it has 9 €/t_{CO2} higher costs compared to the post-combustion technology. This is due to the fact that the increased costs incurred in the pre-combustion systems cannot be balanced by the higher efficiency figures of the SEWGS integration. Moreover, the system requires a reformer unit which negatively affects the specific investments costs. The adoption of an improved sorbent like *Sorbent Beta* brings the cost of CO_2 avoided down to 49 €/t_{CO2}. In connection with CO_2 purity, results showed that there is a negligible impact from economic point of view, thus the

higher CO_2 purity is preferred to reduce transport and storage issues. The optimal SEWGS CO_2 capture ratio, depends on sorbent capacity, and is 95% for *Sorbent Beta*. A sensitivity analysis showed that even by reducing SEWGS investment costs of 50%, the resulting cost of CO_2 avoided would decrease by only 5 €/t_{CO2}, since SEWGS costs share is about 15% of the total investment costs. To summarize, SEWGS has several advantages compared to reference cases which are: (i) higher efficiency, (ii) lower CO_2 emissions, (iii) lower SPECCA and (iv) no environmental issues. From economic point of view, the cost of CO_2 avoided is comparable to amine scrubbing technology although pre-combustion technologies have higher investment costs. SEWGS may be the most cost-effective option in NGCC for fuel prices higher than 8.5 €/GJ_{LHV}.

9.2.2 COAL PLANT

This section presents the economic assessment of SEWGS integrated in IGCC plants previously presented. As for chapter 7, firstly plant with reference *Sorbent Alfa* are discussed, then *Sorbent Beta* is considered.

The reference cases and the SEWGS systems are compared in terms of total plant costs, cost of electricity and cost of CO_2 avoided. The estimated cost of a SEWGS train, which is composed of 9 vessels with 40 ft length, is 9.47 M€. For the adopted configuration, five or six trains with a vessel length of 40 ft are necessary when reference sorbent, *Sorbent Alfa,* is adopted.

H_2S catalytic combustion and flue gas desulphurization compose the system adopted to separate the H_2S from the CO_2 rich stream as SEWGS products.

Overall total plant costs for four SEWGS and two IGCC reference cases are summarized in Table 9-9. Investment costs for SEWGS are considered assuming *Sorbent Alfa.*

Total plant cost for the reference IGCC without capture is about 900 M€, where 375 M€ depend on equipment costs. In particular, the gasifier is the most expensive component with 94.4 M€, while the entire power section (GT, HRSG and steam turbine) accounts for 120 M€. The specific investment costs is 2100 €/kW_{inst} which is 25% higher than reference ASC determined with similar approach (as a term of comparison an ASC plant cost about 1100 M€ with a net power output of 760 MW [1]). IGCC with CO_2 capture increases total plant costs of 200 M€, mainly because of the CO_2 capture and compression sections. However, the specific investment cost rises of almost 40% because it is affected by the lower net power output. ASC case with CO_2 capture has a total investment cost of 1250.0 M€: cost increase is related to MEA separation systems and CO_2 compression section leading to a specific investment cost of 2536 €/kW_{inst}.

About SEWGS cases, there is no significant variation of Total Equipment Costs [TEC] and Total Plants Costs among the four presented cases: the lowest cost is for 45 vessel case because of the reduced investment for SEWGS (47.3 M€ vs 56.8 M€).

SEWGS working conditions have negligible effect on plant costs, since gasifier island and power section, which account for 75% of the total equipment costs, are not affected. Significant equipment cost variation can be noted in SEWGS expander and CO_2 compressor, since the amount of captured CO_2 and steam usage differ from case to case. Focusing on specific investment costs, differences among cases arise because of the significant impact of SEWGS

working conditions on plant performances and net power output: moving from 98% to 90% CCR, TEC is almost constant, but the net power output increases of 3%, thus reducing specific investment cost. The lowest specific investment costs are achieved for 45 vessel case with small advantages compared to 54 vessel case and 90% CCR.

Table 9-9: total plant and specific investment costs for different purge pressure and CCR in IGCC application.

Vessel number	IGCC	SELEXOL	54			45
Plant Component, [M€]			CCR 90%	CCR 95%	CCR 98%	CCR 90%
Coal handling	28.8	32.1	31.4	31.4	31.4	31.4
Gasifier	94.4	105.1	102.8	102.9	103.0	102.9
Gas Turbine	50.4	51.1	51.1	51.1	51.1	51.2
Steam Turbine	33.4	31.3	27.2	26.3	25.1	25.7
HRSG	36.4	40.0	36.5	35.7	38.4	38.1
LTHR	6.4	7.1	6.9	6.9	6.9	6.9
Cooling	37.5	41.9	41.2	41.7	41.8	40.9
ASU	29.6	33.1	32.4	32.4	32.4	32.4
Ash removal	10.1	11.1	10.9	10.9	10.9	10.9
AGR & Gas Cleaning	16.6	18.5	4.4	4.4	4.4	4.4
Water treatment	11.2	12.5	12.2	12.2	12.2	12.2
Claus	8.4	9.3	-	-	-	-
WGSR	-	12.5	2.9	2.9	2.9	2.9
Selexol	-	33.6	-	-	-	-
CO_2 compressor	-	14.5	19.6	20.3	20.7	19.6
SEWGS	-	-	56.8	56.8	56.8	47.3
Nitrogen compressor	11.3	9.3	6.9	6.9	6.9	6.9
SEWGS expanders	-	-	14.3	15.1	15.9	15.5
FGD/catalytic combustion	-	-	7.5	7.9	8.2	7.5
Total Equipment Cost [M€]	**374.7**	**463.4**	**465.0**	**466.0**	**469.2**	**456.9**
Total Plant Cost [M€]	**884.1**	**1093.6**	**1097.3**	**1099.6**	**1107.3**	**1078.1**
Net power Output [MW]	422.4	379.6	400.0	393.1	386.2	394.3
Net Electric efficiency[%]	47.12	36.03	39.27	38.52	37.83	38.64
CO_2 avoided [%]	--	86.5	87.2	92.8	96.6	86.9
Specific costs [€/kW$_{gross}$]	**1781.3**	**2212.4**	**2195.3**	**2221.1**	**2262.6**	**2181.7**
Specific costs [€/kW$_{net}$]	**2093.0**	**2881.1**	**2743.1**	**2797.0**	**2867.0**	**2734.4**

The estimated COE and cost of CO_2 avoided for investigated cases are summarized in Table 9-10.

Table 9-10: cost of Electricity and Cost of CO_2 avoided for SEWGS and reference IGGC cases.

Plant Component	IGCC	SELEXOL	SEWGS 54 vessels			SEWGS 45 vessels
SEWGS CCR/CO_2 purity	-	-	90/99	95/99	98/99	90/99
Net Power Output, [MW]	422.4	379.6	400.0	393.1	386.2	394.3
Thermal Power Input$_{LHV}$, [MW]	896.5	1053.5	1018.6	1020.6	1020.9	1020.3
Net Electric Efficiency$_{LHV}$, [%]	47.12	36.03	39.27	38.52	37.83	38.64
Net Electric Efficiency$_{HHV}$, [%]	45.21	34.58	37.68	36.96	36.30	37.08
CO_2 avoided, [%]	**--**	**86.5**	**87.2**	**92.8**	**96.6**	**86.5**
SPECCA [MJ_{LHV}/kg_{CO2}]	**--**	**3.71**	**2.39**	**2.51**	**2.65**	**2.63**
Investment cost, [€/MWh]	34.51	47.46	45.18	46.07	47.22	45.04
Fixed O&M costs, [€/MWh]	7.07	8.99	8.55	8.71	8.90	8.57
Consumables, [€/MWh]	1.82	3.14	4.61	4.71	4.79	4.35
Fuel costs, [€/MWh]	22.92	29.97	27.50	28.04	28.55	27.95
COE, [€/MWh]	**66.32**	**89.55**	**85.84**	**87.52**	**89.47**	**85.92**
Cost of CO_2 avoided [€/t_{CO2}]	**--**	**36.7**	**30.6**	**31.2**	**32.7**	**30.8**

The cost of electricity for the reference IGCC is about 66 €/MWh. More than 50% of the COE depends on the investment costs, while fuel costs account for about 35%. This result is typical of coal based plants, while natural gas based plants have an opposite trend. COE for the CO_2 capture increases of 35% because of the higher investment cost as well as fuel costs. The resulting cost of CO_2 avoided is 36.7 €/t_{CO2} which is in the range of similar studies proposed in literature [2] [14] [15] [16] supporting the reliability of this analysis.

As a term of comparison, the cost of electricity for the reference ASC is 54.8 €/MWh, which is lower than IGCC of about 20%; this result is consistent with the fact that all coal based power plant being built worldwide are based on this technology. When CO_2 capture is applied to ASC, the cost of electricity goes up to 85.5 €/MWh leading to a cost of CO_2 avoided of 46 €/t_{CO2} (the cost of CO_2 avoided in this case is calculated assuming as reference the ASC without capture). The higher cost of electricity is related to the investment cost of the capture section together with a reduced net power output and efficiency of 25%.

The application of SEWGS to IGCC allows reducing the cost of electricity to about 86 €/MWh with a CO_2 avoidance of about 87%. The cost of CO_2 avoided increases for higher CO_2 avoidance meaning that economic and thermodynamic penalties for high CCR balance lower CO_2 emissions.

Compared to reference capture with SELEXOL, SEWGS reduces investment and fuel costs thanks to the high temperature sulphur removal with consequent equipment savings, and higher efficiency. Only consumables, which mainly depend on sorbent replacement, are higher.

Comparing SEWGS cases with 45 and 54 vessels, they achieve very similar results with minimal advantage for the cases with 54. This means that the higher efficiency of 54 case is more important than the higher investment cost related to nine additional vessels. It must be

outlined that the COE for 54 and 45 vessels case were determined with the same equivalent hours whilst higher vessels could be less reliable as a consequence of the higher number of valves. Cost of CO_2 avoided for four cases are very similar being in a bandwidth of 2 €/t_{CO2}.

Concerning different CO_2 purities for SEWGS case with 54 vessel, Figure 9-4 shows that there are minimal differences from 98% to 99.5% which are negligible considering economic assessment uncertainties. In particular, the cost is the same for 90% CCR and there is a small increase with CO_2 purity for higher CO_2 avoidance. This result was expected since similar trends were achieved from thermodynamic point of view with no significant investment differences.

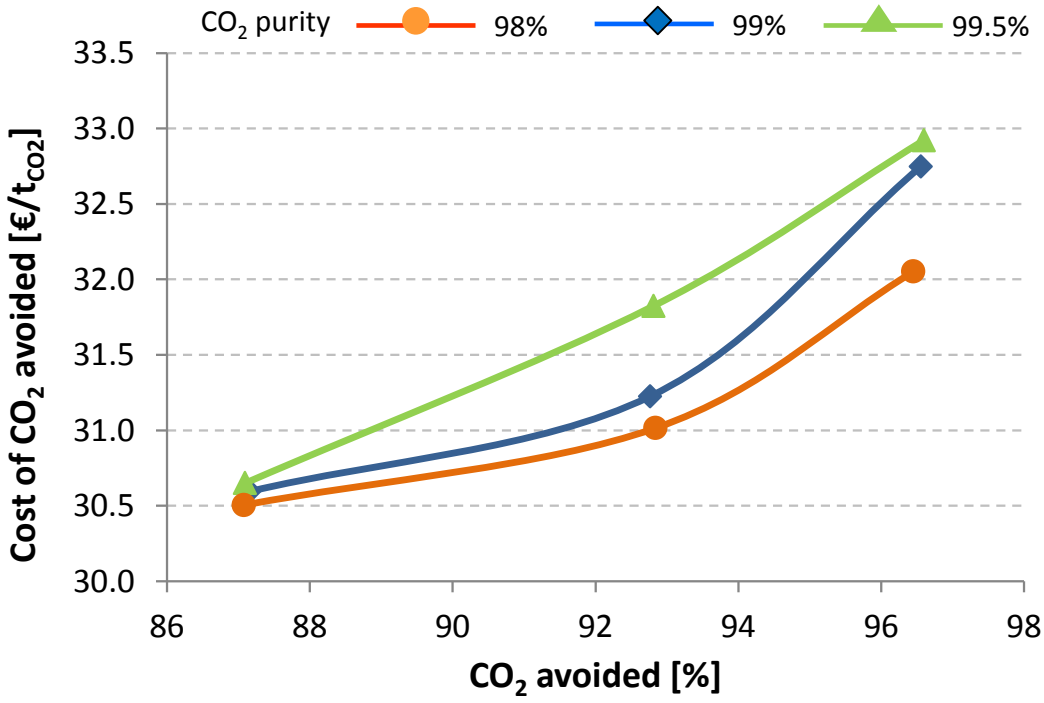

Figure 9-4: cost of CO_2 avoided as a function of CO_2 avoidance and CO_2 purity for SEWGS with 54 vessels.

Summarizing, the adoption of SEWGS with reference sorbent performances (*Sorbent Alfa*) allows reducing the cost of CO_2 avoided of 15% compared to conventional CO_2 capture by Selexol. SEWGS endows lower investment costs and efficiency penalties thanks to: i) the simultaneous CO_2 and H_2S separation and ii) the limited energy consumption for CO_2 capture. About optimal SEWGS working conditions, the lowest cost of CO_2 avoided is achieved for 87% CO_2 avoidance. CO_2 purity has negligible impact on final results, for this reason, 99% purity is assumed.

When *Sorbent* Beta is adopted, total sorbent volume can be significantly reduced either by reducing vessel number or vessel length. For simplicity, constant vessel number was considered and equal to 45, while vessel length range from 22 ft to 34 ft was investigated. In the 34ft case, the cost of a SEWGS train is about 8.7 M€ and would drop to 7.2 M€ for 22 ft. Vessel number reduction can lead to slightly different investment costs; the main advantage comes from a reduced number of valves with benefits from the reliability of the process. However, these considerations are beyond the scope of this preliminary assessment. Compared to *Sorbent Alfa*, cases with SEWGS 90% CCR were not considered, since the reduced steam usage suggested to move towards higher CO_2 avoided.

As shown in chapter 8 of this work, plant efficiency and CO_2 avoided with *Sorbent Beta* are higher than corresponding *Sorbent Alfa* cases, even with lower number of vessels. For this reason, it is expected a similar advantage also from economic point of view.

Figure 9-5 shows the CO_2 avoided cost for the investigated cases with *Sorbent Beta*: results are close to 23 €/t_{CO2}, significantly lower than *Sorbent Alfa* (31 €/t_{CO2}), reference Selexol (36.5 €/t_{CO2}) and ASC with CO_2 capture (45.9€/t_{CO2}).For 22ft and 28ft vessel length, optimum SEWGS CCR is 95% (which corresponds to 91.5% CO_2 avoidance), while for 98% CCR the optimum corresponds to 34ft. This is because short bed (22ft and 28 ft) requires a significant increase of steam moving from 95% to 98%% CCR, while this does not happen in 34 ft, leading to the abovementioned results. Results suggest that there is a minimal advantage of 22ft and 28ft vs. 34 ft which means that the additional costs for SEWGS are not balanced by the higher efficiency. As anticipated before, the analysis on SEWGS volume was performed changing the vessel length and keeping constant vessel number.

However, similar results could be achieved assuming constant vessel length and reducing vessel number because the governing parameter is the total sorbent volume which is the product of the two. For example, 45 vessels of 22ft and 28 ft corresponds to about three and four SEWGS trains of nine vessels, respectively.

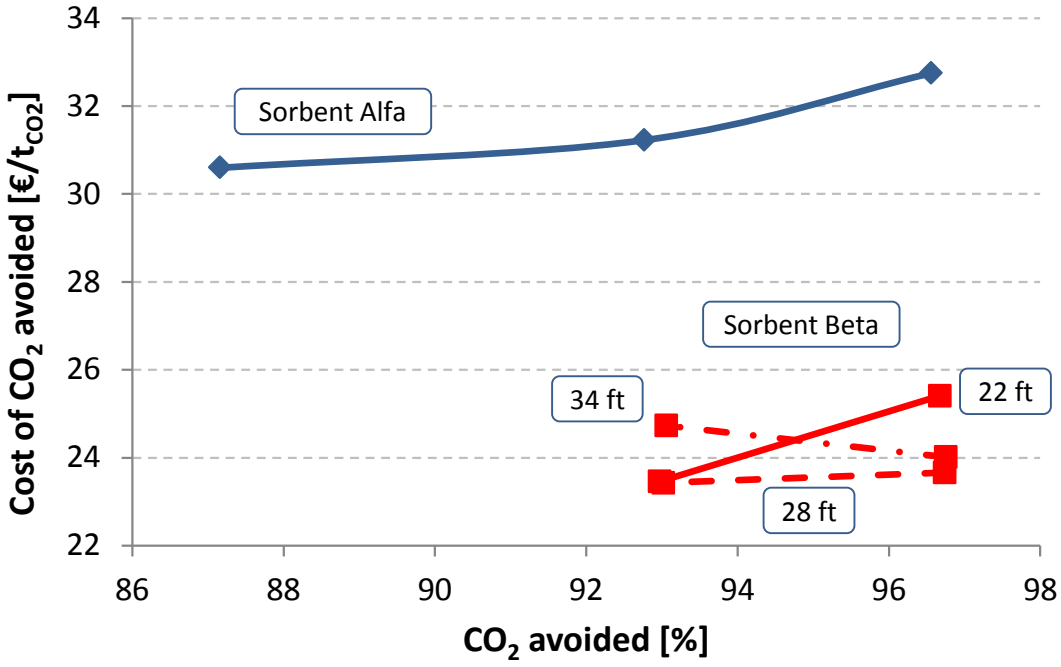

Figure 9-5: cost of CO_2 avoided as a function of CO_2 avoidance and vessel length for SEWGS with *Sorbent Beta*; IGCC application.

Detailed results (see Table 9-11) show that SEWGS investment cost with the advanced sorbent capacity is less than 10% of the entire plant. Specific investment costs are around 2600 €/kWinst which is about the same as ASC with capture. Compared to reference sorbent, the higher capacity reduces consumables costs of about 25%. The resulting COE is about 81.5 €/MWh which is 4 €/MWh and 7 €/MWh lower than reference ASC with capture and Selexol, respectively.

As a term of comparison, an ideal plant with no energy requirements for CO_2 separation can be considered; the additional energy penalties and costs would be related only to the CO_2 compression section. Resulting cost of electricity would be 71 €/MWh while the cost of CO_2 avoided would be 8€/t_{CO2}. These figures are determined adding to the reference IGCC without capture the CO_2 compressor costs and power consumptions. Hence, the additional costs related to the separation process within the SEWGS accounts for only 15 €/t_{CO2}.

Table 9-11: thermodynamic performances and economic calculations for SEWGS with *Sorbent Beta* in IGCC application.

CCR [%]		95			98	
Vessel lenght [ft/m]	22/6.7	28/8.5	34/10.4	22/6.7	28/8.5	34/10.4
Net Power Output, [MW]	**401.5**	**404.2**	**403.3**	**393.3**	**400.7**	**403.2**
Thermal Power $Input_{LHV}$, [MW]	1020.3	1017.0	1013.9	1021.1	1018.8	1021.1
Net Electric $Efficiency_{LHV}$, [%]	**39.35**	**39.75**	**39.78**	**38.52**	**39.33**	**39.49**
Net Electric $Efficiency_{HHV}$, [%]	37.76	38.14	38.17	36.96	37.74	37.89
SEWGS Costs	35.9	39.7	43.5	35.9	39.7	43.5
Total equipment costs [M€]	440.0	443.7	448.8	442.5	444.0	448.4
Total Plant Costs [M€]	1043.6	1052.3	1064.3	1049.6	1053.1	1063.4
Specific Investment costs [€/kW]	2599.2	2603.2	2639.2	2668.3	2627.9	2637.6
Investment cost, [€/MWh]	43.03	43.09	43.68	44.17	43.50	43.66
Fixed O&M costs, [€/MWh]	8.27	8.26	8.34	8.47	8.33	8.33
Consumables, [€/MWh]	3.54	3.75	4.00	3.63	3.79	3.99
Fuel costs, [€/MWh]	27.44	27.17	27.15	28.04	27.46	27.35
COE, [€/MWh]	**82.28**	**82.27**	**83.17**	**84.30**	**83.08**	**83.33**
Cost of CO_2 avoided [€/t_{CO2}]	**23.5**	**23.4**	**24.7**	**25.4**	**23.7**	**24.0**

Assuming as optimal SEWGS length 28 ft for both 95% and 98% CCR, a sensitivity analysis on carbon tax was performed. Figure 9-6 shows cost of electricity for SEWGS cases as a function of carbon tax. Reference cases are added too, considering different yearly equivalent operating hours.

Sensitivity analysis on equivalent operating hours only for reference case without capture is justified by the possible assimilation of capture plants to renewable energy with priority of dispatchability. For this reason, the power plant with carbon capture could work as base load with 7500 equivalent hours. Results show that for 4000 operating hours, the cost of electricity of ASC is similar to SEWGS and the situation is inverted for a carbon tax of 8 €/t_{CO2}. This value rises to 26 €/t_{CO2} and 37 €/t_{CO2} when ASC operating hours are assumed equal to 5500 and 7500, respectively. For IGCC, the trend is similar even if the breakeven is achieved for 5500 operating hours as a consequence of the higher initial COE.

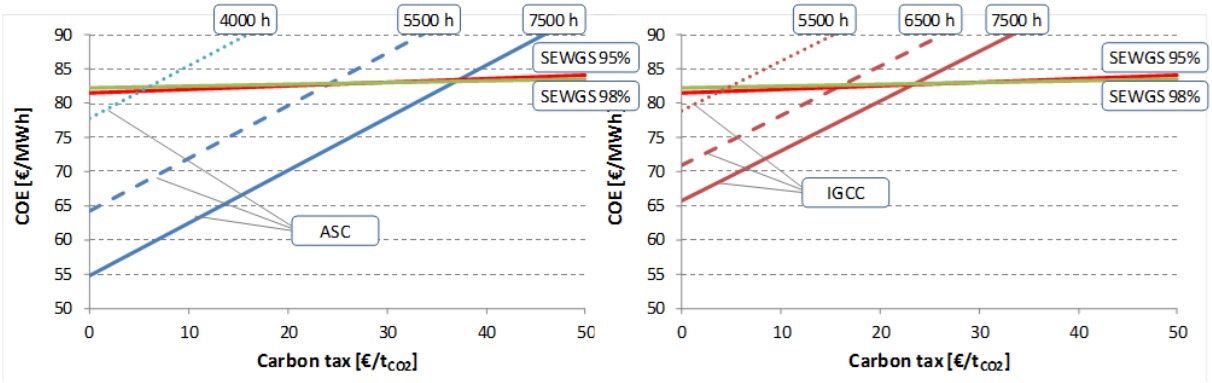

Figure 9-6: cost of electricity for SEWGS and reference cases without CO_2 capture as a function of carbon tax and equivalent operating hours.

9.2.2.1 Sensitivity analysis

A detailed sensitivity analysis on cost of CO_2 avoided was performed, in order to verify the consistency of results achieved. In particular, SEWGS investment costs and sorbent costs are evaluated for *Sorbent Beta* performances.

Figure 9-7 shows the cost of CO_2 avoided for different vessel lengths and CCR assuming a SEWGS investment cost variation of ±50% than reference price. Even with 50% higher SEWGS investment costs, the resulting cost of CO_2 avoided is about 26 €/t_{CO2} which is well below reference cases (i.e. 36.5 €/t_{CO2}). Higher SEWGS investment cost of 50% leads to a cost of CO_2 avoided increase of only 12%. It is worth noting that optimal vessel length varies with the assumed SEWGS equipment cost: when higher investment costs are assumed, the optimal case moves towards shorter length.

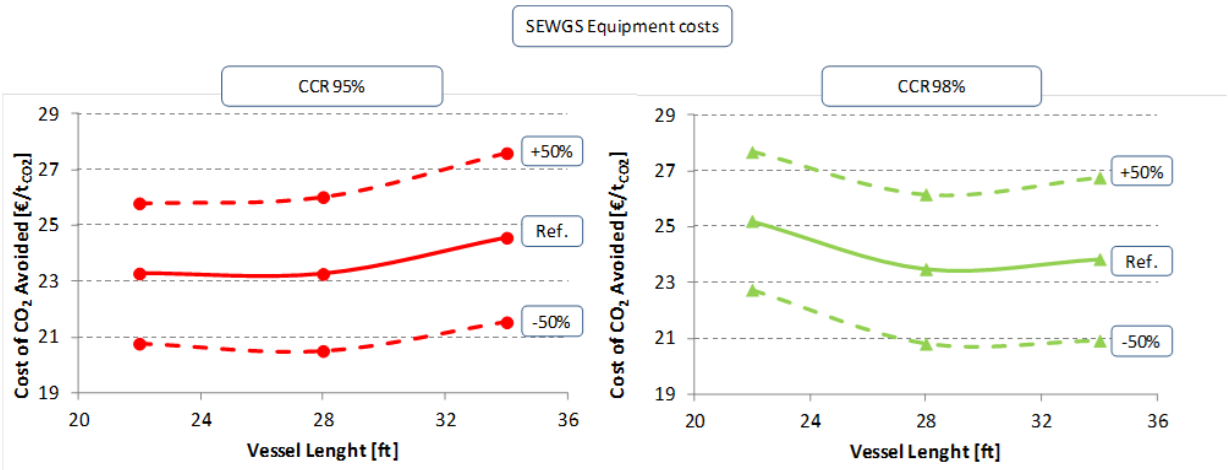

Figure 9-7: cost of CO_2 avoided as a function of vessel length and SEWGS equipment costs for SEWGS with Sorbent Beta. Left side 95% CCR SEWGS and right 98% CCR SEWGS.

Another sensitivity analyses were performed on fuel costs, SEWGS equipment and sorbent costs only for SEWGS 95% CCR case with vessel length of 28 ft (considered one of the most promising).

Results show that sorbent cost have negligible impact on the final cost of CO_2 avoided, while fuel cost variation from 1.5 to 4.5 €/GJ_{LHV} leads to a higher CO_2 avoidance cost of 6 €/t_{CO2}. This is a consequence of the capture plant efficiency penalty.

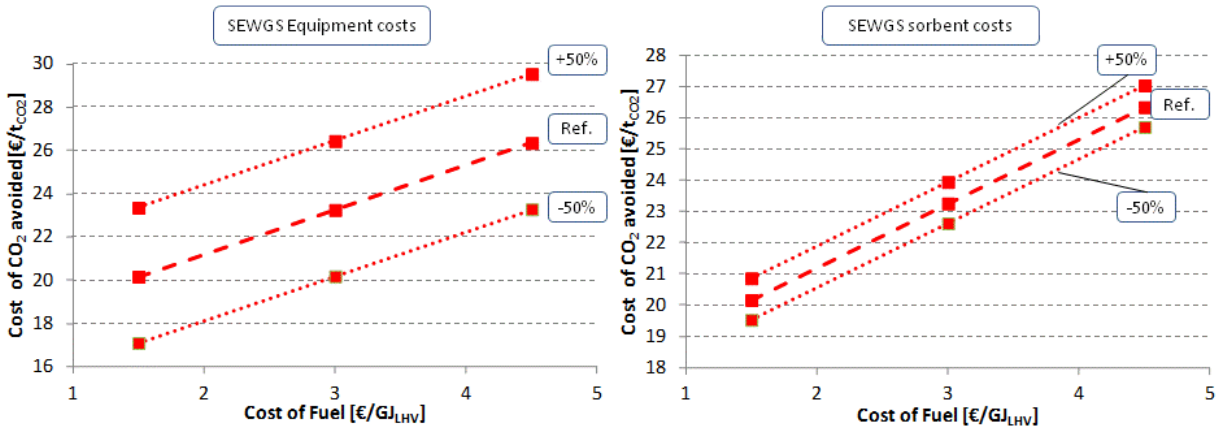

Figure 9-8: cost of CO_2 avoided as a function of fuel cost and SEWGS equipment costs (left side) and sorbent cost (right side). The case considered is SEWGS with Sorbent Beta 95% CCR and 28ft vessel length.

Finally, it was evaluated the impact of eventual financial support for CCS development. The financial support can be granted from government/institution as European Community [17]. This subsidy reduces the COE from 82.3 €/MWh (SEWGS case with 45 vessels and 95% CCR) to 76 €/MWh, which is still 10 €/MWh above the reference IGCC without capture. The cost of CO_2 avoided will reduce from 23.4 €/t_{CO2} to 14.1 €/t_{CO2}, which is not so far from actual CO_2 trading values.

9.2.2.2 Conclusions

SEWGS performances were analyzed and compared towards reference technologies for power production from coal: integrated gasifier combined cycle and pulverized coal plant. SEWGS working conditions were optimized as a function of the carbon capture ratio, CO_2 purity in the by-product and total sorbent volume. In addition, two different SEWGS sorbents, named *Sorbent Alfa* and *Sorbent Beta*, were compared from economic point of view. Results showed that SEWGS with *Sorbent Alfa*, which is the most reliable of the two but less performing, reduces the cost of CO_2 avoided than reference cases of 6 €/t_{CO2}.

The adoption of *Sorbent Beta* can further reduce the cost of CO_2 avoided down to 23 €/t_{CO2} which is 35% lower than reference cases. Moreover, *Sorbent Beta* reduces the total vessel volume with potential advantages also from vessel and valves reduction.

COE for SEWGS would be competitive towards ASC without capture, if about 4000 equivalent operating hours are assumed for ASC or a carbon tax of 35 €/t_{CO2} is applied.

A sensitivity analysis showed that even increasing SEWGS investment costs of 50%, the resulting cost of CO_2 avoided would increase of only 3 €/t_{CO2}, since SEWGS costs share is about 10% of total investment costs.

To summarize, SEWGS has several advantages compared to reference cases which are: i) higher efficiency, ii) lower CO_2 emissions, iii) lower SPECCA, iv) no environmental issues, and, last but not least, v) lower cost of CO_2 avoided.

9.3 HYDROGEN MEMBRANES ECONOMIC ANALYSIS

This section presents the economic assessment of membrane cases discussed in chapter 8 from thermodynamic point of view. This analysis aims at indicating the optimal membrane working conditions and configurations from economic point of view. Moreover, the competitiveness of membranes compared to reference technology is assessed. For this reason, specific investment costs will be firstly presented and discussed, while the cost of electricity and CO_2 avoided will be afterwards considered.

The specific investment costs computation is based on NOAK plant. The cost of the membrane module was assumed equal to 5800 €/m^2 for a membrane length of 6 m. This was finally proposed by Technip after long discussion within CACHET-II. The cost of the membrane module is taken constant for all feed pressure. In fact, most of the cost of the reactor are related to membrane manufacturing and layer deposition (which is not affected by the membrane) as well as manifolding (which is assumed to be independent from the feed pressure for simplicity).

9.3.1 NITROGEN-BASED GASIFIER

Since Selexol case indicated no advantages towards Rectisol, only the latter cases are discussed. The overall results for the base case are presented in Table 9-12.

Considering the very high plant costs with feed pressure of 37 bar, only the cases with higher feed pressure are going to be discussed. Focusing on specific investment costs, differences among cases become significant as a consequence of the membrane module costs. The resulting entire membrane separation section will cost between 140 M€ and 2600 M€ depending on the HRF and feed pressure. Only the case with HRF 90% and feed pressure equal to 54 bar with three reactor in series has a total equipment cost similar to reference cases. This case is slightly penalized by the cost of an additional WGS compared to the two membrane in series configuration, which however accounts for only 1.8 M€, negligible if compared to the reduced cost of the membrane of 70 M€. As anticipated, higher feed pressure than 54 bar was not investigated because of the CO_2 purity issues. A possible option not investigated in this work can be a feed compression at about 70 bar and, after the membrane, an expansion. This solution will increase the hydrogen permeation driving force with penalties from plant efficiency point of view.

The most expensive plant component besides membrane module is the gasifier, which is 25% cheaper than the membranes. Considering that membrane has to be replaced every five years, it is fundamental to achieve a membrane cost reduction or flux increase in order to make this technology competitive.

Table 9-12: equipment, total plant and specific investment costs for membrane integration in base case layout (N_2 feed gasifier). Results are presented for different HRF (90, 95 and 98 %) and different feed pressure (37, 47, 54 bar).

	Base case, Rectisol						
HRF [%]	**90**			**95**		**98**	
Feed pressure [bar]	37	47	54	37	47	37	47
Plant Component [M€]							
Coal handling	30.61	30.30	30.31	30.64	30.36	30.64	30.39
Gasifier	104.52	103.45	103.50	104.61	103.67	104.61	103.75
Gas Turbine	52.44	52.03	52.01	52.58	52.21	52.65	52.31
Steam Turbine	30.20	30.67	30.72	29.85	30.33	29.61	30.12
HRSG	38.08	38.08	38.08	38.08	38.08	38.08	38.08
LTHR	7.05	6.97	6.98	7.05	6.99	7.05	6.99
Heat rejection	34.79	36.14	36.24	34.22	35.47	33.93	35.06
ASU	34.27	33.90	33.91	34.30	33.98	34.30	34.00
ASH	11.09	10.99	10.99	11.10	11.01	11.10	11.01
AGR	15.03	14.87	14.88	15.04	14.91	15.04	14.92
Gas cleaning	4.46	4.42	4.42	4.47	4.43	4.47	4.43
Water Treatment	11.87	11.75	11.76	11.88	11.78	11.88	11.79
Claus	9.64	9.54	9.54	9.65	9.56	9.65	9.57
CO_2 compressor	8.74	8.26	8.12	8.51	8.13	8.37	8.08
Membrane	**716.06**	**188.42**	**134.96**	**1215.46**	**450.50**	**2594.22**	**621.03**
Sweep compression	12.83	12.74	12.74	12.84	12.76	12.84	12.76
Saturator	0.23	0.23	0.23	0.23	0.23	0.23	0.23
HTS	5.61	5.55	5.55	5.61	5.56	5.61	5.56
Air expander	5.66	5.61	5.61	5.67	5.62	5.67	5.62
Criogenic	0.80	0.80	0.80	0.80	0.80	0.80	0.80
LT heat exchangers	3.45	3.45	3.45	3.45	3.45	3.45	3.45
HT heat exchangers	8.49	8.49	8.49	8.49	8.49	8.45	8.49
Total Equipment Cost	**1145.91**	**616.67**	**563.29**	**1644.52**	**878.31**	**3022.62**	**1048.45**
Total Plant Cost	**2062.65**	**1110.00**	**1013.93**	**2960.14**	**1580.96**	**5440.72**	**1887.21**
Net power Output [MW]	407.67	403.21	401.67	407.94	404.06	407.70	404.43
Net Electric efficiency[%]	39.04	39.21	39.04	39.02	39.17	39.00	39.16
CO_2 avoided [%]	81.77	84.51	85.62	85.00	87.15	86.97	88.81
Specific costs [€/kW_{gross}]	5282.43	2870.34	2621.49	7581.81	4081.31	13949.33	4868.47
Specific costs [€/kW_{net}]	**6633.07**	**3609.05**	**3309.30**	**9512.95**	**5129.54**	**17495.18**	**6117.58**

As expected after thermodynamic results and investment cost assessment, the lowest cost of electricity and CO_2 avoided is achieved when the membrane surface area is minimized (HRF 90% and feed pressure at 54 bar, see Figure 9-9 and Table 9-13). This is because membrane costs have a significant share on the overall plant costs, while they have a negligible impact on system efficiency. Besides higher TPCs for membrane cases than Selexol reference case with CO_2 capture, which affect investment and fixed costs, membrane cases are penalized also from consumables costs. This is because membrane lifetime is assumed equal to 5 years; hence substitution costs must be included (in this case, module costs are not included since only the membrane must be replaced). The best membrane case has a cost of CO_2 avoided equal to 48

€/ton_{CO2} which is higher than the reference Selexol (36.7€/ton_{CO2}). From Figure 9-9, it can be outlined that a further increase in the feed pressure may not coincide with a lower cost of CO_2 avoided as consequence of the membrane area trend.

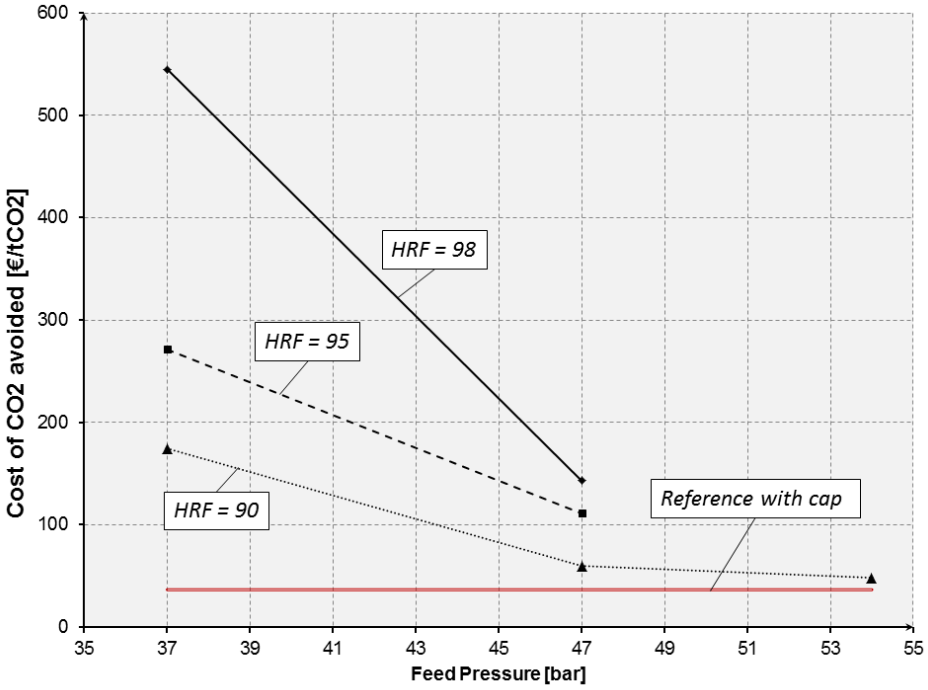

Figure 9-9: cost of CO_2 avoided as function of the feed pressure. Values are plotted for different HRF (90, 95 and 98%); in red the cost of CO_2 avoided for the reference IGCC with Selexol capture.

Table 9-13: cost of Electricity and Cost of CO_2 avoided for base case membrane integration (N_2 feed gasifier).

	Base case, Rectisol						
HRF [%]		90		95		98	
Feed pressure [bar]	37	47	54	37	47	37	47
Investment cost	108.96	59.38	54.46	156.17	84.31	287.04	100.51
Fixed O&M costs	16.40	10.28	9.69	22.26	13.37	38.50	15.38
Consumables	17.75	5.96	4.75	28.99	11.91	60.11	15.77
Fuel costs	27.66	27.54	27.66	27.68	27.57	27.69	27.58
COE, €/MWh	170.77	103.17	96.57	235.10	137.16	413.35	159.23
Cost of CO_2 avoided, €/ton_{CO2}	174.49	59.56	48.26	271.25	111.03	545.04	142.92

Table 9-14 reports the investment costs when advanced integrations, either post-firing and Rectisol and post-firing and HGD, are considered. The HRSG cost was corrected with a multiplicative factor when the maximum steam temperature is 620°C. In all cases with post-firing and Rectisol the membrane cost is considerately lower than the other plant solutions, either without PF or with PF +HGD. It can also be noted that the membrane cost range for different HRF is narrower; this is due to the limited area of the fourth membrane which works with permeate at ambient pressure.

It was difficult to accurately predict the cost of the entire desulphurization process because of three different reactors required. The kinetic model presented in chapter 5 can compute the cost

only for the desulfurizer section (differently from the complete Zn system). For this reason, the economic assessment was performed by determining the cost of the HGD system which makes the cost of CO_2 avoided competitive with the best case without post-firing. These calculations indicate that the actual cost of the system must be about 12.2 M€, which is lower than the corresponding cost of the Rectisol. This result is a consequence of the larger membrane surface area which significantly penalizes the economics.

Table 9-14: equipment, total plant and specific investment costs for membrane integration in advanced layout (N_2 feed gasifier). Results are presented for different HRF (90, 95 and 98 %) and different feed pressure (37, 47, 54 bar).

	Post-firing, Rectisol				Post-firing, HGD	
HRF [%]	90	90	95	98	90	90
Feed pressure [bar]	54	54	54	54	47	54
T steam HRSG	565	620	565	565	565	565
Plant Component [M€]						
Coal handling	31.95	31.90	32.10	32.08	31.81	31.81
Gasifier	109.10	108.92	109.59	109.54	108.61	108.60
Gas Turbine	51.65	51.62	51.82	51.95	51.67	51.66
Steam Turbine	36.25	36.76	36.22	35.88	36.40	36.60
HRSG	39.29	52.40	45.79	46.08	45.59	45.09
LTHR	7.35	7.34	7.39	7.38	7.32	7.32
Heat rejection	40.63	40.18	40.38	39.89	41.00	41.24
ASU	35.84	35.77	36.01	35.99	35.67	35.66
ASH	11.52	11.51	11.57	11.56	11.48	11.47
AGR	15.69	15.66	15.76	15.75	12.49	12.49
Gas cleaning	4.66	4.65	4.68	4.68	4.64	4.64
Water Treatment	12.39	12.37	12.45	12.44	12.34	12.34
Claus	10.06	10.04	10.11	10.10	10.01	10.01
CO_2 compressor	8.52	8.50	8.59	8.60	8.50	8.50
Membrane	**82.93**	**82.93**	**97.58**	**138.43**	**153.42**	**122.66**
Sweep compression	16.19	16.16	16.27	16.26	15.15	15.15
Saturator	0.24	0.24	0.25	0.25	0.00	0.00
HTS	4.46	4.45	4.48	4.48	4.44	4.44
Air expander	6.76	6.75	6.79	6.79	6.73	6.73
Criogenic	0.80	0.80	0.80	0.80	0.80	0.80
LT heat exchangers	3.45	3.45	3.45	3.45	3.45	3.45
HT heat exchangers	8.49	8.49	8.49	8.49	8.49	8.49
Total Equipment Cost	**538.25**	**550.91**	**560.55**	**600.87**	**610.01**	**579.14**
Total Plant Cost	**1270.16**	**1300.04**	**1322.80**	**1417.92**	**1439.51**	**1366.66**
Net power Output [MW]	435.20	439.67	437.53	437.21	445.57	443.81
Efficiency [%]	39.09	39.60	39.04	39.04	40.30	40.15
CO_2 avoided [%]	86.0	86.1	86.2	86.5	83.1	83.0
Specific costs [€/kW_{gross}]	2312.00	2349.29	2394.24	2568.40	2612.36	2473.20
Specific costs [€/kW_{net}]	**2918.59**	**2956.85**	**3023.34**	**3243.09**	**3230.69**	**3079.41**

If the permeability of the sulphur tolerant membranes is assumed equal to the non sulphur tolerant once, the cost of the HGD power plant can increase to about 50 M€ (more than twice the

Rectisol costs). Hence, the success of the HGD when applied to membranes configuration is strictly related to the impact of membrane costs itself.

The cost of CO_2 avoided ranges from 34 €/t_{CO2} to 45 €/t_{CO2} depending on steam maximum temperature and HRF. At 90% HRF and 54 bar feed pressure, the cost of CO_2 avoided is about 34 €/t_{CO2}, which is lower than the reference case (see Figure 9-10). All the 90% HRF cases result to have a lower CO_2 capture cost than the reference IGCC. Compared to the base case the reduction is significant and equal to 10-14 €/t_{CO2}.

It must be reminded that the cost of CO_2 avoided with the innovative cases is lower than the reference case one, even with the high cost of membrane area assumed. Hence, foreseen advancements in membrane technologies can lead to further cost reduction.

Table 9-15: cost of Electricity and Cost of CO_2 avoided for advances cases membrane integration (N_2 feed gasifier).

		Post-firing, Rectisol				Post-firing, HGD	
HRF	[%]	90		95	98	90	
Feed pressure	[bar]		54			47	54
T steam HRSG	[°C]	565	620	565	565	565	565
Investment cost	[€/MWh]	48.13	48.75	49.84	53.45	53.24	50.76
Fixed O&M costs	[€/MWh]	8.66	8.71	8.86	9.31	9.23	8.94
Consumables	[€/MWh]	3.28	3.23	3.56	4.41	4.67	4.06
Fuel costs	[€/MWh]	27.63	27.28	27.66	27.66	26.80	26.90
COE	[€/MWh]	87.70	87.97	89.93	94.83	93.94	90.66
Cost of CO_2 avoided	[€/ton_{CO2}]	33.95	34.34	37.41	45.01	45.42	40.07

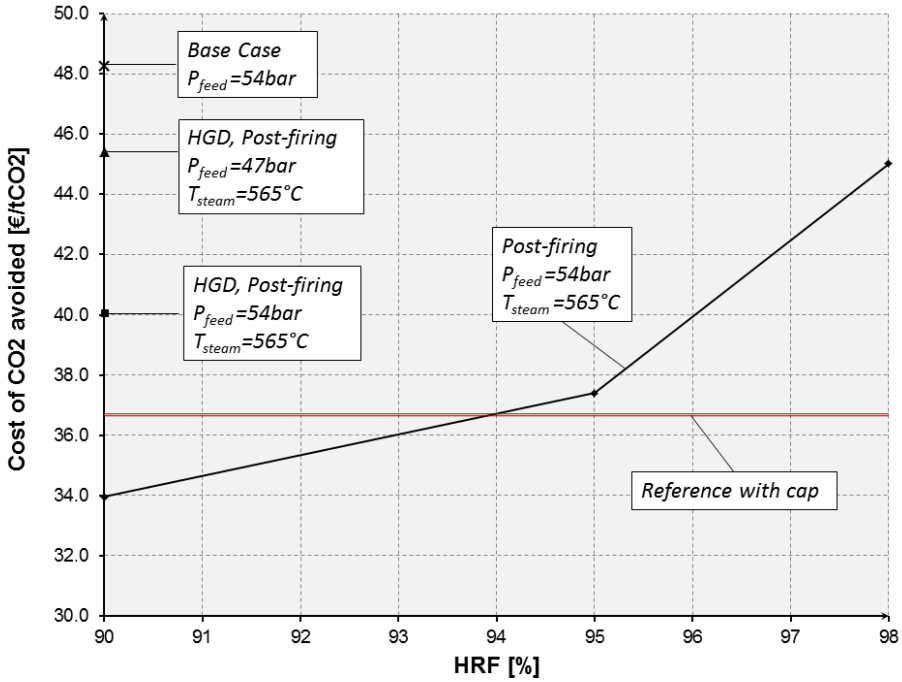

Figure 9-10: Cost of CO_2 as function of the HRF for post firing configuration and comparison with other plants at 90% HRF.

9.3.2 CO_2 FED GASIFIER

Focusing on results reported in Table 9-16, Total Equipment costs [TEC] ranges between 1500 and 5600 M€ outlining that membrane operating conditions strongly affects the economics, even more than the system performances. Again, total equipment cost shows a trend function of the membrane surface area: the smaller the membrane surface area, the lower the membrane cost, the lower the total equipment cost. Compared to membrane area, the other components have negligible variations.

Focusing on specific investment costs, differences among cases are also significant as a consequence of the different TPC. The membrane costs are significant since they account for 25% to 80% of total plant costs depending on the considered HRF and feed pressure. Only the case with 90% HRF and 54 bar of feed pressure has a specific investment costs comparable to the reference case (3434 €/kWel), suggesting a necessary improvement for the membranes in terms of costs for this gasifier feeding technology.

As shown in Table 9-17, the calculated cost of electricity covers a wide range depending on membrane operating conditions. Nevertheless, the COE is always higher than reference capture plant with Selexol. Comparing different contributions, only fuel costs are lower for the membrane cases thanks to the higher efficiency. About investment and fixed O&M costs, they depend on the total plants costs which are significantly higher for membrane cases as shown in previous section.

Focusing on the cost of CO_2 avoided, with actual feeding performances, the minimum cost of CO_2 avoided is about 64 €/t_{CO2}, while it reduces to 46 €/t_{CO2} when improved performances are considered.

The hybrid feeding shows no improvements compared to the conventional nitrogen feeding (55 vs 48€/t_{CO2}). All cases with hybrid feeding have a cost of CO_2 avoided higher than respective N_2 feeding ones.

Table 9-16: equipment, total plant and specific investment costs for membrane integration in base case layout (CO_2 feed gasifier). Results are presented for different HRF (90, 95 and 98 %) and different feed pressure (37, and 54 bar).

	Rectisol, CO_2 feeding					
HRF [%]	90		95		98	
Feed pressure [bar]	37	54	37	54	37	54
Coal handling	31.92	31.91	30.97	30.97	30.43	30.44
Gasifier	108.99	108.95	105.73	105.73	103.91	103.92
Gas Turbine	51.30	51.30	51.66	51.60	51.86	51.84
Steam Turbine	36.89	37.35	33.48	34.02	31.09	31.93
HRSG	42.58	33.88	39.05	32.36	37.12	31.94
LTHR	7.35	7.34	7.13	7.13	7.01	7.01
Heat rejection	48.80	48.80	48.80	48.80	48.80	48.80
ASU	38.21	38.21	35.20	35.16	33.48	33.47
ASH	11.51	11.51	11.20	11.20	11.03	11.03
AGR	15.67	15.67	15.20	15.20	14.94	14.94
Gas cleaning	4.65	4.65	4.51	4.51	4.44	4.44
Water Treatment	12.38	12.38	12.01	12.01	11.80	11.81
Claus	9.29	9.28	9.01	9.01	8.85	8.85
CO_2 compressor	7.50	8.09	7.27	7.70	73.20	7.57
Membrane	1158.51	163.34	1705.58	350.89	1867.70	429.98
Sweep compression	17.25	17.25	15.99	15.96	15.20	15.20
Saturator	0.24	0.24	0.24	0.24	0.23	0.23
HTS	6.68	5.84	5.67	5.67	5.57	5.57
Air expander	5.19	5.19	4.80	4.80	4.58	4.57
Oxy-combustor	2.58	2.58	1.29	1.29	0.65	0.65
LT heat exchangers	8.95	8.95	8.22	8.22	7.83	7.83
HT heat exchangers	10.02	10.02	7.81	7.81	6.52	6.52
Total Equipment Cost [M€]	1636.48	632.74	2160.82	800.25	2376.24	868.53
Total Plant Cost [M€]	3861.76	1493.15	5099.10	1888.44	5607.46	2049.56
Net power Output [MW]	428.37	434.77	415.25	419.40	417.07	407.64
Net Electric efficiency[%]	38.6	39.2	39.2	39.5	39.3	39.4
Specific costs [€/kW_{gross}]	7231.35	2756.52	9983.35	3662.46	11277.62	4080.60
Specific costs [€/kW_{net}]	9015.01	3434.31	12279.48	4502.70	13445.02	5027.82

Table 9-17: cost of Electricity and Cost of CO_2 avoided for base case and hybrid membrane integration (CO_2 feed gasifier).

	Base case					Hybrid	
HRF [%]	90		95		98	90	
Feed pressure [bar]	37	54	37	54	37	54	54
Investment cost, [€/MWh]	148.0	56.5	201.5	74.0	220.6	83.6	54.81
Fixed O&M costs, [€/MWh]	21.1	9.7	27.8	12.0	30.2	13.1	9.74
Consumables, [€/MWh]	26.8	5.4	39.8	9.7	43.2	11.8	4.84
Fuel costs, [€/MWh]	28.0	27.6	27.6	27.3	27.5	27.4	27.71
COE [€/MWh]	223.9	99.2	296.7	123.0	321.5	135.9	97.11
Cost of CO_2 avoided [€/ton_{CO2}]	221.6	46.2	323.9	79.7	354.7	97.7	55.55

9.3.3 CONCLUSIONS

Membrane performance was analyzed and compared towards reference IGCC. Membrane working conditions were optimized as a function of the HRF and feed pressure for all the developed plant solutions. Results showed that membranes with nitrogen-based gasifier, which is the traditional integration layout, have a very high specific investment cost as consequence of the membrane price. The resulting cost of CO_2 avoided is not competitive with reference technology at the present membrane state-of-the-art.

On the other hand the adoption of the post-firing configuration can reduce the cost of CO_2 avoided down to 34 €/t_{CO2} which is lower than reference case (36.7 €/t_{CO2}). Moreover, this plant solution allows increasing the HRF with limited cost penalization.

COE for Pd-alloy membrane and HGD will be competitive only if a flux increase will be achieved.

As far as CO_2-based gasifier is concerned, resulting specific investment costs are affected by the membrane cost as in the nitrogen case. The COE is slightly lower than the nitrogen-based case if a recovery of the lock hopper gas is considered. Anyway, COE is higher than the reference capture technology.

REFERENCES

[1] **Franco F, Anantharaman R, Bolland O, Booth N, van Dorst E, Ekstrom C, Sanchez Fernandes E, Macchi E, Manzolini G, Nikolic D, Pfeffer A. Prins M, Rezvani S, Robinson L.** D4.9 European Best practice guidelines for assessment of CO2 capture technologies. 2011.

[2] **GCCSI, Global CCS Institute, 2011.** http://www.globalccsinstitute.com/sites/default/files/eco-assess-ccs-tech-2010-4b.pdf. Accessed June 2011.

[3] **IEA.** *Leading options for the capture of CO2 emissions at power stations.* s.l. : IEA, Februray 2000. PH3/14.

[4] —. *Improvement in power generation with post-combustion capture of CO2.* s.l. : IEA, November 2004. PH4/33.

[5] **Thermoflow Inc.** http://www.thermoflow.com. *Thermoflow website.* [Online] visited june 2011.

[6] **Aspentech website.** http://www.aspentech.com/. *visited October 2011.*

[7] **DOE-NETL.** *Cost and performance baselines for fossil energy plants, Volume 1.* 2007-1281.

[8] EPCCI website. *http://www.cera.com/aspx/cda/client/knowledgeArea/serviceDescription.aspx?KID=229.* [Online]

[9] **Cambridge Energy Research Associaters.** [Online] June 2010. http://www.cera.com/aspx/cda/public1/news/pressReleases/pressReleaseDetails.aspx?CID=10429.

[10] *Gas Turbine World Handbook.* Southport 06890 USA : Pequot Publishing INC, 2009-2010.

[11] **Manzolini, G, Gazzani, M and Macchi, E.** SEWGS INTEGRATION IN NATURAL GAS COMBINED CYCLE: Part 2 Economic Assessments. Vol. submitted to International Journal of Greenhouse Gas Control.

[12] **CAESAR.** *D4.7 Test cases and preliminary benchmarking results from the three projects.* 2010.

[13] **Project, Carbon Capture.** *http://www.co2captureproject.org/ccp2_capture.html.* [Online] [Cited: January 7, 2010.]

[14] **Finkenrath, Matthias.** Cost and perforamnce of carbon dioxide capture for power generation. s.l. : International Energy Agency, 2011.

[15] **European Benchmark Task Force.** European best practice guide for assessment of CO2 capture technologies. 2011. Vol. http://www.energia.polimi.it/news/D%204_9%20best%20practice%20guide.pdf.

[16] **Valenti G, Bonalumi D, Macchi E.** A parametric investigation of the Chilled Ammonia Process from energy and economic perspective. *Fuel.* In press, 2011. doi:10.1016/j.fuel.2011.06.035.

[17] **European Commission communication.** http://ec.europa.eu/competition/sectors/energy/legislation en.html. Strasburg : s.n., 2012. 3230.

[18] **Manzolini G, Dijkstra JW, Macchi E, Jansen D.** Technical Economic Evaluation of a system for electricity production with CO2 capture using membrane reformer with permeate side combustion. 2006.

[19] **INC, Fluor Daniel.** *CO2 capture via partial oxidation of natural gas.* s.l. : IEA, 2000. PH3/21.

[20] **Tom Kreutz, Prineton university, personnal communication, 2007.**

[21] **Manzolini G, Macchi E, Binotti M, Gazzani M.** Integration of SEWGS for carbon capture in Natural Gas Combined Cycle. Part B: Reference case comparison. *International Journal of Greenhouse Gas Control.* 2011. Vol. 5, 2, Pag 214-225.

[22] **Gazzani, M, Manzolini, G and Macchi, E.** Co2 capture in natural gas combined cycle with SEWGS. Part A: Thermodynamic performances. 2012. Vol. International Journal of Greenhouse Gas Control. 10.1016/j.ijggc.2012.06.010.

[23] **Politecnico di Milano.** Software presentation: GS (Gas-Steam Cyckes). *http://www.gecos.polimi.it/software/gs.html.* [Online] 2009. [Cited: January 8, 2010.]

[24] **Mark Prins, Shell employee, personnal communication, March 2010.**

[25] **Chiesa P, Campanari S, Manzolini G.** CO2 cryogenic separation from combined cycle integrated with molten carbonate fuel cells. s.l. : Internatonal Journal of Hydrogen Energy . Vols. 2011, In press. DOI: 10.1016/j.ijhydene.2010.09.068.

[26] **Manzolini G, Campanari S, Chiesa P, Giannotti A, et. al.** CO2 separation from combined cycle using molten carbonate fuel cells. *Submitted to ASME Fuel Cell Science, Engineering and Technology conference 2011.*

[27] **Aspentech Documentation.** Aspen Physical Property System. *V 7.2.*

[28] **Politecnico di Milano.** D4.2 Base case report. *CACHET II Project.*

[29] **Gazzani M, Manzolini G, Macchi E, Ghoniem A.F.** Reduced order modeling of the Shell-Prenflo entrained flow gasifier. *Fuel, in press.* 2012.

[30] **van Vliet, Oscar P.R., Faaij, Andrè P.C. and Turkenburg, C.** Fischer-Tropsch diesel production in a well-to-wheel perspective: a carbon, energy flow and cost analysis. s.l. : Elsevier, 2009. 50, pp. 855-876.

[31] **Tijmensen, M.J.A. et al.** Exploration of the possibilities for production of Fischer Tropsch liquids and power via biomass gasification. 2002. Vols. Biomass and Bioenergy, Volume 23, Pages 129-152.

10 CONCLUSIONS

The multi-level simulation work carried out in the PhD permitted to investigate in detail both the proposed pre-combustion CO_2 capture technologies: SEWGS and hydrogen membranes. Thanks to the FP7 projects framework, all the technology issues have been addressed, making the theoretical simulation consistent with experimental data. Thermodynamic and economic results for the best cases in term of minimum cost of CO_2 avoided are reported in the next paragraphs.

10.1 THERMODYNAMIC COMPARISON

SEWGS technology showed good thermodynamic results both in NGCC and IGCC power plants.

As far as NG is considered (Figure 10-1), the SEWGS allows limiting the efficiency penalty compared to the reference technologies; any of the developed sorbents achieve 51% electric efficiency and SPECCA lower than 3.0 MJ/kg_{CO2}. The minimum SPECCA is about 2.5 MJ/kg_{CO2}. Hydrogen membranes were not investigated in natural gas applications.

Concerning coal-IGCC plant, both SEWGS and hydrogen membranes improve the thermodynamic performance: all the configurations feature an efficiency higher than 39% and a SPECCA lower than 2.6 MJ/kg_{CO2}. The efficiency improvement is in the order of 3-4 percentage points compared to the reference pre-combustion technology. It can be noted that the efficiency and SPECCA intervals are narrow despite of the significant technology differences. SEWGS allows achieving the lowest SPECCA because of the higher CO_2 avoided value among the reported cases. Nevertheless, membranes with higher HRF (95 or 98%) further decrease the SPECCA; these cases were not considered in this section because of the bad economic results.

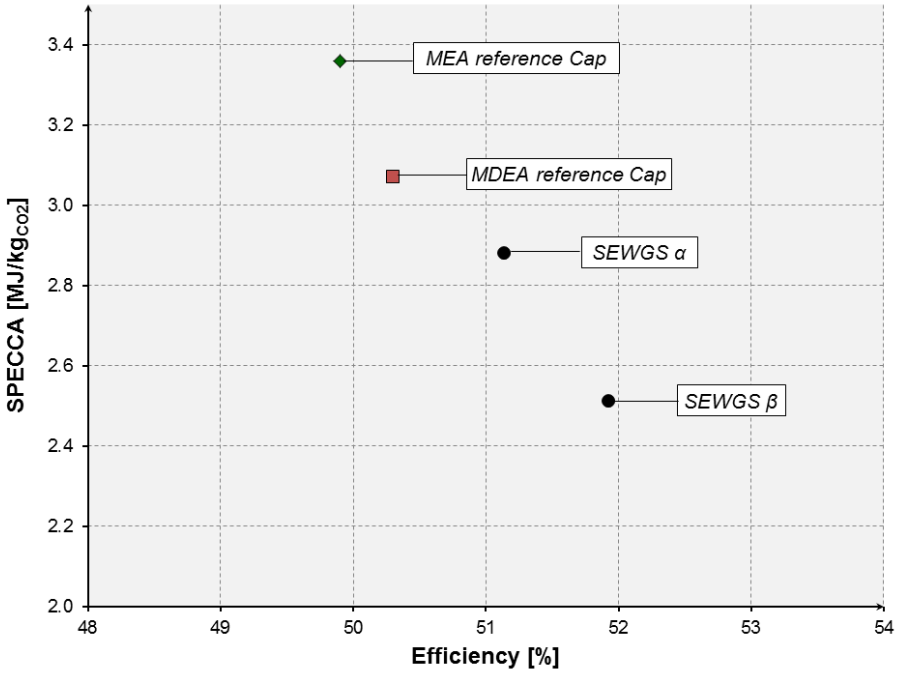

Figure 10-1: SPECCA and electric efficiency for different technologies in natural gas fuelled pre-combustion capture plant. All cases feature about 90% CCR. MEA is the reference technology for CO_2 capture in general; MDEA is the reference for pre-combustion CO_2 capture.

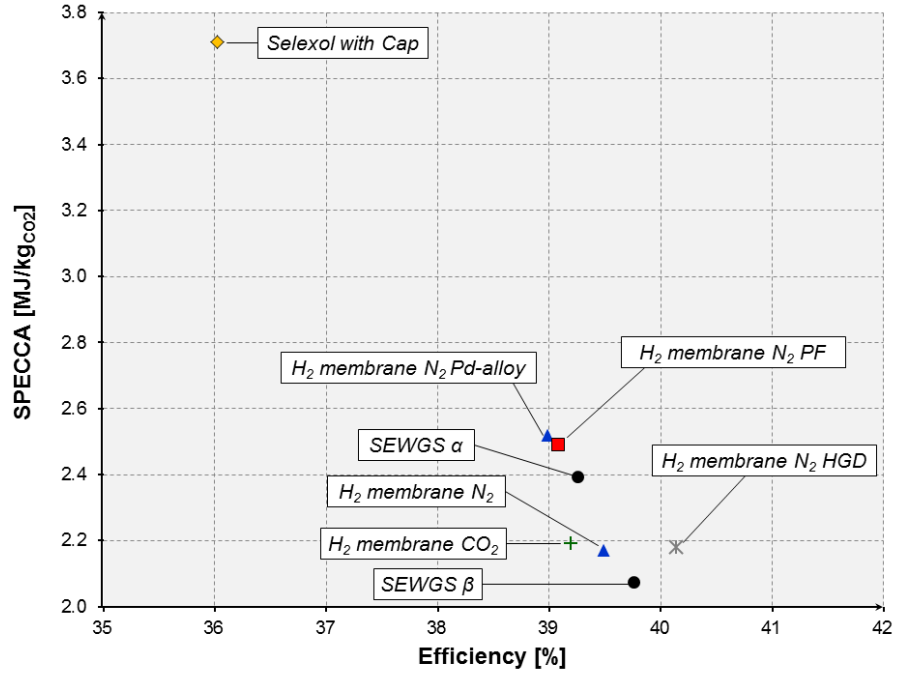

Figure 10-2: SPECCA and electric efficiency for different technologies in coal fuelled pre-combustion capture plant. SEWGS features 95% CCR, all hydrogen membranes have 90% HRF but for Pd-Alloy which has 98% HRF. Selexol with capture is the reference technology.

10.2 ECONOMIC COMPARISON

From an economic point of view, the application of SEWGS to NGCC does not show evident advantages compared to commercial ready technology. As far as pre-combustion reference is concerned (MDEA), SEWGS allows sharply decreasing the cost of CO_2 avoided from 64 to 49 €/ton$_{CO2}$. On the other hand, considering reference post-combustion capture (MEA), the cost of CO_2 avoided established by SEWGS is not competitive. Provided the very good thermodynamic results, this suggests that pre-combustion capture in natural gas plant is not competitive even with advanced technologies.

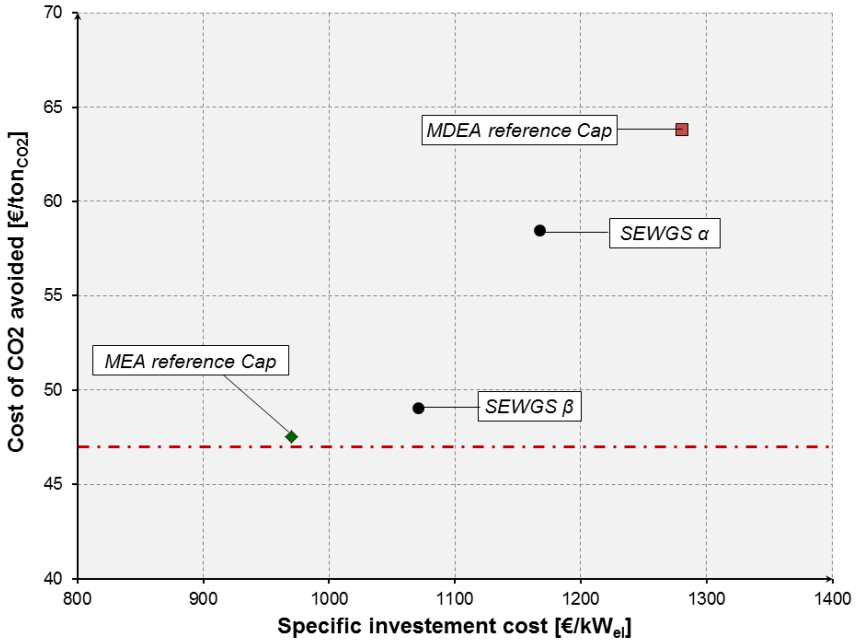

Figure 10-3: Cost of CO_2 avoided for different technologies in natural gas fuelled pre-combustion capture plant. SEWGS features 90% CCR. MEA is the reference technology for CO_2 capture in general; MDEA is the reference for pre-combustion CO_2 capture.

On the other hand, SEWGS application to IGCC leads to a substantial decrease in the cost of CO_2 avoided, in the order of 35%. Compared to the reference IGCC Selexol, both sorbent alfa and beta achieves a lower cost of CO_2 avoided. Considering sorbent beta, the cost of CO_2 avoided approaches 20 €/ton$_{CO2}$. Provided that about 8 €/ton$_{CO2}$ are directly linked to the penalization and cost of the CO_2 compression standalone, the separation cost is very attractive compared to all the CO_2 capture technologies. Indeed, sorbent beta was a breakthrough of the SEWGS technology both from economic and thermodynamic point of view.

Concerning hydrogen membrane application, the cost of CO_2 avoided is not competitive as far as all the hydrogen is produced and sent to the gas turbine. Any of the base configurations (nitrogen or CO_2 feeding gasifier) features a high cost, in the range of 45-50 €/ton$_{CO2}$. On the other hand, considering the solution developed in this work where part of the hydrogen is sent to the HRSG, the cost of CO_2 avoided decreases below the reference technology at about 30 €/ton$_{CO2}$. With the actual membrane technology, this solution looks mandatory in order to limit the membrane surface area. It must be stressed that the post-firing is extensively adopted in

modern power plants and there are no evident drawbacks and no reasons to discard this layout also in more complex plant solutions.

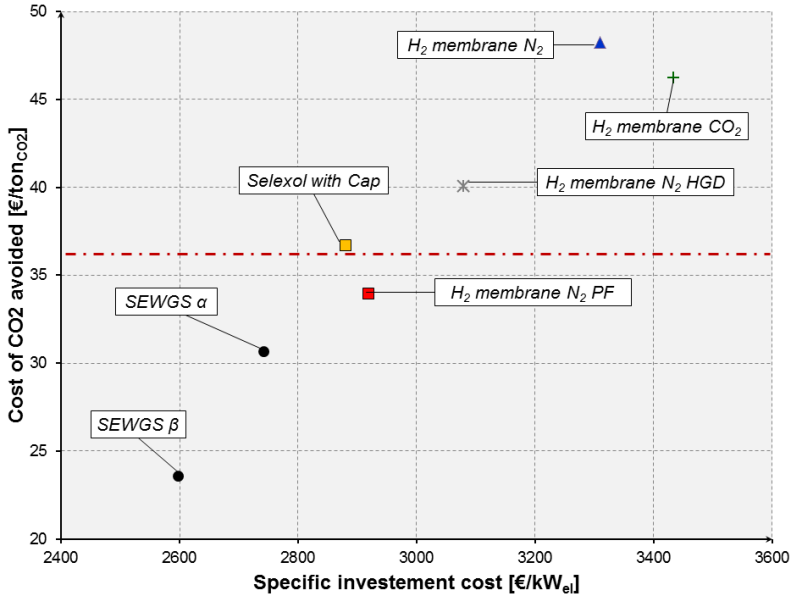

Figure 10-4: : Cost of CO_2 avoided for different technologies in coal fuelled pre-combustion capture plant. SEWGS features 95% CCR, all hydrogen membranes have 90% HRF but for Pd-Alloy which has 98% HRF. Selexol with capture is the reference technology.

Table 10-1 and Table 10-2 report a summary of the numbers shown in Figure 10-1, Figure 10-2, Figure 10-3 and Figure 10-4, respectively.

Table 10-1: main thermodynamic end economic values for all the natural gas-based plant investigated.

	Reference NGCC			SEWGS	
	No cap	MEA Cap	MDEA Cap	α	β
Net Electric Efficiency $_{LHV}$, %	58.34	49.9	50.3	51.1	51.9
SPECCA, MJLHV/kg_{CO2}	N/A	3.36	3.07	2.88	2.51
Specific costs, €/kW	630.4	969.9	1280.6	1168.1	1072
COE, €/MWh	54.1	69.1	74.6	72.8	69.9
Cost of CO_2 avoided €/t_{CO2}	N/A	47.5	63.8	58.4	49

Table 10-2: main thermodynamic end economic values for all the coal-based plant investigated.

	Reference		SEWGS		Pd-membrane			
COAL	No Cap	Cap	α	β	base N_2	N_2 PF	HGD	Base CO_2
Net Electric Efficiency$_{LHV}$, %	47.12	36.0	39.3	39.8	39.0	39.1	40.2	39.2
SPECCA, MJ_{LHV}/kg_{CO2}	N/A	3.71	2.39	2.07	2.52	2.49	2.18	2.19
Specific costs, €/kW	2093	2881	2743	2599	3309	2918	3079	3434
COE, €/MWh	66.32	89.6	85.8	82.3	96.6	87.7	90.7	99.2
Cost of CO_2 avoided, €/t_{CO2}	N/A	36.7	30.6	23.5	48.3	33.9	40.1	46.2

Figure 10-5 reports the final comparison between SEWGS and membranes. Provided the very attractive thermodynamic performance of the two, SEWGS score is higher in the economics and technology readiness. Concerning the plant complexity, both the technologies feature quite high complexity: membranes require some hundred modules while SEWGS several medium-temperature switching valves (with the latter less critical in author' opinion).

Globally SEWGS can be considered more attractive for nowadays application. From a medium-long term perspective, membranes can play a major role because of the higher efficiency and the expected lower capture cost. Eventually, the process type and requirements (sulfur/not sulfur tolerant, high/not high hydrogen purity) will make one technology more or less attractive.

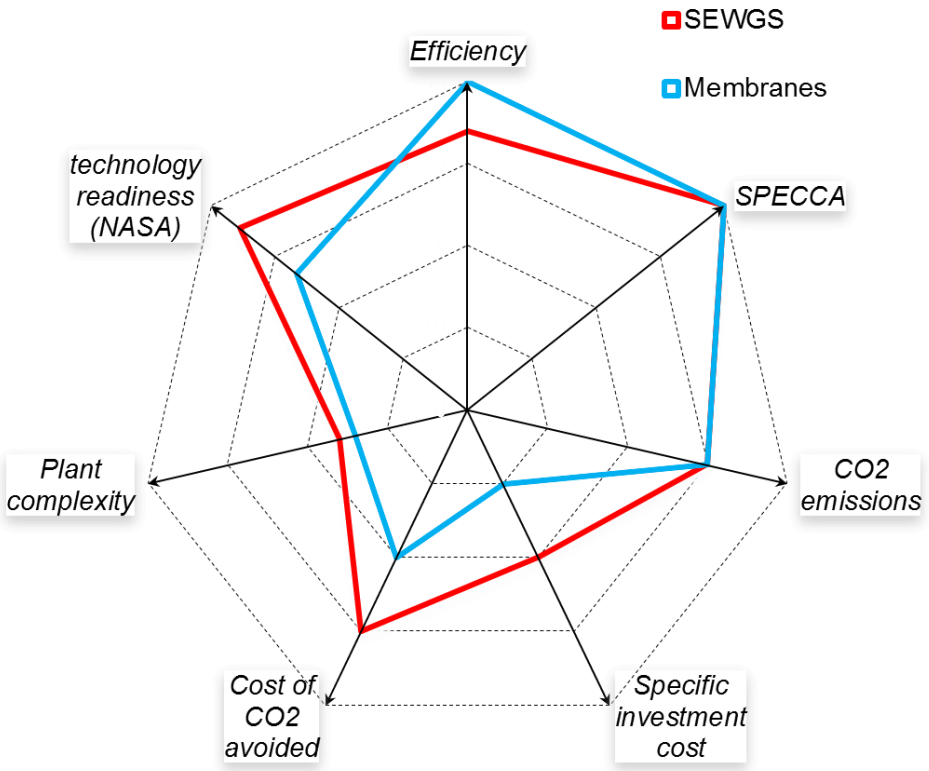

Figure 10-5: qualitative comparison between SEWGS and hydrogen membrane. The higher the score in a category, the better. Both the technologies feature good scores but currently SEWGS is cheaper and ready for scale up.

10.3 FUTURE WORKS

This work assessed that both SEWGS and hydrogen membranes are promising CO_2 capture technologies. In order to make further developments different actions should be taken:

- SEWGS: move and scale up the process in an industrial site, verify the correct operation of the valves at 400°C, test the sorbent with a real process syngas, verify possible sorbent contaminations in the hydrogen mixture.
- Membranes: test full scale modules, verify the seal operations in full scale modules, verify the membrane reliability, improve the simulation modeling to compute more accurately the area and predict inhibition effects.

Finally, it is author opinion that both SEWGS and membranes can play an important role in future CO_2 capture plants provided that CCS will become a real option for power generation with limited emissions.